Smac mimetic compounds engage peripheral and neuroimmune action against Glioblastoma

Kyle Malone

A thesis submitted to the University of Ottawa in partial fulfilment of requirements for the Doctoral degree in Microbiology and Immunology

Department of Biochemistry, Microbiology and Immunology

Faculty of Medicine

University of Ottawa

© Kyle Malone, Ottawa, Canada, 2024

Abstract

The Inhibitor of Apoptosis (IAP) proteins promote cell survival and are at the nexus of multiple inflammatory pathways. Smac mimetic compounds (SMCs) are small molecule drugs that inhibit the IAPs, sensitize cancer cells to TNFα-induced cell death, and alter NF-κB signaling to provide immunostimulation. SMCs are currently under evaluation as therapeutic agents against a wide array of cancers. We have previously shown that SMC combination with immunotherapies durably cures up to 40% of syngeneic, orthotopic murine glioblastoma (GBM) models. GBM is the commonest and deadliest primary brain tumor, with near uniformly fatal prognoses and no significant changes to standard of care in decades. Given key roles of IAPs in gliomagenesis and GBM therapy resistance, optimizing SMC-based therapies for GBM has significant potential for improving outcomes for this fatal cancer. Here, I aimed to identify and exploit resistance mechanisms to SMC-based immunotherapies for GBM. I show that GBM cells sensitive to SMC-mediated cell death remain sensitive under a diverse array of microenvironmental conditions. I further show that the central nervous system location limits primary immune responses against GBM, and that the tumor-associated macrophage (TAM) population represents a significant source of potential death ligands for GBM eradication. I elucidate a key role for astrocytes and TGFβ in GBM and TAM resistance to SMC treatment and show increasing dose of SMC and TGFβ blockade significantly improve efficacy of SMC-based immunotherapies. Further evaluating precise timing, delivery methods and other immunosuppressive targets for blockade will establish SMCs as potent immunostimulants promoting anti-GBM immunity. Collectively, SMCs can potently remodel the GBM microenvironment and provide significant immunostimulation allowing for enhancement of anti-GBM immunotherapies, thereby producing substantial survival benefit for this highly resistant and fatal cancer.

Acknowledgments

I would like to thank Dr. Shawn Beug for the opportunity to contribute to the work being done in his lab. His expertise and openness to discussion fostered a phenomenal research environment where I was able to explore all my ridiculous ideas, affording me the space to learn and grow as a researcher. I would like to thank Dr. Eric LaCasse for constantly being available for discussion, for having the widest net I've ever witnessed regarding relevant papers, and for his invaluable knowledge on the IAPs and Smac mimetics. I would further like to thank Dr. Robert Korneluk for initially hiring me on as a student, for his tremendous insights on the IAPs, the never-ending roasts, and for including me in the after-work hockey which has become a highlight of my weeks. I also thank him for telling me I was the only person in the lab who looked better in a COVID mask. I owe my minimal infections to his influence. I thank Dr. Tommy Alain for including me in his Mitacs projects and for his constant openness to answer questions and guide the project. Similarly, I thank Dr. Subash Sad and Dr. Ian Lorimer for their guidance and expertise as members of my TAC committee.

I would like to thank Martine St-Jean for her endless patience in answering my stupid questions and for sharing her immense experience in helping me optimize all my lab work. Similarly, I would like to thank Allan Humphrey for his help in ensuring all my lab work was performed correctly, and for not losing his patience every time I texted him I'd forgotten my badge. I would especially like to thank Nathalie Earl for her help with the animal work. Without her only a fraction of the presented *in vivo* work would have been done, and my trips down to the animal care dungeon would have been immeasurably bleaker absent those hilarious podcasts and stories.

I would like to thank Melanie Dugas not only for being one of the most gifted researchers and problem solvers I've ever worked with, but also for breathing fresh enthusiasm into my project. The multiplex staining would not have been done even a fraction as well as it has been had she not joined the lab, and I know I would have long grown bored without her influence. You truly changed the lab and my project for the better. Another thank you to Elyn Rowe for sending me that book on managing burnout. The book and your example in persevering through insane circumstances were more help than I ever told you, and you're due the world in wins after the last few years.

To all the members of the CHEO community, thank you for keeping the institute such a fantastic place to work. Thank you Lynn Kyte for being invaluable to the research, and for always being available to chat when I seem to just pop up out of nowhere with some half-assed hockey take. Thank you Keith Wilson for being an endless source of positivity and your encyclopedic knowledge of the weirdest sayings I've ever heard. Thank you Jarred Lau for being one half of our Hillbilly voice-offs, and for organizing the football pools I definitely should have won (Pat Mahomes is useless). And thank you Noah Robert for taking the oddball pressure off by somehow being weirder than me (and also for being hilarious).

Finally and most importantly, I would like to thank Sufi Baba Budan, the first person to smuggle coffee out of the Middle East in 1670 by strapping beans to his chest, setting off an explosion in trade and ultimately allowing me the mental faculties to get any work done. Thank you Sufi you brilliant sneak, and apologies to Bob the Janitor for the coffee spills.

Table of Contents

List of Figures:

List of Tables:

List of Abbreviations

ABC – ATP binding cassette

AIF – apoptosis inducing factor

Akt – Protein kinase B

ALDH1A3 – aldehyde dehydrogenase 1A3

AMPK – 5' adenosine monophosphate-activated protein kinase

APC – antigen presenting cell OR allophycocyanin (fluorescent antibody conjugate)

AVPI – alanine valine proline isoleucine

BBB – blood brain barrier

BDNF – brain derived neurotrophic factor

BFGF – basic fibroblast growth factor

BIR – baculovirus IAP repeat

BMDM – bone marrow derived macrophages

C3c – complement 3c

CAR – chimeric antigen receptor

CCL2 – chemokine (C-C motif) ligand 2

CCR2 – C-C chemokine receptor 4

CD – cluster of differentiation

CDKN2A/B – cyclin dependent kinase inhibitor 2A

cIAP – cellular IAP

CK2 – protein kinase 2

CMV - cytalomegalovirus

CNS – central nervous system

CSF – cerebrospinal fluid

CSF1 – colony stimulating factor 1

CSF1R - colony stimulating factor 1 receptor

CTLA4 – Cytotoxic tumor lymphocyte antigen 4

CXCL10 – C-X-C motif chemokine ligand 10

CXCR4 – C-X-C motif chemokine receptor 4

CYLD – cylindromatosis/ CYLD lysine 63 deubiquitinase

c-FLIP – cellular FLIC-like inhibitory protein

DAMP – damage associated molecular pattern

DC – dendritic cell

DED – death effector domain

DIC2 – death inducing complex 2

DISC – death-inducing signaling complex

DMSO – dimethyl sulfoxide

DR – death receptor

EC – endothelial cell

ECM – extracellular matrix

EGF – epidermal growth factor

EGFR – epidermal growth factor receptor

ERK1/2 – extracellular signal-regulated kinase 1/2

FADD – fas-associated death domain

FCS/FBS – fetal calf/bovine serum

FDA – food and drug administration

FSC – forward scatter

GABA – gamma-aminobutyric acid

GABRA1 -gamma-aminobutyric acid type A receptor subunit alpha1

GBM – glioblastoma multiforme

GDNF – glial cell-derived neurotrophic factor

GFAP – glial fibrillary acidic protein

GFP – green fluorescent protein

GLUT3 – glucose transporter 3

GM-CSF – granulocyte-macrophage colony-stimulating factor

GSC – glioma/GBM stem cell

HA – hyaluronic acid

HER2 – human epidermal growth factor receptor 2/ receptor tyrosine-protein kinase erbB-2

HDHF – high dose high frequency

HDSF – high dose standard frequency

HIF-1α – hypoxia inducible factor-1 alpha

IAP – inhibitor of apoptosis protein

ICB – immune checkpoint blockade

ICV – intracerebroventricular

IDH – isocitrate dehydrogenase

IDO1 – indoleamine 2,3-dioxygenase 1

IFNγ – interferon gamma

IGF1 – insulin-like growth factor 1

IGF1R– insulin-like growth factor 1 receptor

IKK – inhibitor of nuclear factor kappa beta kinase

IL – Interleukin

IT – intratumoral, used in reference to injections/implants

IV - intravenous

JNK – c-jun N-terminal kinase

KLRG1 – killer cell lectin-like receptor G1

LAG3 – lymphocyte activated gene-3

LUBAC – linear ubiquitin chain assembly complex

MAPK – mitogen-activated protein kinase

MDSC - myeloid-derived suppressor cell

M-MDSC - monocytic myeloid-derived suppressor cell

MGMT – o^6-methylguanine DNA-methyltransferase

MHC - major histocompatibility complex

MLKL – mixed lineage kinase domain like pseudokinase

MMP - matrix metalloproteinase

MOMP - mitochondrial outer membrane permeabilization

MRI – magnetic resonance imaging

MT1-MMP – membrane type 1-matrix metalloproteinase

NEFL – neurofilament light polypeptide/chain

NF1 – neurofibromatosis type 1

NF-κB - nuclear factor kappa-light-chain-enhancer of activated B cells

NP - nanoparticle

NPC – neural progenitor cell

NSC – neural stem cell

OPC – oligodendrocyte progenitor cell

PAMP – pathogen associated molecular pattern

PARP – poly (ADP-ribose) polymerase

PD-1 – programmed death-1

PDGFRA1 – platelet-derived growth factor receptor A

PD-L1 – programmed death ligand-1

PEA-15 – phosphoprotein enriched in astrocytes -15

PIK3CA – phosphatidylinositol-4,5-bisphosphate 3-kinase catalytic subunit alpha

PIK3R1 – phosphoinositide-3-kinase regulatory subunit 1

PI3K – phosphoinositide 3-kinase

PTEN – phosphatase and tensin homolog

RING - really interesting new gene

RIPK1 – receptor interacting serine/threonine-protein kinase 1

RIPK3 – receptor interacting serine/threonine-protein kinase 3

RT - radiotherapy

RTK – receptor tyrosine kinases

SASP – senescence associated secretory phenotype

ScFv – short chain variable fragments

SDF-1α – stromal cell-derived factor 1alpha

SDSF – Standard dose standard frequency

SERPINA3 – serine (or cysteine) proteinase inhibitor, clade A, member 3

SHP-1 – src homology 2 domain-containing protein tyrosine phosphatases-1

siRNA – small interfering RNA

SLC12A5 – solute carrier family 12 member 5

Smac – second mitochondria-derived activator of caspases

SMC – smac mimetic compound

SSC – side scatter

STAT3 – signal transducer and activator of transcription 3

SVZ – subventricular zone

SYT1 – synaptotagmin 1

TAB2/3 – tgf-beta activated kinase 1 binding protein 2/3

TAK1 – tgf-beta activated kinase 1/mitogen-activated protein kinase kinase kinase 7

TAM – tumor-associated macrophage/microglia

TCR – T-cell receptor

TERT – telomerase reverse transcriptase

TGFβ – transforming growth factor β

TGFβR - transforming growth factor β receptor

Th – T-helper cell, usually Th1 or Th2

TIL – tumor-infiltrating lymphocyte

TIM3 – T-cell immunoglobulin and mucin domain containing protein-3

TLR – toll-like receptor

TME – tumor microenvironment

TMZ - temozolomide

TNFα – tumor necrosis factor alpha

TNFR1 – tumor necrosis factor receptor 1

TRADD – tumor necrosis factor receptor type 1-associated death domain protein

TRAF2/3 – tnf receptor associated factor 2/3

TRAF3IP2 – traf3 interacting protein 2

TRAIL – tnf-related apoptosis-inducing ligand

TRAILR – trail receptor

Treg – Regulatory T-cell

VEGF – vascular endothelial growth factor

VGF – VGF nerve growth factor inducible

WT - wildtype

XIAP – x-linked inhibitor of apoptosis

XAF1 – XIAP associated factor 1

1.0 Introduction

1.1 Cell Death, Inhibitor of Apoptosis Proteins and Smac Mimetic Compounds

1.1.1 Inhibitor of Apoptosis Proteins

The inhibitor of apoptosis (IAP) proteins represent a class of eight anti-apoptotic proteins defined by the presence of 1-3 baculovirus IAP repeat (BIR) domains at the N-terminus[1]. Aside from vital roles in cell survival, the IAPs are essential for proper immune function and are ubiquitously expressed in immune cells and lymphoid organs[2–4]. Deficiency or aberrant functioning of the IAPs is associated with numerous clinical presentations, most notably cancer. X-linked IAP (XIAP; BIRC4) deficiency presents with excess immune cell death in response to numerous stimuli resulting in immunodeficiency, with further impaired pattern recognition signaling contributing to heightened sensitivity to infection and frequent severe inflammatory bowel disease and splenomegaly[5,6]. Cellular IAP 1 and 2 (cIAP1/2; BIRC2/3) directly interact with and ubiquitinate receptor interacting protein kinase 1 (RIPK1) downstream of tumor necrosis factor receptor 1 (TNFR1) signaling, and thus also have vital roles in immune cell survival and proper functioning. Dysfunctional RIPK1 signaling is associated with increased susceptibility to infection, lymphopenia, and autoinflammatory diseases including TNFR-associated periodic syndrome[7,8]. The IAPs are therefore crucial to proper cell survival and immunity.

Some mammalian IAP family members also possess a really interesting new gene (RING) E3 ubiquitin ligase at the C-terminal. The actions of these two domains allow the IAPs, most notably cIAP1/2 and XIAP, to suppress apoptosis via direct caspase inhibition (via BIR domains and linker regions) and signal transduction through survival pathways (RING E3 ubiquitin ligase activity)[9]. Among said pathways, induction of nuclear factor –kappa beta (NF-κB) by tumour necrosis factor alpha (TNF-α) binding to its cognate receptor (TNFR1) requires the interaction of

cIAP1/2 with the NF-κB adaptor protein TNF receptor associated factor 2 (TRAF2) [10,11]. A series of ubiquitination steps[12,13] leads to the downstream activation of both mitogen activated protein kinase (MAPK) and NF-κB, with consequent upregulation of anti-apoptotic proteins (including Bad, Bax, BCL-2, Bid, cellular FADD-like IL-1β-converting enzyme inhibitory protein (c-FLIP), survivin, cIAP1/2 and XIAP[14]) and TNF-α for positive feedback[9,15,16].

XIAP is the most potent caspase inhibitor, capable of directly inhibiting Caspase-3, Caspase-7 (BIR2 domain and linker region) and Caspase-9 (BIR3 domain) at neoepitopes formed upon procaspase cleavage into activated caspases[17–19]. Second mitochondria-derived activator of caspases (Smac), released from the mitochondria during apoptosis, directly binds the BIR2 and BIR3 domains of XIAP and cIAP1/2 via an alanine-valine-proline-isoleucine (AVPI) tetrapeptide at its N-terminus[20,21]. In the case of XIAP, Smac binding at BIR3 directly interferes with its capacity to bind caspase-9, while also causing steric interference preventing caspase-3 and caspase-7 binding[22,23]. Smac binding to cIAP1/2 allosterically promotes autoubiquitination via RING E3 ubiquitin ligase activity, with consequent proteasomal degradation[24].

Survivin (BIRC5), another IAP family member, is also activated by NF-κB (and STAT3). While survivin has no enzymatic activity, it has key roles in mitosis and survival via actions as an adaptor protein. Its anti-apoptotic functions are through its binding to XIAP, wherein it can enhance caspase interactions, stabilize and enhance the actions of cIAP1/2[25,26], prevent Apaf1 release, and sequester Smac[27]. Survivin is also involved in the trafficking of the chromosomal passenger complex to centromeres during mitosis, a crucial step ensuring proper chromosomal alignment prior to segregation[28].

1.1.2 Mitochondrial apoptotic cascade

The intrinsic apoptotic pathway (Figure 1) is initiated by cytotoxic stimuli and results in mitochondrial outer membrane permeabilization (MOMP). This permeabilization is effected by the monomeric BCL-2 family proteins Bax and Bak. Upon exposure to an apoptotic signal, Bax translocates to the mitochondria; Bak is constitutively inserted in the mitochondrial outer membrane. Activation exposes their BH3 domain, which binds hydrophobic grooves in other Bax or Bak monomers. Subsequent oligomerization results in the formation of a pore in the outer mitochondrial membrane[29–31]. This allows for release of cytochrome C, Smac, Htra serine peptidase 2 (Htra2), endonuclease G, and apoptosis-inducing factor (AIF) into the cytosol[32,33]. Htra2 acts similar to Smac in its IAP inhibitory capabilities, and at high concentrations is able to induce a serine protease-dependent cell death that does not engage caspases[34]. XIAP-associated factor 1 (XAF1) interacts with XIAP to prevent its caspase inhibitory functions, seemingly without need for an activation signal[35]. As a result of these actions, the inhibitory effect of the IAPs is removed and apoptosis can proceed. For most cells, release of cytochrome C (and Smac) represents the point at which the apoptotic cascade becomes irreversible[36,37]. Cytosolic apoptotic protease activating factor-1 (Apaf-1) is then activated via cytochrome C binding to its C-terminal WD-40 repeats, and seven Apaf-1/cytochrome C complexes oligomerize through caspase recruitment domain (CARD) and nucleotide-binding and oligomerization domain (NOD) conjugation to form the apoptosome[38–41]. The CARD domains of seven procaspase-9 zymogen monomers bind the CARD domains of the apoptosome[40], resulting in cleavage and activation of caspase-9. This activated complex in turn cleaves and activates the effector caspases-3 and -7[42,43], which subsequently cleave their targets (most notably poly-ADP ribose polymerase; PARP, enzymes critically involved in DNA repair)[44,45] and effect apoptosis.

Regulation of MOMP is achieved through expression of other pro- and anti-apoptotic BCL-2 family members. Anti-apoptotic members, which include BCL-2, BCL-xL, BCL-w, and MCL-1, can bind and sequester Bax and Bak[46,47], preventing MOMP. Pro-apoptotic BH3-only proteins (Bim, Bid, Puma, Bad, Noxa, Bmf, Blk, and Hrk) can bind and inactivate these anti-apoptotic proteins and, in the case of Bid, Bim and Puma, directly bind and activate Bax and Bak[48–51]. Genetic knockout of anti-apoptotic BCL-2 proteins has revealed that Bax and Bak spontaneously activate and oligomerize, with the outer mitochondrial membrane itself sufficient to trigger Bax/Bak activation; BCL-2 family members prevent this tendency[52].

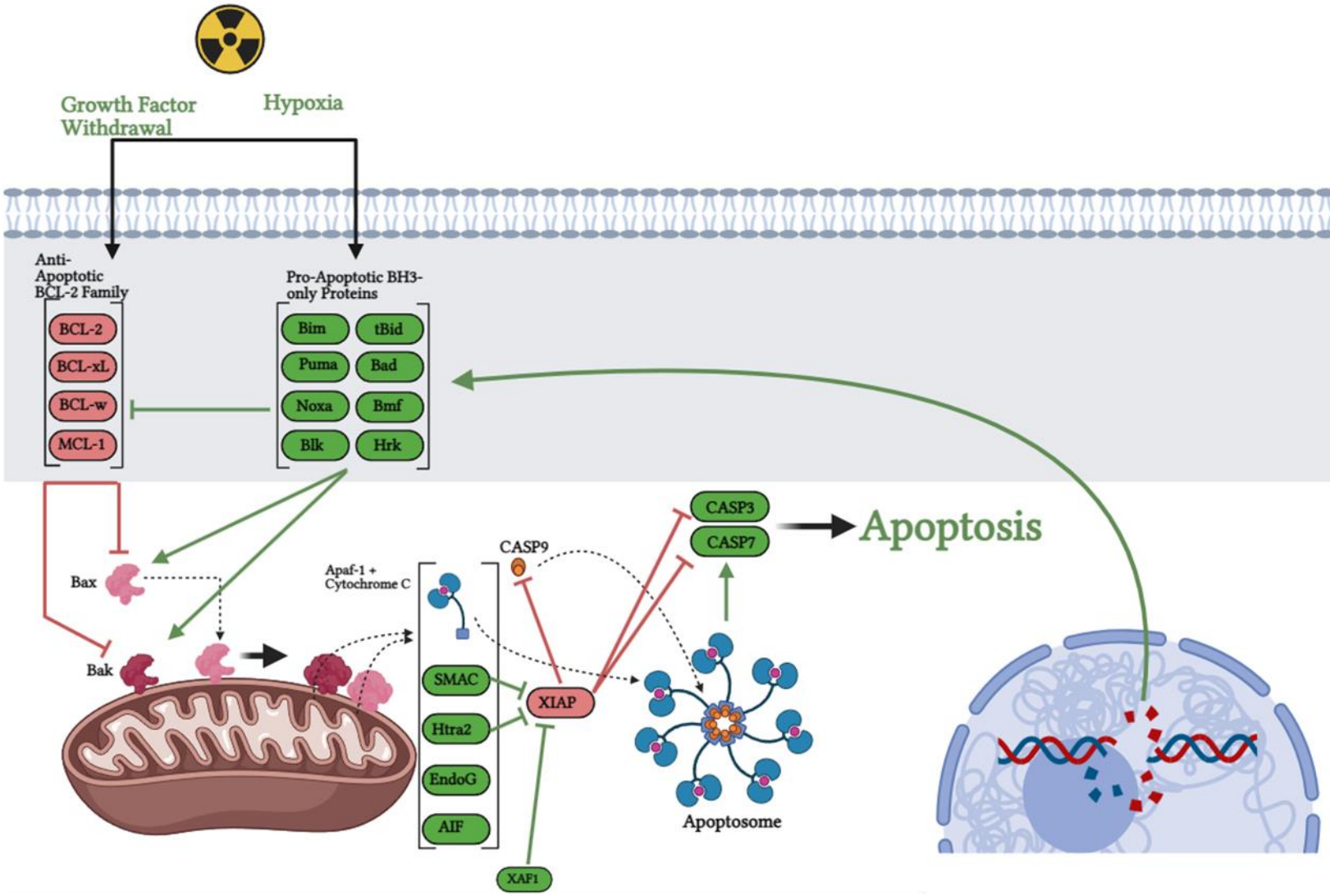

Figure 1: Intrinsic apoptotic pathway. DNA damaging agents including chemotherapy and radiation induce expression of pro-apoptotic BH3-only proteins, exceeding the balance with anti-apoptotic BCL-2 family proteins and permitting Bax and Bak oligomerization in the mitochondrial outer membrane. This outer membrane is consequently permeabilized, allowing release of pro-apoptotic factors including Apaf-1 and cytochrome C, which form the apoptosome with Caspase-9 and cleave downstream effector Caspases-3 and -7. Smac release from the mitochondria inhibits XIAP, a crucial step in permitting apoptosis. Figure was generated in BioRender.

1.1.3 Death receptor apoptotic cascade and necroptosis

The extrinsic apoptotic pathway (Figure 2) is initiated by engagement of TNFR superfamily death receptors. Such receptors include Fas, TNF-related apoptosis inducing ligand receptor 1/2 (TRAILR1/2, also referred to as Death Receptor 4/5 (DR4/5) respectively), and, if cIAP1/2 are absent or inhibited, TNFR1. These receptors are characterized by cytoplasmic death domains (DD). Fas trimerizes upon FasL binding, resulting in the recruitment of the adaptor protein Fas-associated protein with death domain (FADD), binding to Fas via its own DD. FADD in turn recruits procaspase-8 through death effector domain (DED) interactions, forming the death inducing signaling complex (DISC). The multiple procaspase-8s recruited to the DISC then undergo two autocatalytic cleavages, setting off the caspase cascade and consequently apoptosis[53–57]. Caspase-8 can also cleave Bid to truncated Bid (tBid), allowing for further Bax/Bak activation and concurrent initiation of the mitochondrial apoptosis pathway[58]. TRAILR1/2 (DR4/5) engagement similarly results in apoptosis through receptor trimerization, DISC formation, and caspase cascade initiation[59], although cancer cells appear most susceptible to TRAIL-induced cell death[60].

Under homeostatic conditions, TNF-α binding to TNFR1 recruits the adaptor protein TNFR1-associated death domain (TRADD) via DD interactions, as well as RIPK1[61]. TRADD subsequently recruits TRAF2/3[62], which recruits and interacts with cIAP1/2 BIR1 domains[63]. cIAP1/2 then act as E3 ubiquitin ligases to K63 polyubiquitinate RIPK1[64], forming the RIPK1 signalsome and serving as a scaffold for the formation of further signaling complexes. Linear ubiquitin chain assembly complex (LUBAC), an E3 ubiquitin ligase that generates Met1 (M1) ubiquitin chains to stabilize the signalsome, is then recruited[65]. A TGF-beta activated kinase 1 (TAK1) binding protein 2/3 (TAB2/3)-TAK1 complex binds to the K63 ubiquitin chains on

RIPK1 via their zinc finger domains[66]. The TAK1-TAB2/3 complex phosphorylates and activates inhibitor of kappa beta (IκB) kinase (IKK) complex, which in turn tags IκBα for proteasomal degradation. IκBα sequesters p50-p65 (NF-κB) in the cytoplasm, and its degradation allows for NF-κB to translocate to the nucleus and promote expression of target genes[66,67], including the aforementioned survival factors.

A key component informing IAP-targeted cancer immunotherapies is that the presence or absence of cIAP1/2 determines whether TNFR1 signaling is a cell survival or cell death signal. In the absence of RIPK1 ubiquitination by cIAP1/2, TRADD interacts with FADD through their DDs, and FADD recruits and activates procaspase-8, forming the death inducing complex 2 (DIC2) and effecting downstream apoptosis[68]. The presence/absence or inhibitory status of Caspase-8 determines the mode of cell death, as Caspase-8 protease activity can cleave RIPK1, RIPK3, and cyclindromatosis (CYLD), preventing the formation of the necrosome[69–71]. Inhibition or absence of caspase-8 upon death receptor engagement can result in a form of regulated necrosis called necroptosis[72]. Without Caspase-8, CYLD deubiquitinates RIPK1, which then recruits and interacts with RIPK3 via their RIP homotypic interaction motifs. Activated RIPK3 (which can trigger necroptosis by itself when overexpressed[73]) phosphorylates mixed lineage kinase domain-like pseudokinase (MLKL), which results in exposure of a 4-helix bundle at the N-terminus. This RIPK1-RIPK3-MLKL complex is the necrosome. Activated MLKL oligomerizes, interacts with phosphatidylinositol phosphates at the plasma membrane, and creates membrane pores leading to substantial ion flux, release of inflammatory damage associated molecular patterns (DAMPs), and necrotic cell death[73–76].

Aside from cIAP1/2 action as a switch between cell survival and cell death in TNF-α signaling, regulation of the extrinsic apoptotic pathway is primarily achieved through the actions of cFLIP

and XIAP. The two major cFLIP isoforms, long and short ($cFLIP_L$ and $cFLIP_s$) contain two N-terminal DEDs and structurally resemble caspase-8. Both isoforms bind FADD through DED interactions and prevent caspase-8 DIC2 or DISC recruitment and activation, thereby inhibiting apoptosis. $cFLIP_L$ cleavage products activate cell survival (Akt, JNK, Wnt, NF-κB) and proliferation pathways through its C-terminal caspase-like domain, which allows for TRAF2 and RIPK1 binding[77–79]. Upregulation of cFLIP represents a major strategy used by cancer cells to resist TRAIL-induced apoptosis. The direct caspase-inhibitory effects of XIAP also determine whether extrinsic apoptosis is type 1 or type 2. Type 1 cells die through the caspase cascade initiated by procaspase-8 processing and activation, while type 2 cells require the further cleavage of Bid to tBid by caspase-8 and engagement of the mitochondrial apoptotic pathway. This is due to altered ratios between effector caspases and XIAP, with cells possessing high XIAP showing compensatory increases upon exposure to death ligands, requiring mitochondrial smac release and IAP inhibition to effect apoptosis[80,81].

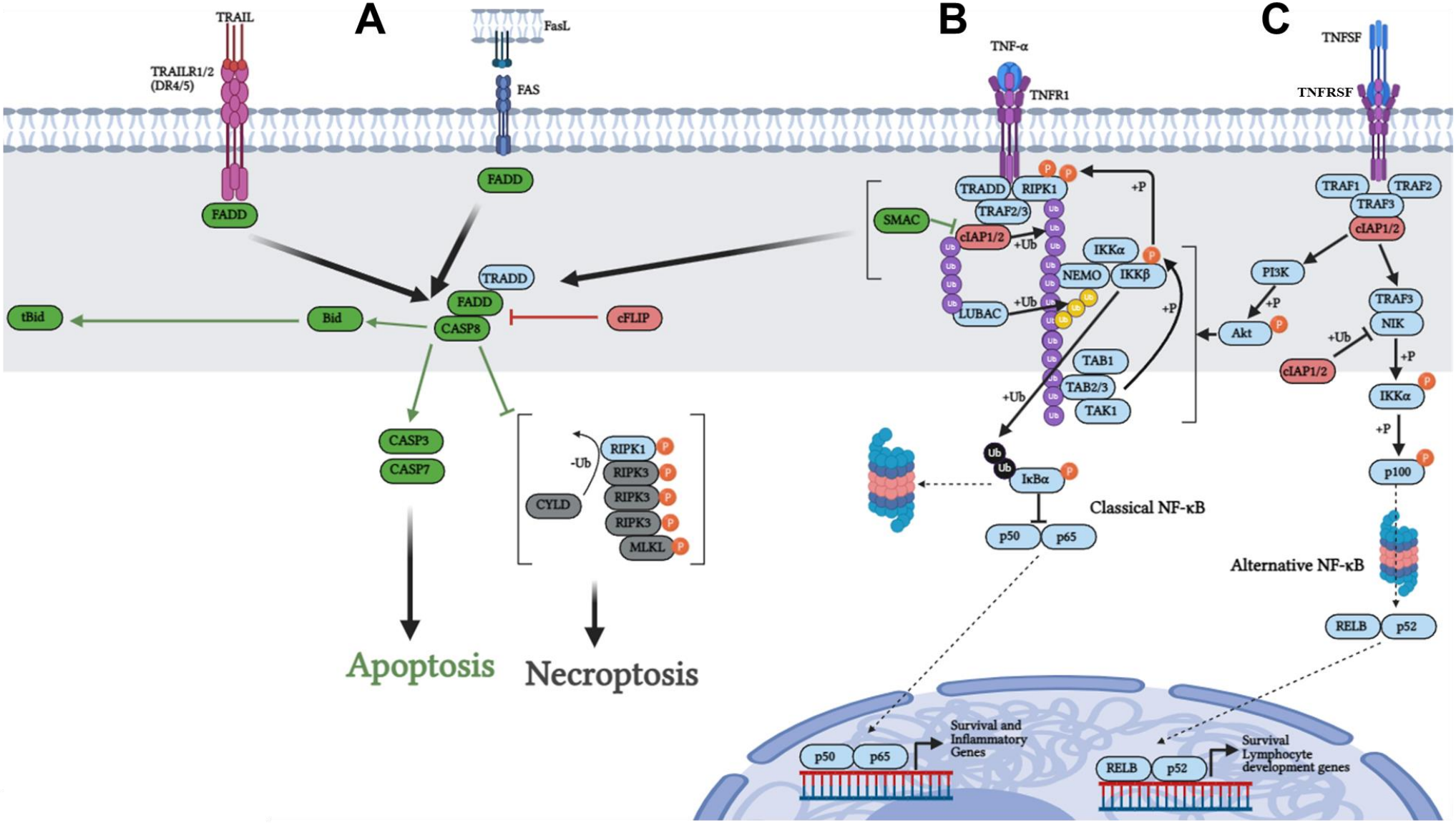
A
TRAIL
TRAILR1/2
(DR4/5)
FADD
FasL
FAS
FADD
TRADD
FADD
CASP8
tBid
Bid
cFLIP
CASP3
CASP7
RIPK1
RIPK3
RIPK3
RIPK3
MLKL
-Ub
CYLD
Apoptosis
Necroptosis
B
TNF-α
TNFR1
TRADD
RIPK1
TRAF2/3
SMAC
cIAP1/2
+Ub
IKKα
NEMO
IKKβ
LUBAC
+Ub
+P
TAB1
TAB2/3
TAK1
+Ub
Ub
Ub
IκBα
p50
p65
Classical NF-κB
C
TNFSF
TNFRSF
TRAF1
TRAF2
TRAF3
cIAP1/2
PI3K
+P
Akt
TRAF3
NIK
+Ub
cIAP1/2
+P
IKKα
+P
p100
Alternative NF-κB
RELB
p52
p50
p65
Survival and
Inflammatory
Genes
RELB
p52
Survival
Lymphocyte
development genes

Figure 2: Death receptor apoptotic pathway. A) Engagement of TNFR superfamily death receptors (DR4/5, Fas, TNFR1) by their ligands (TRAIL, FasL, TNFα) leads to FADD recruitment. FADD in turn recruits multiple procaspase-8s, forming the DISC. Procaspase-8 cleavage to activated Caspase-8 leads to cleavage and activation of Caspases-3 and -7, effecting apoptosis, and Bid cleavage to tBid, engaging the mitochondrial pathway. cFLIP binding FADD inhibits subsequent procaspase-8 binding and DISC or DIC2 formation. B) In TNFR1 signaling, TRADD and RIPK1 are initially recruited following TNFα binding. TRAF2/3 is subsequently recruited, and in turn recruits cIAP1/2 which ubiquitinate RIPK1. This ubiquitinated RIPK1 represents a scaffold for downstream signaling to activate IKK to degrade IκBα, permitting NF-κB activation. In the absence of cIAP1/2, lack of RIPK1 ubiquitination results in TRADD recruitment of FADD and formation of the DIC2. Engagement of death receptors in the absence of Caspase-8 results in RIPK1-RIPK3-MLKL dependent necroptosis. C) TNF superfamily members (ex. 4-1BB, OX40) binding their cognate receptors can initiate the 'Classical' or 'Alternative' NF-κB signaling pathway, wherein cIAP1/2 ubiquitination of NF-κB inducing kinase (NIK) leads to its degradation and signaling via p65 (RelA)-mediated 'Classical' NF-κB. Loss of cIAP1/2 via Smac or SMC binding frees NIK to permit signaling through 'Alternative' NF-κB mediated by RelB. Figure was generated in BioRender.

1.1.4 SMCs as cancer therapeutics

Smac mimetic compounds (SMCs) were developed to mimic the IAP binding AVPI tetrapeptide of endogenous Smac to suppress the ability of XIAP to block caspase activity. SMCs have since been found to have the highest affinity for cIAP1/2, with treatment resulting in altered NF-κB signaling towards NIK-mediated 'Alternative' NF-κB (Figure ii) and consequent immunomodulation, sensitizing a diverse array of cancer cells to inflammatory cytokine-induced cell death[15,82–90]. LCL161, a monomeric SMC used in all experiments herein, has an IC_{50} of 35nM and 0,4nM for XIAP and cIAP1, respectively[91]. Given the extensive roles of both classical and alternative NF-κB in immunity[92–95] and the vital roles of the IAPs in that signaling, it is unsurprising the SMCs have significant inflammatory effects and impact multiple steps of the cancer immunity cycle (Figure iii). These include: induction of TNFα and IFNγ expression by macrophages; induction of inflammatory macrophage phenotypes and type I interferon signaling; CD40 agonism and increased macrophage and dendritic cell (DC) phagocytosis; increased T-cell co-stimulatory signaling; reduced regulatory T-cell (Treg) differentiation and programmed death-1 (PD-1) expression; and induction of chemokine expression improving immune cell trafficking[96]. Given these substantial pro-inflammatory effects and the ability to sensitize cancer cells to apoptosis through many signaling molecules used by immune cells (TRAIL, FasL, TNFα), SMCs have demonstrated potent anti-cancer properties and have produced promising preclinical results in a variety of different cancer models. SMCs are only effective as single agents for cancers producing high levels of TNFα. Combination with innate immune stimuli inducing significant pro-inflammatory cytokine expression within the TME allows for substantial SMC-mediated killing even in the absence of tumor-derived TNFα[97]. There are therefore

numerous clinical trials underway exploring different SMC formulations and immunotherapeutic combinations for treatment of diverse solid and liquid tumors[98].

In a GBM context, SMC targeting of XIAP and cIAP1/2 sensitizes GBM cells to temozolomide (TMZ) and radiotherapy[99–103]. Aside from canonical SMC targets XIAP and cIAP1/2, targeting survivin (BIRC5) using YM155 results in significant reduction in U87 and U251 human GBM cell viability, proliferation and migration and sensitizes to further radiation-induced DNA damage *in vitro* and, following direct intratumoral (IT) injection, significantly enhances mouse survival *in vivo* in combination with RT[104].

1.2 Overview of Glioblastoma Multiforme

1.2.1 Incidence, prognosis, current treatment regimens

GBM is the most common and lethal tumor of glial origin. It is seen in greatest proportions in patients 50-80 years old, with no significant differences in occurrence between lobes of the brain[105]. GBM incidence rates are increasing[106,107], with few known risk factors and a median overall survival of 16-21 months, making it one of the deadliest malignancies. This prognosis has shown minimal improvements in decades despite significant research effort in understanding its biological underpinnings, substantial clinical trials of novel therapeutics, and the highest treatment cost per-patient of any cancer in the United States[107–110].

Current treatment for GBM (colloquially referred to as the Stupp Protocol) consists of maximal surgical resection, followed by RT (total 60 Gy) with concurrent TMZ chemotherapy (75 mg/m^2 per day for entire RT course), then adjuvant TMZ treatments (150 to 200mg/m^2 across two 28-day cycles)[111]. TMZ is an oral DNA methylating agent that readily crosses the blood-brain barrier (BBB) and is intracellularly converted into its active form to methylate nucleobases,

especially guanine residues[112]. Methylation of guanine damages DNA, interferes with replication and activates cell death processes if not repaired. Repair depends on pre-existing amount, synthesis rate and activation status of methylguanine DNA methyltransferase (MGMT), which directly removes O^6-methylguanine lesions via transfer to an active site cysteine residue, permanently inactivating that MGMT polypeptide. Thus, subsequent lesions require further synthesis of new MGMT, creating a vulnerability wherein repair capacity can be overwhelmed. Other main TMZ lesions (N^3-methyladenine and N^7-methylguanine) are removed by base excision repair mechanisms[113,114]. Interestingly, smaller slow-growing tumors respond poorer than larger fast growing ones, with lower median survival[115]. MGMT levels are low in brain relative to breast tumors[114], and MGMT promoter methylation is a common feature of GBM, with methylated tumors responding significantly better to TMZ treatments than unmethylated[116].

1.2.2 Disease Subtypes

World Health Organization (WHO) classifications based on histological, morphological and genetic features classified GBM into isocitrate dehydrogenase (IDH) wildtype (IDH^{WT}) or IDH-mutant (IDH^{Mut}) subtypes, based on mutation status of IDH1 or IDH2. The IDH^{WT} group is significantly more commonly diagnosed and tends to have low levels of MGMT promoter methylation, epidermal growth factor receptor (EGFR) amplification (associated with chromosome 7 gains), *PTEN* mutations (associated with chromosome 10 loss), as well as *CDKN2A/B, PDGFRA1, NF1* and *tp53* mutations. IDH^{Mut} GBM are also associated with tp53 mutations and chromosome 10 and *CDKN2A/B* losses, with nearly all bearing MGMT promoter methylations, significantly earlier age of onset and longer median overall survival[117].

Verhaak *et al*.[118] identified four GBM subtypes based on gene expression profiles in the Cancer Genome Atlas Network: Classical, associated with EGFR amplifications and EGFRvIII

mutations, *CDKN2A* deletions and lack of *tp53, NF1, PDGFRA* or *IDH1* mutations; Mesenchymal, associated with deletion of *NF1*, *PTEN* mutations, and high NF-κB, TNF superfamily, CD44, and MERTK expression; Proneural, associated with *PDGFRA* amplification, IDH1 point mutations, frequent tp53 mutations, and high oligodendrocyte development gene program expression; and Neural, with high similarity to normal brain and expression of neuron markers *SLC12A5, GABRA1, SYT1*, and *NEFL*. Consistent with substantial disease heterogeneity, a single tumor can possess characteristics of several subtypes. Among these, treatment shows enhanced survival in classical and mesenchymal, with little to no efficacy in neural and proneural[118].

1.2.3 Disease Heterogeneity and Glioma Stem Cell Concept

GBMs are characterized by substantial inter- and intratumoral heterogeneity. Within a tumor, heterogeneity exists spatially between hypoxic and inflammatory regions; transformed versions of oligodendrocyte progenitor cells (OPCs), radial glia, and neural progenitor cells (NPCs/NSCs) coexist along reactivity gradients depending on regional differences in metabolic and inflammatory molecules[119,120]. Despite this intra- and intertumoral heterogeneity, the combined deregulation of receptor tyrosine kinase (RTK)-Ras-PI3k, p53 and retinoblastoma (Rb) pathways are seen in nearly all GBMs, and are considered potential core requirements for GBM pathogenesis[121]. TMZ treatment selects for mismatch repair deficient hypermutated clones resistant to further therapy[121]. NF-κB is also constitutively active in many gliomas, downstream of which are numerous stemness, pro-survival and inflammatory genes[122]. Consistent with a central role for this pathway in many aspects of GBM biology, blocking TRAF3IP2, an upstream regulator of NF-κB, significantly reduces GBM proliferation, sphere forming capacity, tumor

size, angiogenesis, matrix metalloproteinase (MMP) expression and consequently invasive capacity, and expression of inflammatory cytokines (including TNF-α)[123].

Amplification of RTKs (EGFR and PDGFR, chief among them), coupled with constitutive PI3K-AkT signaling resulting from PTEN inactivation and mutations in PIK3CA and PIK3R1, overcome normal mitogenic controls and contribute to substantial apoptotic resistance[121,124]. EGFR amplification occurs in nearly half of all GBMs[125,126], and deletion of exons 2-7 coding for the EGF binding site (EGFRvIII) confer constitutive activation even in the absence of ligand binding[127]. This mutation occurs in nearly 25% of GBMs[128], with some figures as high as 50%[129]. PI3K-Akt signaling is consequently increased[130], with increases in anti-apoptotic BCL-2 family member expression and proliferation[131,132], contributing to enhanced survival and treatment resistance[133,134]. Impact on median overall survival is not clear and may differ based on age[128,135], although high EGFR expression tends to correlate with poorer prognosis[136]. Tyrosine kinase inhibitors are relatively ineffective for GBM given numerous RTKs are amplified and the BBB limits access of both chemical inhibitors and blocking antibodies[137].

GBM stem cells (GSCs) are thought to represent the proliferative cell of origin of the tumor, retaining tumor initiation capacity and coexisting with more differentiated GBM cells[138,139]. Cellular hierarchies of GSCs, intermediate progenitors and more differentiated, lineage restricted GBM cells exist within a tumor. More differentiated cells can dedifferentiate to a GSC based on treatment, with TMZ selecting for GSCs, or due to microenvironment pressures. As such, different anatomical regions within the same tumor can be classed as different subtypes[140]. Indeed, several distinct subtypes have been identified based on unique gene expression profiles. Tumors resulting from proneural and mesenchymal GSCs differ in tumor growth rate, DNA repair capacity, metabolism and extent of angiogenesis and necrosis. Within a single tumor,

proneural and mesenchymal GSCs can coexist and treatment allows for interconversion between subtypes[141]. Proneural and mesenchymal GSCs have different tumorigenicities, proliferation rates, invasive patterns, histologic features and survival times[141,142]. GSCs within a tumor exist along a gradient of transcriptional states akin to those seen in normal neurodevelopment and in neuroinflammatory wound responses[143]. GSCs can also switch between glycolytic and oxidative metabolic mechanisms depending on microenvironmental constraints, allowing GSCs to survive in most compartments within a tumor[144]. Patient-to-patient heterogeneity also exists in responses of GSCs to hypoxic and inflammatory stimuli[145]. CD44 has key roles in GSC self-renewal and consequent poor prognosis[146], and along with CD133 represent the canonical GSC markers. Individual patient derived GSC lines show unique proportions of CD44 and CD133-expressing subpopulations. Treatment increases CD44+ and double positive GSC proportions[142], with aldehyde dehydrogenase 1A3 (ALDH1A3)-induced NF-κB signaling driving much of this 'proneural to mesenchymal transition'[147] and consequent increases in invasiveness and treatment resistance[148].

Cues that would normally differentiate NSCs do not terminally differentiate GSCs, with partially differentiated progeny uniquely able to dedifferentiate back to the GSC state as a result of substantial changes to the GSC DNA methylation landscape[149]. Further, GSC-derived hyaluronic acid (HA) acts in autocrine and paracrine fashions following exposure to differentiation cues, signaling through upregulated TLR4 to activate NF-κB and promoting proliferation and evasion of senescence or terminal differentiation[150]. In the normal CNS, HA is involved in NSC self-renewal and maturation. In GBM, high HA (and its receptor CD44) is associated with increased proliferation and invasiveness through PI3K-Akt and Ras/MAPK increases in MMP-2 and -9 expression, allowing for HA to signal for its own degradation in order to facilitate migration

through ECM[151]. Jagged1-Notch-NF-κB signaling is substantial in GSCs, with high Jagged1 expression correlating with poor prognosis and increased GSC invasiveness[152].

GSCs have key roles in GBM invasion, angiogenesis and recurrence[153]. Within a tumor they occur in highly proliferative, hypoxic, cell dense areas of necrosis near the core of the tumor[154,155], and are major resistance factors for chemoradiotherapy[156] due to higher expression of drug efflux transporters and MGMT, XIAP, cIAP1/2 and survivin relative to their more differentiated counterparts[154,157], as well as high Notch signaling and quiescence[158]. GSCs inhabit protective niches that maintain their stemness properties, wherein they coexist with immune, CNS and blood vessel cells primarily around hypoxic and necrotic regions, with bidirectional signaling between cell types maintaining GSC stemness. GSCs remain in their niches due to CD44-osteopontin and CXCR4-SDF-1α signaling, and disruption of these interactions causes differentiation and induces sensitivity to chemoradiotherapy[158,159]. GSCs migrate towards areas of hypoxia and necrosis, even when experimentally injected into normal contralateral hemisphere[145]. Tumor vasculature is often structurally and functionally abnormal. In part this is due to GSCs in perivascular niches differentiating into pericytes in the presence of TGFβ, both within tumor and in peritumoral brain. These pericytes have abnormal morphology and function but allow for increased tumor vessel supply at the cost of BBB maintenance[160]. In the absence of interactions with more differentiated GBM cells, tumor forming potential and proliferation of GSCs are significantly reduced. This is likely due to BDNF, as differentiated cells express significant BDNF and GSCs express high levels of the BDNF receptor TrkB. BDNF signaling through PI3k-Akt induces GSC secretion of VGF, acting in paracrine and autocrine fashions to enhance differentiated cell survival and promote GSC self-renewal and stemness[161].

1.2.4 Cell death in GBM

High, unregulated PI3K-Akt signaling results in significant alterations to mitochondrial apoptotic cascade members. Apaf-1 and procaspase-9 are expressed at significantly lower levels in GBM relative to HeLa cells. TMZ-sensitive GBM cell lines show significantly higher expression of procaspase-3 compared to TMZ-resistant cells. High procaspase-3 levels were associated with longer progression-free survival times; Apaf-1, Smac or XIAP showed no such correlation[162]. While expression of Apaf-1 and procaspase-9 may be low, they are expressed, and GBM cells should therefore still be sensitive to strong enough apoptotic triggers. The pro-apoptotic BH3-only protein Bad is phosphorylated and inactivated by Akt[163], freeing BCL-2 and BCL-xL to inhibit further apoptotic signaling. Procaspase-9 is also phosphorylated and inhibited by Akt. In many cancers, overactivation of Akt results in resistance to numerous apoptotic stimuli[164]. Reintroduction of PTEN via adenoassociated virus application results in reduced viability and proliferation in several human GBM lines[165]. High NF-κB activation via Akt phosphorylation of IKKα results in transcription of multiple anti-apoptotic genes, including BCL-2 family members, cIAP1/2, XIAP and survivin. Inhibition of Akt via induction of PTEN expression or chemical inhibition of PI3K results in significant decreases in NF-κB activity[164,166–168]. Overactivated Notch signaling is a common feature of GBMs, and crosstalk with the Akt pathway further promotes apoptosis resistance[169,170]. EGFRvIII overexpression correlates with increased expression of anti-apoptotic BCL-2 family members[171], which are overexpressed in GBMs relative to normal brain[172] and especially high in GSCs[173], which also show high levels of survivin[174]. Conversely, Bax levels are significantly reduced, consistent with p53 mutations[172].

Interestingly, almost all human GBM cell lines express the full extrinsic apoptotic[175,176] and necroptotic machinery[177]. High caspase-8 expression was associated with worse survival. Sublethal actions of caspase-8 contributed to tumour growth, angiogenesis, and cytokine

secretion via alterations to NF-κB signaling and nuclear localization. Further roles of caspase-8 have been found in migration and metastasis through enhancing the activity of Calpain[178]. TNF-α acts as a growth factor for GBM cells; TNF-α neutralization or gene inhibition substantially reduces U251 GBM proliferation[179]. TNFR1 is highly expressed in GBM relative to low grade gliomas and healthy brain tissue[180] and represents the major mechanism of NF-κB activation in GBM along with Akt[181]. Almost half of the commonly used human GBM cell lines are sensitive to TNF-α-induced cell death following cIAP1/2 blockade using SMCs[97,182]; cFLIP represents the major mechanism of *in vitro* resistance in the remaining lines. While cFLIP is relatively homogeneously expressed among human GBM lines, differential effects of SMCs on JNK-ITCH induced cFLIP degradation account for variation in sensitivity[176]. Inhibition of TNF, JNK and/or ERK signaling sensitizes GBM cells to EGFR inhibition, both *in vitro* and *in vivo*[183,184].

Most human GBM cell lines are resistant to TRAIL-induced apoptosis, with DR5 (but minimal DR4) expression[175], yet both at substantially higher levels than seen in astrocytes[185,186]. Expression of DR5 has been found to correlate with survival but not glioma grade[187]. U87 human GBM cells respond to SMC and TRAIL cotherapy *in vivo*[188]. Arsenic trioxide increases DR5 expression and sensitizes GBM cells to TRAIL without affecting cFLIP or Akt[189]; other agents acting to similarly increase DR4/5 also sensitize GBM cells to TRAIL[190]. Reduced NF-κB signaling and consequent cFLIP reductions enhance TRAIL-induced apoptosis[191]. Radiation induces soluble TRAIL expression and secretion by U87 GBM cells, as well as modest increases in DR5[192]. U87 and U251 GBM cells are sensitive to irradiation and/or TRAIL-induced, caspase-8-mediated apoptosis. Isolated GSCs from these cell lines are significantly more resistant to either and express significantly lower levels of DR5 and caspase-8[193]. Combination TRAIL and compound C (an AMPK inhibitor) significantly reduced U87 and U138 GBM cell BCL-2, XIAP

and cFLIP levels and increased BAX expression, with consequent increases in cleaved caspase-3 and PARP. *In vivo*, combined SMC and compound C treatment severely hindered tumour growth[194]. cFLIP is cleaved to its active form in TRAIL resistant GBM cell lines but not in sensitive ones[195].

1.2.5 IAPs in GBM

XIAP and survivin have been extensively studied for their roles in GBM biology and treatment resistance. Both proteins are expressed at significantly higher levels in GBM than normal astrocytes[189], although XIAP at lower levels compared to bulk brain tissue[196]. XIAP knockdown in multiple GBM cell lines sensitizes them to resveratrol, vincristine and doxorubicin-induced cell death[197], illustrating a crucial role of XIAP in GBM chemoresistance and that despite significant inhibition the intrinsic apoptotic cascade remains functional and targetable. Similar experiments using shRNA knockdowns of survivin in GBM cell lines demonstrate increased apoptosis and reduced proliferation characterized by mitotic catastrophe[198]. Survivin also plays roles in GBM resistance to RT[199] and high expression is associated with a more aggressive phenotype[200]. YM155, a small molecule survivin inhibitor, substantially reduces viability of U87 and U251 human GBM cells, impairs homologous recombination, reverses epithelial to mesenchymal transition (and consequently reduces migration), reduces STAT3 activation, and potently sensitizes to radiation[201–203]. Survivin inhibition synergizes with the BH3-only protein mimetic ABT-737 to induce apoptosis through the mitochondrial cascade in numerous human GBM cell lines. As EGFR signaling through PI3K-Akt regulates survivin expression, U87 cells with upregulated EGFR or bearing the EGFRvIII mutation exhibited enhanced protection against this cotreatment; EGFR inhibition enhanced sensitivity[204]. In keeping with high survivin expression, SurVaxM, an immunogenic, modified version of survivin, has been used to vaccinate

against GL261 murine GBM, producing potent $CD8^+$ T-cell responses and significantly improved overall mouse survival[205]. This survivin-targeted vaccine strategy also shows promising clinical results[206].

Heterogeneous expression of cIAP1, cIAP2 and XIAP are seen in human GBMs. Long-term IAP inhibition using intravenous (IV) SMC administrations resulted in dose-dependent long-term survival of mice bearing U87 human GBMs[207], and IAP inhibitors could trigger differentiation of more resistant GSCs under normoxic conditions. Further, while hypoxia had no significant effect on IAP levels, SMC treatment was more effective, resulting in decreased proliferation, increased apoptosis and little to no differentiation, regardless of GSC subtype[208]. The majority of immortalized human GBM cell lines are sensitive to TMZ, with further sensitization achieved via IAP blockade using dimeric SMC birinapant. Primary GBM cells tend to be more resistant, showing heterogeneous responses to IAP blockade and/or TMZ treatment[209]. High cIAP2 (BIRC3) is associated with significantly poorer prognosis. cIAP2 levels increase dose-dependently following standard treatments (RT and TMZ), and recurrent tumours showed significantly higher levels than primary. Survivin was found to be increased upon recurrence, and XIAP upon RT; both of these IAPs are able to stabilize cIAP2 directly or indirectly. These BIRC3 responses to treatment and in recurrence were found to be due to differences in PI3K and STAT3 signaling[210]. Other groups have made similar findings using TCGA analysis, confirming a central role of cIAP2 in GBM prognosis and progression[196].

cIAP2 is significantly increased during gliomagenesis. Direct binding of XIAP to cIAP2 through its RING domain is required for XIAP stabilization of cIAP2, and this stabilizing effect may explain the slower kinetics of SMC cIAP2 degradation relative to cIAP1[211]. High levels of hypoxia and necrosis are associated with mesenchymal phenotype, aggressive disease and poor

survival; cIAP2 is found at the highest levels in mesenchymal GBMs. NF-κB signaling mediates the mesenchymal transformation as well as cIAP2 expression. Hypoxia also increases cIAP2 expression, with hypoxia inducible factor-1α (HIF-1α) binding the BIRC3 promoter; cIAP2 inhibition of caspase activation subsequently promotes survival under hypoxic conditions and upon exposure to RT[212]. Increases in cIAP2 during hypoxia depend on concurrent increases in XIAP. TNF-α also specifically increases cIAP2 in GBM cells[211]. Between low grade glioma and GBM, only BIRC3 and BIRC4 showed significant upregulation. In low grade glioma, high cIAP1/2 were associated with poor survival, while only cIAP2 had prognostic value in GBM. BIRC3 was found to promote malignant progression[213].

1.2.6 CNS Cells in GBM biology

Cell of origin for GBM has not been firmly established, however recent studies have identified subventricular zone (SVZ) NSCs as likely candidates. NSCs with low level driver mutations in *EGFR*, *tp53* and *PTEN* and *TERT* promoter mutations can migrate out from the SVZ, aberrantly grow along the OPC lineage, and develop into GBM – OPC cells are a major contributor to glioma formation[214]. Modeling of OPC dynamics suggests gradual replacement of normal OPCs with those lacking capacity for differentiation, increased proliferation and impaired contact inhibition can result in gliomagenesis[215]. Differentiation of these cells along the neuron lineage did not lead to GBM development[214], consistent with more recent findings suggesting NSCs and astrocytes with *PTEN, NF1, tp53* and *Rb1* depletion can be induced to form gliomas, whereas differentiation along the neuronal lineage reduces this capacity correlating with maturity, illustrating dedifferentiation from mature postmitotic neurons is highly unlikely[216].

In the normal CNS, neuron signalling affects progenitor cell survival, proliferation and differentiation[217–219]. GBM growth is increased by neuron activity, with release of neuroligin-3

found to be a requirement for progression[220,221]. GBMs also affect neuron activity, with significant glutamate secretion and reductions in GABAergic interneurons contributing to hyperexcitability and frequent seizures[222–224]. NPC/OPC-like GBM cells integrate into neural circuits, forming functional networks wherein GBM-induced neuron hyperexcitability induces depolarization of GBM cell membranes, engaging proliferation pathways and increasing growth. Blockade of glutamate receptors significantly decreases tumor size[225]. Greater integration of GBM into neural networks is associated with worse prognosis[226,227], consistent with findings that increased neuron-GBM signaling is associated with increased invasion[228], and that neuron- and NPC-like GBM cells unconnected to astrocytes that form synapses with healthy neurons were the major drivers of GBM invasion[229].

Variable cell types and differentiation states exist within a GBM tumor[230,231]. Thrombospondin-1 expressing cells within GBM have been identified as the subpopulation maintaining functional connections and remodeling circuits and are characterized by gene expression profiles enriched in synaptogenic, integrative, invasive and proliferative gene sets[226]. GBMs exhibit unique resting state network patterns and progressively functionally sequester themselves from the rest of the brain[232]. GBM migration occurs along white matter tracts and blood vessels via basement membrane disruption[124,233], with a heterogeneity between cells in speeds and directions. This movement occurs in an EGFR-dependent saltatory fashion characterized by elongated cell shape and fast bursts of motion[234] and through continuous motion via short protrusions at the leading edge of rounded cells, illustrating flexible invasion strategies based on levels of MMPs and hyaluranon synthase[235].

Astrocyte reactivity is governed by NF-κB signaling[236]. Under neuroinflammatory conditions such as traumatic brain injury, astrocytes adopt a reactive (A1, inflammatory) state characterized

by secretion of a broad range of proinflammatory cytokines, including IL-1β, IL-6, GM-CSF and TNF-α, which act in autocrine and paracrine manners to induce and maintain further reactivity and inflammation[236–238]. Tumor-associated astrocytes are highly proliferative and form a glial 'scar' around GBM[239,240] as a result of high tumor microenvironment (TME) glutamate secretion, with this 'scar' contributing to slowed GBM growth and reductions in TMZ delivery to tumor[241]. These astrocytes adopt varied reactivity states depending on location within and around tumor[242] and the specific neuroinflammatory milieu[238]. Anti-inflammatory (A2) astrocytes reprogram microglia to a tumor-promoting phenotype characterized by high IL-10, IFNγ and TGFβ expression. These phenotypes are maintained by tripartite crosstalk between astrocytes, GBM cells and microglia and lay the foundation for further development of the immunosuppressive TME[243]. Astrocytes surrounding GBM cells express MHCII and secrete CCL2, leading to Treg and macrophage recruitment[244–246]. Astrocytes have key roles in both the recruitment and programming of TAMs towards their immunosuppressive phenotypes, with CCL2-CCR2, CSF1-CSF1R and PD1-PDL1 signaling axes crucial for these alterations[247].

Astrocyte derived factors such as IL-1β, SDF1, TNF-α, TGFβ, IL-6, IGF1, BDNF, GDNF and MMPs[239,242,248] enhance GBM proliferation, treatment/apoptotic resistance and invasion. These astrocyte secreted factors increase expression of anti-apoptotic proteins in GBM cells[237,248], and astrocyte-GBM gap junctions provide further protection from chemotherapies[249,250]. Through their multifaceted means of communication, astrocytes reduce GBM sensitivity to a plethora of chemotherapies in part due to increases in NF-κB signaling, promoting expression of anti-apoptotic proteins including BCL-2 family members and IAPs[251,252] and reducing Bax expression[253]. Sensitivity to RT is also reduced in the presence of astrocyte secreted factors and gap-junction mediated interactions increasing JAK/STAT, MAPK/JNK and NF-κB signaling[254].

Astrocytes further aid in GBM progression via supply of metabolic requirements[247]. Ablation of reactive astrocytes around the TME significantly reduces GBM progression and enhances survival[247]. IL-10 secretion from astrocytes reduces MHCII and IFNγ expression within the tumor, restricting antigen presentation capacity, and astrocyte-mediated activation of STAT3 signaling in TAMs promotes adoption of anti-inflammatory states[242]. Astrocytes and microglia also represent key resistance factors against oncolytic virotherapy, able to act as virus 'traps' to preferentially uptake viral particles and protect GBM cells[255].

Cerebrospinal fluid (CSF) of GBM-bearing mice enhances STAT3-induced SERPINA3 and CD44 expression, significantly increasing proliferation and migration of GBM cells *in vitro* and increasing tumor growth rate *in vivo*[256]. Contact with the SVZ of the cerebral ventricles is a poor prognostic factor for GBM, associated with more aggressive disease and poorer overall survival[257,258]. CSF plays a key role in maintenance of normal NSC pools[259], and GBM cells close to CSF show increased cancer stem cell gene signatures, including increased CD133 and MGMT expression and significantly poorer survival[260].

Along with generation of new blood vessels via angiogenesis, GBM is also characterized by vessel co-opting, wherein GBM cells displace astrocyte endfeet from perivascular regions. GBM-associated or -derived pericytes express anti-inflammatory IL-10 and TGFβ, and hyperpermeability ('leaky' BBB) is a common feature of GBMs[261]. GBM confers immunosuppressive functionality to pericytes, inhibiting T-cell responses via TGFβ and IL-10 secretion, decreasing CD80 and CD86 expression, increasing PD-L1 and disrupting BBB integrity[262]. The BBB represents a key protective structure for the brain, excluding blood-borne neurotoxic pathogens and molecules from the brain interstitial fluid. The BBB is a highly complex mix of unique cellular interactions. Cerebrovascular endothelial cells (ECs) have high

mitochondrial content to facilitate extensive active efflux and influx transport mechanisms, with only gases and small lipophilic molecules able to passively diffuse[263,264]. They are connected via adherens junctions on the basolateral (brain-facing) side, limiting immune cell trafficking[265], and tight junctions at the apical (blood-facing) side, with high electrical resistance limiting ion and solute diffusion and maintained by EC-EC gap junction communication[265,266]. A basement membrane consisting of ECM proteins separates ECs from the glia limitans, which is made up of astrocyte endfeet that wrap around the vessel[265]. These cover nearly all cerebral capillaries and are crucial for induction and maintenance of the BBB[267,268] through BFGF, TGFβ and BDNF secretion and gap junction communication with ECs[269,270]. Astrocyte-derived apolipoprotein E3 maintains proper pericyte function at the BBB[271]. Pericytes reside in the basement membrane and contribute to BBB integrity via production of basement membrane proteins[265] and secretion of developmental cues such as sonic hedgehog, Wnt and retinoic acid[272–275]. Together, these form a significant barrier against solute and cellular trafficking into the brain.

Inflammation, as well as changes in astrocyte, pericyte and neuron function during aging, result in BBB breakdown via reduced tight junction integrity[265,276], rendering the CNS more susceptible to harmful blood components and cellular infiltration, including by immune cells. In GBM, integrity of the BBB is inversely correlated with density of tumor cells – areas of high density show completely compromised BBB, whereas areas at leading edge of invasion (i.e low GBM cell density) show intact BBB[277]. Neovasculature is abnormal and heterogeneous, with some subsets of GBM-derived ECs also expressing BBB drug efflux transporters, adding to the complexity of effective drug delivery for CNS tumors[277]. Dual IL-6 signaling from both microglia and GBM cells impair formation of EC barrier properties, with IL-6R signaling through JAK/STAT reducing expression of intercellular junction proteins[278]. ATP-binding

cassette (ABC) transporters are major efflux pumps allowing for exclusion of toxic molecules and drugs from tissues. Of these, ABCB1 (p-glycoprotein) and ABCG2 are the major transporters responsible for multidrug resistance in the brain, and ABCB1 is significantly expressed at the BBB, pumping toxins back into circulation. ABCG2 is also found at the BBB and may be functionally redundant with ABCB1 as inhibition of both is required for effective crossing of certain drugs. ABCB1 is expressed at significantly higher levels in GSCs than their more differentiated counterparts, which may account for increased drug resistance, and ABCB1 and ABCG2 levels represent poor prognostic markers for GBM[279].

1.3 Innate and adaptive immunity in GBM

1.3.1 Cancer-immunity cycle

The immune system plays key roles in tumor development and progression, a concept termed cancer immunoediting[280]. The three broad stages of immunoediting are: elimination, wherein transformed cells are recognized by the presence of neoantigens and DAMPs and cleared; equilibrium, wherein transformed cells surviving elimination (due to a myriad of mechanisms, including increased anti-apoptotic protein expression, downregulated MHC or costimulatory molecule expression, lack of strong neoantigens, presence of immunosuppressive cytokines, and expression of immune checkpoints) persist and can remain dormant for years; and escape, wherein surviving transformed cells begin to rapidly divide and form clinically relevant, invasive tumors with neoangiogenesis and immunosuppressive TMEs hindering effective anti-tumor immunity[281,282]. Cancer immunoediting occurs during immunotherapies as well, with the goal of therapies to counter the mechanisms that allowed for equilibrium and escape[283].

Multiple methods of stratifying tumors have been proposed based on the tumor-immune relationship. For example, one means of classification is based on mutational burden and extent

of intratumoral inflammation, with tumors exhibiting high and/or low measures of each and a convergence of immune checkpoints, impaired neovasculature functionality, immunosuppressive cytokine expression and myeloid cell infiltrates maintaining immune escape[284]. Another method is through identifying the mechanisms allowing for persistent escape, classifying tumors as oncogene-driven, stromal-cell driven, immunosuppressive-cell driven, or exhausted T-cell driven[285]. More broadly, tumors are classified based on overall inflammatory status and fall under one of three general categories: immune desert, wherein poor antigen quality and presentation and minimal expression of immune activation or co-stimulation signals result in little to no T-cell infiltration in the tumor or stroma and consequently lack of response to immune checkpoint blockade (ICB); immune excluded, wherein immune cells are recruited but do not migrate into the tumor parenchyma, and ICB is associated with T-cell activation but minimal infiltration; and immune inflamed, wherein significant T-cell infiltration and proinflammatory cytokine expression is observed, but escape is maintained through high checkpoint expression, T-cell exhaustion, and large suppressive myeloid cell and Treg populations, resulting in better but not total responses to ICB[286].

Immune checkpoints are inhibitory receptors involved in normal peripheral immune tolerance to avoid autoimmunity[287], particularly by the adaptive immune system[288] and which are expressed by cancer cells to evade immune clearance. T-cell exhaustion is characterized by high expression of inhibitory checkpoint receptors, altered metabolism, and loss of mitogenic and effector/killing capacity (characterized by reduced IL-2, IFNγ, TNFα and Granzyme B production) resulting from continuous antigen presentation and signaling through immune checkpoints[289,290]. Among the myriad of checkpoint receptors, PD-1, T-cell immunoglobulin and mucin domain containing protein-3 (TIM-3), and lymphocyte activated gene-3 (LAG-3) represent the three classically

upregulated markers of exhausted T-cells, binding PD-L1, MHC and Galectin-9 on cancer cells, respectively[291,292]. Cytotoxic tumor lymphocyte antigen 4 (CTLA-4) represents one of the first checkpoints discovered[293], along with PD-1[294], and ICB for a wide array of liquid and solid tumors are currently being investigated in numerous clinical trials, alone or in combination[295].

PD-1/PD-L1 signaling inhibits T-cell function through four major mechanisms[296]: direct T-cell receptor (TCR) inhibition, where recruitment of Src-homology 2 domain-containing protein tyrosine phosphatases (SHP)-1 and -2[297] inhibits ZAP70 (associated with TCR) and PI3K (associated with co-stimulatory domains such as CD28) and consequently downstream TCR signals are blunted; indirect TCR inhibition, where SHPs recruited by PD-1/PD-L1 engagement decrease expression and activation of the protein kinase 2 (CK2), normally involved in T-cell activation and proliferation following TCR stimulation via activation of NF-κB, JAK/STAT and PI3K/Akt pathways[298]; TCR surface expression regulation, wherein PD-1/PD-L1 signaling increases CBL E3 ubiquitin ligase expression resulting in ubiquitination of TCR chains and their subsequent removal from cell surface and degradation[299,300]; and alterations in T-cell metabolism, wherein PD-1/PD-L1/SHP-mediated inhibition of PI3K-Akt and ZAP70 signaling results in a transition from glycolysis to β-oxidation[296]. ICB against PD-1 is generally more effective than against PD-L1, as PD-L1 is continuously internalized and recycled[296,301].

The cancer-immunity cycle outlines seven key phases in T-cell immune responses to cancer, wherein immunotherapeutic manipulation of one phase is theoretically capable of enhancing the rest (Figure 3). Briefly, these stages are: 1) cancer cell death and consequent antigen release; 2) phagocytosis of dying cancer cells by antigen presenting cells (APCs) and subsequent antigen presentation; 3) APC trafficking to lymph nodes and subsequent T-cell priming and activation; 4) T-cell trafficking from lymph nodes to blood and along chemokine gradients to tumor; 5) T-cell

migration out of blood into tumor; 6) T-cell recognition of antigen presented on MHC molecules; and 7) T-cell killing of cancer cell, via perforin-granzyme or death receptor mechanisms[302,303]. Immune desert, excluded or inflamed tumors use mechanisms to disrupt multiple steps of the cancer-immunity cycle, and the goal of immunotherapies is to overcome these and restart or accelerate the cycle[303].

1.3.2 CNS immunity

The brain has long been considered an immune 'privileged' site, excluding immune responses to protect neurons incapable of self-renewal. These assumptions were in part due to seminal skin graft experiments, wherein skin grafts from non-identical rabbits generated immune reactions and were rejected when implanted in the periphery but, markedly, not in the brain[304,305]. Further contributing to this notion was the finding that the brain lacked classical lymphatic vessels[306]. T-cell responses are observed following initial neutrophil and macrophage engagement against sub-dermally injected heat killed bacille Calmette-Guérin (BCG) bacteria, whereas in the CNS macrophages are recruited but T-cell responses absent[307,308]. Multiple other models fail to demonstrate T-cell infiltration and action against CNS-specific antigens[309–311], leading to the idea that the CNS was isolated from the immune system. Nonetheless, T-cell responses are possible within the CNS – skin grafts can be rejected when implanted into the brain, however only after a preceding subdermal implant of the same tissue[304,312].

More recent work has illuminated a far more complex CNS-immune system relationship. CNS border regions allow for immune surveillance, particularly the dural sinuses (large meningeal vascular structures), choroid plexus, perivascular spaces, meninges, draining lymph nodes, and the bone marrow of the skull, wherein CNS antigens are sampled and immune responses generated[313,314]. Unlike with the BBB, meningeal vasculature expresses significant adhesion

molecules and ligands allowing for substantial T-cell trafficking[315], and the dura mater of the meninges are innervated by lymphatic vessels[316,317] that transport CNS antigens for sampling in cervical lymph nodes[318,319]. CSF from the subarachnoid space has been found to drain to lymphatic vessels[320]. In the recently characterized glymphatic system, CSF from the cerebral ventricles and subarachnoid space flows along supply arteries (periarterial spaces) via arterial pulsations to supply nutrients, wherein it enters and coats the brain, in turn mixing with interstitial fluid. This mixing allows for metabolic waste removal, and the brain interstitial fluid is cleared along perivascular routes (perivenous spaces) via astrocyte aquaporin-4-mediated fluid flux into subarachnoid space and dura mater or along draining veins to cervical lymph nodes[321–325]. CSF- and interstitial fluid-borne antigens are then processed by dural sinus APCs and presented to circulating T-cells[315,326], activating them through TCR-MHCII signaling[315] and permitting CNS immune surveillance[313]. T-cells within CSF can attach to the leptomeninges via CCR5/CXCR3 signaling following appropriate antigen stimulation and migrate into the parenchyma[327]. Chemical-induced increases in activity of this glymphatic pathway allows for improved CNS parenchymal delivery of drugs following injection into CSF[328]. Interestingly as well, the skull itself possesses a pool of bone marrow from which immune cells derive and gain access to the aforementioned border regions via direct channels[329,330]. Normal aging is associated with poor meningeal lymphatic function and CSF drainage driven by $CD4^+$ and $CD8^+$ T-cell expansion and increased IFNγ signaling, resulting in impaired lymphatic endothelial cell adherens junctions. These impairments allow for buildup of misfolded proteins[331].

Microglia represent the only resident leukocytes in the brain parenchyma under homeostatic conditions, branching in development from bone-marrow derived monocytes during the embryonic yolk sac stage[332] and able to renew independent of hematopoietic stem cell

involvement[333,334]. Microglia express little MHCII under homeostatic conditions but expression is increased drastically in response to neuroinflammatory insults. They can act as APCs, although they do not migrate to cervical lymph nodes[335], and constantly monitor for DAMPs and pathogen associated molecular patterns (PAMPs). Damage or injury results in rapid migration to the injury site, wherein microglia form a barrier between injured and healthy tissue[336]. Activation is associated with a change from ramified, branched surveillance/resting phenotype to a de-branched, M1 or M2 polarized phenotype depending on stimulus. M1 microglia are characterized by high oxidative metabolism and inflammatory cytokine and chemokine production (especially IL-1β, TNFα and IL-6), while M2 microglia produce enzymes involved in wound healing and resolution of inflammation, such as IL-10 and TGFβ[336]. Microglia play roles in modulating effector T-cell function rather than recruitment[337].

CNS border regions (choroid plexus, meninges) are significantly more populated by immune cells, with significant macrophage and DC populations orchestrating T-cell activation[338,339]. Neuroinflammation stemming from disease or normal aging results in activation of resident immune cells and permits infiltration of peripheral leukocytes[340,341]. Recent mass cytometric analyses of mouse brain and meningeal tissue have revealed that while microglia make up most CNS immune cells under resting conditions, neutrophils, DC's and resident macrophages also significantly populate the meninges and choroid plexus (i.e parenchymal border regions). These border macrophages show incredible phenotypic diversity. Further, these border regions are also surveilled by NK-, T- and B-cells, but lymphocytic populations are relatively minimal[341,342]. Nonetheless, these meningeal DC's are able to recruit CNS-infiltrating T-cells in animal models of multiple sclerosis[338].

Astrocytes, the largest cell population within the CNS, play critical roles in neuron survival and CNS homeostasis. Among them, astrocytes have key roles in neuroinflammation, wherein they can act as phagocytes and APCs, producing IL-12/IL-23p40[343]. Astrocytes have minimal capacity to prime naïve T-cells or stimulate infiltrating lymphocytes, however, with the exception of the less inflammatory Th2 subset which they effectively stimulate as a means of protecting neurons from inflammation-induced cell death[344]. Further to this, astrocytes regulate immune infiltration via chemokine release[236], barrier formation/maintenance/loosening (depending on context) that gates immune cell entry from CNS border regions, leukocyte instruction based on astrocyte secretory profile[345], and via Fas-FasL[344,346] or Galectin-9 expression[347] signaling to induce T-cell apoptosis and consequent resolution of neuroinflammation. Astrocytes can adopt reactive states similar to monocytes, coined A1 (inflammatory) and A2 (anti-inflammatory)[243]. Astrocyte reactivity is mediated by NF-κB downstream of IL-1β and TNFα signaling[236] resulting from neuroinflammatory conditions such as neurodegenerative disorders or traumatic brain injury. Reactive astrocytes secrete further IL-1β, IL-6, IFNγ and TNFα[237], which can act in autocrine and paracrine fashions to induce further reactivity[236]. On the other end of this spectrum, IL-10 induces astrocytes to release TGFβ, suppressing further neuroinflammation[345]. Astrocyte PD-L1 inhibits effector T-cell function[348]. Normal aging has been found to be accompanied by increased proinflammatory microglia[349], which in turn increase the expression of A1-associated genes in astrocytes, hindering their normal homeostatic functions, allowing increased peripheral immune infiltration, and increasing vulnerability to neurotoxic insult[350,351].

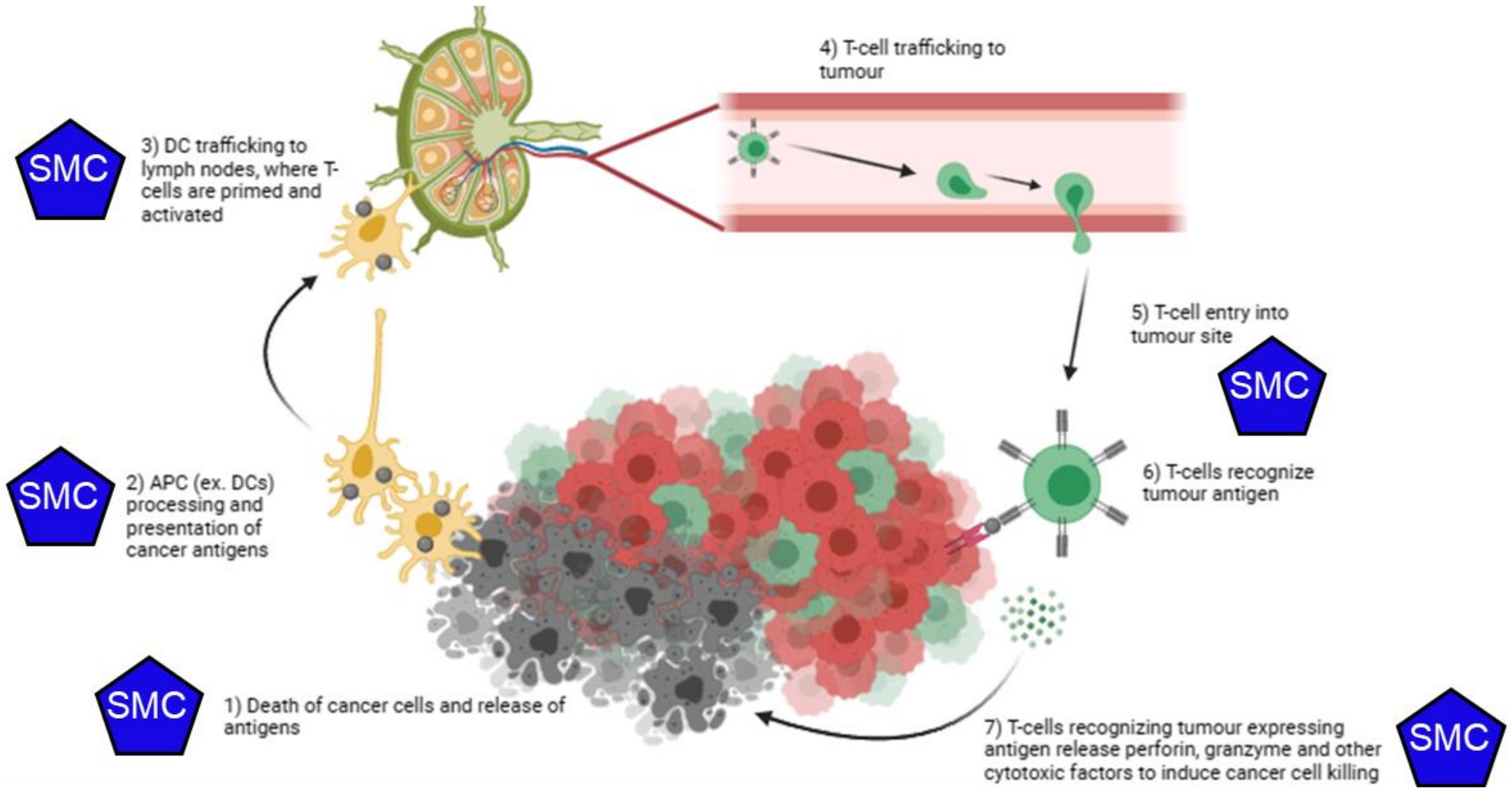
SMC
3) DC trafficking to lymph nodes, where T-cells are primed and activated
4) T-cell trafficking to tumour
5) T-cell entry into tumour site
SMC
SMC
2) APC (ex. DCs) processing and presentation of cancer antigens
6) T-cells recognize tumour antigen
SMC
1) Death of cancer cells and release of antigens
7) T-cells recognizing tumour expressing antigen release perforin, granzyme and other cytotoxic factors to induce cancer cell killing
SMC

Figure 3: The cancer-immunity cycle. Outline of the seven key steps of the cancer-immunity cycle, wherein tumor antigens are presented to T-cells and cells expressing these antigens are subsequently recognized and cleared. Multiple mechanisms are used by tumors to escape immune elimination, a process termed immunoediting. Immunotherapies look to enhance aspects of the cancer-immunity cycle and remove tumor-derived inhibition of immune recognition and attack. Blockade of IAPs via SMC treatment has been found to enhance multiple aspects of this cycle, including: sensitizing tumor cells to death through conventional chemotherapy or death receptor signaling[97,102,188,352,353]; increased type I interferon signaling, DC maturation, phagocytosis and antigen presentation[354,355]; increased chemokine production allowing for enhanced immune cell trafficking from lymphoid organs to tumor[356]; increased T-cell costimulation, proliferation and cytokine production[82,357]; and reducing T-cell PD-1 expression and Treg differentiation[358]. Figure was generated in BioRender and adapted from Ali *et al*[359] and Chen and Mellman[302].

1.3.3 Immune microenvironment

GBM is immunologically 'cold', with little T-cell infiltration due to multiple mechanisms, including alterations to tumor vasculature hindering trafficking, ECM features not conducive to T-cell migration, and minimal chemotactic signaling[360,361]. Despite variations between patients and subgroups, GBM is often considered an immune 'desert'[362]. Indeed, HA, a major component of the brain ECM, is key for T-cell exclusion, as HA-rich areas are typically devoid of T-cells. HA degradation increases CD8+ T-cell infiltration, promotes M1 TAM phenotypes and enhances oncolytic virotherapy efficacy[363]. GBM cells expressing FasL can induce T-cell apoptosis, maintaining immune privilege[364] similar to normal astrocytes. Some T-cells do infiltrate and encounter a potently immunosuppressive TME, adopting exhausted phenotypes that further limit anti-GBM responses[289,290]. Tregs, which make up a significant proportion of infiltrating T-cells, are mainly recruited from the periphery and potently suppress anti-tumor immunity[365], contributing to exhaustion. TGFβ plays a role in Treg recruitment to, and action within, the tumor, as blockade significantly reduces Treg and enhances $CD8^+$ T-cell proportions and effector functions[366]. Intratumoral $CD4^+$ T-cells can also become Tregs via induction of FoxP3 expression upon exposure to the immunosuppressive TME[367], notably by TGFβ as downstream SMAD binds the FoxP3 gene[368]. Treg proportions vary with glioma grade, and are highest in GBM[369,370]. Among the mechanisms used by Tregs, high CD25 sequesters IL-2, limiting effector cell functionality[371,372], while IL-10 and TGFβ further suppress anti-tumor immunity[290,373,374]. Treg immunosuppression and persistence within the TME is enhanced by hypoxia, which is high in GBM. Tregs thrive in low-glucose environments compared to conventional T-cells given higher surface expression of fatty acid transporters, readily switching to lipid metabolism which in turn enhances suppressive effects[375]. Among the inhibitory receptors involved in T-cell exhaustion are

the immune checkpoints CTLA-4, PD-1, LAG-3 and TIM-3. Reducing T-cell exhaustion via ICB has shown significant clinical benefit for numerous cancers, potently enhancing anti-cancer immunity. Their efficacy in GBM is discussed in **section 1.4.4**.

Interestingly, while T-cells represent the major TME components of brain metastases, tumor-associated microglia/macrophages (TAMs) dominate glioma TMEs[376], suggesting it is not the CNS alone limiting anti-brain tumor action but features of gliomas themselves. Microglia are the first myeloid cells recruited, however as the tumor develops monocyte-derived macrophages dominate[377,378]. In GBM, TAMs are found mostly in GSC-rich areas such as around blood vessels, invasive tumor margins, and especially in hypoxic areas where TAMS are found in high proportions with necrotic cells[379]. GSCs are key for TAM recruitment to the tumor, with said TAMs having roles in invasion, angiogenesis and tumor growth[380,381]. CSF-1 produced in high levels by GBM cells acts to recruit microglia, which in turn activate EGFR signaling in GBM and stimulates invasion[382]. Differential proportions of microglia or macrophages observed between patients are a result of individualized GBM mutation patterns, resulting in unique chemoattractant secretion patterns[383], contributing to further intertumoral heterogeneity. These distinct TAM cell types have been found to infiltrate and colonize different intratumoral regions[384]. Substantial variation in TAM proportions are seen between patients with IDH^{WT} GBMs, with proportions significantly decreased in IDH^{MUT} tumors[385], in part explaining the better response to therapy amongst IDH^{MUT} GBMs. Indeed, resistance to antiangiogenic therapy is associated with increased infiltration of myeloid cells[386]. TAMs negatively correlate with T-cell, neutrophil and DC proportions and activation, secreting immunosuppressive cytokines such as IL-10, -4 and -13 and enhancing Treg proportions[376]. TAMs and MDSCs also represent the

major source of TGFβ, acting in autocrine and paracrine fashions to induce and maintain anti-inflammatory (M2) phenotypes[387].

TGFβ is highly expressed in GBM, signaling via SMAD to enhance epithelial-to-mesenchymal transition and increase GBM invasiveness[388]. Cancer stem cells are regarded as both the initiating cells for tumors as well as the major orchestrators of invasion[389,390]. Indeed, $CD133^+$ GSCs express higher TGFβR2 levels than more differentiated cells, and TGFβ from TAMs increases MMP-9 expression by GSCs, enhancing invasive potential. This is significantly reduced upon TGFβ blockade[380]. TGFβ from GBM cells induces reductions in microglial MHCII expression, proliferation and pro-inflammatory cytokine production, in turn increasing expression of IL-10 and further TGFβ[391,392]. Despite the numerous roles in immunosuppression and GBM biology, intratumoral TGFβ blockade in phase II trials showed enhanced survival benefit for anaplastic astrocytoma patients but none in GBM[393]. Little IFNγ, TNFα, IL-2 or IL-12 is expressed within the tumor, and TAMs show reduced NF-κB signaling in GBM relative to those in lower grade gliomas, with lower TLR and T-cell costimulatory molecule (CD40, CD80, CD86) expression[394]. Microglia also secrete MMP-9[395] and MT1-MMP[396], and GBM cells induce TAMs to secrete MMP-2, further contributing to ECM degradation and invasion into normal parenchyma[397].

Increased bone marrow derived macrophage (BMDM) infiltration is a feature of more aggressive gliomas and poorer survival[376], and these peripheral macrophages are also more closely associated spatially with infiltrating T-cells. GBM TAMs show unique and diverse transcriptional profiles, existing on a spectrum between M1 and M2 polarizations and not neatly purely pro- or anti-inflammatory. They alter ECM protein composition and function[398]. GBM promotes monocyte maturation to MDSC phenotypes[399], and high MDSC levels are a marker of

poor prognosis[400]. TAM and GBM cell-derived p-selectin levels have been found to correlate with poor survival, increased GBM cell proliferation and invasion, and increased Arg19, IL-10, and TGFβ expression. P-selectin blockade significantly enhances anti-GBM T-cell responses, reduces neovasculature and tumor volume, and enhances survival[401]. Given their potent immunosuppressive and tumor-promoting features, it is not surprising that IDH^{MUT} GBM tumors, characterized by lower TAM infiltration, have greater microglia than macrophage content, significantly greater pro-inflammatory gene signatures, respond better to treatment and have better long term survival than IDH^{WT}[385].

Meningeal lymphatic vessels have been identified as essential components of anti-GBM immune response, necessary for GBM interstitial fluid drainage and DC trafficking to draining cervical lymph nodes. Presence of intracranial tumors remodels meningeal lymphatics to limit immune responses and reduce efficacy of immunotherapy. VEGF-C treatment enhances angiogenesis within meningeal lymphatics and improves immune surveillance and immunotherapy efficacy for GBM[402,403].

1.3.4 Peripheral immunosuppression

Metastasis of GBM out of the brain is rare[404]. Despite this, systemic immunity is severely disrupted in GBM patients. Through as yet-unidentified mechanisms, GBM induces significant T-cell lymphopenia in the periphery, specifically among the $CD4^+$ compartment and accompanying reduced MHCII expression. Increased proportions of circulating Tregs and increased numbers of immunosuppressive monocytes and MDSCs relative to healthy controls further exacerbate peripheral immune defects[399,400,405–407]. Accompanying this lymphopenia are findings of contracted lymphoid organs including involuted thymuses, impaired T-cell functionality and sequestration of abnormal numbers of T-cells in bone marrow due to loss of

egress signals on T-cell surfaces[408,409]. IL-6 from GBM cells increased PD-L1 expression on peripheral myeloid cells, which consequently adopt immunosuppressive function and induce T-cell apoptosis[410]. Soluble tumor necrosis factor receptor-1 (sTNFR1), which may act as a decoy receptor for TNFα, is significantly reduced in circulation in both newly diagnosed and recurrent GBM[411].

1.4 Immunotherapies for GBM

1.4.1 T-cell transfer therapies

Adoptive transfer of patient- or donor-derived cancer-targeting T-cells, termed adoptive T-cell therapy, has shown significant preclinical and clinical benefit for hematologic and select solid tumors[412]. Isolation and expansion of tumor-infiltrating lymphocytes (TILs) specific for tumor antigens has shown significant benefit for melanoma patients with brain metastases[413,414], suggesting anti-tumor T-cell responses against brain malignancies are possible. Adoptive cytalomegalovirus (CMV)-specific T-cell immunotherapy in GBM patients post RT and TMZ did not provide survival benefits. CMV-specific T-cells were dysfunctional within the TME and located mostly within perivascular regions and not throughout the tumor[415], illustrating significant immunosuppressive hurdles.

Chimeric antigen receptor (CAR) T-cells are patient T-cells expanded *ex vivo* and genetically modified (typically via lentivirus) to confer antibody specificity without the need for engagement of TCR-MHC signaling. The extracellular component of the CAR construct consists of the light and heavy chains of single chain variable fragments (scFv) of antibodies specific for a defined tumor surface antigen, a transmembrane hinge region, and intracellular signaling domains consisting of aspects of normal T-cell activation, such as 4-1BB, CD28 and CD3ζ[416–418]. While initial CARs had no costimulatory domain, second generation constructs and beyond add one or

more, conferring *in vivo* efficacy. Tailoring ratios of subsets of $CD4^+$ and $CD8^+$ T-cells (eg. Naïve, memory or effector), as well as: the size of the hinge region; specific combinations of costimulatory domains; scFv affinity depending on level of antigen expression; bispecific scFv's gating activation or inhibition depending on expression of multiple ligands; 'suicide' genes allowing for inducible cell death in the case of toxicity; and CARs containing inducible gene cassettes signaling for expression of inflammatory cytokines or cytotoxic payloads represent significant flexibility of the CAR design for tailoring treatment to specific cancers and TMEs[418–422].

While CAR-T cells have shown significant benefit for hematologic ('liquid') tumors[423], with FDA approved CAR-T therapies for lymphomas, leukemias and myelomas[424], 'solid' tumors pose numerous issues, including suboptimal CAR-T expansion and persistence *in vivo*, poor trafficking, antigen loss and potently immunosuppressive TMEs[416]. Primary resistance to CAR-T infusion results from impairments in cancer cell death receptor signaling, allowing for antigen persistence and gene signatures in CAR-T reminiscent of T-cell exhaustion. Relapse represents secondary resistance, acquired due to loss of antigen[425]. All of these play a role in CAR-T treatment of GBM, with the added hurdles of long manufacturing times incongruent with the low survival times for GBM patients, and overcoming CNS-specific anti-immune mechanisms - CAR-T cells for patients with leukemia appear in the CSF[426], suggesting access to CNS is possible following peripheral administration. Intracranial (IC) or intracerebroventricular (ICV) administration of CAR-Ts allows for overcoming trafficking defects to GBM tumors[427]; ICV and IT administration significantly improves CAR-T trafficking to tumor site and consequently therapeutic benefit relative to IV[428].

Among the aforementioned hurdles, a lack of defined and consistently expressed neoantigens represents a severe limiting factor. Identified and targetable GBM-specific antigens include EGFRvIII, HER2, and IL13Ra2[422]. These are heterogeneously expressed, however, and antigen escape is common. Phase 1 trials of HER2+ recurrent GBM patients receiving HER2 targeted CARs IV showed little *in vivo* expansion of infused T-cells, although overall survival was improved in nearly half of patients[429] and combination HER2-targeted CAR-T cells with PD-1 blockade *in vitro* significantly enhanced IL-2 and IFNγ production[430], suggesting a rational combination for future GBM treatments. IL13Ra2 is overexpressed in over half of GBM patients[431] and shows little expression in normal brain[432], increasing with glioma grade and associated with mesenchymal subtypes, greater immune activation and poor prognosis[431]. IL13Ra2 is expressed by both GSCs and more differentiated cells, and CAR-T cells targeting this antigen reduced GSC tumor initiation capacity and tumor size in *in vivo* mouse models, with increases in IFNγ, GM-CSF and TNFα production[433,434]. In early patient trials of IL13Ra2-targeted CAR-Ts for recurrent GBM, IC injection of cells into tumor cavity using an implanted catheter system allowed for repeat targeted doses. Significant increases in tumor necrosis volume, loss of IL13Ra2 expressing cells, and CAR-T cell detection within tumor and away from catheter suggested effective anti-GBM action. Recurrence occurs via expansion of cells not expressing IL13Ra2[435]. Anti-EGFRvIII CAR-T cells show *in vitro* and *in vivo* cytotoxicity against human GBM cell lines, trafficking to tumor, significantly reducing tumor size, and extending median survival in mice[436,437]. CAR-Ts targeting both overexpressed EGFR and EGFRvIII extend survival in mice bearing human GBM cells following IV administration, showing trafficking into tumor, persistence and proinflammatory cytokine production *in vivo*[438]. EGFRvIII is also expressed by GSCs, and CAR-T cells recognize and kill this population *in vitro*

as well as more differentiated cells[439,440]. Early trials of IV delivered CAR-Ts targeting EGFRvIII had no impact on survival despite persistence, with reductions in EGFRvIII expression between primary and recurrent disease[441].

Phase I trials of CAR-Ts targeting both IL13Ra2 and EGFR administered into the subarachnoid space show promising early results in terms of tumor size reduction, expansion and rapidly increased IFNγ, IL-2, and TNF-α expression in CSF[442]. Numerous Phase I clinical trials using anti-GBM CAR-T are underway, with multiple combinatorial approaches, CAR designs and novel target antigens such as CD44/CD133 (GSC markers) and B7-H3 (a novel immune checkpoint)[424,443]. Novel CAR designs and rational immunotherapy combinations attempting to overcome antigen heterogeneity, antigen loss, delivery and trafficking issues and the immunosuppressive TME are all under preclinical investigation by numerous research groups (reviewed in [444]). Targeting the GSC pool represents a promising new avenue for engineered T-cell-based GBM therapies. CD133-targeted CART cells injected IT persisted in the brain and almost completely eliminated all CD133-expressing cells, significantly extending survival[445].

1.4.2 Vaccination strategies

Given the efficacy of memory but not primary immune responses against CNS skin grafts (**Section 1.3.2**), vaccination strategies aiming to induce memory responses against GBM antigens represents a promising strategy. DC's pulsed with EGFRvIII peptide and reinfused into patients induced anti-EGFRvIII immune responses and extended overall and progression-free survival, with heterogeneity in antigen expression limiting efficacy[446]. EGFRvIII peptide vaccination induces antigen specific immune responses and improves overall survival when given concurrently with TMZ. Chemotherapy-induced lymphopenia increases the relative proportion of antigen-specific lymphocytes along with Tregs[447]. Immunologic escape was

associated with elimination of EGFRvIII expressing cells and expansion of WT EGFR expressing ones[448,449]. Phase III clinical trials failed to extend median and overall survival[450].

IDH1-specific peptide vaccines induce antigen-specific $CD4^+$ T-cell responses and extended survival in IDH1-mutated astrocytoma patients[451]. DC's pulsed with IL13Ra2 peptide infused intradermally into recurrent, IL13Ra2+ GBM patients showed induction of antigen-specific $CD8^+$ T-cell responses, although the time course of the study was too short to evaluate long-term impacts on tumor growth[452]. Tumor lysate-pulsed DC's administered concurrent with TMZ following surgery and radiation showed extended survival times in a phase 3 study[453].

1.4.3 TAM depletion or reprogramming

As microglia and macrophages are major components of the GBM TME and play significant roles in numerous aspects of GBM biology (**Section 1.3.3**), targeting these populations for depletion or reprogramming towards more anti-tumor phenotypes will likely represent a vital component of any successful anti-GBM immunotherapy. Microglia[454] and subpopulations of neural progenitors[455] express CSF1R in the CNS under homeostatic conditions. CSF1 or IL-34 signaling through CSF1R is required for microglia survival, with blockade using CNS-permeable PLX compounds able to dose-dependently eliminate nearly all microglia in the brain[456]. In preclinical GBM models, CSF1R blockade using PLX3397 significantly reduces tumor volume[457] and invasiveness[382], depleting brain microglia. Interestingly, TAMs were spared from depletion by GBM TME-derived survival factors, including IFNγ, CXCL10 and GM-CSF. TAMs were, however, depolarized from the M2 state and GBM cells were sensitized to subsequent RTK inhibition[457]. Mouse models of GBM show significant benefit upon CSF1R blockade. However, resistance to further blockade results from TAM secretion of IGF1, signalling through IGF1R on GBM cells and increasing PI3K signaling. Combined inhibition of IGF1R and CSF1R blockade

significantly enhances median and overall survival[458]. However, clinical trials of PLX3397 showed limited efficacy in patients with recurrent GBM[459].

Aside from depletion strategies, multiple groups have explored TAM reprogramming towards anti-tumor phenotypes. Antibody blockade of TLR2 on microglia reduces GBM invasion via reduced microglial MT1-MMP expression[460], and IV administration of anti-TLR2 antibodies is effective and safe in humans[461], but no followup clinical trials have been performed in GBM[383]. Increasing phagocytic capacity of TAMs using TMZ and CD47 blockade improves APC cross priming of antigen-specific $CD8^+$ T-cells, accompanied by increased myeloid and T-cell infiltrates into TME and increased serum TNFα and IL-2 levels, culminating in significantly reduced tumor volume and improved median survival in murine GBM[462,463]. Myeloid cells within the GBM TME, especially M-MDSCs, have the highest PD-L1 expression of any immune infiltrate, and both this expression and bulk myeloid infiltration are increased by RT. Direct intracranial implant of lipid nanoparticles containing dinaciclib (a kinase inhibitor targeting CDK5, limiting PD-L1 recycling and production) and surface expressed αPD-L1 antibodies reduces TAM proportions, increases T-cell proliferation and significantly improves overall survival, with long term cures across two murine GBM models[464].

1.4.4 Immune checkpoint blockade

ICB has revolutionized cancer therapy for multiple solid and hematologic tumors (**Section 1.3.1**), and high checkpoint-induced T-cell exhaustion in GBM (**Section 1.3.3.**) makes this a logical strategy for enhancing anti-GBM T-cell attack. A phase 3 clinical trial of monotherapy αPD-1 treatment for recurrent GBM showed no survival benefit[465], nor did the combination with RT and TMZ in newly diagnosed GBM[466]. A systematic review of clinical trials using αPD-1 ICB for GBM showed improved median overall survival for newly diagnosed GBM, although no

differences in progression free survival and no efficacy for recurrent GBM[467]. Phase 2 trials in relapsed GBM patients showed trends towards increased immune cell infiltration and increased TCR clonality following αPD-1 ICB[468]. One trial using αPD-1 blockade in the neoadjuvant setting significantly improved survival in recurrent GBM patients, increasing IFNγ responses by infiltrating T-cells, a shift towards memory phenotypes, and tumor-specific TCR clonal expansion without changes in TCR diversity[469]. Combination with CTLA-4 blockade in recurrent GBM showed no improvements in survival[470]. PD-1 shows increased expression on tumor-infiltrating lymphocytes after DC vaccination strategies. In murine GBM, αPD-1 ICB significantly enhances the efficacy of tumor lysate-pulsed DC vaccine strategies, with long-term cures, increased T-cell infiltration into tumor, improved intratumoral $CD8^+$ T-cell activity characterized by increased IL-2 and IFNγ expression and enhanced anti-GBM cytotoxicity[471].

Hypermutation is a common feature of recurrent GBM post-Stupp protocol, with TMZ selecting for mismatch repair deficient, resistant cells. Despite increases in neoantigens, anti-GBM immune responses are not improved, with no differences in total T-cell infiltrates based on hypermutation status. This appears unique to CNS tumors, as hypermutated colorectal cancers do exhibit enhanced T-cell infiltration. Glioma hypermutations tend to be subclonal, with high missense mutations and low frameshift indels generating poor quality neoantigens, and consistently poor response to ICB regardless of mutation status[472]. TAMs express significant TGFβ and are major contributors to ICB resistance[398]. In keeping with this, number and clonality of mutations does not correlate with significant differences in responses to ICB. Non-responders show reduced T-cell infiltration, proliferation, and killing capacity and increased Tregs and TAMs expressing high PD-L1, MHCII and TNFα. Tumors that respond to ICB have lower T AM frequencies, and the TAMs that are present show higher pro-inflammatory gene signatures

associated with promoting Th1 T-cell responses[473]. PD-L1 is highly expressed across TAM subgroups and contributes to high Treg proportions and exhausted phenotypes. Interestingly as well, TAMs promote $CD4^+CD8^+$ double positive T-cell phenotypes, which further produce significant IL-10, IDO1 and TGFβ[474]. Functional alteration of TAMs enhances efficacy of αPD-1, generating long-term survivors in murine GBM[462].

Age-related immunosenescence affects both the CNS and peripheral immune system, with lymphopenia and reduced TCR diversity resulting from thymic involution[475–479], greater Treg proportions in circulation[109], and greater TGFβ and IL-10 production by microglia[480,481]. Age is also associated with increased IDO1 and PD-L1 expression, most drastically in the brain of individuals 60-69 years old, coinciding with median age of GBM onset[109]. IDO1 expression is typically limited to placenta and lymphoid tissues and is increased in response to inflammation, mediating T-cell suppression via tryptophan depletion. High IDO1 is associated with effector T-cell apoptosis and expansion of Treg populations[482]. The confluence of age-related and GBM-induced immune impairments results in significantly worse responses to ICB as patient age increases[483]. Glucocorticoid-induced TNFR-related receptor (GITR) is highly expressed by Tregs within GBM, and blockade reduces Treg anergy, converts Tregs to Th1 T-cells, repolarizes TAMs towards a more M1 phenotype, and frees up $CD8^+$ T-cell action, all acting to enhance αPD-1 ICB efficacy in murine GBM[484]. Overcoming intracranial tumor-induced bone marrow sequestration via sphingosine-1-phosphate knock-in and 4-1BB agonism significantly improves overall survival in murine GBM[409].

An issue affecting many GBM clinical trials is they are tested on primary or recurrent tumors post-Stupp protocol, fundamentally selecting for more resistant cell populations and altering the patient's immune system and TME. Systemic carmustine chemotherapy regimens for GBM have

been found to cause lymphopenia in the blood, lymph nodes, bone marrow and tumor itself, significantly reducing the efficacy of αPD-1 blockade. Conversely, direct IT chemotherapy administration robustly enhances anti-GBM immune responses via localized cell death, boosting phagocytosis and antigen presentation without the cytotoxic effects on lymphoid organs noted in systemic schedules and consequently doubling the number of long-term survivors[485]. Similar anti-immune effects have been noted with TMZ, as addition of this chemotherapy to αPD-1 blockade induces lymphopenia, myelosuppression, inhibits anti-GBM immune memory formation and increases Treg numbers[486]. Dose schedule of TMZ demonstrates significant intricacies in effects on the immune system. Standard doses of TMZ (50 mg/kg, 5 days) have been found to increase exhaustion marker expression on T-cells (especially PD-1), increase Treg proportions, decrease IFNγ production by T-cells and impairs efficacy of αPD-1 blockade in murine GBM. Conversely, reducing dose but extending schedule (25 mg/kg, 10 days) resulted in increased IFNγ production, increase antigen specific T-cell proportions in peripheral lymphoid organs and lower intratumoral exhaustion signatures with improved numbers of long-term survivors[487].

1.4.5 Combination immunotherapy with SMCs

Taken together, it appears clear that anti-GBM immune responses are possible. Overcoming innate CNS immune and drug exclusion mechanisms, the immunosuppressive GBM TME, GBM anti-apoptotic oncogenic changes, CNS- and GBM-derived peripheral immunosuppression, age-associated immunosenescence, and standard of care-induced lymphopenia represent significant hurdles unlikely to be adequately overcome by single target immunotherapies. Combinatorial approaches targeting multiple pillars of the GBM-immune relationship are required for maximal therapeutic benefit. The addition of SMCs to immunotherapy regimens represents a promising

new avenue of treatment given the multifaceted roles of SMCs in modulating immune responses via enhancements to many steps of the cancer immunity cycle. Notably, SMCs induce alterations in NF-κB signaling[96,357], including enhancing T-cell costimulation, proliferation and inflammatory cytokine production[82,357,488] in microenvironmental context and T-cell subset dependent manners[489–491] while simultaneously sensitizing cancer cells to chemoradiotherapy (intrinsic pathway) and through signaling via many common cytokines and death ligands (extrinsic pathway)[492]. This is especially noteworthy given the high TNFα-TNFR1-NF-κB signaling crucial to multiple aspects of GBM biology (**Section 1.2.4, 1.2.5. 1.2.6, 1.3.3**). Indeed, SMCs are under investigation as combinatorial agents for numerous immunotherapy clinical trials[493–495]. SMCs have been found to provide costimulatory signals to engineered T-cells following antigen exposure, with a limiting factor being sensitization of T-cells to Fas-FasL mediated death[496]. LCL161 has been found to inhibit ABCB1 drug transport activity[497], and birinapant (a dimeric SMC)-induced reductions in cIAP1 resulted in a mesenchymal transition of GSCs, characterized by increases in self-renewal potential and increased expression of CD44, TNFα, MMP9, vimentin and ALDH1A3[498].

In the context of GBM, our lab has shown combination of SMCs with ICB, notably αPD-1, enhances anti-tumoral immunity and produces long-term durable cures characterized by potent anti-GBM immune memory[182]. Despite these promising extensions in survival, not all tumors are cured and much of its neuroimmune effects remain unexplored.

1.5 Hypothesis and Objectives

I hypothesized that exposure to the CNS milieu provided GBM cells intrinsic and extrinsic mechanisms of resistance against SMC-mediated cell death and to SMC and αPD-1

immunotherapy. My overall objective was to identify and exploit these resistance mechanisms. My specific aims are to:

1) Characterize resistance of murine GBM to SMC-mediated inflammatory cell death
2) Characterize the role of astrocytes and macrophages/microglia in SMC-mediated GBM killing
3) Explore dose-escalation for improved SMC and αPD-1 therapeutic efficacy
4) Explore the role of TGFβ in treatment resistance

2.0 Materials and Methods

2.1 Cell culture

Cells were maintained at 37ºC and 5% CO_2 in DMEM media supplemented with 10% heat inactivated calf serum, 1% non-essential amino acids, and penicillin-streptomycin (Invitrogen; Waltham, Massachusetts, USA). All cell lines were obtained from ATCC, with the following exceptions: BV2 (Dr. Shawn Hayley, Carleton University) and SMA-560 (A-9051, EMD Millipore; Burlington, Massachusetts, USA). BV2-EGFP cells were generated using IncuCyte NucLight Green reagent (4626) from Sartorius/Essen Bioscience (Ann arbor, Michigan, USA). For hypoxia experiments, oxygen levels were altered using ProOx 110 Compact O2 controller (RRID: SCR_021129) from Biospherix Ltd (Parish, New York, USA). No glucose conditions were achieved using DMEM complete media without glucose (11966025) from Thermo Fisher (Waltham, Massachusetts. USA). Mouse primary cortical astrocytes (M1800-57) and microglia (M1900-57) were purchased from ScienCell (Carlsbad, California, USA). Astrocytes were cultured in astrocyte media from ScienCell (1801), supplemented with 2% FCS, 1% penicillin/streptomycin and 1% astrocyte growth serum (ScienCell). For culture on ECM

proteins, cells were seeded on culture plates coated with HyStem-C cell culture scaffold kit (HYSC020) from Sigma Aldrich (St. Louis, Missouri, USA).

For brain slice cultures, slices were generated and maintained as previously described[499]. Briefly, naïve 5-7 week old C57BL/6 mice were sacrificed and their cortices isolated. Forebrain was fixed in ultra low melting point agarose. Embedded brain was cut on ice into 250µm slices using as Leica Biosystems (Wetzlar, Germany) VT1000 S vibratome. Slices were placed into a 0.4µm Millicell cell culture insert from Sigma (PICM0RG50), which was in turn placed in a 6 well plate overtop NeuroCult Neural Stem Cell Media (05700), supplemented with recombinant basic FGF (79003) and EGF (78006) from StemCell (Vancouver, British Columbia, Canada). Two days later slices were imaged and visually assessed for viability or contamination; healthy slices were kept and the rest discarded. Following this, an indentation was made in the left striatum using a 10µL pipette tip and $5x10^3$ CT2A-mKate cells were implanted in and around the indentation pit. The following day, adherence of cells on brain tissue was confirmed using an EVOS fluorescent microscope. Media was changed every 2-3 days. After five days of growth, whole slices were imaged using an EVOS FL Auto fluorescent microscope (Thermo Fisher) to give a baseline CT2A-mKate2 count. Following this, either fresh media, 1µM LCL161 + 10ng/mL TNFα or 10µM LCL161 + 10ng/mL TNFα was added to the culture media below the insert. After 24 hours, slices were again imaged using the EVOS fluorescent microscope. Surviving red CT2A-mKate nuclei were manually counted using ImageJ, and the percent change from baseline prior to treatment was calculated.

For spheroid cultures, 400 cells/well of CT2A or GL261 cells were plated on Corning (Corning, New York, USA) Costar ultra low attachment well plates (CLS7007) in NeuroCult Neural Stem Cell media supplemented with bFGF and EGF. Growth was tracked using Incucyte live cell

analysis system. T-cell:GL261 co-cultures were performed as previously described[500]. Briefly, 200μL of peripheral blood was drawn from animals 7 days post-reimplantation. Red blood cells were lysed using ACK lysing buffer (A1049201) from Thermo per manufacturers protocol. GL261 cells were plated at $1x10^5$ cells/well in a 96 well plate and treated for 24h with 75U IFNγ. Media was removed, cells were washed and isolated leukocytes were plated with monolayer GL261 cells in triplicate per animal. All wells were treated with GolgiPlug (1μL/mL media). Negative control was naïve leukocytes. Positive control was treatment with PMA (20ng/mL) and Ionomycin (1μg/mL). Following 4 hours of co-culture or stimulation, cells were collected for flow cytometric analysis.

2.2 *In vitro* viability assays

Cell lines were seeded at $1x10^4$ cells/well in 96-well plates and incubated overnight. Cells were treated with 50% dilution series of LCL161, TNFα, TRAIL, the combination, YM155 or matched DMSO and media control for 24h, 48h or 72h. Viability was assessed using Alamar blue (7x resazurin sodium salt (R7017;Sigma)). Spectral absorbance was assessed using a spectrophotometer (Synergy microplate reader, Biotek). Wavelength corrections and absorbance readings were quantified using associated Gen5 software. Treated cell readouts were normalized to matched vehicle control. All viability assays were performed with at least 3 technical replicates.

2.3 Chemical compounds and cytokines

LCL161 (S7009) was purchased from SelleckChem (Houston, Texas, USA) or provided by Novartis (Basel, Switzerland). AZD-5582 (A-9051) was purchased from Active Biochem. YM155/Sepantronium Bromide (S1130) was purchased from SelleckChem.

Mouse TNFα (410-MT-010), IL-1β (401-ml) and TGFβ (7666-MB-005) were purchased from R&D systems (Minneapolis, Minnesota, USA). Murine IFNγ was purchased from R&D systems (4875-M1) or Peprotech (315-05; Cranbury, New Jersey, USA). Murine IL-4 (214-14) was purchased from Peprotech. Mouse IL-10 (575806) was purchased from BioLegend (San Diego, California, USA). LPS (Tlrl-peklps) was purchased from Invivogen (San Diego, California, USA). Recombinant mouse TRAIL (1121-TL-010) was purchased from R&D Systems.

zVAD-FMK (FMK001) was purchased from R&D systems. Necrostatin-1 (N9037) and Evan's Blue dye (E2129-10G) were purchased from Sigma Aldrich. GolgiPlug protein transport inhibitor (555029) was purchased from BD Biosciences (Franklin Lakes, New Jersey, USA). Ionomycin calcium salt was purchased from Millipore Sigma (P1585) or Life Technologies (I24222; Carlsbad, California, USA). PMA (P1585) was purchased from Millipore Sigma.

2.4 Brain tumor models

All animal experiments were conducted with the approval of the University of Ottawa Animal Care and Veterinary Service in concordance with guidelines established by the Canadian Council on Animal Care. Female 6-week old C57BL/6 mice were anesthetized with isofluorane and the surgical site prepared. $5x10^4$ CT2A or GL261 cells were implanted stereotactically over 1 minute in a 10μL volume in the left striatum at coordinates: 0.5mm anterior, 2mm lateral from bregma, 3.5mm deep. Skin was closed using surgical glue. Features of murine GBM cells are reviewed in Table 1.

Mice were treated via oral gavage with either vehicle (30% 0.1M HCl, 70% 0.1M NaOAc pH 4.63) or LCL161 (75mg/kg or 100mg/kg) resuspended in 30% 0.1N HCl and 70% CH3COONa. For treatment with checkpoint inhibitors, mice were treated with anti-PD-1 clones J43 (BE0033-

2), 29F.1A12 (BE0273) or RMP1-14 (BE0146) or IgG2A isotype control (BE0089 or BE0091, where applicable) from BioXcell (Lebanon, New Hampshire, USA). For experiments using anti-VEGFR2 (BioXcell, BE0060-25MG-A), treatments were 40mg/kg initially followed by 20mg/kg maintenance every 3-4 days over 2 weeks for a total of 3 treatments. For experiments using anti-TGFβ (BioXcell, BE0057), treatments were 5mg/kg 3x/week for 2 weeks concurrent with anti-PD-1 treatments. Animal endpoint criteria include loss of >20% body weight, hunched posture, lethargy and significantly impaired ambulation. For isolation of endpoint tumor cells, animals at endpoint were sacrificed, tumor bulk dissected from brain, and CT2A or GL261 cells isolated using Tumor Cell Isolation Kit (130-110-187) from Miltenyi Biotec (Bergisch Gladbach, North Rhine-Westphalia, Germany). Experimental groups were not blinded and no randomization of treatment groups were performed. Sample size was consistent with previous reports but no statistical methods were used to determine sample size [97,182,501].

For tumor vasculature permeability assessments, 100μL Evan's blue dye was injected into tail vein. After 45 minutes of circulation, mice were euthanized and tumor, brain and kidneys were collected and weighed. Tissues were submerged in formamide overnight in a water bath at 55ºC. Next day samples were centrifuged at 10,000G for 40 mins and 100μL of resulting solutions were added in triplicate to 96-well plates. Absorbance was read at 620nm using spectrophotometer and ng/mL Evan's blue was calculated using organ weights.

Table 1: Features of common murine GBM cell lines

	CT2A	GL261	SMA560
Original Description	Seyfried *et al*., 1992[502]	Zimmerman *et al*., 1941[503]	Fraser, 1971[504]
Method of Generation	20-methylcholanthrene (20-MC) implantation into B6 mice. Tumours arise 450 days post 20-MC implant. CT2A generated following serial subcutaneous passages	3-methylcholanthrene pellet implantation into C57BL/6 mice brains, maintained via serial passaging[505]	Spontaneous, generated line following SC implant[506]
Histology	Highly malignant, poorly differentiated anaplastic astrocytoma Pleomorphic, hyperproliferative, infiltrative. Pseudopalisading necrosis, vascular proliferation[507]	Radial growth pattern[505] Poorly differentiated Highly proliferative, angiogenic Centralized necrosis[508]	Little pleomorphism Anaplastic astrocytoma[504] Grows well circumscribed mass, infiltrative Rare focal necrosis, vascular proliferation Secretes TGFβ[509–511]
Background	C57BL/6	C57BL/6	VM/Dk

2.5 Western Blotting

Cells were scraped, collected by centrifugation and lysed in RIPA lysis buffer (Thermo Fisher) containing protease inhibitor cocktail (Roche; Basel, Switzerland). Equal amounts of protein were separated on polyacrylamide gels followed by transfer to 0.2µm nitrocellulose membranes (1620112, Bio-Rad (Hercules, California, USA)). Membranes were blocked using Intercept blocking buffer (927-65001, LI-COR Biosciences (Lincoln, Nebraska, USA)). Individual proteins were detected using antibodies for: cIAP1/2 (1:1000, CY-P1041, Cyclex); XIAP (1:1000, 20422S, Cell Signaling (Massachusetts, USA)); Caspase-8 (1:1000, R&D Systems); Caspase-3 (1:1000, 9662S, Cell Signaling); and PARP (1:1000, P532S, Cell Signaling). Antibodies were diluted in Intercept antibody diluent (927-65001, LI-COR Biosciences). Primary antibodies were incubated overnight at 4ºC and subsequently detected using AlexaFluor 680 (Invitrogen) incubated for 1 hour at room temperature. β-tubulin (E7, DSHB (Iowa City, Iowa, USA)) loading control was detected using IRDye 800 (926-32211, LI-COR Biosciences) incubated for 1 hour at room temperature. Fluorescent signals were detected using Odyssey Infrared Imaging System (LI-COR Biosciences).

2.6 Microscopy

Detection of CT2A-mKate2 and BV2-EGFP cells were performed in an incubator outfitted with an Incucyte Zoom microscope under 10x objective. For assessment of cell counts, numbers immediately before and at indicated timepoints after treatments were used for calculations of percent change from baseline. For assessment of cleaved caspase-3, Incucyte Caspase-3/7 dye for apoptosis from Essen Bioscience (4440) was used. For assessment of phagocytosis, Incucyte pHrodo red E.coli bioparticles from Essen bioscience (4615) were used. Quantification of fluorescent signal was processed using Incucyte Zoom software. For brain slice cultures, phase

and fluorescent images were acquired using EVOS FL Auto on stitched 20x objective images. For astrocyte GFAP fluorescence, mouse cortical astrocytes were grown on ibidi microslide 8 well chambered coverlips (80826) and treated for 24h with DMSO, 10μM LCL161, 500ng/mL LPS or 10ng/mL TNFα. Cells were then stained in-well for GFAP expression (ab10062, Abcam, 1:100) and images were acquired on Zeiss (Baden-Wurttemberg, Germany) Axio Imager.M2 at 20x objective. For tumor-bearing whole brain stains, mice were transcardially perfused on day 18 post-implant and formalin-fixed in 4% paraformaldehyde for 48h. Fixed brains were sent to the Louise Pelletier Histology Core at the University of Ottawa for paraffin embedding and slicing (4μm thick slices). Slices were stained using the Akoya (Marlborough, Massachusetts, USA) Opal polaris 7-color IHC detection kit (NEL811001KT) using previously established protocols[515]. Background autofluorescence was quenched using TrueBlack lipofuscin autofluorescence quencher (1:20, 10119-144, Biotium (Fremont, California, USA)). Brains were stained with DAPI (0.5μg/mL, PerkinElmer (Waltham, Massachusetts, USA)), anti-moouse GFAP (1:100, MA5-12023, Life Technologies) following pH9 antigen retrieval, Opal Polymer HRP Ms+Rb (ARH1001EA, Akoya Biosciences) and signal generated using Opal 570 dye (1:100 in 1x Plus amplification diluent, FP1609, Akoya). Slides were mounted and IHC images acquired using Zeiss AxioImager Z2 widefield microscope with Colibri 5/7 and Apotome at 10x. Images were stitched in Zeiss Zen Black software. Analysis was performed using ImageJ.

2.7 Flow Cytometry

All antibodies and associated details used for flow cytometry are listed in Table 2. For chronic LCL161 treatments, GL261 and CT2A cells were treated daily for 10 days with 10μM LCL161 or matched DMSO. Cells were lifted from plates using non-enzymatic cell dissociation buffer (C5914) from Sigma and stained for viability using Zombie Violet fixable viability dye. For flow

on *in vivo* tissues, organs were collected on day 11 (*in vivo* TGFβ treated) or day 18 (all other *in vivo* flow) post-implant. Tissues were dissociated using gentleMACS dissociator (130-096-427) from Miltenyi Biotec. Resulting solutions were strained through 70µm cell strainers (352350, Corning (Corning, New York, USA)) prior to counting and normalization of populations across analyzed groups. Cells were stained with Fc block (anti-CD16/CD32) and Zombie viability dyes at 1:300 dilution prior to surface stains. Cells were fixed using intracellular fixation solution (ThermoFisher/eBioscience, 88-8824-00). If intracellular targets were being analyzed, cells were permeabilized using permeabilization buffer as per manufacturers protocol. Intracellular targets were stained same day as analysis. Antibody stains were performed at 1:200 dilution unless otherwise indicated. Cells were analysed on a BD Fortessa (BD Biosciences) flow cytometer. Data was analysed using FlowJo software (BD Biosciences). Compensation was performed using UltraComp eBeads (01-222-42) from ThermoFisher/Invitrogen.

2.8 Statistical Analysis

Comparison of Kaplan-Meier survival plots was conducted by log-rank analysis and subsequent pairwise multiple comparisons were performed using the Holm-Sidak method (GraphPad). Comparison between multiple treatment groups was analysed using one- or two-way ANOVA followed by post hoc analysis using Tukey's multiple comparison test (GraphPad). Comparison of treatment pairs was analysed by two-sided t-tests (GraphPad). Lines within bar graphs represent mean with standard error. Area under curve was calculated using GraphPad.

Table 2: Antibodies used in Flow Cytometric Analyses

Target	Conjugate	Manufacturer	Catalogue #
TruStain FcX (anti-mouse CD16/32)		BioLegend	101320
Zombie Violet Fixable Viability Kit	BV421 Equivalent	BioLegend	423114
Zombie Green Fixable Viability Kit	AF488/GFP Equivalent	BioLegend	423112
Anti-mouse phosphatidylserine	AF488	Sigma Aldrich	16-256
Anti-mouse calreticulin	PE	Novus	NBP1-47518PE
Anti-mouse IFNγ	PE	BioLegend	505808
Anti-mouse TNFα	APC	BioLegend	506308
Anti-mouse IDO1	AF647	BioLegend	654004
Anti-mouse KLRG1	FITC	BioLegend	138410
Anti-Mouse MHCI (H-2Kd/H-2Dd)	AF647	BioLegend	114712
Anti-Mouse MHCII (I-A/I-E)	BV605	BioLegend	107639
Anti-mouse Qa-1b	BV786	BD Biosciences	744390
Anti-mouse Qa-2	FITC	BioLegend	121710
Anti-Mouse CCR7	BV605	BioLegend	120125
Anti-mouse CTLA4	BV605	BioLegend	106323
Anti-mouse PD-L2	APC	BioLegend	107210
Anti-mouse PD-L1	BV421	BioLegend	124315
Anti-mouse CD86	BV786	BioLegend	105043
Anti-mouse CD80	AF488	BioLegend	104716
Anti-mouse Galectin-9	APC	BioLegend	136110
Anti-mouse OX40	PE	BioLegend	119409
Anti-mouse Ki67	BV711	BD Biosciences	563755
Anti-mouse PD-1	BV605	BioLegend	135220
Anti-mouse LAG3	BV711	BioLegend	125243
Anti-mouse TIM3	PE	BioLegend	119703
Anti-mouse Ly6C	AF488	BioLegend	128022
Anti-mouse Ly6G	BV786	BioLegend	127645
Anti-mouse F4/80	AF700	BioLegend	123130
Anti-mouse F4/80	APC	eBioscience Thermofisher	17-4801-80
Anti-mouse CD3	BV786	BioLegend	100232
Anti-mouse CD3	APC/Cy7	BioLegend	100222
Anti-mouse CD3	Pacific Blue	BioLegend	100214
Anti-mouse CD3	FITC	BioLegend	100306 & 100204
Anti-mouse CD4	AF700	BioLegend	100536
Anti-mouse CD8	FITC	BioLegend	100706
Anti-mouse CD8	FITC	Invitrogen	MA5-16759
Anti-mouse CD11b	APC	BioLegend	101212

Anti-mouse CD11b	PE	BioLegend	101207
Anti-mouse CD25	APC	eBioscience	17-0251-81A
Anti-mouse CD44	APC	BioLegend	103012
Anti-mouse CD44	PE	eBioscience	12-0441-82
Anti-mouse CD45	BV786	BioLegend	103149
Anti-mouse CD45	PE	BioLegend	147712
Anti-mouse CD69	BV605	BioLegend	104529
Anti-mouse CD86	PE	BioLegend	105007
Anti-Mouse CD127	AF488	BioLegend	135018

3.0 Results

3.1 Dose, CNS location and age limit SMC-based GBM killing

3.1.1 SMC and TNFα significantly reduce viability of GBM cells

To evaluate GBM sensitivity to SMC treatments, the viability of human GBM cell lines was assessed following application of a dilution series of LCL161 and TNFα. Of the 9 analyzed cell lines, 5 were resistant (SF539, SNB19, U343, U373, SF268) and four were sensitive (SF295, SNB75, M059K, U118) in a dose-dependent fashion to the combination (Figure 4A), in keeping with previous findings showing differences in cFLIP processing mediate sensitivity to SMC and TNFα despite intact death receptor pathways[176]. All human lines are sensitive to chemical inhibition of survivin via YM155 treatment (Figure 4B,C), while no murine GBM cells are (Figure 4D), suggesting differential IAP expression and dependencies between species. Previous reports have shown primary patient GBM cells express TRAIL receptors and several GBM cell lines are sensitive to TRAIL treatment[516]. I aimed to evaluate sensitivity of a panel of GBM cell lines to TRAIL, alone or in combination with SMCs. No dose-dependent reductions in viability were observed following TRAIL treatment in human (Figure 5A) or murine (Figure 5C) GBM cells. Combination with LCL161 reduced viability in a dose-dependent manner only in SNB75 cells (Figure 5B). CT2A and GL261 murine GBM cells were completely resistant (Figure 5D).

Murine GBM cell lines were treated with a dilution series of LCL161, TNFα or the combination and viability assessed as before. Single agent treatments had no effect on viability (Figure 6A,B), except in the case of LCL161 at 50μM, a dose previously characterized to cause lytic cell death[517]. The combination LCL161 and TNFα resulted in significant reductions in viability in a dose dependent fashion across all three examined murine GBM lines (Figure 6C).

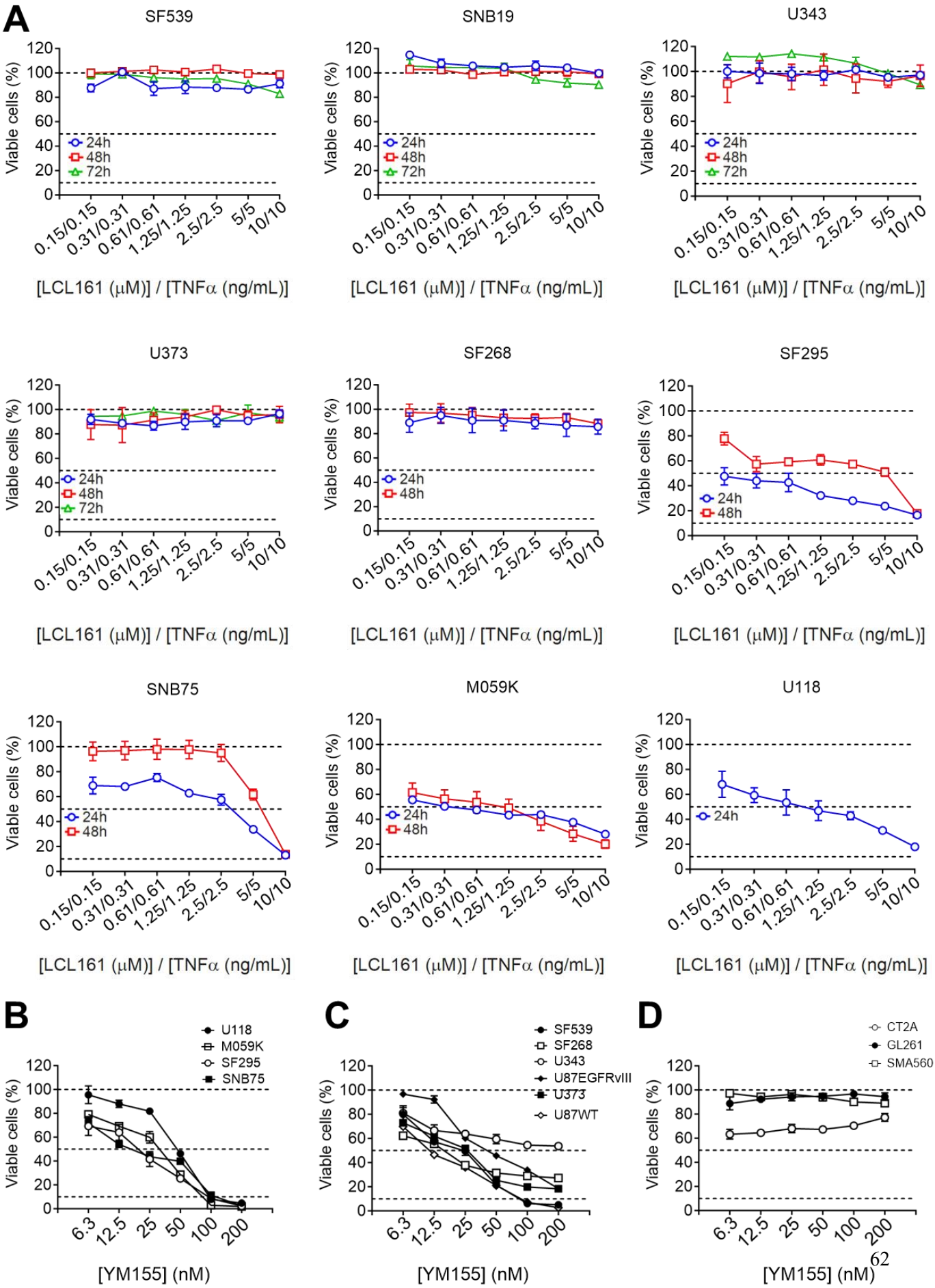
A
SF539
SNB19
U343
U373
SF268
SF295
SNB75
M059K
U118
Viable cells (%)
24h
48h
72h
0.15/0.15
0.31/0.31
0.61/0.61
1.25/1.25
2.5/2.5
5/5
10/10
[LCL161 (μM)] / [TNFα (ng/mL)]
B
U118
M059K
SF295
SNB75
[YM155] (nM)
C
SF539
SF268
U343
U87EGFRvIII
U373
U87WT
[YM155] (nM)
D
CT2A
GL261
SMA560
[YM155] (nM)

Figure 4: Human GBM cells respond to IAP inhibition. A) SF539, SNB19, U343, U373, SF268, SF295, SNB75, M059K and U118 immortalized human GBM cells were treated with a dilution series of combined LCL161 and TNFα for indicated treatment times. N=3 technical replicates per treatment group. Cell viability was assessed using Alamar blue. N=1 independent experiment per timepoint. B,C) Human GBM lines sensitive (B) and resistant (C) to combination LCL161 and TNFα were treated with a dilution series of YM155 for 24h. N=3 technical replicates per treatment group. Cell viability was assessed using Alamar blue. N=1 independent experiment per timepoint. D) Murine GBM cells were treated with dilution series of YM155 for 24h. N=3 technical replicates per treatment group. Cell viability was assessed using Alamar blue. N=1 independent experiment per timepoint.

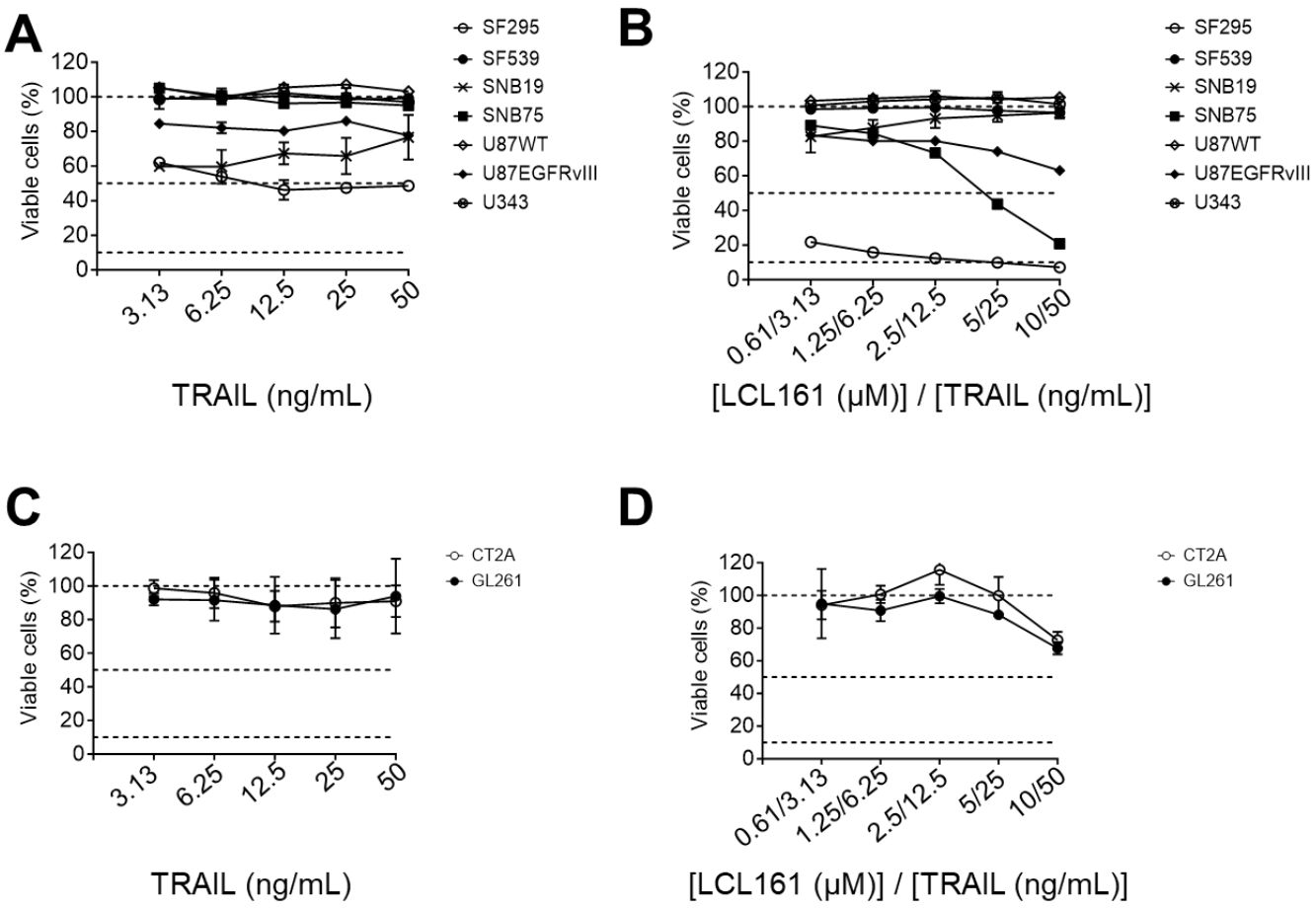

Figure 5: Few GBM lines respond to TRAIL. A,B) SF295, SF539, SNB19, SNB75, U87WT, U87EGFRvIII and U343 immortalized human GBM cells were treated with indicated dilution series of TRAIL (A) or TRAIL in combination with LCL161 (B) for 24hr. C,D) The same treatments as in A) and B) were performed on CT2A and GL261 murine GBM cells. N=3 technical replicates per treatment group. Cell viability was assessed using Alamar blue. N=1 independent experiment per timepoint.

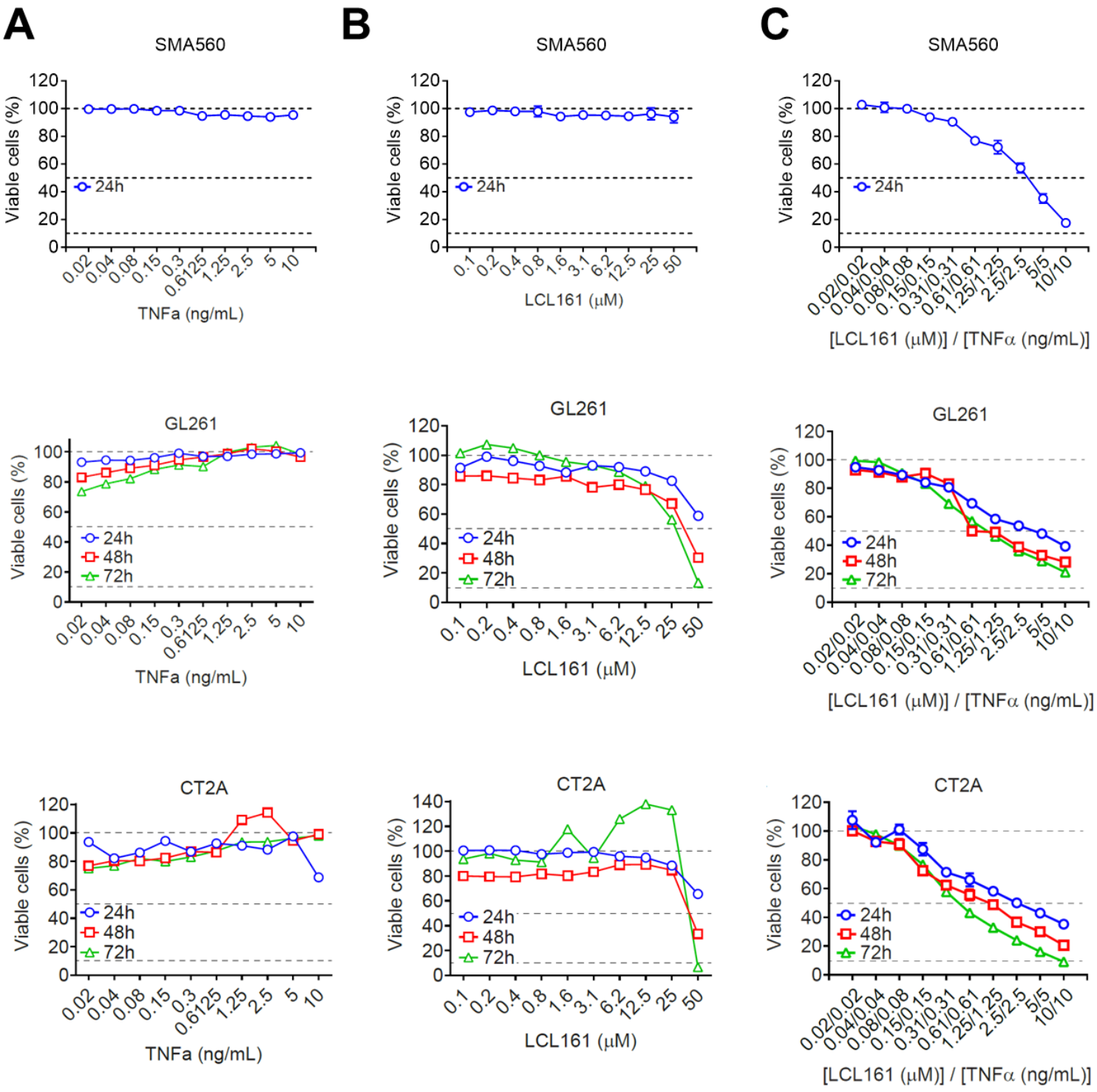
A
B
C
SMA560
GL261
CT2A
Viable cells (%)
24h
48h
72h
TNFa (ng/mL)
LCL161 (μM)
[LCL161 (μM)] / [TNFα (ng/mL)]
0.02
0.04
0.08
0.15
0.3
0.6125
1.25
2.5
5
10
0.1
0.2
0.4
0.8
1.6
3.1
6.2
12.5
25
50
0.02/0.02
0.04/0.04
0.08/0.08
0.15/0.15
0.31/0.31
0.61/0.61
1.25/1.25
2.5/2.5
5/5
10/10

Figure 6: Murine GBM cells respond to SMC-mediated treatments *in vitro*. SMA560, GL261 and CT2A murine GBM cells treated with dilution series of A) TNFα, B) LCL161 or C) the combination for indicated treatment times. Viability was assessed using Alamar blue. N=3 technical replicates per treatment group. N=1 independent experiment per timepoint.

Given that TNFR1-mediated cell death can occur through apoptotic or necroptotic mechanisms, and given that necroptosis represents a more inflammatory mode of cell death[518], I sought to determine the preferential mechanism for each cell line. Robust caspase-3/7 activation is seen following high dose LCL161 (10μM) and TNFα (10ng/mL) treatment in both cell lines (Figure 7A,B). Concurrent treatments with pan-caspase (zVAD-FMK) or RIPK1 (necrostatin-1) inhibitors showed that CT2A cells die in a RIPK1 and caspase-dependent manner, consistent with apoptosis (Figure 7C), while GL261 dies in a caspase-independent, RIPK1-dependent manner, consistent with necroptosis (Figure 7D).

To assess whether CT2A and GL261 cells express immunomodulatory proteins conducive to T-cell activation and recognition, and whether these are inducible via cytokine stimulation or LCL161 treatment, expression of various surface peptides was assayed via flow cytometry. Both cell lines express MHCI at a basal level, which is significantly increased following treatment with IFNγ (Figure 8A,B). CT2A shows no basal or inducible expression of MHCII, while IFNγ induces substantial increases in expression in GL261 cells (Figure 8C). No differences in expression of PD-L2, PD-L1, CD86, CD80 or Galectin-9 were observed following treatment with LCL161 (Figure 8D). Both CT2A and GL261 cells undergoing LCL161 and TNFα-mediated cell death express and expose the DAMP phosphatidylserine (Figure 8E,F).

Together, these data indicate that murine GBM cells express surface markers conducive to phagocytosis by APCs (phosphatidylserine), to T-cell recognition (MHCI and MHCII), and immune checkpoint ligands able to restrict T-cell killing (PD-L1, Galectin-9). Given these and results from the previous viability assays, it is reasonable to presume murine GBM cells will undergo SMC-mediated inflammatory cell death *in vivo* in combination with ICB, leading to long-term cures. Orthotopic intracranial implants of CT2A or GL261 were cleared by

combination LCL161 (75mg/kg) and αPD-1 (10mg/kg) treatment over 2 weeks (Figure 8G), with long term cures in CT2A (40%) and GL261 (20%)-bearing animals (Figure 8H,I respectively) similar to previously published findings[182]. Thus, despite the significant cytotoxicity of SMCs *in vitro*, several tumors fail to respond *in vivo*, suggesting TME features are limiting SMC efficacy.

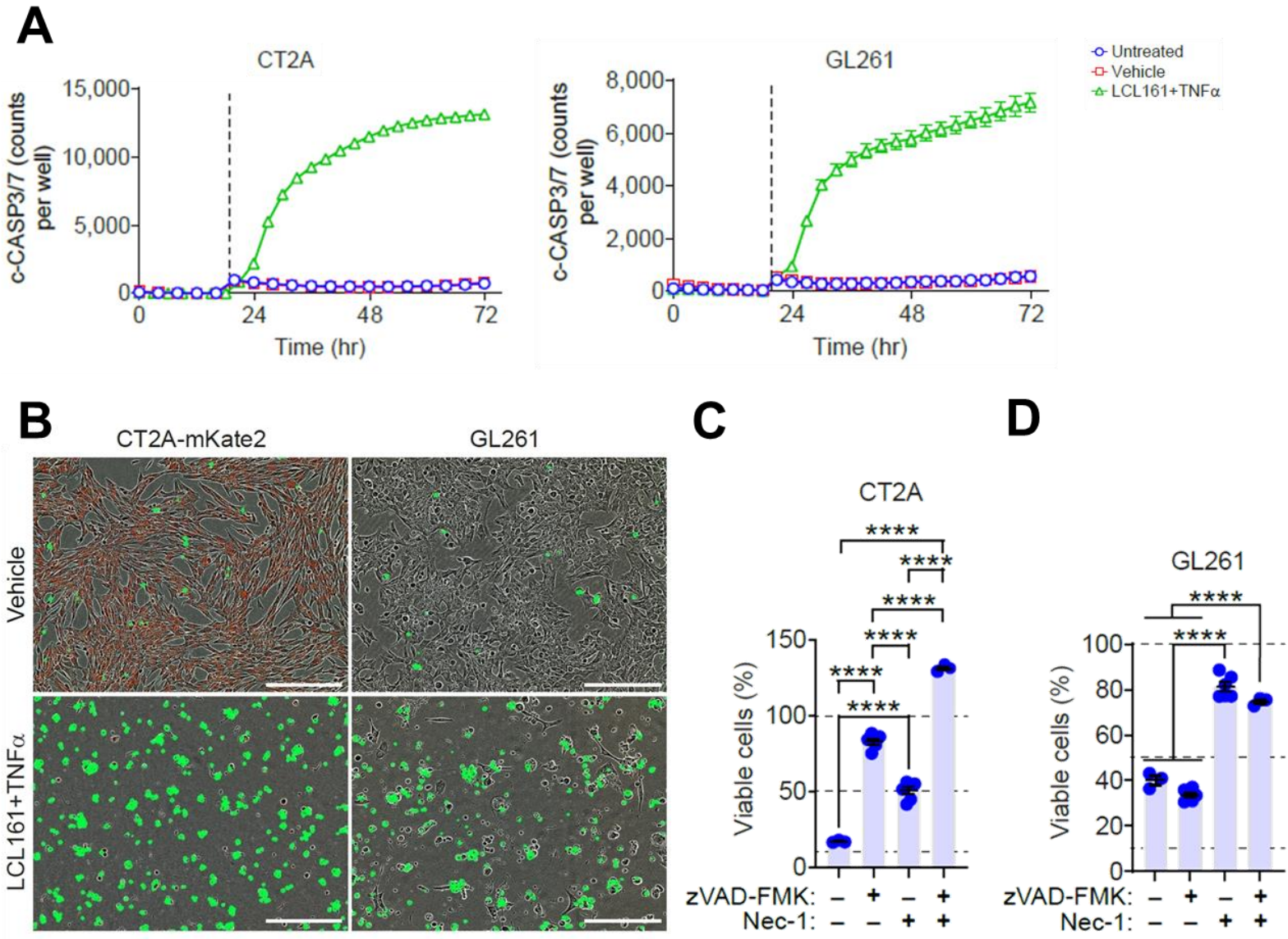

Figure 7: SMC-induced murine GBM cell death requires RIPK1. A,B) CT2A-mKate2 and GL261 cells were treated with vehicle or 10μM LCL161 and 10ng/mL TNFα in the presence of the caspase-3/7 substrate DEVD488. Images were acquired via time-lapse microscopy and DEVD488 positivity quantified and plotted. N=3 per treatment group. Imaged in B) are representative micrographs at 24h post-treatment. Scale bar: 300μm. C) CT2A and D) GL261 cells were treated with 10μM LCL161 and 10ng/mL TNFα in the presence of the pan-caspase inhibitor zVAD-FMK (20μM) and/or the RIPK1 inhibitor necrostatin-1 (50μM). Cell viability was assessed using Alamar blue. N=3 technical replicates for naïve or double-inhibitor treatment groups. N=5 technical replicates for individual inhibitor treatments. N=1 independent experiment per timepoint. ****P<0.0001 by Two way ANOVA using Tukey's HSD multiple comparison test.

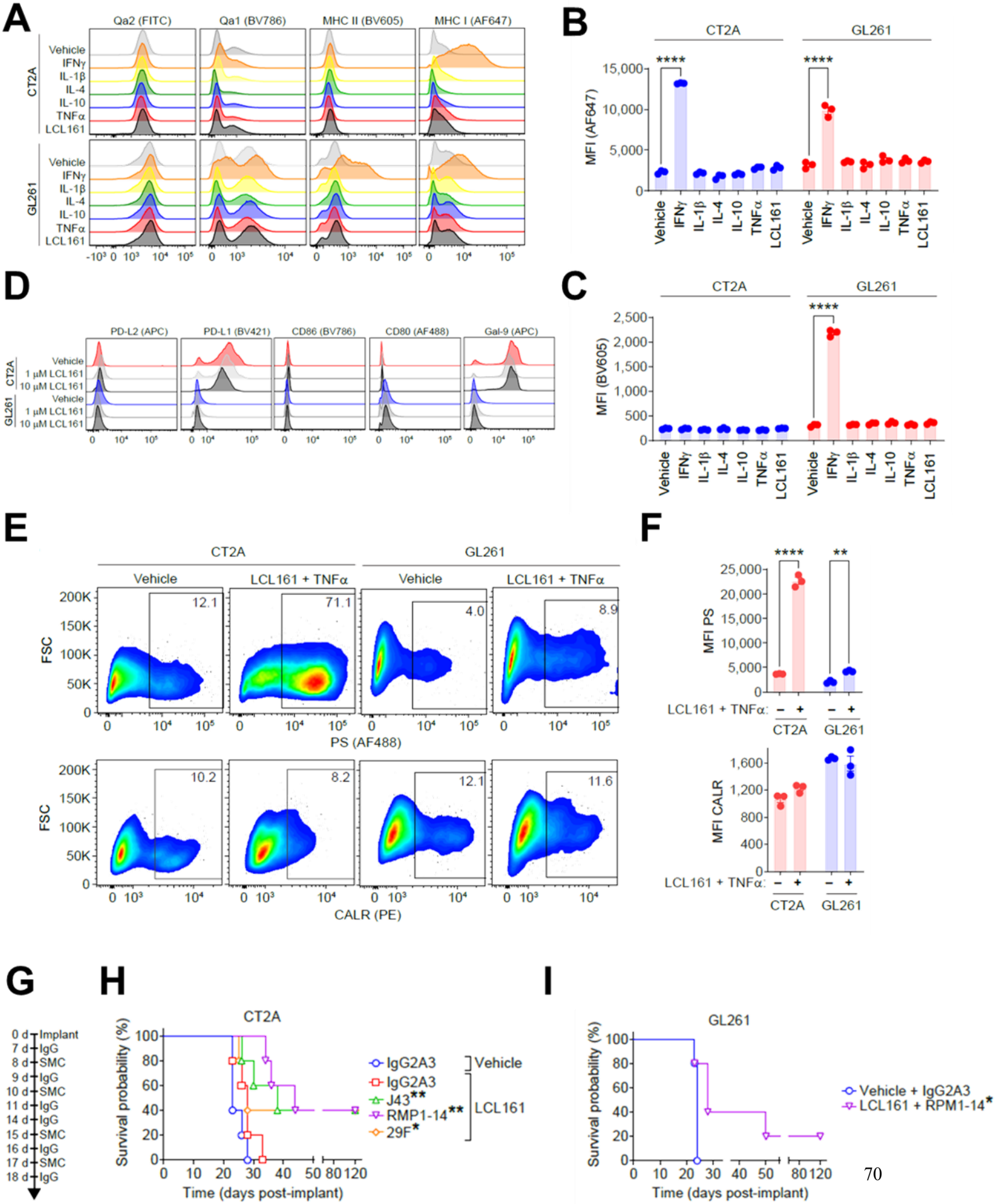
A
Qa2 (FITC)
Qa1 (BV786)
MHC II (BV605)
MHC I (AF647)
CT2A
GL261
Vehicle
IFNγ
IL-1β
IL-4
IL-10
TNFα
LCL161
B
CT2A
GL261
MFI (AF647)
****
C
MFI (BV605)
D
PD-L2 (APC)
PD-L1 (BV421)
CD86 (BV786)
CD80 (AF488)
Gal-9 (APC)
1 μM LCL161
10 μM LCL161
E
LCL161 + TNFα
FSC
PS (AF488)
CALR (PE)
12.1
71.1
4.0
8.9
10.2
8.2
12.1
11.6
F
MFI PS
**
MFI CALR
G
0 d Implant
7 d IgG
8 d SMC
9 d IgG
10 d SMC
11 d IgG
14 d IgG
15 d SMC
16 d IgG
17 d SMC
18 d IgG
H
Survival probability (%)
Time (days post-implant)
IgG2A3
J43**
RMP1-14**
29F*
Vehicle
LCL161
I
Vehicle + IgG2A3
LCL161 + RPM1-14*

Figure 8: Murine GBM cells express immunomodulatory proteins and respond to SMC-mediated treatments *in vivo*. A) Flow cytometric analysis of Qa2 (FITC), Qa1 (BV786), MHCII (BV605) and MHCI (AF647) expression on CT2A and GL261 cells treated with IFNγ (50U), IL-1β (20ng/mL), IL-4 (20ng/mL), IL-10 (20ng/mL), TNFα (10ng/mL) or LCL161 (10μM). B,C) Mean fluorescent intensity (MFI) of B) MHCI and C) MHCII in response to treatments in CT2A and GL261 cells. N=3 for all treatment groups. ****P<0.0001 by two-way ANOVA using Tukey's HSD multiple comparison test. D) Flow cytometric analysis of PD-L2 (APC), PD-L1 (BV421), CD86 (BV786), CD80 (AF488) and Galectin-9 (APC) expression on CT2A and GL261 cells treated with vehicle (DMSO) or LCL161 (1μM or 10μM) for 24 hr. E,F) Flow cytometric analysis of phosphatidylserine (PS; AF488) and calreticulin (CALR; PE) expression on CT2A and GL261 cells treated with 10μM LCL161 and 10ng/mL TNFα. Bar plots are MFI of PS and CALR expression. N=3 per treatment group. **P<0.01; ****P<0.0001 by two-way ANOVA using Tukey's HSD multiple comparison test. G-I) Mice were implanted with $5x10^4$ CT2A or GL261 cells and treated orally with vehicle or 75mg/kg LCL161 and intraperitoneally with 10mg/kg of indicated control or αPD-1 antibody (J43, RMP1-14 or 29F clones). Data represent Kaplan-Meier curve of mouse survival, log-rank with Holm-Sidak multiple comparison. N=5 per treatment group. *P<0.05; **P<0.01.

3.1.2 In vivo features minimally protect against SMC and TNFα cytotoxicity

To assess whether exposure to the CNS microenvironment and SMC and αPD-1 cotherapy lead to the acquisition of cell intrinsic resistance mechanisms to SMCs, and in so doing identify potential novel targets for rational combination, I isolated tumor cells from mice treated with LCL161 and αPD-1 that reached endpoint and evaluated responsiveness to LCL161 and TNFα ex vivo. In all cases, GBM cells remained sensitive to LCL161 and TNFα cotreatment in a dose-dependent fashion (Figure 9A,B), suggesting resistance was a transient effect of the *in vivo* microenvironment.

To determine whether the BBB limited drug delivery to tumor, Evan's blue dye was administered on day 18 post-implant of CT2A cells. In each of the three mice examined, dye was excluded from normal brain (intact BBB) and accumulated in significantly greater proportions in tumor and kidney (Figure 9C,D), suggesting the BBB is not a limiting factor for LCL161 delivery to tumor bulk. This is in keeping with previous findings illustrating a tumor-specific degradation of cIAP1/2 following LCL161 treatments[182]. Repeat cotreatments of LCL161 and TNFα failed to produce populations resistant to subsequent treatments (Figure 9E), suggesting resistant clones are not generated and escape was due to availability of drug or cytokine.

To determine whether aspects of the in vivo setting conferred resistance to SMC-mediated cell death, individual *in vivo* tumor features were recapitulated *in vitro*. Both CT2A and GL261 cells express CD44, the ligand for HA (Figure 9F,G), and sensitivity to LCL161 and TNFα is reduced in both when cultured on HA-containing ECM protein mixes (Figure 9H). When cultured under hypoxic and/or hypoglycemic conditions, GL261 cells again showed slight but significant protection from the combination (Figure 9I). Conversely, no significant effects were observed in CT2A cells under the same conditions, and lack of glucose significantly reduced baseline

viability (Figure 6J). Therefore, brain ECM and hypoxic, hypoglycemic conditions provide minimal protection against SMC-induced cell death.

To better recapitulate three-dimensional *in vivo* tumor structure and microenvironment and determine whether these contribute to reduced sensitivity to SMCs, CT2A-mKate2 and GL261 cells were grown under sphere-forming conditions. High dose LCL161 and TNFα contributed to significant reductions in sphere size (Figure 10A-C), suggesting the three-dimensional nature of *in vivo* tumors does not diminish efficacy of SMC-mediated cell death. When CT2A-mKate2 cells were grown on organotypic brain slice cultures (Figure 10D) sensitivity to medium dose LCL161 and TNFα was abolished, although significant reductions in cell numbers were still observed at high doses (Figure 10E,F). Together, these data suggest sensitivity remains even when exposed to common CNS and TME conditions assessed *ex vivo*, assuming sufficient dose of SMC and TNFα reaches the tumor site.

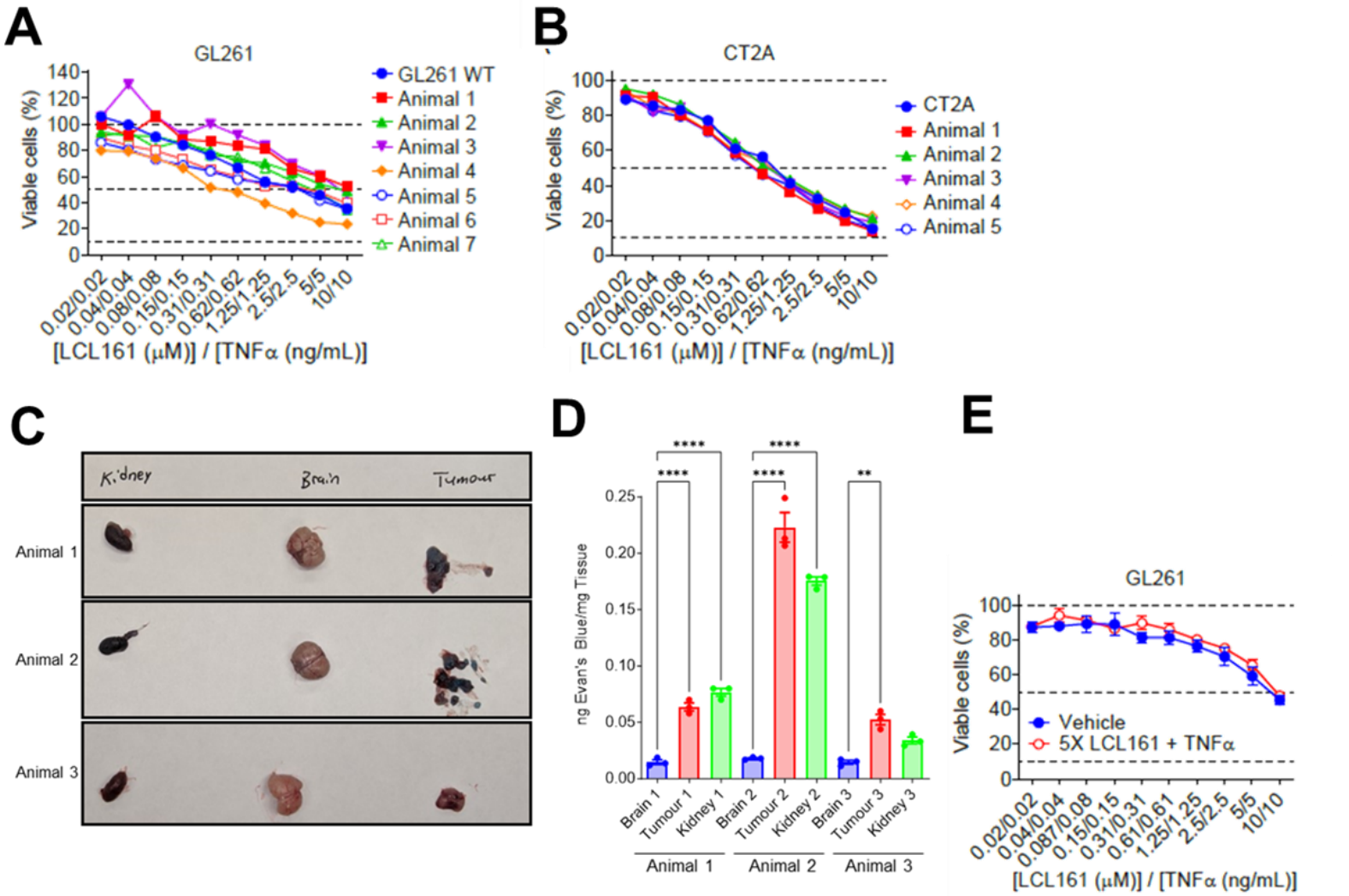
A
GL261
Viable cells (%)
GL261 WT
Animal 1
Animal 2
Animal 3
Animal 4
Animal 5
Animal 6
Animal 7
0.02/0.02
0.04/0.04
0.08/0.08
0.15/0.15
0.31/0.31
0.62/0.62
1.25/1.25
2.5/2.5
5/5
10/10
[LCL161 (μM)] / [TNFα (ng/mL)]
B
CT2A
Viable cells (%)
CT2A
Animal 1
Animal 2
Animal 3
Animal 4
Animal 5
[LCL161 (μM)] / [TNFα (ng/mL)]
C
Kidney
Brain
Tumour
Animal 1
Animal 2
Animal 3
D
ng Evan's Blue/mg Tissue
Brain 1
Tumour 1
Kidney 1
Brain 2
Tumour 2
Kidney 2
Brain 3
Tumour 3
Kidney 3
Animal 1
Animal 2
Animal 3
E
GL261
Viable cells (%)
Vehicle
5X LCL161 + TNFα
[LCL161 (μM)] / [TNFα (ng/mL)]
F
Vehicle
LCL161
Vehicle
LCL161
CT2A
GL261
CD44 (PE)
G
CT2A
GL261
MFI (CD44 PE)
LCL161:
H
Viable cells (%)
Hystem
Normal
GL261
Hystem
Normal
CT2A
[LCL161 (μM)] / [TNFα (ng/mL)]
I
GL261
Viable cells (%)
Normoxia
Hypoxia
+ glucose
Normoxia
Hypoxia
– glucose
[LCL161 (μM)] / [TNFα (ng/mL)]
J
CT2A
Viable cells (%)
Normoxia
Hypoxia
+ glucose
Normoxia
Hypoxia
– glucose
[LCL161 (μM)] / [TNFα (ng/mL)]

Figure 9: Hypoxia and extracellular matrix proteins do not affect the ability of SMCs to induce GBM cell death. A) GL261 and B) CT2A cells from LCL161 and αPD-1 resistant tumors were treated *in vitro* with the indicated dilution series of LCL161 and TNFα for 24hr. Viability was assessed by Alamar blue. N=3 technical replicates per animal. C,D) Mice bearing CT2A tumors received a tail vein injection of Evan's blue dye. Bar plots are quantification of Evan's blue dye signal in each tissue. N=3 technical replicates per animal. **P<0.01; ****P<0.0001 by one-way ANOVA using Tukey's HSD multiple comparison test. E) GL261 cells were treated five times with 10μM LCL161 and 10ng/mL TNFα for 24hr per treatment. Viability was assessed via Alamar blue. N=3 technical replicates per treatment. F) Flow cytometric analysis of CD44 (PE) expression on CT2A and GL261 cells treated with 10 doses of 10μM LCL161. Bar plots are MFI of CD44 expression. N=3 technical replicates for all CT2A groups and GL261 naïve group; N=6 technical replicates for GL261 LCL161 treated. *P<0.05; ****P<0.0001 by two-way ANOVA using Tukey's HSD multiple comparison test. H) Alamar blue viability of GL261 and CT2A cells cultured on Hystem extracellular matrix gel and treated with indicated dilution series of LCL161 and TNFα for 24hr. N=3 technical replicates per treatment group. **P<0.01;***P<0.001 by two-way ANOVA using Tukey's HSD multiple comparison test. I,J) GL261 and CT2A cells treated with indicated dilution series of LCL161 and TNFα under hypoxia and/or no glucose conditions. N=6 technical replicates for normoxia complete glucose. N=3 technical replicates for all other groups. *P<0.05; **P<0.01;***P<0.001 by two-way ANOVA using Tukey's HSD multiple comparison test. N=1 independent experiment per condition.

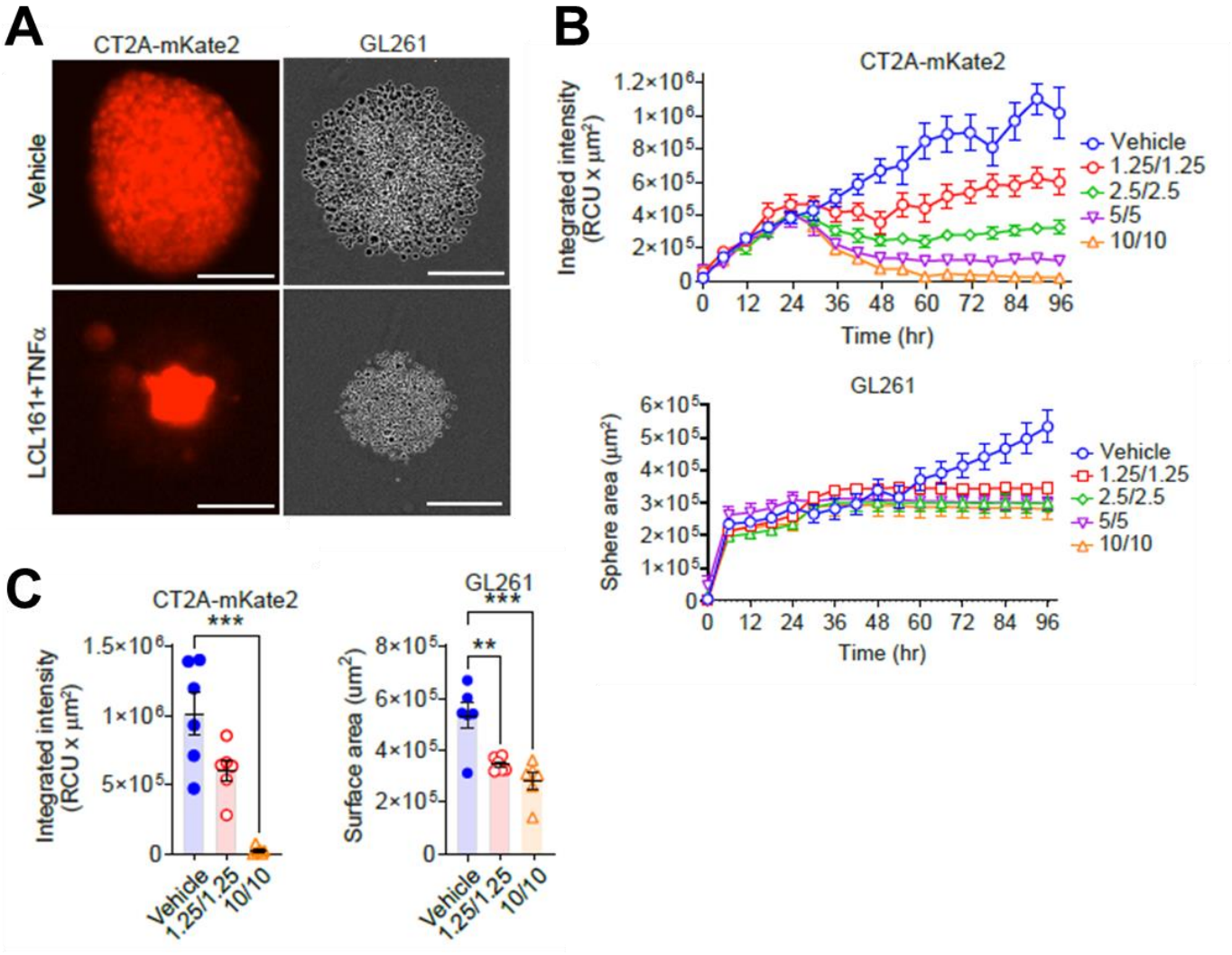
A
CT2A-mKate2
GL261
Vehicle
LCL161+TNFα
B
CT2A-mKate2
Integrated intensity (RCU x μm²)
Time (hr)
Vehicle
1.25/1.25
2.5/2.5
5/5
10/10
GL261
Sphere area (μm²)
C
CT2A-mKate2
GL261
Integrated intensity (RCU x μm²)
Surface area (um²)
Vehicle
1.25/1.25
10/10

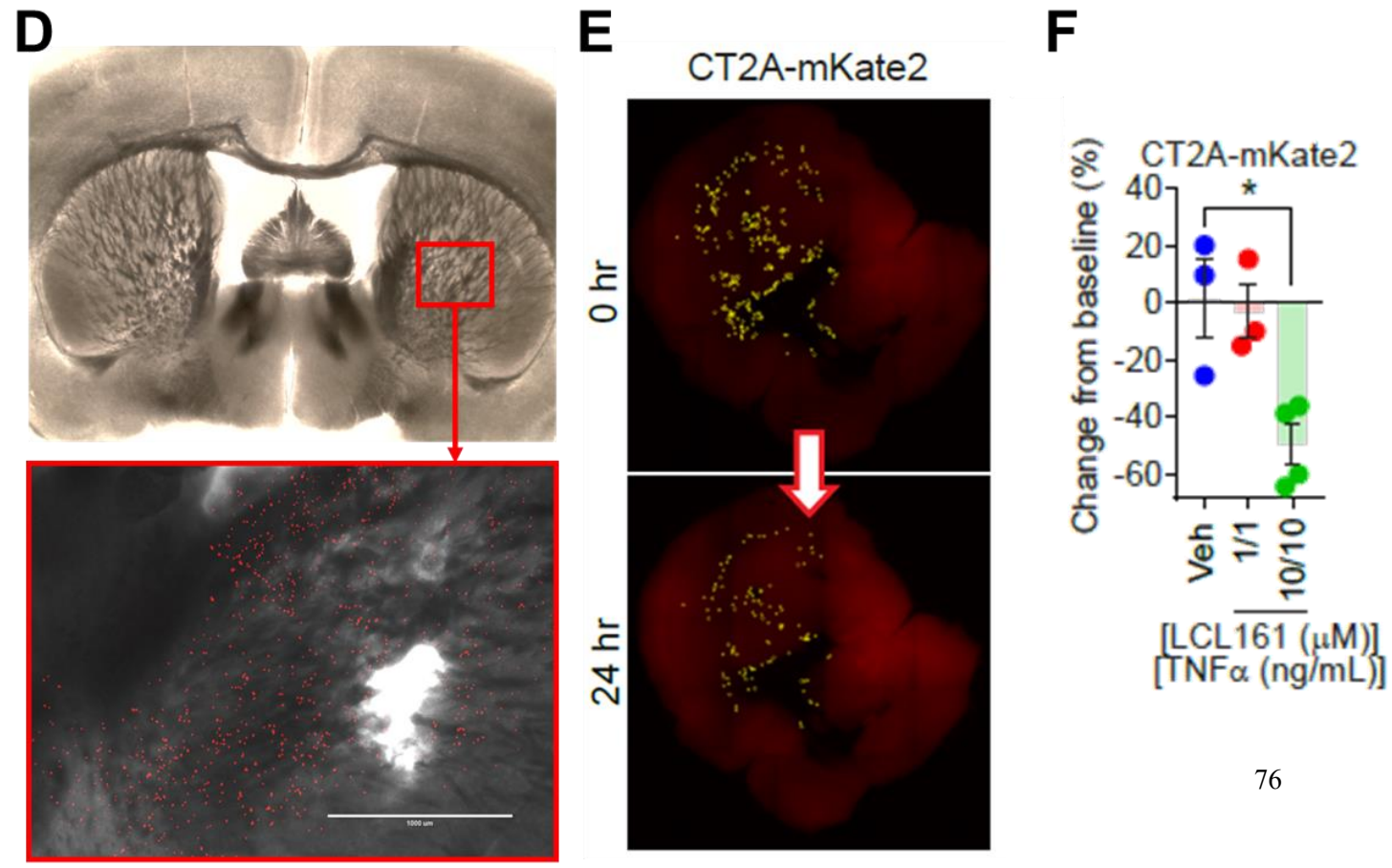
D
E
CT2A-mKate2
0 hr
24 hr
F
CT2A-mKate2
Change from baseline (%)
Veh
1/1
10/10
[LCL161 (μM)]
[TNFα (ng/mL)]

Figure 10: GBM cells remain sensitive to SMC-induced cell death under spheroid or explant conditions. A-C) CT2A-mKate2 and GL261 cells were cultured as spheres and treated with indicated dilution series of LCL161 and TNFα following 24hr in culture. Fluorescence intensity (CT2A-mKate2) and size (GL261) were measured using time-lapse imaging and plotted at 72hr post-treatment. N=6 technical replicates per-treatment group. Scale bar: 800μm. D) Mouse brains were sectioned into 250μm slices and 48hr later implanted with $5x10^3$ CT2A-mKate2 cells in the left striatum. Scale bar: 1mm. E,F) CT2A-mKate2 cells were enumerated before and 24hr after 10μM LCL161 and 10ng/mL TNFα treatment (E) or of the indicated concentrations (F). N=3 technical replicates for vehicle and 1/1 treatment groups. N=4 technical replicates for 10/10 treatment. *P<0.05; **P<0.01; ***P<0.001 by one-way ANOVA using Tukey's HSD multiple comparison test. N=1 independent experiment per assay.

3.1.3 Anti-GBM immune responses are hindered by CNS location and age

To determine whether efficacy of the cotherapy is hindered by the CNS location, GL261 cells were implanted subcutaneously (SQ) and treated as in Figure 7G. No tumors were visible 35 days post-implant regardless of treatment (Figure 11A). A second SQ GL261 implant on the opposite flank was performed on day 35 and tumors were cleared despite no subsequent treatments. On day 100, GL261 cells were once again implanted SQ and peripheral blood collected 3 days later. Peripheral blood mononuclear cells (PBMCs) were isolated and co-cultured with GL261 cells. IFNγ and TNFα expression was assessed via flow cytometry (Figure 11B). Co-culture with GL261 cells significantly increased the expression of IFNγ, specifically among $CD4^+$ T-cells (Figure 11C,D), suggesting an immune memory had formed against GL261 antigens. To determine whether this immune memory was functional against subsequent IC challenges, GL261 cells were implanted intracranially in these same animals. All tumors were cleared and all animals survived despite receiving no further treatments (Figure 11E), suggesting memory responses against GBM are effective even within the CNS. To determine whether this effect could be induced against a primary intracranial tumor, GL261 cells were implanted intracranially and received saline or GL261 cells SQ 7 days later. All animals bearing intracranial tumors reached endpoint within 30 days (Figure 11F), regardless of subsequent SQ implants. All SQ tumors were cleared, even in animals bearing intracranial tumors, suggesting the CNS location limits anti-GBM T-cell immunity. When CT2A cells were implanted SQ, tumor growth was significantly greater than for GL261 cells. A subset of SQ tumors were cleared even when untreated (Figure 11G), and endpoint CT2A tumors were substantially more infiltrated by $CD3^+$ cells than intracranial tumors (Figure 11H). Together, these data corroborate the findings of Figure 4, providing functional evidence of immune recognition, antigen presentation, T-cell-

mediated clearance and immune memory against GBM cells, with the limiting factor being the CNS location.

GBM is primarily a disease of individuals over 50 years old. I therefore undertook experiments in aged animals. Equivalent human and C57BL/6 mouse ages were based on previously published data, with human middle age (38-47 years old) corresponding to 10-14 month old mice, and human old age (56-69 years old) corresponding to 18-24 month old mic. Efficacy of SMC and αPD-1 cotherapy was abolished in middle aged animals bearing intracranial CT2A tumors (Figure 12A) but remained in GL261-bearing animals (Figure 12B). Across both lines LCL161 monotherapy provided significant median survival extensions relative to vehicle, with the most long-term survivors of any treatment cohort in the GL261 model. IDO1[109] and KLRG1[519–521] are upregulated in aging brain and immune systems, respectively, corresponding with the timeframes of increased GBM occurrence, immunosenescence and impaired capacity for anti-tumor immunity. Endpoint tumors from middle aged animals bearing either CT2A or GL261 intracranial tumors show significant, tumor-specific expression of IDO1 among $CD45^+$ cells (Figure 12C), as well as significant KLRG1 among tumor-infiltrating $CD4^+$ and $CD8^+$ T-cells only (Figure 12D); minimal KLRG1 or IDO1 are expressed within lymph nodes from the same animals, and combination SMC and αPD-1 had no impact on this expression. Cotherapy provided no survival benefit in old animals (Figure 12E).

Together, these data indicate the CNS uniquely limits primary but not memory anti-GBM immune responses. Aging further limits the ability of the immune system to clear tumor and respond to therapeutic interventions. IDO1 and KLRG1 are highly expressed specifically among tumor-infiltrating immune cells and represent potential future targets to overcome age-induced immune limitations.

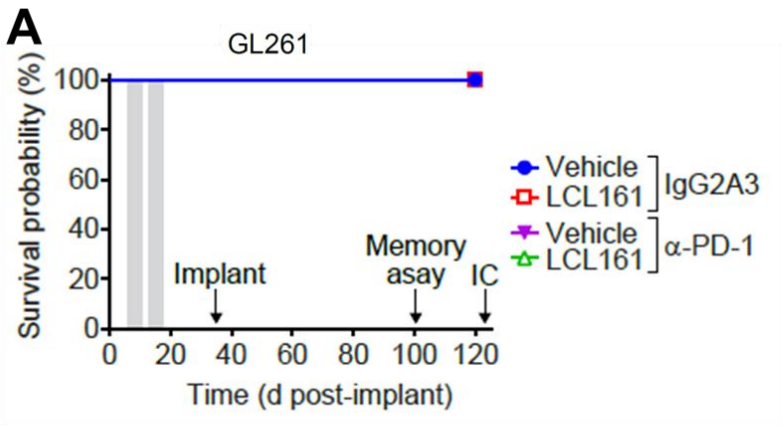
A
GL261
Survival probability (%)
Time (d post-implant)
Implant
Memory asay
IC
Vehicle
LCL161
IgG2A3
Vehicle
LCL161
α-PD-1

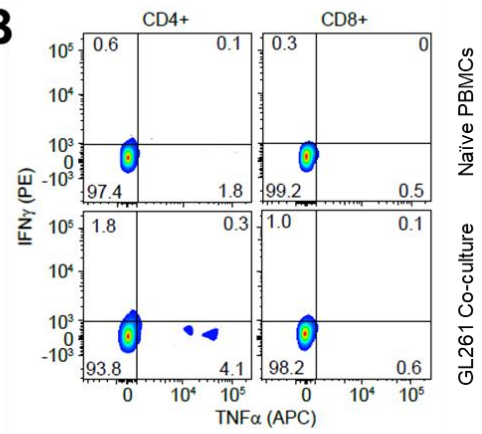
B
CD4+
CD8+
IFNγ (PE)
TNFα (APC)
Naïve PBMCs
GL261 Co-culture

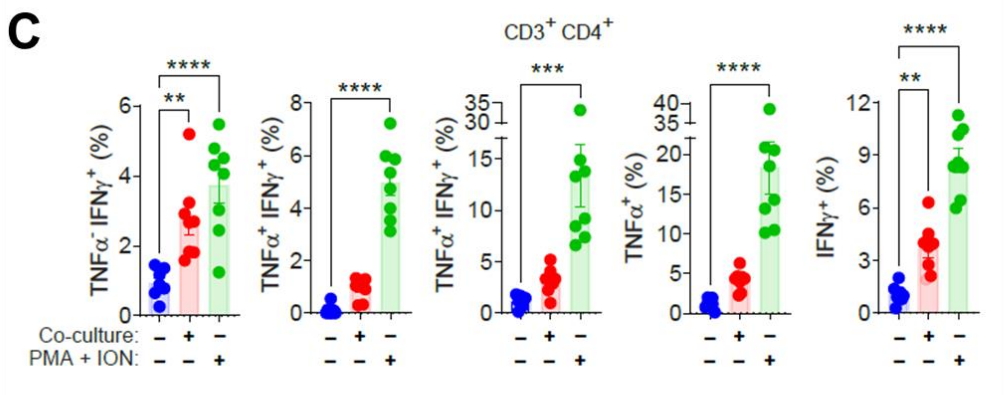
C
CD3+ CD4+
TNFα- IFNγ+ (%)
TNFα+ IFNγ+ (%)
TNFα+ IFNγ+ (%)
TNFα+ (%)
IFNγ+ (%)
Co-culture:
PMA + ION:

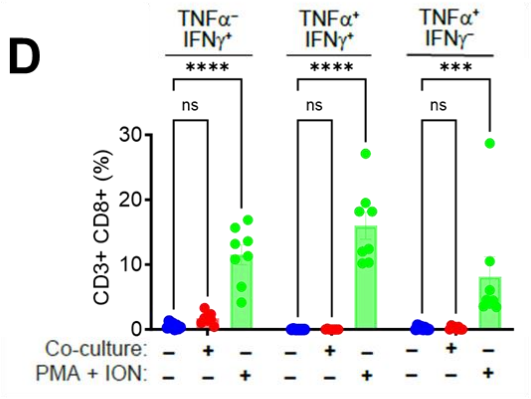
D
TNFα- IFNγ+
TNFα+ IFNγ+
TNFα+ IFNγ-
CD3+ CD8+ (%)
ns
Co-culture:
PMA + ION:

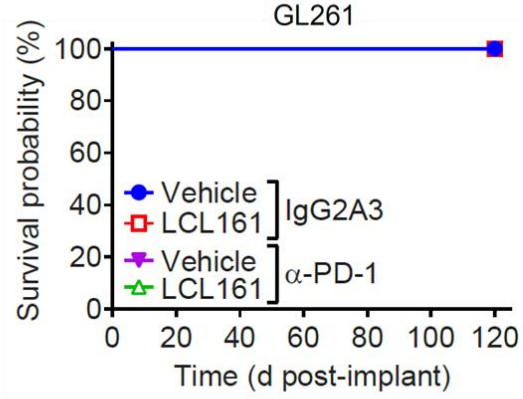
E
GL261
Survival probability (%)
Time (d post-implant)
Vehicle
LCL161
IgG2A3
Vehicle
LCL161
α-PD-1

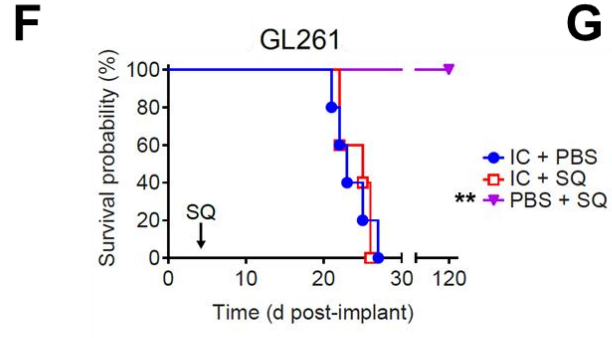
F
GL261
Survival probability (%)
Time (d post-implant)
SQ
IC + PBS
IC + SQ
PBS + SQ

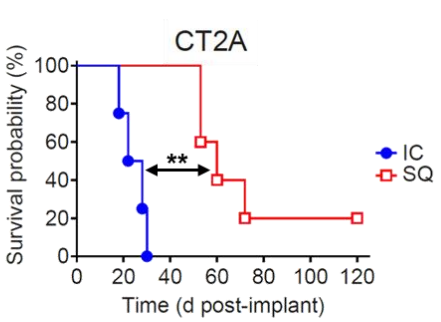
G
CT2A
Survival probability (%)
Time (d post-implant)
IC
SQ

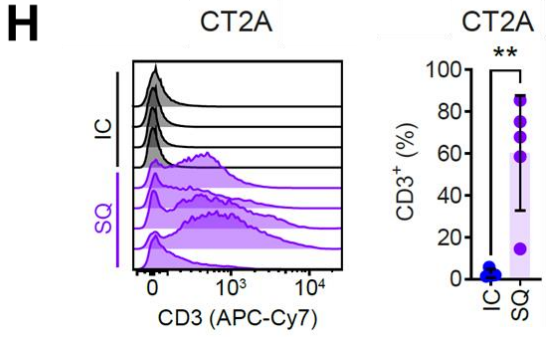
H
CT2A
CT2A
IC
SQ
CD3 (APC-Cy7)
CD3+ (%)

Figure 11: CNS location limits primary but not memory anti-GBM immune responses. A) Mice were implanted with $5x10^5$ GL261 cells subcutaneously (SQ) and treated orally with vehicle or 75mg/kg LCL161 and intraperitoneally with 10mg/kg αPD-1 or isotype control. On Day 35 mice were implanted with $1x10^6$ GL261 cells in opposite flank. On day 100, mice were implanted with $5x10^5$ GL261 cells SQ. Peripheral blood was drawn 3 days later. On day 125, mice were implanted with $5x10^4$ GL261 cells intracranially (IC). N=5 per treatment group. Data represent Kaplan-Meier curve depicting mouse survival. B-D) Flow cytometric analysis of IFNγ (PE) and TNFα (APC) expression by $CD3^+CD4^+$ and $CD3^+CD8^+$ cells following 6-hour co-culture with GL261 cells or treatment with PMA and ionomycin (ION). Bar plots are percentage of C) $CD3^+$ $CD4^+$ and D) $CD3^+$ $CD8^+$ cells positive for indicated TNFα and IFNγ subgroups. N=8 for all treatment groups. **P<0.01; ***P<0.001; ****P<0.0001 by one-way ANOVA using Tukey's HSD multiple comparison test for C). ***P<0.001;****P<0.0001 by two-way ANOVA using Tukey's HSD multiple comparison test for D). E) Kaplan-Meier curve depicting mouse survival following IC implant indicated in A). No further treatments were administered. F) Mice were implanted with $5x10^4$ GL261 cells IC. 7 days later, mice were implanted with $5x10^5$ GL261 cells SQ. N=5 per treatment group. Data represent Kaplan-Meier curve depicting mouse survival. Log-rank with Holm-Sidak multiple comparison. N=5 per treatment group. **P<0.01. G) Mice were implanted with $5x10^4$ CT2A cells IC or $5x10^5$ SQ. Data represent Kaplain-Meier curve depicting mouse survival. Log-rank with Holm-Sidak multiple comparison. N=5 per treatment group. **P<0.01. H) Flow cytometric analysis of CD3 (APC-Cy7) expression in IC and SQ CT2A tumors at endpoint. Bar plots represent percent of total live cells that are $CD3^+$. N=5 per indicated implant site. **P<0.01 by unpaired t-test.

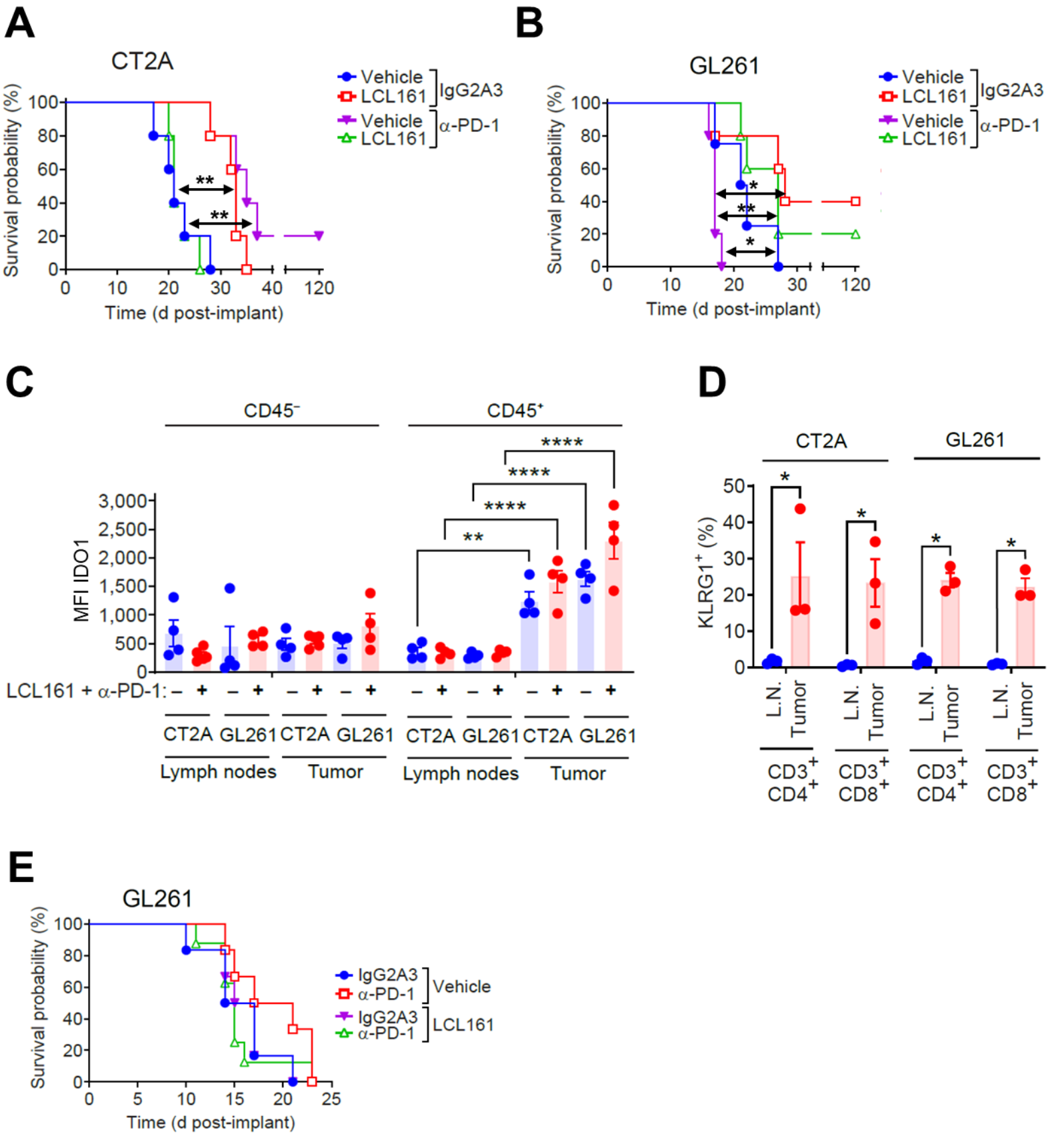
A
CT2A
Survival probability (%)
Time (d post-implant)
Vehicle
LCL161
IgG2A3
Vehicle
LCL161
α-PD-1
B
GL261
C
CD45⁻
CD45⁺
MFI IDO1
LCL161 + α-PD-1:
CT2A GL261 CT2A GL261 CT2A GL261 CT2A GL261
Lymph nodes
Tumor
Lymph nodes
Tumor
D
CT2A
GL261
KLRG1⁺ (%)
L.N. Tumor
CD3⁺CD4⁺
CD3⁺CD8⁺
E
GL261
IgG2A3
α-PD-1
Vehicle
IgG2A3
α-PD-1
LCL161

Figure 12: Advanced age hinders anti-GBM immunotherapy. A) Middle aged (10–11-month-old) mice were implanted with $5x10^4$ CT2A or B) GL261 cells and treated orally with 75mg/kg LCL161 and intraperitoneally with 10mg/kg αPD-1 or isotype control. Data represent Kaplan-Meier curves depicting mouse survival. Log-rank with Holm-Sidak multiple comparison. N=5 per treatment group. *P<0.05; **P<0.01. C) Flow cytometric analysis of IDO1 (AF647) expression on $CD45^+$ and $CD45^-$ cells from lymph nodes and tumors of endpoint middle aged mice with CT2A or GL261 intracranial implants. D) Flow cytometric analysis of KLRG1 (PE-CF594) positivity among $CD3^+CD4^+$ and $CD3^+CD8^+$ cell subsets within lymph nodes and tumor of endpoint middle aged mice. *P<0.05;**P<0.01; ****P<0.0001 by two-way ANOVA using Tukey's HSD multiple comparison test. E) Old (18-month-old) mice were implanted with $5x10^4$ GL261 cells and treated orally with LCL161 or vehicle and αPD-1 or isotype control. Data represent Kaplan-Meier curves depicting mouse survival. Log-rank with Holm-Sidak multiple comparison. N=5 per treatment group.

3.2 TNFα ablates astrocyte protection of GBM cells in presence of SMCs

3.2.1 SMCs kill murine macrophages and microglia in vitro

Microglia and macrophages represent the major immune infiltrates within GBMs, contributing significantly to numerous aspects of tumor biology (See **Section 1.3.3**). I sought to determine the impact of SMCs on murine microglia and macrophage functionality. RAW264.7 (herein referred to as RAW) immortalized murine macrophages were assayed for phagocytic capacity in the presence of varying doses of LCL161, as M2 macrophages generally show higher phagocytosis than M1[522]. LCL161 completely abolished RAW phagocytic capacity at doses 1μM and above (Figure 13A), coinciding with robust, dose-dependent induction of cleaved caspase-3 and -7 (Figure 13B), suggesting LCL161 induces macrophage cell death. Differences in IAP expression levels mediate responsiveness to SMC-induced cell death of human macrophages, with M1 being the more sensitive subtype[523]. To determine whether the sensitivity of murine macrophages was affected by the presence of immunosuppressive cytokines, RAW cells were pre-treated with LPS or common GBM TME anti-inflammatory cytokines IL-4 or IL-10. No impact on sensitivity to high dose LCL161 was observed (Figure 13C). As bovine serum affects the differentiation capacity and cytokine secretion profile of mesenchymal stem cells[524], I undertook the same experiment under serum free conditions. In cultures lacking FCS, IL-4 and IL-10 protect macrophages against the cytotoxicity of medium dose (1μM) LCL161. Protective effects disappear at high doses (Figure 13D). To recapitulate these findings with primary cells, bone marrow progenitors were differentiated into bone marrow derived macrophages (BMDMs) over 8 and 12 days, with successful differentiation confirmed via flow cytometric analysis for $CD11b^+$ $F4/80^+$ $Ly6C^-$ cells (Figure 13E). Confirmed BMDMs treated with LCL161 showed dose-dependent reductions in viability regardless of cytokine pre-treatment (Figure 13F). RAW cell death was confirmed as RIPK1- and caspase-dependent (Figure 13G), consistent with apoptosis.

BV2 immortalized microglia also showed dose-dependent reductions in phagocytosis (Figure 14A) and activation of caspases (Figure 11B) regardless of cytokine pretreatment (Figure 14C). Caspase activation was delayed relative to RAW cells, and significantly less in cultures treated with 1μM LCL161. BV2 viability was reduced at a basal level under FCS-free conditions (Figure 14D). Primary mouse microglia showed minimal caspase activation in response to LCL161. Only LPS pre-treated cultures were responsive (Figure 14E). BV2 cells die through RIPK1- and caspase-dependent mechanisms (Figure 14F), with caspase-3 and PARP-cleavage and cIAP1/2 degradation confirmed via Western Blot. Consistent with the findings in Figure 13B and 14B, caspase-3 cleavage was observed at 1μM LCL161 treated RAW cells but not in BV2 (Figure 14G). Coupled with findings from BMDMs and primary microglia, this suggests that macrophages are more sensitive to SMC-induced cell death than microglia.

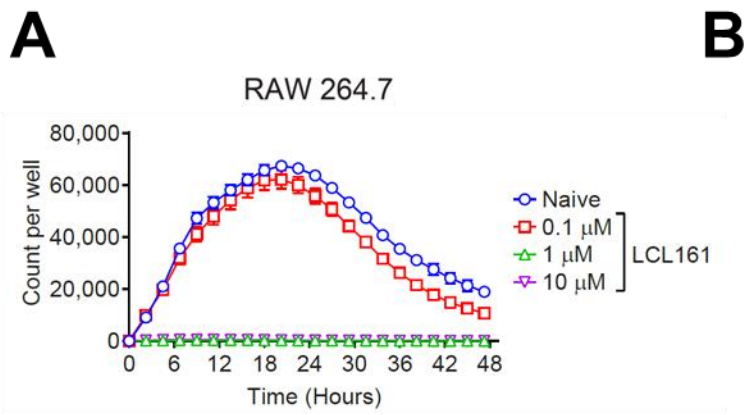
A
RAW 264.7
Count per well
80,000
60,000
40,000
20,000
0
0 6 12 18 24 30 36 42 48
Time (Hours)
Naive
0.1 μM
1 μM
10 μM
LCL161

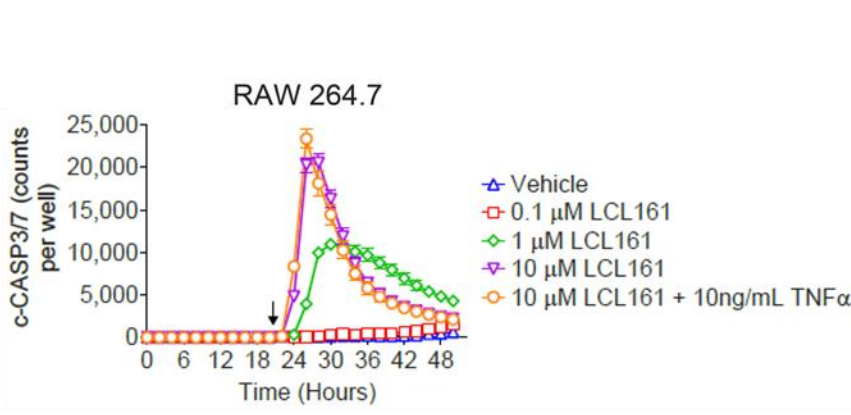
B
RAW 264.7
c-CASP3/7 (counts per well)
25,000
20,000
15,000
10,000
5,000
0
0 6 12 18 24 30 36 42 48
Time (Hours)
Vehicle
0.1 μM LCL161
1 μM LCL161
10 μM LCL161
10 μM LCL161 + 10ng/mL TNFα

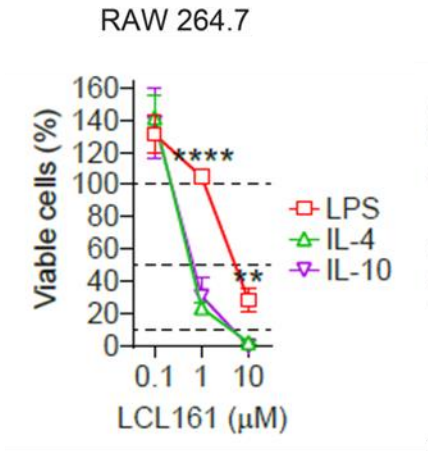
C
RAW 264.7
Viable cells (%)
160
140
120
100
80
60
40
20
0
****
**
0.1 1 10
LCL161 (μM)
LPS
IL-4
IL-10

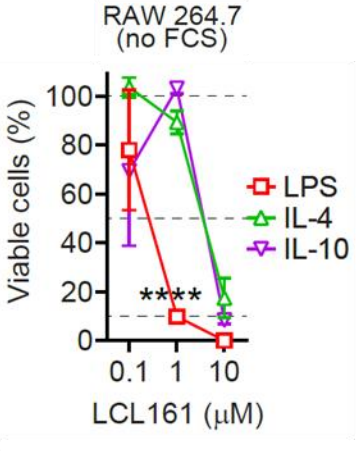
D
RAW 264.7
(no FCS)
Viable cells (%)
100
80
60
40
20
0
****
0.1 1 10
LCL161 (μM)
LPS
IL-4
IL-10

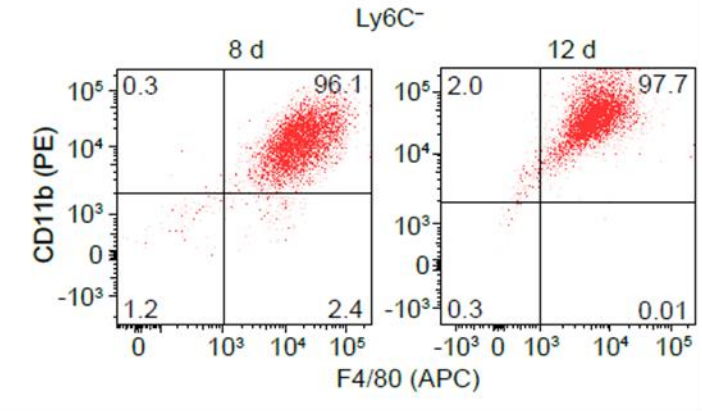
E
Ly6C⁻
8 d
12 d
CD11b (PE)
0.3
96.1
1.2
2.4
2.0
97.7
0.3
0.01
F4/80 (APC)

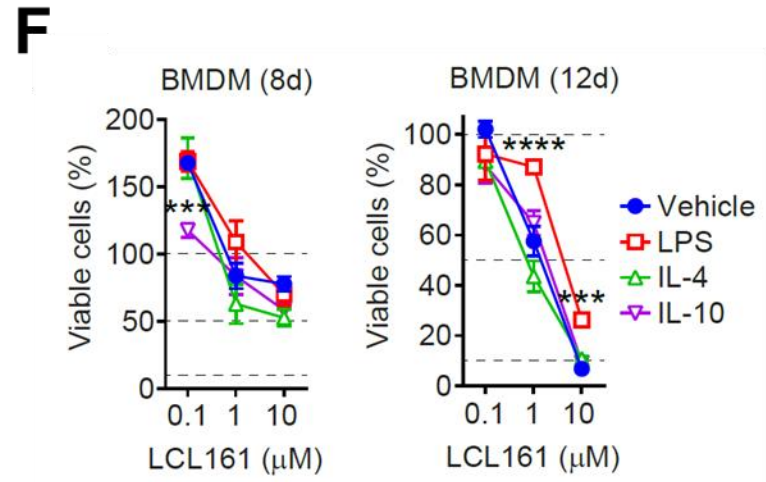
F
BMDM (8d)
BMDM (12d)
Viable cells (%)
200
150
100
50
0
***
****
***
0.1 1 10
LCL161 (μM)
Vehicle
LPS
IL-4
IL-10

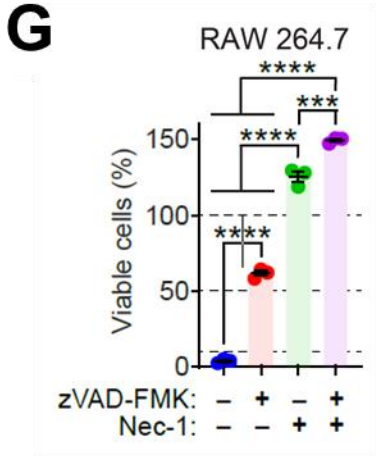
G
RAW 264.7
Viable cells (%)
150
100
50
0
****
***
****
****
zVAD-FMK: – + – +
Nec-1: – – + +

Figure 13: SMC treatment induces the death of murine macrophages. A) RAW macrophages were assayed in the presence of the indicated concentrations of LCL161 for phagocytic activity of pHrodo bioparticles via live cell microscopy. N=6 per treatment group. B) RAW cells were treated with indicated doses of LCL161 and assayed for activated caspase-3/7 via live cell microscopy. Arrow denotes time of treatment. N=6 technical replicates per group. C,D) RAW cells were treated for 24hr with LPS (100ng/mL), IL-4 (20ng/mL) or IL-10 (20ng/mL), with (C) or without (D) FCS and subsequently treated with indicated concentrations of LCL161. Viability was assessed using Alamar blue. N=3 technical replicates per treatment group. E) Bone marrow progenitors isolated from femurs were differentiated using conditioned L929 media for 8 or 12 days. Cells were evaluated for expression of Ly6C (AF488), CD11b (PE) and F4/80 (APC) via flow cytometry, with $Ly6C^{-}CD11b^{+}$ $F4/80^{+}$ cells considered differentiated macrophages (BMDMs). F,G) BMDMs were treated with cytokines as in C) and subsequently treated with indicated doses of LCL161. Viability was assessed using Alamar blue at 24hr. N=3 technical replicates per treatment group. **P<0.01; ***P<0.001; ****P<0.0001 by two-way ANOVA using Tukey's HSD multiple comparison test. G) RAW macrophages were treated with 10μM in the presence of zVAD-FMK (20μM) and/or necrostatin-1 (50μM) for 24hr. Viability was assessed by Alamar blue. ***P<0.001;****P<0.0001 by one-way ANOVA using Tukey's HSD multiple comparison test. N=1 independent experiment per timepoint.

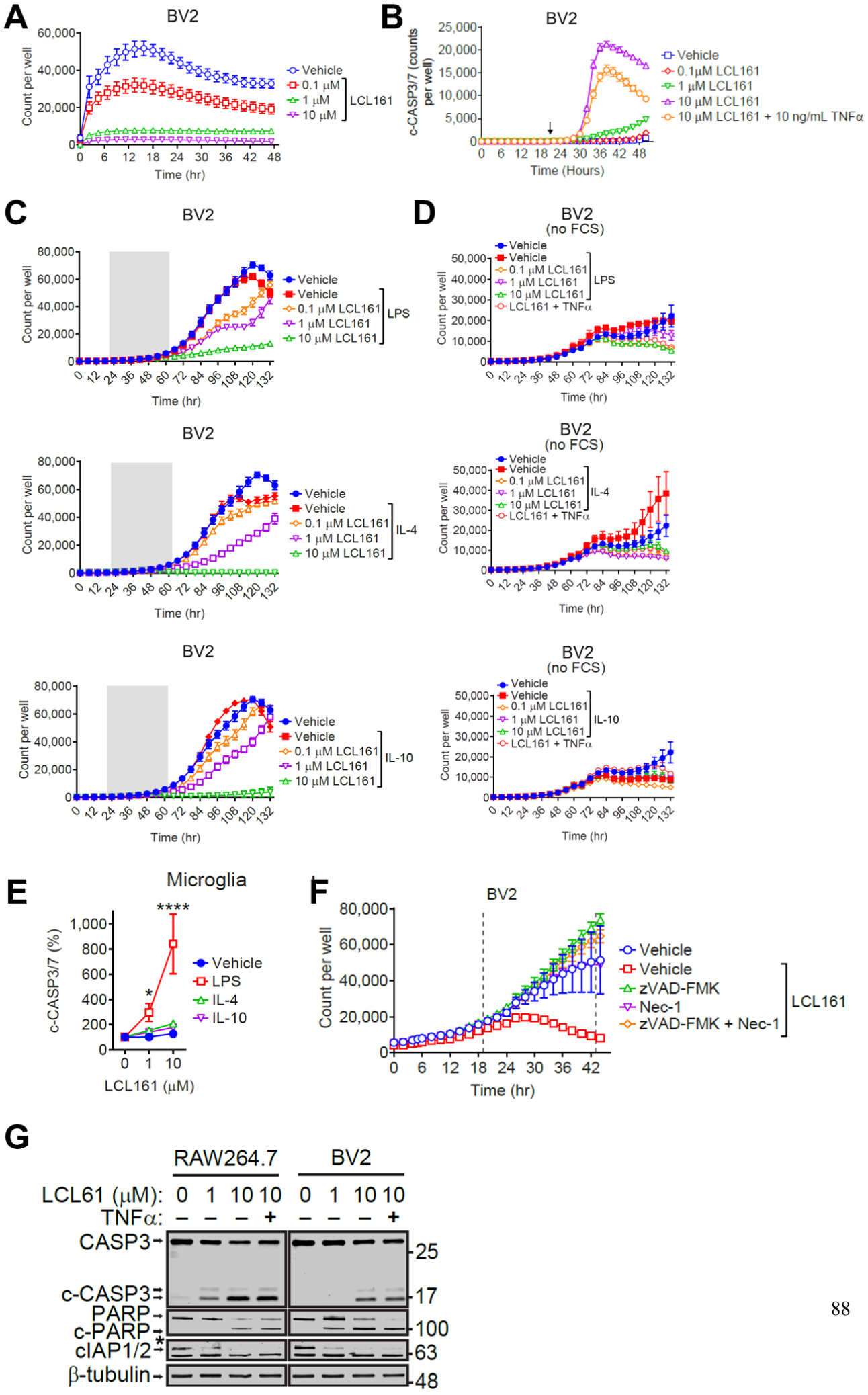
A
BV2
Count per well
Time (hr)
Vehicle
0.1 μM
1 μM
10 μM
LCL161
B
BV2
c-CASP3/7 (counts per well)
Time (Hours)
Vehicle
0.1μM LCL161
1 μM LCL161
10 μM LCL161
10 μM LCL161 + 10 ng/mL TNFα
C
BV2
LPS
IL-4
IL-10
Vehicle
0.1 μM LCL161
1 μM LCL161
10 μM LCL161
D
BV2
(no FCS)
LCL161 + TNFα
E
Microglia
c-CASP3/7 (%)
LCL161 (μM)
Vehicle
LPS
IL-4
IL-10
F
BV2
Vehicle
zVAD-FMK
Nec-1
zVAD-FMK + Nec-1
LCL161
G
RAW264.7
BV2
LCL61 (μM):
TNFα:
CASP3
c-CASP3
PARP
c-PARP
cIAP1/2
β-tubulin
25
17
100
63
48

Figure 14: SMC treatment induces death of mouse microglia. A) BV2 cells were treated with the indicated doses of LCL161 and assayed for phagocytic activity using pHrodo bioparticles via live cell microscopy. N=6 technical replicates per treatment group. B) BV2 cells were assayed for activated caspase-3/7 using live cell imaging. Arrow denotes time of treatment. N=6 technical replicates per treatment group. C,D) BV2-EGFP cells were treated for 24hr with LPS (100ng/mL), IL-4 (20ng/mL) or IL-10 (20ng/mL) and subsequently treated with indicated concentrations of LCL161 in complete (C) or FCS-free (D) media conditions. EGFP positive events were quantified over time via live microscopy imaging. Shaded area represents pre-treatment time with indicated cytokine. End of shaded area represents introduction of LCL161. N=3 technical replicates per treatment group. E) Primary mouse microglia were pre-treated with LPS, IL-4 or IL-10 and subsequently treated with indicated doses of LCL161. Activated caspase-3/7 was quantified using live imaging at 24hr post-treatment. N=3 technical replicates per treatment group. *P<0.05;****P<0.0001 by two-way ANOVA using Tukey's HSD multiple comparison test. F) BV2-EGFP cells were treated with 10μM LCL161 in the presence of zVAD-FMK (20μM) and/or necrostatin-1 (50μM) for 24hr. Line indicates treatment point. EGFP counts were obtained using live cell imaging. N=3 technical replicates per treatment group. N=1 independent experiment per timepoint. G) Western blot illustrating cIAP1/2 degradation and caspase-3 and PARP cleavage in response to LCL161 treatment.

3.2.2 SMC-induced macrophage and microglia killing provide death cues to GBM cells

Given that GBM cells and TAMs coexist within a tumor and communicate via direct cell-cell contact and via secreted factors, I aimed to determine whether co-culture of murine microglia or macrophages with GBM cells affected sensitivity to SMCs. LCL161 alone does not affect CT2A growth rate in monocultures (Figure 15A,C,D). Co-culture of BV2 cells with CT2A does not protect BV2 from LCL161-mediated cytotoxicity (Figure 15B). Concurrent with this loss of BV2 viability, CT2A cells in co-culture with microglia show substantially reduced growth relative to monocultures in response to LCL161 treatment (Figure 15C,D), suggesting LCL161-induced BV2 cell death results in release of factors that act in autocrine and paracrine fashions to induce death of LCL161 sensitized GBM cells, even without the addition of exogenous TNFα. Primary microglia also enhanced LCL161 cytotoxicity without added TNFα and did not affect CT2A sensitivity to LCL161 and TNFα cotreatment (Figure 15E,F). These findings were recapitulated in CT2A-RAW (Figure 16A,B) and CT2A-BMDM (Figure 16C,D) cultures, suggesting that both microglia and macrophages are sensitive to SMC-induced cell death, releasing secreted factors that act on sensitized GBM cells to initiate cascades of GBM cell death. Thus, TAMs represent a potential source of death ligands for SMC-based GBM killing, and SMC-induced reductions in these cell populations may represent a key component of their *in vivo* efficacy in combination with ICB.

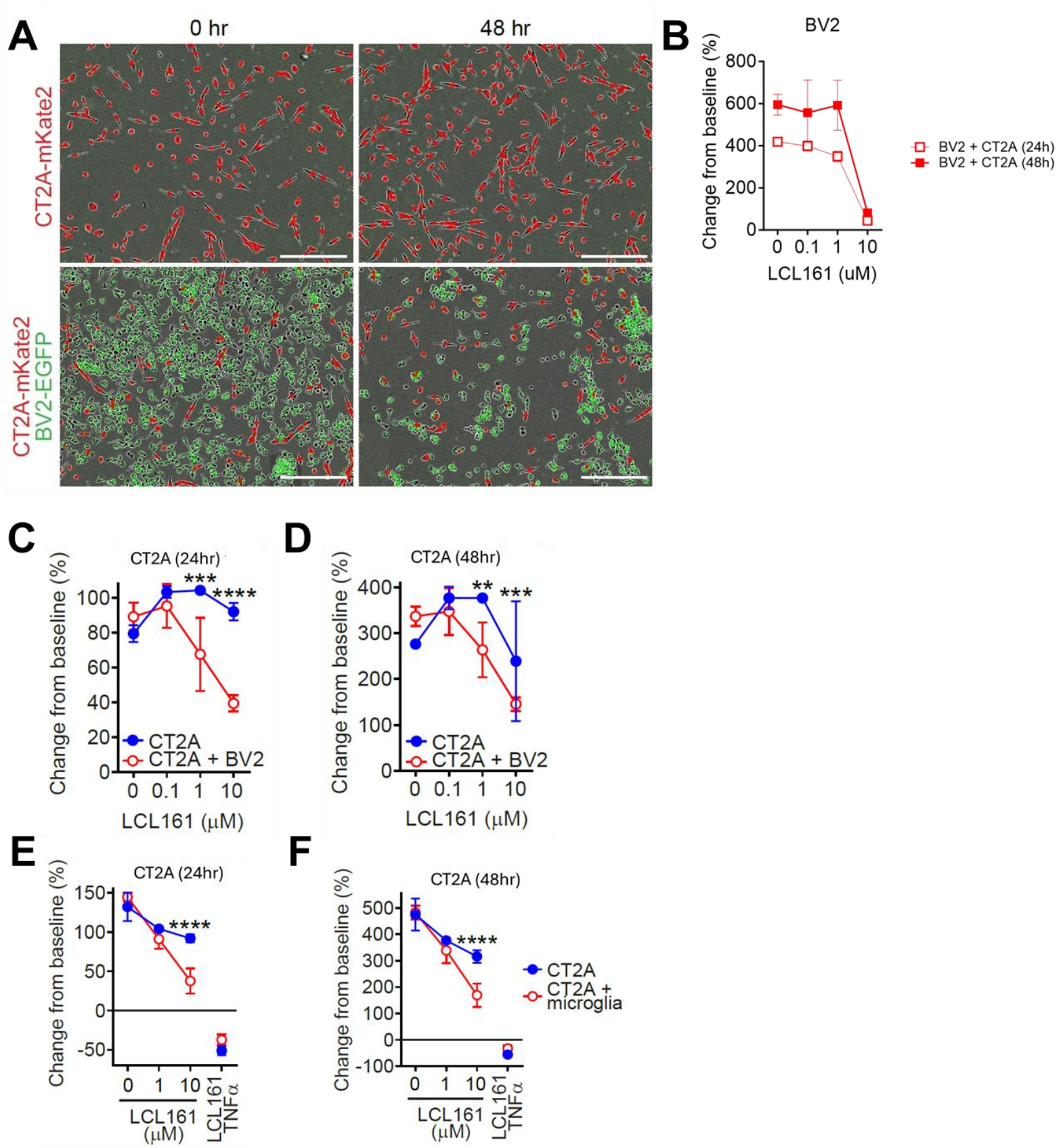
A
0 hr
48 hr
CT2A-mKate2
CT2A-mKate2
BV2-EGFP
B
BV2
Change from baseline (%)
800
600
400
200
0
0 0.1 1 10
LCL161 (uM)
BV2 + CT2A (24h)
BV2 + CT2A (48h)
C
CT2A (24hr)
***
****
Change from baseline (%)
100
80
60
40
20
0
CT2A
CT2A + BV2
0 0.1 1 10
LCL161 (μM)
D
CT2A (48hr)
**
***
Change from baseline (%)
400
300
200
100
0
CT2A
CT2A + BV2
0 0.1 1 10
LCL161 (μM)
E
CT2A (24hr)
Change from baseline (%)
150
100
50
0
-50
****
0 1 10
LCL161 (μM)
LCL161
TNFα
F
CT2A (48hr)
Change from baseline (%)
500
400
300
200
100
0
-100
****
CT2A
CT2A + microglia
0 1 10
LCL161 (μM)
LCL161
TNFα

Figure 15: Microglia enhance ability of SMCs to induce GBM cell death. A,B) BV2-EGFP cells were cultured 1:1 with CT2A-mKate2 cells and treated 24hr later with tenfold dilution series of LCL161. Viable cells were enumerated by tracking EGFP positive events using live cell imaging over 48hr post-treatment. N=6 per treatment group. Scale bar: 300μm. C,D) CT2A-mKate2 cell counts in co-culture with BV2-EGFP cells over C) 24hr and D) 48hr following treatment with dilution series of LCL161. N=3 for monocultures and N=6 for co-cultures per treatment group. E,F) CT2A-mKate2 cell numbers were analysed and treated as in C,D) in co-culture with primary mouse microglia over 48hr. Response to treatment with 10μM LCL161 and 10ng/mL TNFα was also assessed. N=4 technical replicates per treatment group. **P<0.01;***P<0.001;****P<0.0001 by two-way ANOVA using Tukey's HSD multiple comparison test. N=1 independent experiment per timepoint.

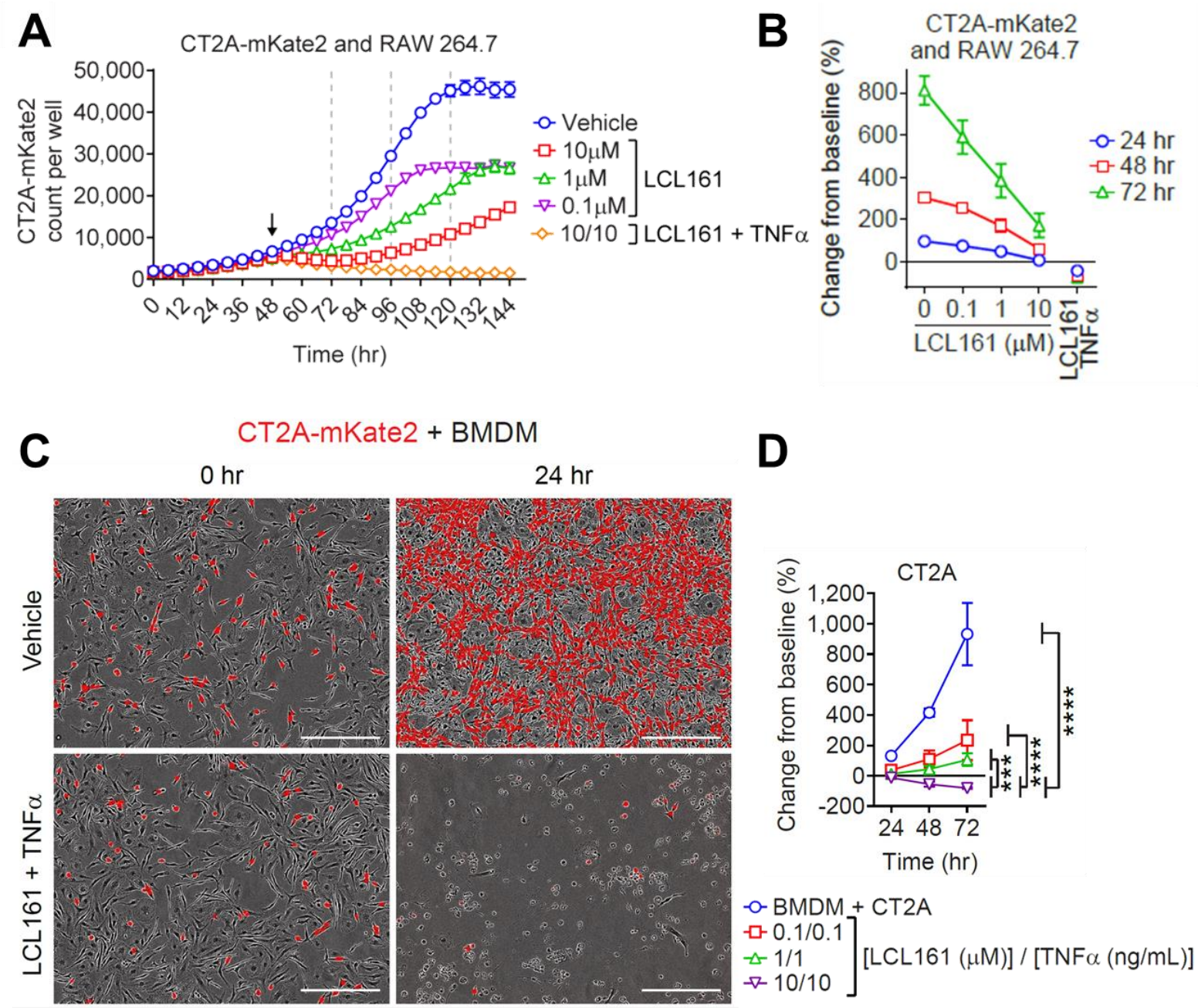
A
CT2A-mKate2 and RAW 264.7
CT2A-mKate2 count per well
50,000
40,000
30,000
20,000
10,000
0
0 12 24 36 48 60 72 84 96 108 120 132 144
Time (hr)
Vehicle
10μM
1μM
0.1μM
LCL161
10/10
LCL161 + TNFα
B
CT2A-mKate2 and RAW 264.7
Change from baseline (%)
800
600
400
200
0
0 0.1 1 10
LCL161 (μM)
LCL161 TNFα
24 hr
48 hr
72 hr
C
CT2A-mKate2 + BMDM
0 hr
24 hr
Vehicle
LCL161 + TNFα
D
CT2A
Change from baseline (%)
1,200
1,000
800
600
400
200
0
-200
24 48 72
Time (hr)
***
****
****
BMDM + CT2A
0.1/0.1
1/1
10/10
[LCL161 (μM)] / [TNFα (ng/mL)]

Figure 16: Macrophages enhance ability of SMCs to induce GBM cell death. A,B) CT2A-mKate cells were cultured with RAW macrophages and treated with indicated doses of LCL1612 and 10ng/mL TNFα. mKate2-positive events were assessed using live cell microscopy. Percent change over 72hr was calculated from bulk mKate2-positive events (A) and plotted (B). Arrow indicates treatment point, dashed lines indicate time point for subsequent calculations. N=3 technical replicates per treatment group. C,D) CT2A-mKate2 cells were co-cultured with BMDMs and treated with indicated doses of LCL161 and TNFα. mKate2 positive events were enumerated via live cell microscopy imaging (C) and quantified over 72hr (D). ***P<0.001; ****P<0.0001 via two-way ANOVA using Tukey's HSD multiple comparison test. N=1 independent experiment per timepoint.

3.2.3 Astrocytes protect microglia and GBM cells from SMCs in absence of TNFα

Given the multifaceted roles of astrocytes in GBM apoptotic resistance (**Section 1.2.5**) and modulating neuroinflammation (**Section 1.3.2**), I sought to examine the role of astrocytes in SMC-based GBM killing. Astrocytes form a border 'scar' around *in vivo* GL261 tumors, which is significantly increased around the tumor following twice weekly (four total) LCL161 treatments (Figure 17A-C) indicating a significant tumor-local role for these cells in SMC-based therapies. Co-cultures of CT2A-mKate2 cells with murine astrocytes lead to a significant increase in growth rate over 24h and 48h regardless of treatment with high dose LCL161 or TNFα (Figure 18A,B). Conversely, presence of astrocytes enhanced cytotoxicity of LCL161 and TNFα cotreatment (Figure 18C,D). No changes in astrocyte viability were observed following treatment with LCL161, TNFα or the combination (Figure 18E), suggesting this effect is due to alterations in astrocyte functionality rather than paracrine signaling of cell death related factors as seen in microglia/macrophage-GBM cocultures.

To assess whether SMCs could affect astrocyte reactivity directly, murine astrocytes treated with high dose LCL161, LPS (positive control) or TNFα were stained for glial fibrillary acidic protein (GFAP) positivity, which is increased upon adoption of reactive states[525]. Concurrent flow cytometric analyses of GFAP, C3c and PD-L1 expression were undertaken. High dose LCL161 increased GFAP expression concurrent with increased C3c (Figure 19B,C), LCL161 effects were minimal compared to LPS- or TNFα-induced upregulations (Figure 19A).

As LCL161 alone does not induce sufficient death ligand expression from astrocytes to induce GBM cytotoxicity in cocultures (Figure 18A), I sought to determine whether repeat treatments with high dose LCL161 would induce sufficient astrocyte reactivity for induction of GBM cell death. Presence of astrocytes buffered growth inhibitory effects of repeat high dose LCL161

(Figure 19D). Together, these data suggest that the enhanced cytotoxicity of LCL161 and TNFα in astrocyte-GBM cocultures is a result of TNFα-induced astrocyte reactivity (Figure 19A), consequent production of inflammatory factors and death ligands, ultimately acting in a paracrine fashion on LCL161-sensitized GBM cells to induce cell death.

As the GBM TME consists of multiple interacting cell types, I sought to determine the impact of astrocytes on GBM-microglia/macrophage cocultures. Regardless of the presence of CT2A-mKate2 cells or RAW macrophages, astrocytes protected BV2 microglia from LC161 cytotoxicity (Figure 19E). This protective effect contributed to increased growth of CT2A cells compared to cultures lacking astrocytes (Figure 19F). All protective effects are abolished in the presence of exogenous TNFα (Figure 19G), with near complete loss of viable CT2A cells.

Together, these data suggest the highly immunosuppressive and GBM growth-promoting microglia and macrophage populations represent potential sources of death ligands to enhance SMC-based GBM treatments, and that astrocytes can buffer or enhance this cytotoxicity dependent on the presence of TNFα. The results of **Section 3.1** and **Section 3.2** therefore indicate that dose of LCL161 and extent of intratumoral inflammation are limiting factors for the efficacy of SMC-based immunotherapies.

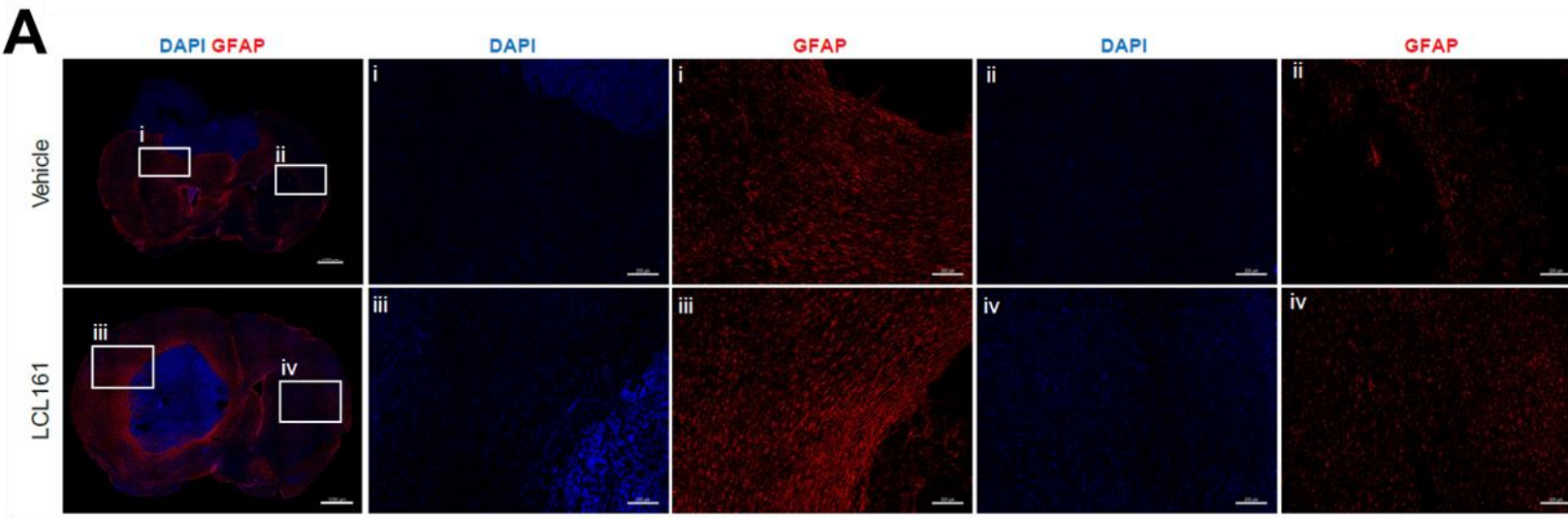
A
DAPI GFAP
DAPI
GFAP
DAPI
GFAP
Vehicle
LCL161
i
ii
iii
iv

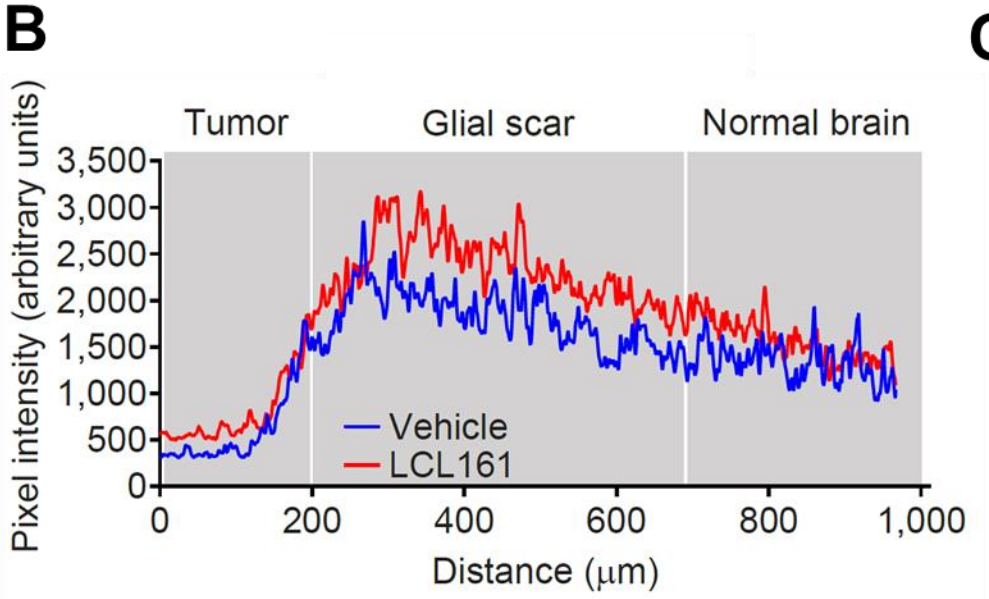
B
Tumor
Glial scar
Normal brain
Pixel intensity (arbitrary units)
3,500
3,000
2,500
2,000
1,500
1,000
500
0
0
200
400
600
800
1,000
Distance (μm)
Vehicle
LCL161

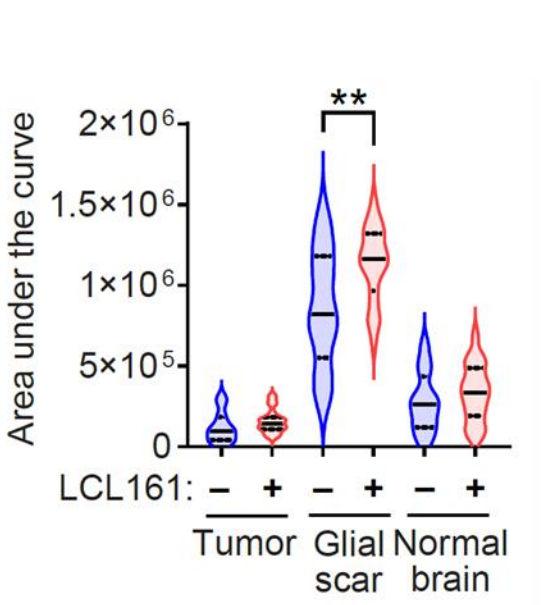
C
Area under the curve
2×10^6
1.5×10^6
1×10^6
5×10^5
0
**
LCL161: – + – + – +
Tumor
Glial scar
Normal brain

Figure 17: SMCs enhance astrocyte reactivity surrounding *in vivo* GBM tumors. A) Mice with inctracranial GL261 tumors were treated orally twice weekly with vehicle or 100mg/kg LCL161 for a total of four doses. At day 18 post-implant, brains were processed for immunohistochemical expression of GFAP surrounding tumor (i, iii) or outwards on contralateral side (ii,iv). B) GFAP intensity was calculated at the tumor border and plotted as mean (B) and area under the curve (C). N=3 vehicle, N=5 LCL161 treated animals per group. Scale bar: 1mm or 200μm as indicated. **P<0.01 via two-way ANOVA using Tukey's HSD multiple comparison test.

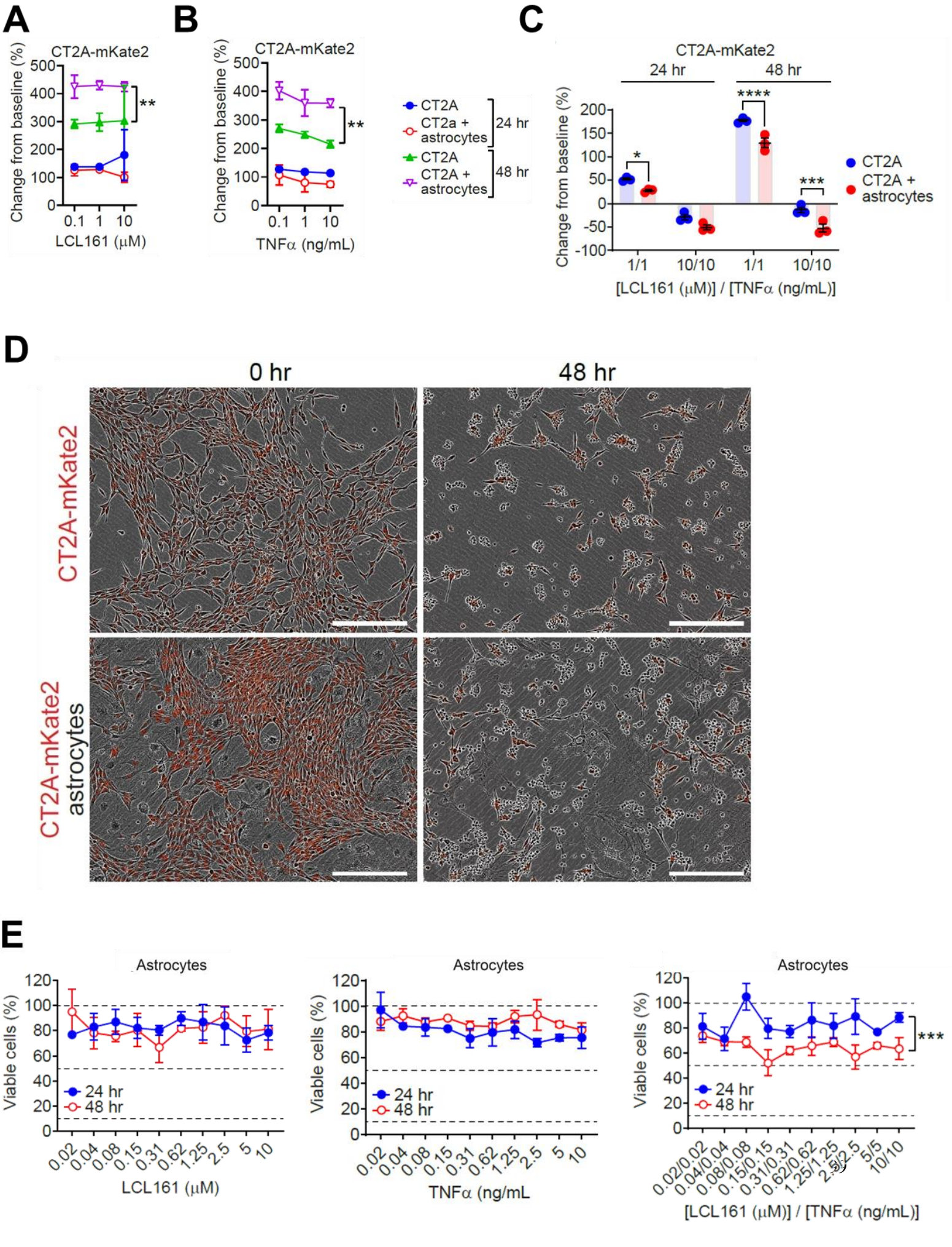
A
CT2A-mKate2
Change from baseline (%)
500
400
300
200
100
0
**
0.1 1 10
LCL161 (μM)
B
CT2A-mKate2
Change from baseline (%)
500
400
300
200
100
0
**
0.1 1 10
TNFα (ng/mL)
CT2A
CT2a + astrocytes
24 hr
CT2A
CT2A + astrocytes
48 hr
C
CT2A-mKate2
24 hr
48 hr
Change from baseline (%)
200
150
100
50
0
-50
-100
*
****
***
1/1
10/10
1/1
10/10
[LCL161 (μM)] / [TNFα (ng/mL)]
CT2A
CT2A + astrocytes
D
0 hr
48 hr
CT2A-mKate2
CT2A-mKate2 astrocytes
E
Astrocytes
Viable cells (%)
120
100
80
60
40
20
0
24 hr
48 hr
0.02 0.04 0.08 0.15 0.31 0.62 1.25 2.5 5 10
LCL161 (μM)
Astrocytes
Viable cells (%)
24 hr
48 hr
0.02 0.04 0.08 0.15 0.31 0.62 1.25 2.5 5 10
TNFα (ng/mL
Astrocytes
Viable cells (%)
***
24 hr
48 hr
0.02/0.02
0.04/0.04
0.08/0.08
0.15/0.15
0.31/0.31
0.62/0.62
1.25/1.25
2.5/2.5
5/5
10/10
[LCL161 (μM)] / [TNFα (ng/mL)]

Figure 18: Astrocytes promote SMC-mediated GBM cell death under inflammatory conditions. A-D) Mouse cortical astrocytes were co-cultured with CT2A-mKate2 cells and treated with LCL161 (A), TNFα (B) or the combination (C,D) over 48hr. Viable cells were enumerated by tracking mKate2-positive events using live cell imaging. Scale bar: 300μm. N=3 per treatment group. E) Astrocytes were treated with dilution series of LCL161 (left), TNFα (middle) or the combination (right) over 48hr. Viability was assessed using Alamar blue. N=3 technical replicates per treatment group. N=1 independent experiment per timepoint. *P<0.05; **P,0.01; ***P<0.001; ****P<0.0001 via two-way ANOVA using Tukey's HSD multiple comparison test.

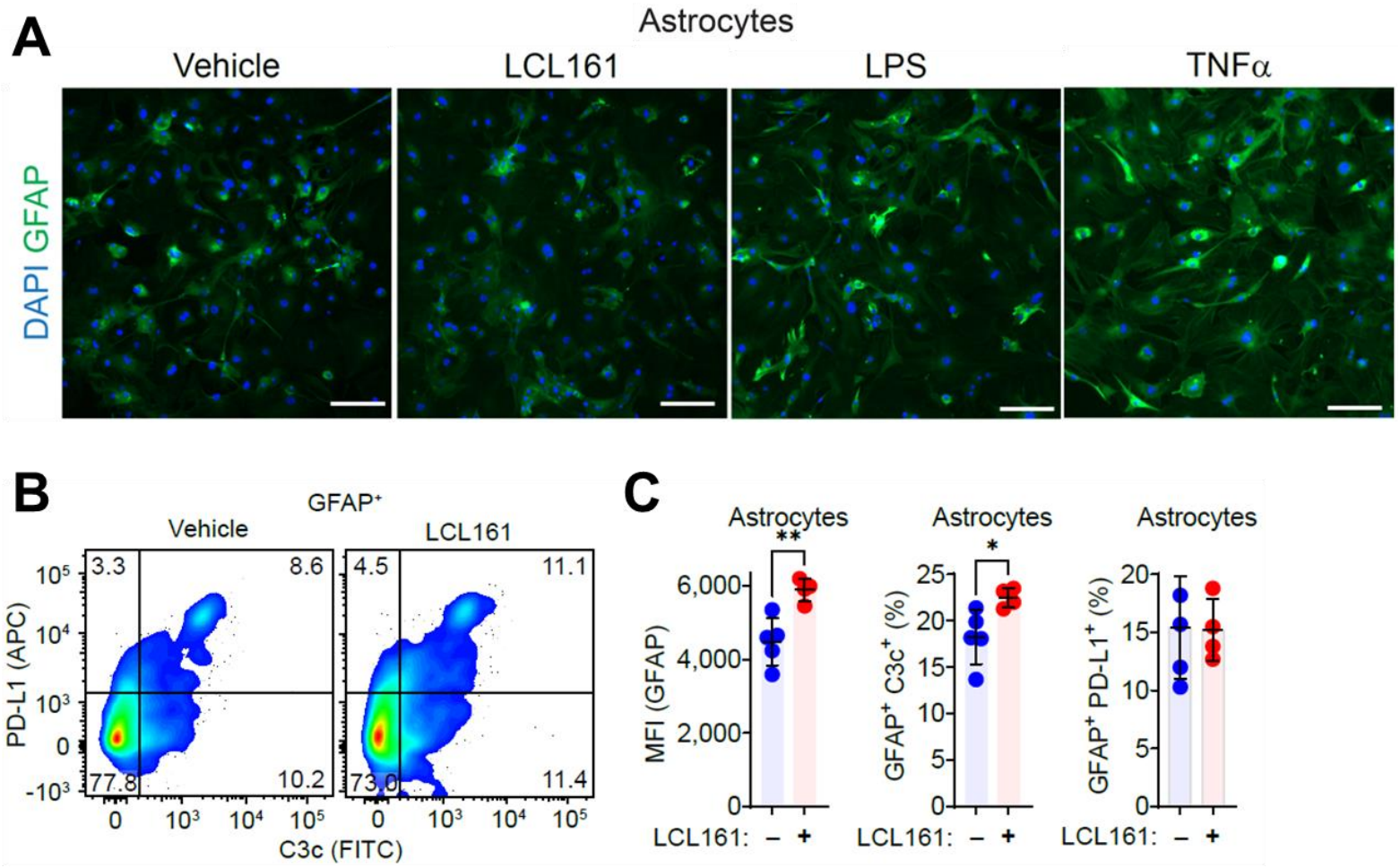
A
Astrocytes
Vehicle
LCL161
LPS
TNFα
DAPI GFAP
B
GFAP+
Vehicle
LCL161
3.3
8.6
77.8
10.2
4.5
11.1
73.0
11.4
PD-L1 (APC)
C3c (FITC)
C
Astrocytes
MFI (GFAP)
GFAP+ C3c+ (%)
GFAP+ PD-L1+ (%)
LCL161: – +
D
CT2A-mKate2
Vehicle
LCL161
CT2A-mKate2
Vehicle
LCL161
CT2A-mKate2
Astrocytes
Count per well
Time (hr)
E
BV2
Change from baseline (%)
Astrocytes:
CT2A:
RAW 264.7:
F
CT2A
Change from baseline (%)
Astrocytes:
BV2:
RAW 264.7:
G
CT2A
Change from baseline (%)
Astrocytes:
BV2:
RAW 264.7:

Figure 19: Astrocytes protect microglia, macrophages and GBM cells from SMC-induced cell death. A) Mouse cortical astrocytes were treated with LCL161 (10μM), LPS (500ng/mL) or TNFα (10ng/mL) for 24hr and assayed for GFAP expression via immunocytochemistry. Scale bar: 200μm. B,C) Flow cytometric analysis of $GFAP^+$ mouse cortical astrocytes treated with 10μM LCL161. Cells were analyzed for MFI of GFAP (PE-CF594) and proportional C3c (FITC) and PD-L1 (APC) expression. N=5 technical replicates per treatment group. *P<0.05; **P<0.01 assessed by t-test. D) Astrocyte and CT2A-mKate2 co-cultures were treated with three daily doses of 10μM LCL161 (arrows) and mKate2-positive events plotted over time. N=3 per treatment group. E,F) BV2-EGFP and CT2A-mKate2 counts in co-cultures with RAW cells and primary mouse astrocytes treated with 10μM LCL161 for 72hr. E) EGFP and F) mKate2-positive events were assessed using live cell imaging. N=3 technical replicates per treatment group. G) Co-cultures in (E,F) treated with combination 10μM LCL161 and 10ng/mL TNFα for 72hr and analysed as before. N=3 technical replicates per treatment group. *P<0.05; **P<0.01; ***P<0.0001 by two-way ANOVA using Tukey's HSD multiple comparison test. N=1 independent experiment per timepoint.

3.3 TGFβ limits efficacy of SMC and ICB

3.3.1 Increasing dose of LCL161 significantly improves efficacy of cotherapy

I next sought to assess the impact of increased SMC dose *in vivo*. Given previous findings on the profound GBM-killing effects of LCL161 in microglia/macrophage cocultures, I examined the effects of LCL161 as a monotherapy at different schedules and doses. Past work has used 75mg/kg twice weekly over two weeks as a standard dose and schedule (Figure 8G). I compared this to 75mg/kg every day for 1-, 2- or 3-weeks post-implant and found no significant survival benefit (Figure 20A). Increasing dose from 75mg/kg to 100mg/kg had no significant survival benefit (Figure 20B). Increased dose and frequency of LCL161 was well tolerated, with no significant alterations to animal body weight (Figure 20C). Mouse spleen size and weights were significantly increased by LCL161 regardless of schedule (Figure 20D,E), a de facto measure of available immune reserves[409]. Tumor size was significantly reduced only in animals receiving high frequency LCL161 (Figure 20F), and this was associated with significant reductions in the TAM populations (Figure 20G,H), characterized as tumor-infiltrating $CD45^+$ $CD11b^+$ $F4/80^+$ cells by flow cytometry. Therefore, increasing dose of LCL161 recapitulates TAM killing effects seen *in vitro*.

I next aimed to assess the impact of this increased dose and schedule on synergism with αPD-1 ICB. GL261 and CT2A tumors treated with 100mg/kg LCL161 2x/week and αPD-1 as done previously (Figure 8G) demonstrated significant improvements in median and overall survival relative to animals receiving 75mg/kg LCL161 at the same schedule (Figure 21A,B). Interestingly, increasing the frequency of 100mg/kg LCL161 treatments to 5x/week significantly reduced the efficacy of combination with αPD-1. This was consistent across both models, however most profound in CT2A. Increasing dose from 75mg/kg to 100mg/kg nearly doubled

the proportion of long-term survivors (3/8 to 7/10). Increasing the frequency of 100mg/kg LCL161 treatments to 5x/week produced less than one third the number of long-term survivors (1/10) compared to original dose and schedule (Figure 21B). This effect was associated with significant toxicity before treatment end. Most animals receiving 100mg/kg 5x/week LCL161 with αPD-1 showed no sign of tumor and normal brain on gross inspection at endpoint (Figure 21C,D), suggesting successful tumor clearance but significant on-target off-tumor effects. In keeping with this, lymph nodes and spleens of animals bearing GL261 tumors and treated with 100mg/kg LCL161 5x/week showed significant reductions in side scatter (SSC) low, forward scatter (FSC) mid populations (Figure 21E-G), suggesting severe immunotoxicity. Therefore, increasing dose of orally administered LCL161 significantly enhances efficacy of combination with αPD-1 ICB in curing murine GBM tumors, however this route of administration is associated with significant treatment frequency-dependent off-tumor effects that reduce survival.

I looked to characterize the effects of this 100mg/kg regimen on peripheral and intratumoral immunity. I used the GL261 model for these experiments, as it best recapitulates the human TME relative to other murine models[526]. Mice bearing IC GL261 tumors showed significant reductions in $CD3^+$ T-cells in both spleen and lymph nodes (Figure 22A,C), with LCL161 treatment further reducing T-cells in the lymph nodes. Implantation of IC GL261 tumors increased splenic CCR7, CD127, and CTLA4 on $CD4^+$ T-cells, with no alterations resulting from LCL161 treatment (Figure 22E-G). Both PD-1 and LAG3 were increased on splenic $CD4^+$ and $CD8^+$ T-cells in GL261 bearing animals. LCL161 reduced expression of both checkpoints, especially on $CD8^+$ T-cells (Figure 22J,K). LCL161 treatment also increased $CD4^+$ T-cell OX40 expression and $CD4^+$ and $CD8^+$ T-cell CD69 expression in the lymph nodes (Figure 22L,M), concurrent with increased frequency of CD25 expressing $CD4^+$ T-cells (Figure 22P). These findings indicate that while IC

implant of GL261 murine GBM cells significantly reduces T-cell proportions in peripheral lymphoid organs, orally administered LCL161 increases expression of T-cell activation markers and reduces immune checkpoint molecule expression.

I then assayed GL261 tumors for immune infiltrates to determine whether these peripheral effects were reflected by changes in the TME. No significant changes in overall T-cell infiltrates were observed (Figure 23A,C). A trend towards increased proportion of $CD4^+$ T-cells was seen, although this did not reach significance (Figure 23B,D,E). Despite promising immune-activating effects in the periphery, no changes in CD69, OX40, PD-1, LAG3 or TIM3 expression were seen following LCL161 treatment (Figure 23F-J), although trends towards decreased PD-1 and LAG3 were seen. A trend towards reduced TAM cells was seen in LCL161 treated animals, although this was not significant (Figure 23K,L,N). Trends towards reduced $Ly6C^+$ $Ly6G^-$ and increased $Ly6C^+Ly6G^+$ cells were seen, although this did not reach significance (Figure 23M,O-Q). Therefore, high dose LCL161 has significant immunostimulatory effects in peripheral lymphoid organs that is not reflected within the tumor, setting the stage for enhanced synergism with αPD-1 ICB. At doses which do cause significant alterations to TAM populations, combination with ICB almost eliminates tumor burden but is associated with severe off-tumor toxicity and reductions in lymphocyte populations. Thus, novel means of enhancing LCL161 effects within the tumor are needed.

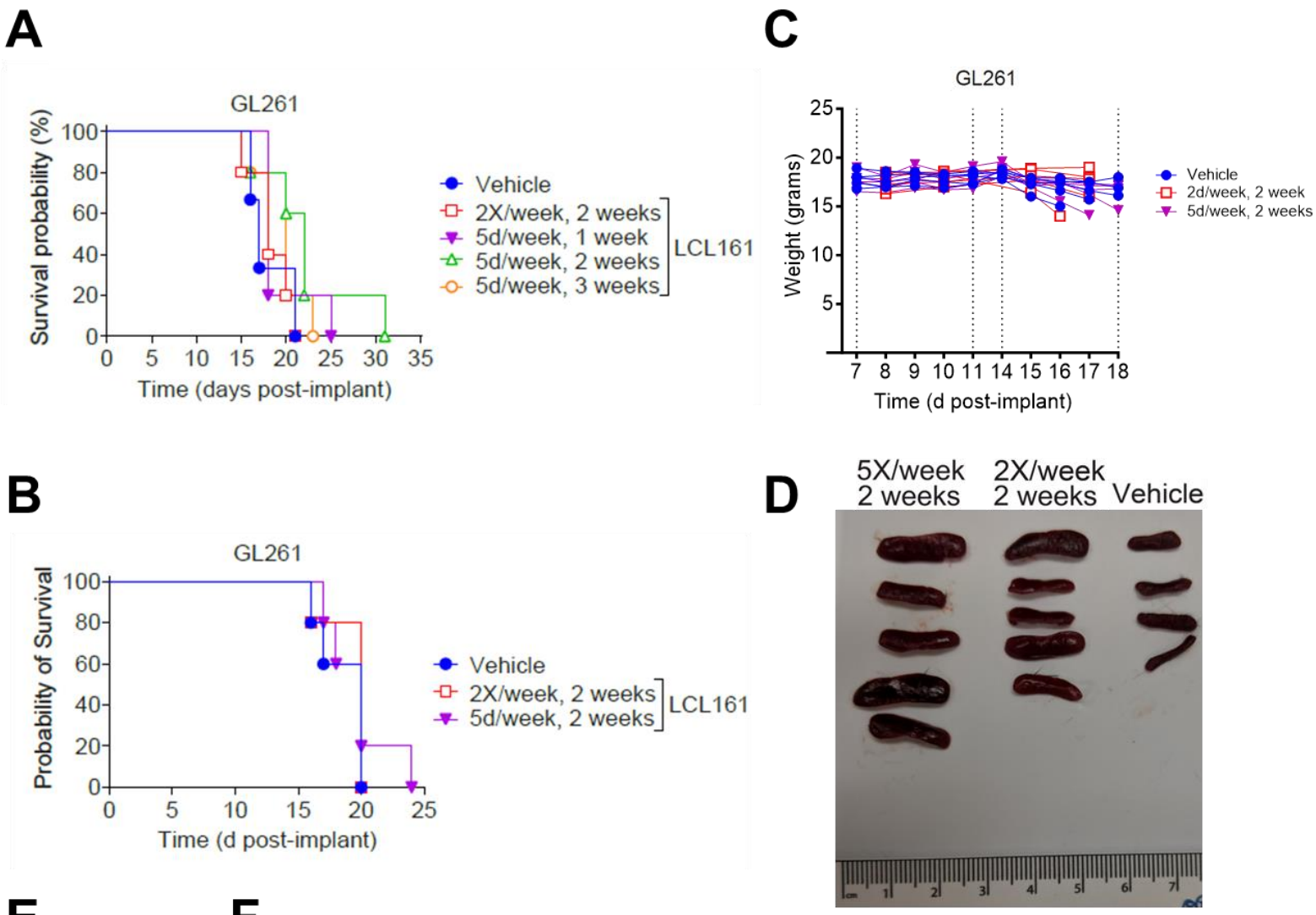
A
GL261
Survival probability (%)
Time (days post-implant)
Vehicle
2X/week, 2 weeks
5d/week, 1 week
5d/week, 2 weeks
5d/week, 3 weeks
LCL161
C
GL261
Weight (grams)
Time (d post-implant)
Vehicle
2d/week, 2 week
5d/week, 2 weeks
B
GL261
Probability of Survival
Time (d post-implant)
Vehicle
2X/week, 2 weeks
5d/week, 2 weeks
LCL161
D
5X/week 2 weeks
2X/week 2 weeks
Vehicle
E
Spleen
Weight (mg)
Vehicle
2X/week, 2 weeks
5d/week, 2 weeks
F
Tumor
Weight (mg)
Vehicle
2X/week, 2 weeks
5d/week, 2 weeks
G
Vehicle
5X/week 2 weeks
CD45+ CD11b+
9.76
1.82
CD45 (BV786)
CD11b (APC)
H
Tumor
Live CD45+CD11b+F4/80+ (%)
Vehicle
2X/week, 2 weeks
5d/week, 2 weeks

Figure 20: High dose LCL161 is well tolerated *in vivo* and reduces tumor size and TAM proportions. A) Mice were implanted with $5x10^4$ GL261 cells and treated orally with vehicle or 75mg/kg LCL161 2x/week for 2 weeks or 5x/week for 1 week, 2 weeks or 3 weeks. N=3 for vehicle, N=5 for all other treatment groups. B) Mice implanted with GL261 cells were treated with vehicle or 100mg/kg LCL161 2x/week or 5x/week for 2 weeks. N=5 per treatment group. Data represent the Kaplan-Meier curve depicting mouse survival. Log-rank with Holm-Sidak multiple comparison. C) Mouse weights plotted over course of 100mg/kg treatments received in B). D-F) Images (D) and weights (E) of mouse spleens and tumor (F) following 100mg/kg LCL161 treatments described in B). G,H) Flow cytometric analysis of CD45 (BV786) and CD11b (APC) expression among live cells in GL261 tumors at end of LCL161 treatment schedule. Bar plots are percent of live cells $CD45^+$ $CD11b^+$ F4/80 $(PE)^+$. N=9 for vehicle, N=3 for 2x/week and N=10 for 5x/week treatment groups. *P<0.05; **P<0.01; ****P<0.0001 via one-way ANOVA using Tukey's HSD multiple comparison test.

A

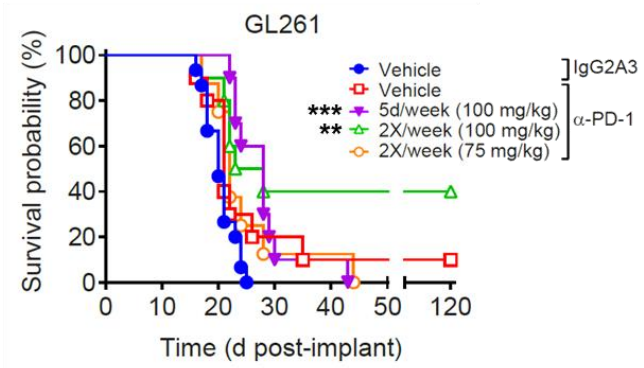

B

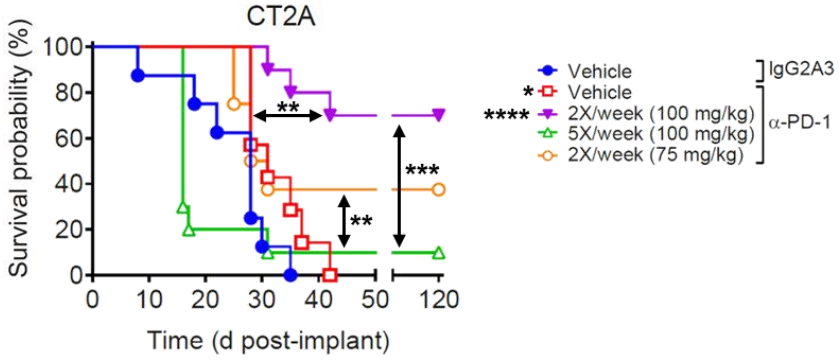

C

CT2A

Treatment group (GL261)	Survivors/total	Proportion with tumors at endpoint
Vehice + IgG2A3	0/9	9/9 (100%)
Vehicle + α-PD-1	0/10	10/10 (100%)
LCL161 (2X/week, 75 mg/kg) + α-PD-1	3/8	5/5 (100%)
LCL161 (2X/week, 100 mg/kg) + α-PD-1	7/10	3/3 (100%)
LCL161 (5X/week, 100 mg/kg) + α-PD-1	1/10	2/9 (22%)

D

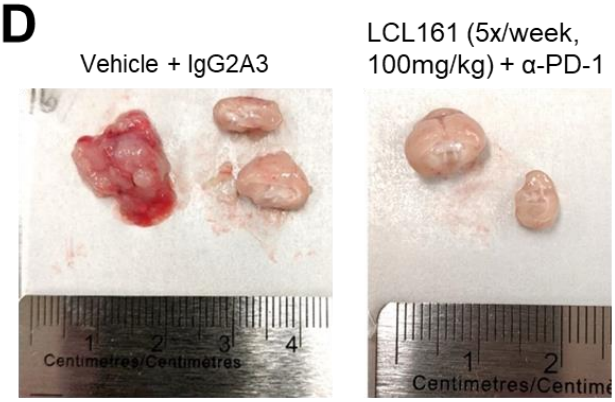

E

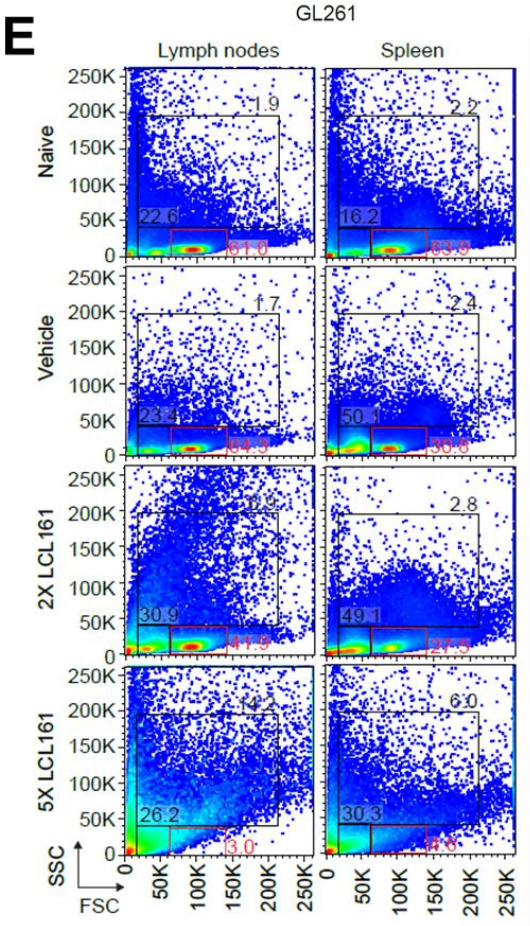

F

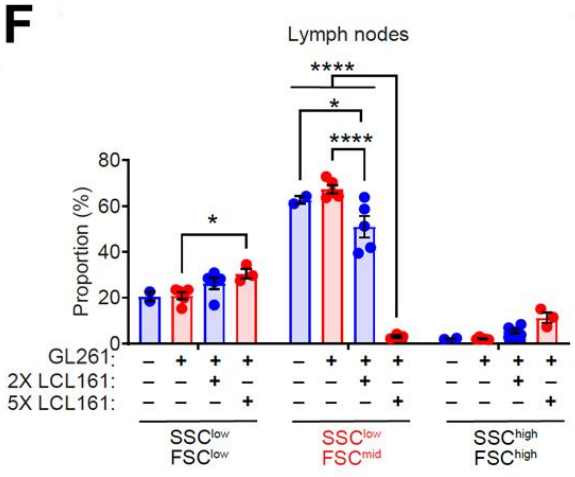

G

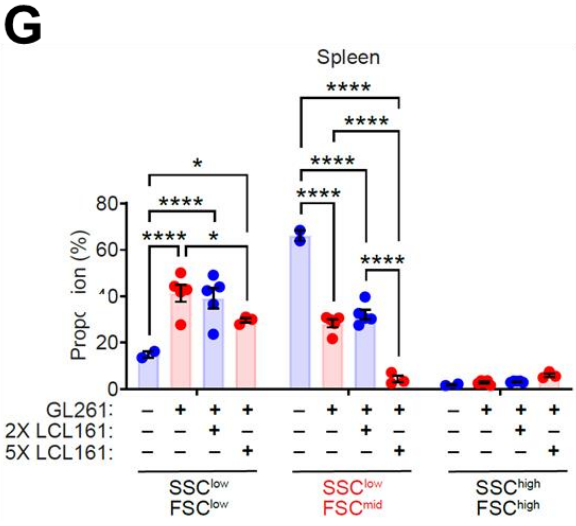

Figure 21: Increased dose of LCL161 significantly enhances efficacy of αPD-1 ICB for GBM. A,B) Mice were implanted with $5x10^4$ GL261 (A) or CT2A (B) cells and treated orally with 75mg/kg or 100mg/kg LCL161 and intraperitoneally with 10mg/kg of isotype control or αPD-1 antibody. Data represent the Kaplan-Meier curve depicting mouse survival. Log-rank with Holm-Sidak multiple comparison. A) N=15 Vehicle/IgG2A3, N=8 Vehicle/αPD-1, N=6 2x/week (100mg/kg)/αPD-1, N=10 5x/week (100mg/kg)/αPD-1, N=8 2x/week (75mg/kg)/αPD-1. B) N=8 Vehicle/IgG2A3, N=8 2x/week (75mg/kg)/αPD-1, N=10 remaining treatment groups. *P<0.05; **P<0.01; ***P<0.001; ****P<0.0001. C) Number of survivors and proportion of animals with observable tumor at endpoint in CT2A treated animals from B). D) Representative images of endpoint mouse brains and CT2A tumors in animals receiving indicated treatments. E-G) Flow cytometric analysis of side scatter (SSC) and forward scatter (FSC) of lymph nodes and spleen from GL261-bearing mice following two-week treatments as in A). Bar plots are proportion of cells within indicated gates and tissues. N=2 for naïve, N=3 for 5x/week, N=5 per remaining treatment group. *P<0.05; ****P<0.0001 via two-way ANOVA using Tukey's HSD multiple comparison test.

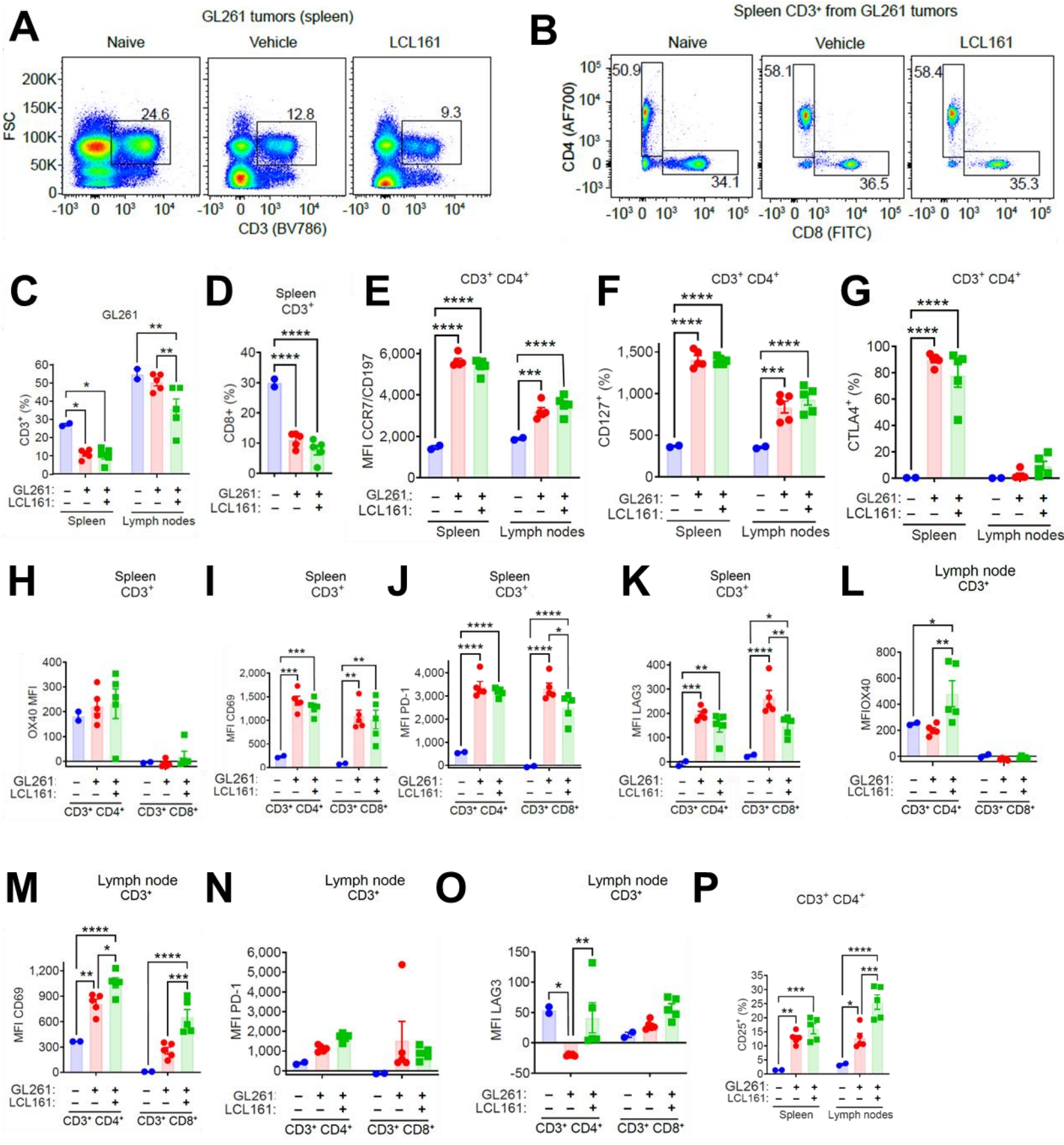
A
GL261 tumors (spleen)
Naive
Vehicle
LCL161
FSC
CD3 (BV786)
24.6
12.8
9.3
B
Spleen CD3+ from GL261 tumors
CD4 (AF700)
CD8 (FITC)
50.9
34.1
58.1
36.5
58.4
35.3
C
GL261
CD3+ (%)
D
Spleen CD3+
CD8+ (%)
E
CD3+ CD4+
MFI CCR7/CD197
F
CD3+ CD4+
CD127+ (%)
G
CD3+ CD4+
CTLA4+ (%)
GL261:
LCL161:
Spleen
Lymph nodes
H
Spleen CD3+
OX40 MFI
I
Spleen CD3+
MFI CD69
J
Spleen CD3+
MFI PD-1
K
Spleen CD3+
MFI LAG3
L
Lymph node CD3+
MFIOX40
CD3+ CD4+
CD3+ CD8+
M
Lymph node CD3+
MFI CD69
N
Lymph node CD3+
MFI PD-1
O
Lymph node CD3+
MFI LAG3
P
CD3+ CD4+
CD25+ (%)

Figure 22: LCL161 upregulates T-cell activation markers in peripheral lymphoid organs. A,B) Flow cytometric analysis of CD3 (BV786), CD4 (AF700) and CD8 (FITC) in spleen from mice bearing GL261 tumors and treated with vehicle or 100mg/kg LCL161 2x/week. C) Quantification of proportion of live cells $CD3^+$ in spleen and lymph nodes across indicated treatment groups. N=2 for unimplanted, N=5 per remaining treatment groups. *P<0.05; **P<0.01 via two-way ANOVA using Tukey's HSD multiple comparison test. D) Quantification of splenic $CD3^+$ $CD8^+$ cells across treatment groups. ****P<0.0001 via one-way ANOVA using Tukey's HSD multiple comparison test. E) MFI of CCR7 (BV605) among $CD3^+CD4^+$ cells in spleens of indicated treatment groups. F,G) Proportion of $CD3^+CD4^+$ cells $CD127^+$ (AF488, F) and $CTLA4^+$ (BV605,G) in spleen and lymph nodes. H-O) MFI of OX40 (PE, H & L), CD69 (BV605, I & M), PD-1 (BV605, J & N), and LAG3 (BV711, K & O) on $CD3^+$ $CD4^+$ and $CD3^+$ $CD8^+$ cells in indicated organ receiving indicated treatment. P) Proportion of $CD3^+CD4^+$ cells in indicated organ expressing CD25 (APC) receiving indicated treatments.

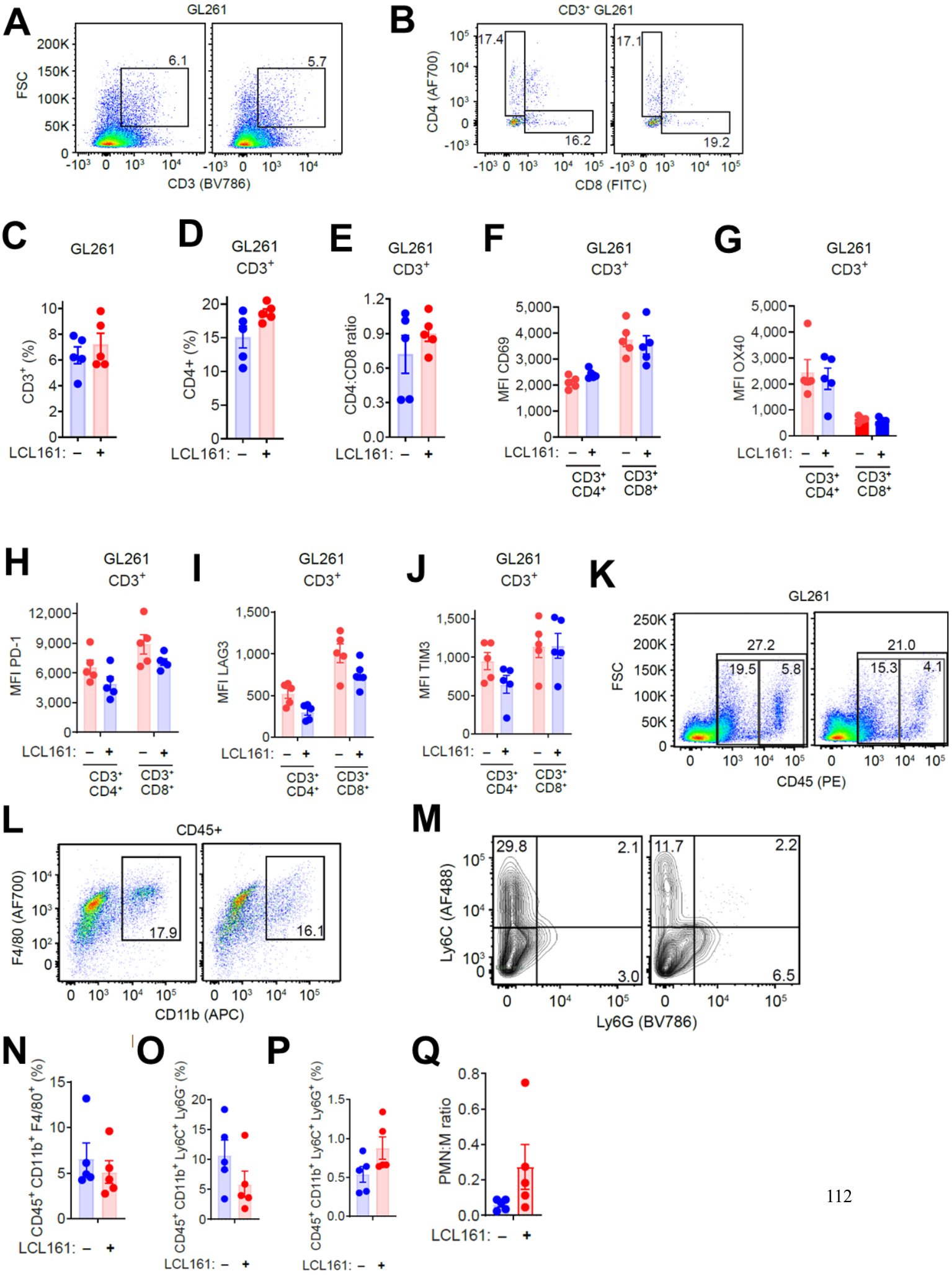
A
GL261
FSC
CD3 (BV786)
6.1
5.7
B
CD3+ GL261
CD4 (AF700)
CD8 (FITC)
17.4
16.2
17.1
19.2
C
GL261
CD3+ (%)
D
GL261
CD3+
CD4+ (%)
E
GL261
CD3+
CD4:CD8 ratio
F
GL261
CD3+
MFI CD69
G
GL261
CD3+
MFI OX40
LCL161: – +
CD3+ CD4+
CD3+ CD8+
H
GL261
CD3+
MFI PD-1
I
GL261
CD3+
MFI LAG3
J
GL261
CD3+
MFI TIM3
K
GL261
FSC
CD45 (PE)
27.2
19.5
5.8
21.0
15.3
4.1
L
CD45+
F4/80 (AF700)
CD11b (APC)
17.9
16.1
M
Ly6C (AF488)
Ly6G (BV786)
29.8
2.1
3.0
11.7
2.2
6.5
N
CD45+ CD11b+ F4/80+ (%)
O
CD45+ CD11b+ Ly6C+ Ly6G- (%)
P
CD45+ CD11b+ Ly6C+ Ly6G+ (%)
Q
PMN:M ratio

Figure 23: LCL161-induced peripheral immunoactivation is not reflected within tumor. A,B) Flow cytometric analysis of CD3 (BV786), CD4 (AF700) and CD8 (FITC) in GL261 tumors treated with vehicle or 100mg/kg LCL161 2x/week. C-E) Proportional CD3, CD4 and CD4:CD8 ratio in GL261 tumors receiving vehicle or LCL161 treatment. F-J) MFI of CD69 (F), OX40 (G), PD-1 (H), LAG3 (I) and TIM3 (J) among indicated $CD3^+$ subsets and treatments. K-M) Flow cytometric analysis of CD45 (PE), CD11b (APC), F4/80 (AF700), Ly6C (AF488) and Ly6G (BV786) in GL261 tumors. N) Proportion of live cells $CD45^+$ $CD11b^+$ $F4/80^+$ between treatment groups. O-Q) Proportion of cells Ly6C and Ly6G single or double positive and ratio between the two subgroups. N=5 per treatment group.

3.3.2 TGFβ blockade significantly enhances the efficacy of SMC and ICB in vivo

TGFβ and hypoxia have numerous roles in GBM biology, GSC phenotypes and niche characteristics, and maintenance of the immunosuppressive TME (**Section 1.2.3, 1.2.5, 1.3.2, 1.3.3**). I first aimed to determine whether TGFβ affects microglia and macrophage sensitivity to LCL161. When pre-treated with TGFβ or cultured under hypoxic conditions, RAW macrophages, BV2 microglia and BMDMs show significantly reduced sensitivity to LCL161-induced cytotoxicity (Figure 24A-D). Hypoxia remains difficult to target pharmacologically, although several hypoxia-reversing strategies are in clinical trials for GBM[527]. One strategy involves normalizing tumor vasculature using low dose αVEGFR2 treatments to improve perfusion, restore regular blood flow and re-oxygenate tissues[528,529]. Treatment of mice bearing GL261 tumors with αVEGFR2 lead to significant increases in long-term survival but did not synergize with LCL161 and αPD-1 cotherapy (Figure 24E), suggesting hypoxia and tumor vasculature are important factors in GL261 tumor biology but not limiting factors for the cotherapy. I therefore continued to examine the role of TGFβ in treatment resistance. BV2 cells pre-treated with a dilution series of TGFβ were significantly protected from high dose LCL161 at 0.8ng/mL and above, with protection plateauing at doses 6.1ng/mL and above (Figure 24F), suggesting protective effects are contingent upon available TGFβ receptors. BV2 microglia showed no significant proliferative responses following TGFβ treatment. As TGFβ signaling has been found increase IAP expression [530], I tested whether administration of AZD5582, a SMC with greater IAP antagonizing capacity than LCL161[531,532], could restore the cytotoxic effects of IAP blockade in TGFβ-treated BV2 and RAW cells. Indeed, while TGFβ pre-treatment rescued viability of both cell types upon exposure to high dose (10μM) LCL161, treatment with AZD5582 abolished this protection (Figure 24G,H). To determine whether GBM-derived TGFβ

was sufficient to protect microglia from the cytotoxic effects of LCL161, BV2 cells were co-cultured with SMA560 murine GBM characterized by TGFβ secretion. Presence of SMA560 significantly protected BV2 cells from LCL161 (Figure 24I), suggesting TGFβ-secreting GBM cells protect TAMs from LCL161-induced cell death. TGFβ enhanced CT2A (Figure 24J) and reduced GL261 (Figure 24K) cell death following treatment with LCL161 and TNFα, although the protective effect on GL261 was minimal compared to that seen in macrophages and microglia. To determine whether TGFβ was a significant resistance mechanism for 100mg/kg LCL161 and αPD-1 ICB cotherapy, I administered αTGFβ concurrently to mice bearing GL261 tumors. Blockade of TGFβ alone had no significant impact on overall survival (Figure 24L), however αTGFβ treatment nearly tripled the number of cured animals relative to cotherapy alone (5/8 vs 2/8 long-term survivors). Therefore, TGFβ is a significant resistance factor to SMC and ICB cotherapy, and blockade of this cytokine significantly enhances cotherapy efficacy.

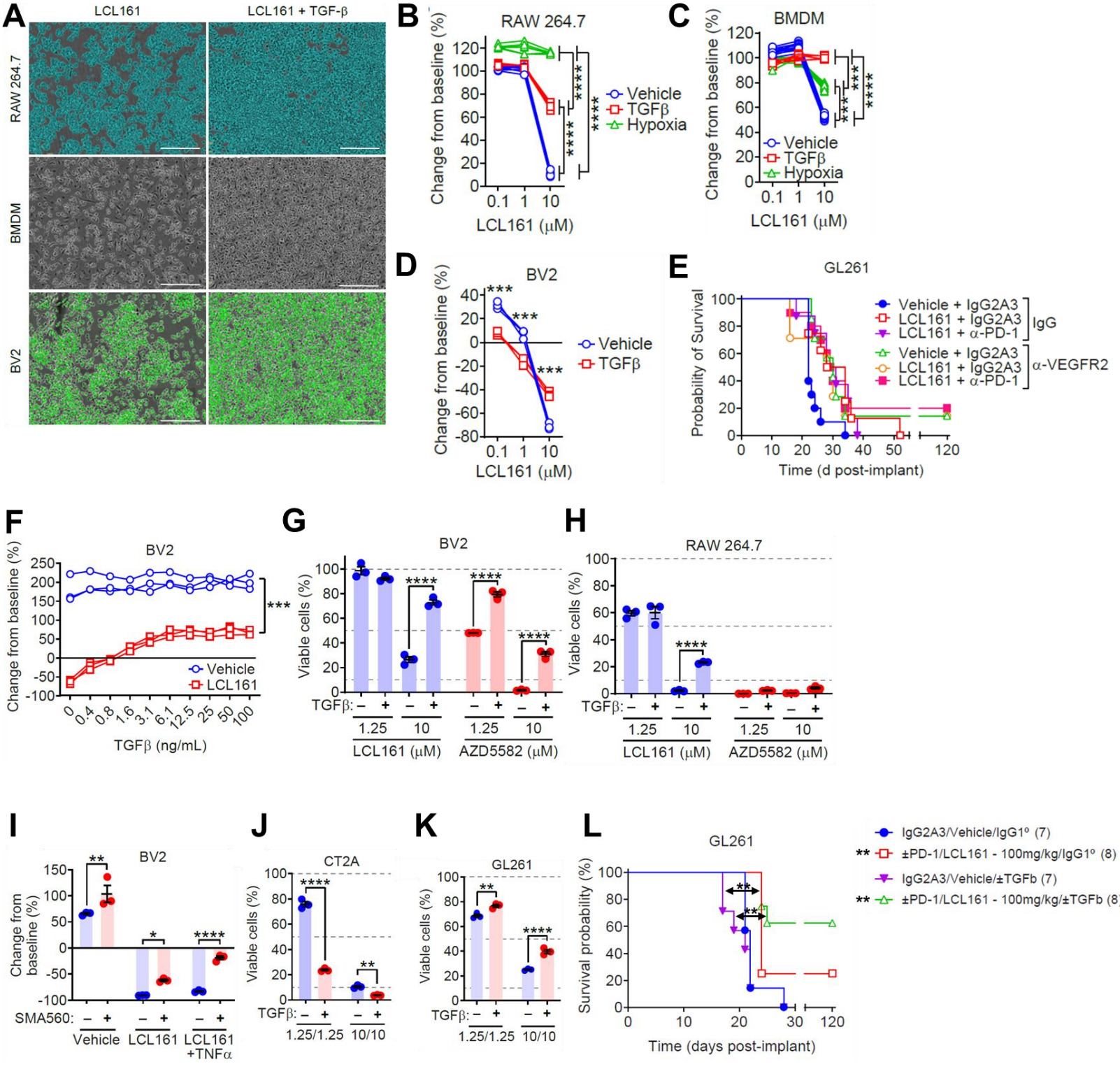
A
LCL161
LCL161 + TGF-β
RAW 264.7
BMDM
BV2
B
RAW 264.7
Change from baseline (%)
Vehicle
TGFβ
Hypoxia
LCL161 (μM)
C
BMDM
D
BV2
E
GL261
Probability of Survival
Vehicle + IgG2A3
LCL161 + IgG2A3
LCL161 + α-PD-1
IgG
α-VEGFR2
Time (d post-implant)
F
BV2
TGFβ (ng/mL)
G
BV2
Viable cells (%)
LCL161 (μM)
AZD5582 (μM)
H
RAW 264.7
I
BV2
Change from baseline (%)
SMA560:
Vehicle
LCL161
LCL161 +TNFα
J
CT2A
K
GL261
1.25/1.25
10/10
L
GL261
Survival probability (%)
Time (days post-implant)
IgG2A3/Vehicle/IgG1° (7)
±PD-1/LCL161 - 100mg/kg/IgG1° (8)
IgG2A3/Vehicle/±TGFb (7)
±PD-1/LCL161 - 100mg/kg/±TGFb (8)

Figure 24: TGFβ represents a significant resistance factor to SMC and ICB immunotherapy for GBM. A-D) RAW (N=6 technical replicates per treatment group), BMDM (N=5 technical replicates for TGF treated, N=12 technical replicates for remaining treatment groups) and BV2 (N=3 technical replicates per treatment group) cells were treated with 20ng/mL TGFβ or cultured in 5% O_2 for 24hr, then treated with DMSO or indicated doses of LCL161. Cell viability was assessed using Alamar blue. N=1 independent experiment per treatment. Scale bar: 300μm. ***P<0.001; ****P<0.0001 via two-way ANOVA using Tukey's HSD multiple comparison test. E) Mice were implanted with $5x10^4$ GL261 cells and treated orally with 100mg/kg LCL161 or vehicle, intraperitoneally with 10mg/kg αPD-1 or isotype control, and 30mg/kg αVEGFR2 or isotype control. Data represent Kaplan-Meier curve depicting mouse survival. Log-rank with Holm-Sidak multiple comparison. N=10 for Vehicle + IgG2A3 + IgG1 and LCL161 + αPD-1 + αVEGFR2. N=8 for LCL161 + IgG2A3 + IgG1 and LCL161 + αPD-1 + IgG1. N=7 for Vehicle + IgG2A3 + αVEGFR2. N=6 for LCL161 + IgG2A3 + αVEGFR2. F) BV2-EGFP were treated with varying concentrations of TGFβ for 24hr and then treated with 10μM LCL161 for 24hr. BV2-EGFP numbers were quantified by counting EGFP positive events via live imaging. Percent change in counts from prior to LCL161 treatment was calculated and plotted. N=3 technical replicates per treatment group. G,H) BV2 and RAW cells were treated with TGFβ for 24hr then treated with indicated doses of LCL161 or AZD5582. Cell viability was assessed using Alamar blue. N=3 technical replicates per treatment group. BV2-EGFP cells were co-cultured with SMA-560 cells and treated with the combination of 10μM LCL161 and 10ng/mL TNFα for 24hr. EGFP counts were enumerated by live cell imaging. N=3 technical replicates per treatment group. N=1 independent experiment per condition. J,K) CT2A (J) and GL261 (K) cells were treated for 24hr with TGFβ then with indicated doses of LCL161 and TNFα. Viability was assessed by Alamar blue. N=3 technical replicates per treatment group. N=1 independent experiment per condition. *P<0.05; **P<0.01; ****P<0.0001 via two-way ANOVA using Tukey's HSD multiple comparison test. L) Mice were implanted with $5x10^4$ GL261 cells and treated with 100mg/kg LCL161 and 10mg/kg αPD-1 and αTGFβ antibodies or vehicle and isotype control. Data represent the Kaplan-Meier curve depicting mouse survival. Log-rank with Holm-Sidak multiple comparison. N=7 or 8 per treatment group where indicated. **P<0.01.

To characterize how αPD-1 and αTGFβ agents synergize with LCL161, spleen and lymph nodes of mice bearing IC GL261 tumors were collected following 1 week of αPD-1, αTGFβ and/or LCL161 treatment and assayed for markers of T-cell activation and myeloid cell numbers. No significant differences in overall $CD3^+$ cells or CD8:CD4 ratios were observed regardless of treatment administered (Figure 25A,B). αPD-1 and αTGFβ treatments did not differ in their impact on OX40 or CD25 expression. Addition of LCL161 to any of the antibody blockade treatments significantly increased $CD4^+$ T-cell OX40 and CD25 expression in the lymph nodes (Figure 25C-E), in keeping with effects noted previously (Figure 22). Addition of LCL161 reduced the proportion of macrophages in the spleen (Figure 25I), with no significant impacts on Ly6C or Ly6G expression (Figure 25J-L). Animals treated with LCL161 showed a trend for increased proportion of $CD11b^+$ cells in the lymph nodes regardless of combination (Figure 25H).

Flow cytometric analysis of peripheral lymphoid organs shows LCL161 is the main immunostimulatory agent, increasing $CD4^+$ T-cell OX40 and CD25 regardless of combinatorial agent. Therefore, TGFβ protects microglia and macrophages from the cytotoxic effects of IAP blockade and hinders the efficacy of high dose LCL161 and αPD-1 cotherapy. Blockade using αTGFβ antibodies significantly enhances the efficacy of the cotherapy, nearly tripling the number of long-term survivors.

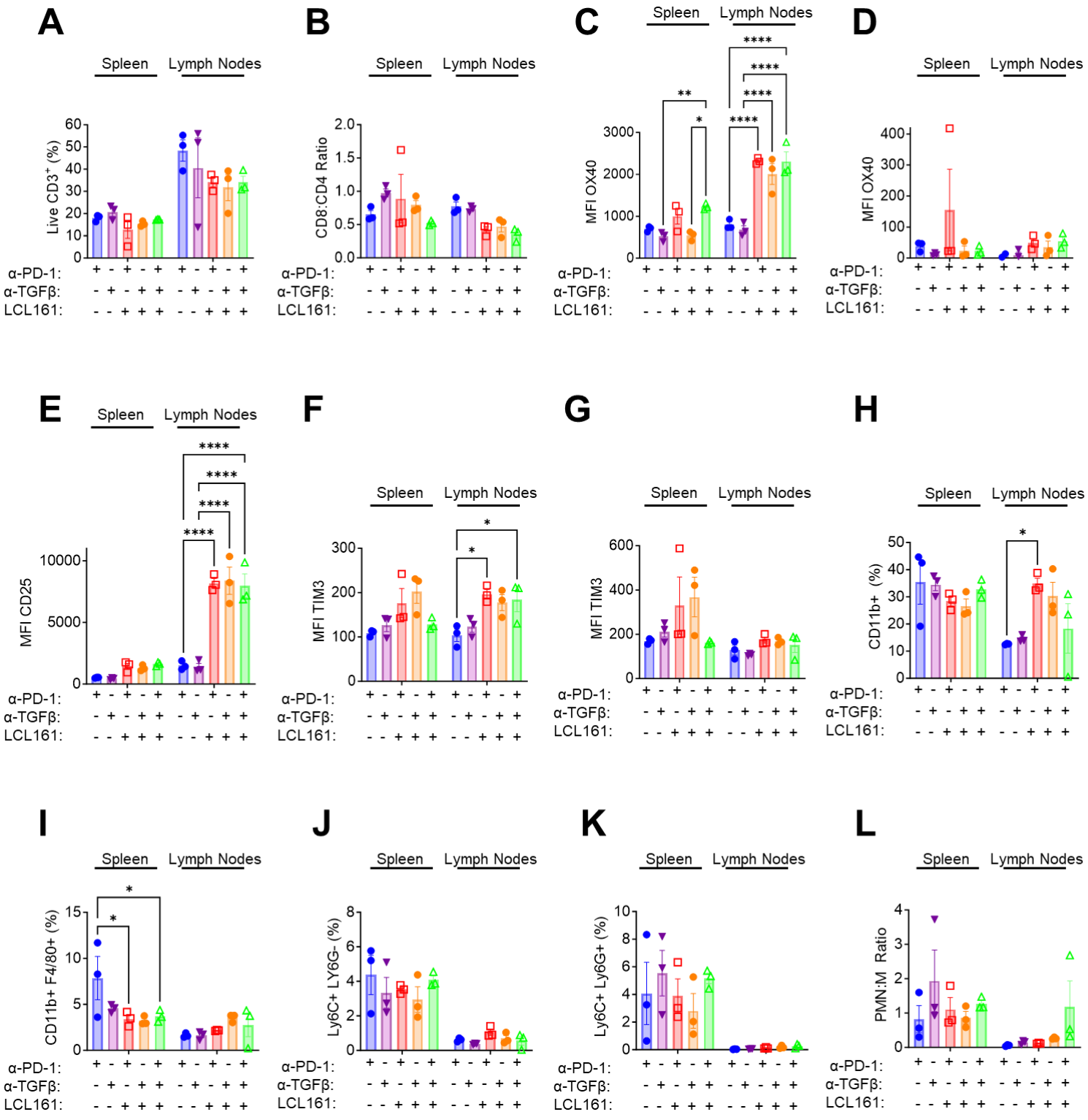
A
Spleen
Lymph Nodes
Live CD3+ (%)
B
CD8:CD4 Ratio
C
MFI OX40
D
MFI OX40
E
MFI CD25
F
MFI TIM3
G
MFI TIM3
H
CD11b+ (%)
I
CD11b+ F4/80+ (%)
J
Ly6C+ LY6G- (%)
K
Ly6C+ Ly6G+ (%)
L
PMN:M Ratio
α-PD-1:
α-TGFβ:
LCL161:

Figure 25: LCL161 is main immunostimulatory agent in cotherapy with αPD-1 and αTGFβ. Flow cytometric analysis of spleen and lymph nodes from mice bearing GL261 tumors and treated with indicated agents. A) Proportion of live cells $CD3^+$. B) Ratio of CD8:CD4 positivity among $CD3^+$ cells. C,D) MFI of OX40 (PE) in $CD3^+$ $CD4^+$ (C) and $CD3^+CD8^+$ (D) cells in indicated organ. E) MFI of CD25 (APC) among $CD3^+CD4^+$ cells. F,G) MFI TIM3 (PE) among $CD3^+$ $CD4^+$ (F) and $CD3^+CD8^+$ (G) cells in indicated organ. H) Proportion of $CD45^+$ (PE) cells $CD11b^+$ (APC) and I) $F4/80^+$ (AF700) in indicated organs. J-L) Ly6C (AF488) and Ly6G (BV786) proportion of $CD45^+CD11b^+F4/80^-$ cells in indicated organs, and ratio of the two subsets (L). *P<0.05; **P<0.01; ****P<0.0001 via two-way ANOVA using Tukey's HSD multiple comparison test. N=3 per treatment group.

4.0 Discussion

4.1 Dose, CNS location and age limit SMC-based GBM killing

cFLIP and PEA-15 as resistance mechanisms to SMC-induced GBM cell death

Herein, I present the most comprehensive characterization to date of GBM cell line sensitivity to inflammatory cell death mediated by IAP blockade. Targeting of the death receptor (extrinsic) apoptotic pathway represents a promising avenue for GBM treatment, as mitochondrial (intrinsic) pathways are significantly perturbed because of alterations to PI3K-Akt and NF-κB signaling, with high BCL-2:BH3 family protein ratios and reduced expression of apoptosome components. The extrinsic pathways are intact, however, with high TNFα-TNFR1 signaling a feature of GBM and a major contributing factor to high constitutive NF-κB activation (**Section 1.2.4**). This dependency represents a targetable vulnerability using agents blocking the IAPs, key regulators of death receptor, TNFR1 and NF-κB survival signaling. Despite intact pathways, I have found most human GBM cells resist SMC and TNFα- or TRAIL-induced cell death. This is in keeping with past findings showing expression of TRAIL receptors at higher levels than normal astrocytes[185,186] but resistance to apoptosis induction[175]. Previous work has elucidated that differences in sensitivity to these treatments are due to cFLIP binding to FADD, inhibiting FADD-Caspase-8 binding and DISC formation. Differential JNK-ITCH signaling in responders and non-responders contributes to differences in sensitivity, as downstream of these pathways are cFLIP degradation and turnover mechanisms[176]. siRNA-mediated genetic knockdown[533] or plant-derived compounds capable of degrading cFLIP[534,535] potently sensitize cancer cells to TRAIL-induced DISC formation and apoptosis. However, no effective, direct cFLIP inhibitors have been identified due to structural similarity of cFLIP DEDs with those of procaspase-8 and -10[536]. Recent work has identified candidate molecules selective for cFLIP DEDs and shows promising *in vitro* inhibition of cFLIP-FADD binding, improved caspase activation and sensitization of

cancer cells to TRAIL-induced apoptosis[537]. Further characterization and *in vivo* preclinical testing are required, but selective cFLIP inhibitors have the potential to drastically improve SMC-mediated GBM cell death.

Further to the actions of cFLIP, CNS cells express the highest RNA and protein levels of phosphoprotein enriched in astrocytes-15 (PEA-15) in the body[538–540]. In CNS cells it appears to play functionally redundant roles to cFLIP, as NSCs/NPCs express minimal cFLIP[541] and cFLIP has little function in NSC/NPC response to extrinsic apoptotic pathway stimulation[542]. Similar to cFLIP, PEA-15 contains an N-terminal DED that inhibits DISC formation through FADD and procaspase-8 binding, blocking death receptor-induced apoptosis[543,544]. This protein has key roles in CNS cell survival, and levels of PEA-15 are commonly reduced in neurodegenerative conditions[545–547]. Through alterations to its phosphorylation status via Akt and CamKII[548–550], which are highly expressed in the CNS[185], PEA-15 can inhibit DISC formation and block apoptosis[551–553]. Human GBMs show high levels of phosphorylated PEA-15 relative to normal brain[186,195] and inhibition of Akt enhances sensitivity of multiple GBM cell lines to TRAIL[554]. The role of PEA-15 in GBM may be more pronounced *in vivo* than *in vitro*, allowing cells to adapt to more diverse cellular stresses. PEA-15 was found in perinecrotic regions and significantly increased upon exposure to hypoxic and low glucose conditions. Upon glucose withdrawal, PEA-15 phosphorylation is increased in GBM cells, with consequent increases in ERK1/2 phosphorylation and GLUT3 expression, each providing further anti-apoptotic effects. siRNA knockdown almost eliminates the ability of U87 GBM cells to form tumours[555]. Thus, *in vitro* efficacy of cFLIP inhibitors may be blunted *in vivo* not only by drug delivery issues but also by compensatory increases in PEA-15. Combination with PI3K-Akt inhibitors and/or RTK inhibitors may remove these roadblocks to death receptor-mediated GBM cell death.

Survivin represents a targetable GSC-enriched resistance factor

In lieu of currently available cFLIP inhibitors, I show that all analyzed human GBM lines are sensitive to survivin inhibition using YM155 at nanomolar concentrations. Previous reports have shown that high survivin expression is associated with worse prognosis in GBM[556], and that YM155 decreases invasion and viability of M059J, M059K[202], U87[203], and LN229[556] human GBM cells. Survivin is increased in GSCs following RT, promoting the plasticity of differentiation states and inhibiting apoptosis. YM155 significantly reverses these effects at non-toxic doses[557]. *In vivo* efficacy is limited by neurotoxicity[558], poor CNS drug delivery and cytotoxicity to normal stem cell pools limiting clinical tolerability[559]. Prodrug formulations show similar GBM killing efficacy and significantly improved CNS penetrance and reduced GBM growth *in vivo*[559]. Nanoparticle delivery of YM155 corroborated our findings of reduced sensitivity of murine GBM cells relative to human, and this encapsulation method allowed for greater delivery to orthotopic tumors and significantly reduced growth relative to vehicle or saline-dissolved YM155[560]. Interestingly, immortalized murine NSCs (NE-4C cells) are sensitive in a dose-dependent fashion to YM155 like human GBM cells (Data not shown), suggesting a vulnerability of stem cell enriched GBMs to survivin inhibition.

GBM cell sensitivity to SMCs is conserved across microenvironment conditions

As opposed to our findings in human lines, murine GBM cells are all sensitive to SMC and TNFα-induced cell death in RIPK1-dependent manners. This sensitivity was conserved across a myriad of conditions. Hypoxia and hypoglycemia minimally protected GL261 cells from high dose LCL161 and TNFα, as did culture on brain ECM-mimicking proteins. Similarly, repeat treatments with LCL161 and TNFα did not affect sensitivity to subsequent treatments, nor did implantation into CNS and resistance to LCL161 and αPD-1 cotherapy. Finally, high dose

LCL161 and TNFα significantly reduced GL261 and CT2A sphere size and CT2A growth on organotypic brain slice cultures. Together, these data show that GBM cells sensitive to LCL161 and TNFα *in vitro* remain sensitive upon exposure to CNS TME components, suggesting resistance in these models is not GBM-cell intrinsic. Likely, then, limiting factors for SMC and αPD-1 ICB derive from GBM-associated immunosuppression, notably poor antigen quality and presentation, impaired T-cell trafficking, and insufficient intratumoral inflammatory signaling (especially by TNFα).

Acquired resistance is a common feature of *in vivo* implantation and subsequent treatment, with numerous validated protocols to test agents for this effect (reviewed in [561]). Sensitivity of resistant renal cell carcinoma cells to anti-VEGFR therapy is reacquired upon implantation of said resistant cells into untreated mice[562,563]. In melanoma clinical trials, personalized chemotherapy regimens based on sensitivities of resected melanoma cells significantly improved overall survival, with *in vivo* responses directly related to *in vitro* drug sensitivity. Notably, however, melanoma brain metastases showed no objective responses to this personalized chemotherapy approach[564]. In clinical trials for melanoma brain metastases, CNS location limited drug delivery and responses to targeted therapy relative to extracranial metastases. Several clinical trials are underway for ICB in melanoma brain metastases[565]. Brain metastases are significantly more infiltrated by T-cells and respond better to ICB than GBMs[566], which are significantly more infiltrated by immunosuppressive TAMs[567]. Interestingly, breast cancer cells resistant to αHER2 therapy *in vitro* are sensitive to HER2 inhibition *in vivo* due to natural-killer cell mediated antibody dependent cellular cytotoxicity[568]. Given the dependence of GBM cells on pathways moderated by TNFR1- and IAP signaling, the sustained sensitivity to SMC and TNFα-induced cell death regardless of exposure to myriad microenvironmental features is

unsurprising and represents a key vulnerability. I concluded that increasing dose of LCL161 *in vivo* would significantly enhance murine GBM killing and ICB efficacy (discussed in **section 4.3**).

Murine GBM cell lines differ in cell death mechanisms and MHC expression

Between the two commonly used mouse GBM lines, CT2A dies through apoptosis and GL261 through mixed apoptosis and necroptosis. Necroptosis is a more inflammatory form of cell death, and GL261 are substantially more enriched for immune related pathways than CT2A[526]. Both cell lines express immunomodulatory proteins, with GL261 alone expressing IFNγ-inducible MHCII, and both show significant survival benefit from combined SMC and αPD-1 therapy. This is in keeping with past work from our lab, which further found that SMC and αPD-1-mediated cures of IC CT2A tumors were dependent on the actions of $CD8^+$ T-cells[182]. Here, I show that anti-GL261 immune memory appears to be $CD4^+$ T-cell mediated, at least in the context of SQ implants, in keeping with GL261-specific inducible MHCII expression.

Research on $CD4^+$ T-cells has focused mainly on their T-helper[569,570] and Treg subset functions in coordinating $CD8^+$ T-cell (and other immune cell) anti-cancer immune action, especially in melanoma[571–575]. Recent work has characterized tumor-infiltrating $CD4^+$ T-cells specific for melanoma MHCII-presented antigens with direct anti-tumor cytotoxic capacity, functioning both in tandem with, and independent of, $CD8^+$ T-cells[576,577]. These cytotoxic $CD4^+$ T-cells act via both classical granzyme-mediated mechanisms as well as unique surface expressed and secreted molecules[578–582]. $CD4^+$ T-cells positively correlate with glioma grade and are highest in GBM; $CD8^+$ T-cells are inversely correlated[583]. LAG-3 binds to MHCII and contributes to $CD4^+$ T-cell exhaustion. GBM patients show increased MHCII expression relative to normal brain due to macrophage-derived TNFα-induced upregulations. High IL-10 contributes to further increase

MHCII and $CD4^+$ T-cell LAG-3 expression, together contributing to $CD4^+$ T-cell exhaustion. Blockade of LAG-3, TNFα and IL-10 significantly improve αPD-1 ICB efficacy in GL261 models[584]. Similar to our SQ implants acting as de facto vaccinations for subsequent IC implants, GBM-specific peptide vaccines have been found to engage $CD4^+$ T-cells to induce tumor cell lysis with consequent antigen spreading allowing for clearance of GBM cells not expressing vaccine-associated antigens[585], suggesting a more nuanced role for $CD4^+$ T-cells than conventionally thought.

Given the intertumoral heterogeneity of GBM, it is feasible that variations between individuals will present with differences in $CD4^+$ or $CD8^+$ T-cell fractions, as well as proportions of $CD4^+$ cells that are cytotoxic, contributing to variable TMEs, exhaustion signatures and responses to immunotherapies. How these cells are affected by IAP blockade needs to be elucidated. Previous work from our lab in CT2A models has shown that CD4 blockade enhances the efficacy of SMC and αPD-1 cotherapy. This was attributed to reductions in Tregs, which also explains the near complete cures observed following addition of CTLA-4 blockade to the cotherapy[182]. More recent work on the CT2A model corroborates this, showing dysfunctional $CD4^+$ T-cells significantly contribute to $CD8^+$ T-cell exhaustion and reduced αPD-1 therapy efficacy[586]. Despite this, GL261 uniquely shows inducible MHCII expression and most closely resembles the immune landscape of human patient GBM samples among common murine GBM lines[526], indicating the potential for greater roles of $CD4^+$ T-cells in this model relative to CT2A. Indeed, $CD4^+$ CAR-T cells show greater GBM killing capacity than $CD8^+$ CAR-T cells within the GBM TME, with reduced exhaustion signatures. Presence of $CD8^+$ cells within the transferred cell populations reduced the efficacy of $CD4^+$ CAR-T cells[428].

Age and CNS location limits anti-GBM immunotherapy

Animal experiments are typically conducted in 5-7 week old mice, including previous results on the synergism between SMCs and checkpoint blockade for GBM[182]. Given the CNS[587–589] and immune system[590–593] undergo significant changes associated with aging, notably with shifts toward memory phenotypes, reduced capacity to respond to novel antigens, immunosenescence, increased permeability of CNS-immune barriers, and baseline neurodegeneration, it is clear that preclinical experiments using young animals do not accurately reflect the GBM patient demographics. Our findings of reduced SMC and ICB efficacy in middle age and old age mice bearing CT2A and GL261 GBM tumors are therefore unsurprising. High IDO1 expression among GBM-infiltrating CD45+ cells is in keeping with literature showing high T-cell IDO1, with expression correlated with worse survival[594] Age-related efficacy of immunotherapy may be therapy- and cancer-dependent. αPD-1 and αCTLA4 show better or equivalent efficacy in patients over 70 relative to under 70 for melanoma, non-small cell lung carcinoma and triple negative breast cancer. Bispecific T-cell engager therapy for B-precursor acute lymphoblastic leukemia efficacy was not affected by age. Conversely, CD40 agonism and IL-2 produced significantly worse outcomes in elderly patients[595]. Age is a negative prognostic factor in mouse models of GBM, with high IDO1 expression[596] consistent with our findings. Age-related immunosenescence represents a key hurdle for immunotherapies of cancer, with decreased T-cell activation, increased Tregs, MDSCs, and immunosuppressive cytokines (IL-10, TGFβ) and reduced naïve and effector T-cells[597]. Aged GBM patients show significantly higher LAG3 and IDO1 and respond poorer to adjuvant αPD-1 and IDO1 inhibition than younger patients. Senescent cells were found to be significantly increased in aged patients treated with radiotherapy, and response to immunotherapy in aged mice bearing GBMs was improved by the addition of senolytic compounds[598].

Senescence represents a state of permanent cell cycle arrest, a characteristic secretory phenotype (SASP) containing high levels of IL-6, apoptosis resistance and high lysosomal content[599]. In GBM and other cancers, senescence is induced by cellular stress and DNA damaging therapies, allowing for escape from cell death and supporting multiple aspects of GBM aggressiveness including induction of MMP expression and enhanced invasion[600]. Radiation induces GBM senescence in a p21-dependent manner, and the SASP enhances RTK signaling and promotes tumor growth. Clearance using a senolytic BCL-2 inhibitor cleared senescent cells, inhibited tumor growth and enhanced survival [601]. TMZ also induces senescence and G2-M cell cycle arrest in a p21 and NF-κB dependent manner, with senescence induced in significantly more cells than apoptosis[602–604]. Contrary to the irreversible nature of conventional senescence, cancer stem cells appear able to enter senescent-like states to avoid therapeutic cytotoxicity and re-enter the cell cycle following escape[605] including in GBM[603]. Mouse and human GBMs possess senescent subpopulations, and extent of senescence is a negative prognostic indicator. Clearance of mouse senescent cells using senolytic compounds significantly improves survival, in part due to reduced TAM populations and increased T-cells[606]. Preclinical studies of senolytic treatments for GBM are underway (reviewed in [600]). Interestingly, SMCs have been found to have senolytic activity against treatment-induced GBM senescence, increasing the apoptotic response[607]. cIAP2 is significantly increased following TMZ-induced senescence, and IAP blockade increases cell death of both senescent GBM cells and those that have subsequently re-entered the cell cycle following senescence-mediated escape[608]. Genome-wide screens identify Smac-IAP interactions as major determining factors for senolytic efficacy, and follow-up cotreatments of senescent cells with BH3 mimetics and SMCs produced significantly reduced viability, clearing senescent cells *in vitro* and *in vivo*[609].

These senescent cell clearing effects may explain the increased efficacy of LCL161 as a monotherapy in middle aged animals relative to young animals, significantly enhancing survival relative to vehicle especially in the GL261 model. The senolytic and immunoactivating effects of IAP blockade may act to counter GBM-associated senescence and increased immunosenescence seen with aging. Confirming these effects *in vivo* represent a promising future area of research, as will combination with IDO1 inhibitors which have shown promising preclinical[610–612] and early clinical trial results[613,614], beneficially reshaping the TME in combination with other agents including αPD-1 checkpoint blockade and Stupp protocol[615,616].

4.2 TNFα ablates astrocyte protection of GBM cells in the presence of SMCs

Microglia and macrophages are sensitive to SMC-induced cell death

Herein, I show that SMCs are cytotoxic to murine macrophages and microglia, and in co-cultures this cell death acts in paracrine fashions on SMC-sensitized GBM cells to effect cancer cell killing. Human macrophages and monocytes have previously been shown to die following IAP blockade[354,523], and cIAP1/2 are required for macrophage survival *in vitro* and *in vivo*[617,618]. Microglial activation is associated with high levels of p19 cleaved caspase-3[619], with further cleavage to p17 and consequent apoptotic cell death controlled by cIAP2[620]. Treatment with SMCs induces p19 to p17 cleavage and microglial cell death[619], in keeping with our findings. The novelty of our work stems from microglia/macrophage-GBM interactions in the context of SMC treatments, wherein this previously characterized TAM cell death produces factors capable of killing SMC-sensitized GBM cells. Whereas microglial depletion using PLX compounds depletes microglia in normal brain but fails to reduce TAMs and provides minimal survival benefit (**Section 1.4.3**), high dose SMCs kill microglia and macrophages *in vitro*, reduces TAMs

in vivo, concurrently reduces tumor size *in vivo*, and sensitizes murine GBM cells to paracrine signaling from dying TAMs.

Astrocytes protect microglia, macrophages and GBM cells from SMC cytotoxicity

I also show that astrocytes blunt this effect and enhance murine GBM growth, in keeping with past findings and their role in maintaining CNS homeostasis and cell survival (**Section 1.2.6**). This is, to our knowledge, the first set of experiments looking at direct impact of SMCs on astrocytes. Given LCL161 appears to be excluded from the normal CNS by the BBB[182] and that the BBB is leaky in murine GBM, effects on astrocytes would either be indirect via impacts on TME component secretory profiles and phenotypes, or direct on cells surrounding tumor. I show increased astrocyte reactivity surrounding IC GL261 tumors following twice weekly LCL161 treatments, suggesting enhanced roles for these cells following SMC-mediated GBM treatment. Combined SMC and TNFα treatment of GBM-astrocyte cocultures significantly enhanced GBM killing relative to monocultures, suggesting inflammatory reactive astrocyte states provide further death ligands acting on sensitized GBM cells. Unlike microglia and macrophages, astrocytes show no change in viability upon treatment with SMCs, suggesting these effects are not due to astrocyte cell death-secreted factors but instead due to changes in inflammatory reactive state. This is in keeping with the general astrocyte resistance to engagement of the extrinsic pathway, with minimal caspase-8 expression[621–623], near complete lack of TRAIL receptor expression[185,624,625] and the combined impact of cFLIP, PEA-15[543,626,627] and the IAPs[628,629]. Inflammatory cytokines and death ligands, especially TNFα, instead induce astrocyte reactivity and further death ligand expression[351,630–633].

Our findings show LCL161 induced modest increases in astrocyte reactivity markers *in vitro* relative to LPS and TNFα and repeat treatments of GBM-astrocyte cocultures with high dose

LCL161 failed to induce death ligand expression sufficient to stem GBM cell growth. Thus, increased astrocyte reactivity surrounding tumor *in vivo* is likely minimally contributed to by direct SMC effects and moreso a result of increased intratumoral inflammatory signaling. This, combined with the effects of inflammatory astrocytes on SMC-sensitized GBM cells and the TAM-GBM killing capacity of SMCs, sets the stage for rational combination of SMCs with any immunotherapy boosting intratumoral inflammatory signaling, recruiting neuroimmune action against the tumor. As astrocyte glial scars form barriers to neuron regrowth following CNS injury, nanoparticle approaches towards increasing astrocyte scar formation surrounding GBMs have shown significant reductions in invasive capacity[634]. Whether these SMC-mediated increases have similar effects represents an interesting future avenue of research.

4.3 TGFβ limits efficacy of SMC and ICB

Increased dose of SMC significantly enhances survival in combination with αPD-1

Given the sustained sensitivity of murine GBM cells to SMC-mediated inflammatory cell death, as well as beneficial effects on microglia/macrophages and astrocytes, I aimed to study dose escalation of LCL161 in GL261-bearing mice. I show that increasing oral dose of LCL161 from 'standard dose' 75mg/kg (SD) to 'high dose' 100mg/kg (HD) is well tolerated, even at increased frequency of treatment. Mouse body weights were not significantly altered by HD 2x/week 'standard frequency' (HDSF) treatments or by HD 5x/week 'high frequency' (HDHF) treatments. Spleen weights were significantly increased following either treatment regimen, with resected tumor weight and TAM proportions reduced only in animals receiving HDHF LCL161, illustrating broad SMC-mediated immunostimulatory effects. These results indicate that *in vivo* TAMs are susceptible to SMC-mediated clearance as found *in vitro* (**Section 4.2**) contingent upon maximal doses of SMC reaching tumor. Further work is looking to examine GBM TME

and normal brain dynamics following HDSF and HDHF treatments, with direct co-staining of cleaved caspase-3 and IBA1 showing active SMC-mediated TAM cell death (data not shown). I further show that despite intracranial GL261-induced reductions of T-cell proportions in peripheral lymphoid organs, consistent with well characterized peripheral immunosuppression (**Section 1.3.4**), HDSF LCL161 treatment significantly increases expression of T-cell activation markers OX40, CD69 and CD25 while reducing PD-1. SMCs have a myriad of previously characterized pro-inflammatory functions via alterations to NF-κB signaling (reviewed in [96]), including enhanced costimulation[82], increased T-cell TNFα and IL-2 production, DC activation and maturation[357] and reduced T-cell Treg differentiation and PD-1 expression[488]. Despite GBM-induced peripheral immunosuppression, SMCs still induce T-cell activation in peripheral lymphoid organs, setting the stage for enhanced anti-GBM immunity in combination with ICB.

In combination with αPD-1 ICB, HDSF significantly extends mouse survival and doubles the number of long-term survivors across both cell lines compared to SDSF. Interestingly, HDHF reduced the efficacy of cotherapy, even to levels below SDSF in CT2A. Despite this reduction in median and overall survival, most deceased animals showed no evidence of residual tumor at endpoint, suggesting substantial anti-GBM action but severe off-tumor toxicity. Consistent with this, $SSC^{low}FSC^{mid}$ populations in peripheral lymphoid organs were nearly completely abolished by HDHF LCL161 treatment alone. This population matches similar reductions in $CD3^{+}$ cells in the spleen seen following intracranial implant of GL261 tumors, suggesting severe lymphodepletion following HDHF LCL161 regimens. Despite costimulatory effects, SMCs have been found to sensitize engineered T-cells to Fas-mediated apoptosis[496]. Astrocyte FasL-induced apoptosis of CNS-infiltrating T-cells is a well characterized mechanism of maintaining immune privilege, especially required given neuron susceptibility to inflammatory cytokines and death

ligands[635–641]. A potential situation therefore arises in which: 1) HDHF LCL161 induces TAM cell death, releasing factors acting on now sensitized GBM cells to clear tumor; 2) enhanced astrocyte reactivity is associated with further increases in death ligand expression, including TNFα and Fas-FasL, acting to enhance GBM cell killing; 3) αPD-1 ICB enhances T-cell proinflammatory function, enhancing GBM cell killing; 4) excess LCL161 from HDHF regimens induces peripheral and intratumoral T-cell killing by Fas-FasL mechanisms, including highly reactive astrocytes, inducing severe toxicity despite clearing tumor.

IT delivery of TMZ or other chemotherapies significantly improves combination with αPD-1 ICB relative to IV, with systemic application causing severe defects in anti-GBM T-cell immunity (**Section 1.4.4**). Altering the schedule of TMZ treatments drastically influences progression-free survival outcomes in GBM[113]. Therefore, elucidating the optimal timing of SMC treatments to maximally boost peripheral and intratumoral immunity while minimizing off-tumor toxicity are key future preclinical research steps. Future work will also examine more direct delivery methods of SMCs in GBM therapy. IT and ICV administration are hindered by the necessity to dissolve LCL161 in DMSO, which has been found to cause severe ventriculomegaly and defects in cilia function and viability of ependymal cells lining the ventricles[642] as well as on cortical neurons[643]. Nanoparticle (NP)-based treatments for GBM have received significant research focus in recent years, allowing for delivery of diverse chemotherapeutic, small molecule, protein or antibody payloads and overcoming many issues of drug delivery or drug specificity for tumor cells[644–647]. Promisingly given their crucial roles in GBM biology and immunosuppressive TME, TAMs primarily uptake NPs and act as delivery mechanisms of nanoparticle payloads to tumor cells[648]. Early experiments in NP-encapsulated LCL161 showed SMC-sensitive MDA-MB231 and murine GBM cells remain sensitive SMC-

based killing. However, cytotoxicity towards microglia and macrophages seen with free drug was completely abolished upon NP encapsulation (previous work done by an MSc student, Melanie Dugas). However, given these findings I propose future work examine direct IT delivery of NP-encapsulated YM155 for direct SMC-resistant GBM cell killing, followed by oral HDSF LCL161 and αPD-1 ICB for maximal GBM-killing, TAM-clearing, neuroimmune engaging and peripheral immune-activating effects.

TGFβ protects microglia and macrophages from SMCs and blockade extends survival

I found that TGFβ and hypoxia are major resistance factors for SMC-mediated microglia and macrophage killing. I focused on targeting TGFβ given its myriad roles in GSC biology (**Section 1.2.3**), astrocyte regulation of neuroinflammation (**Section 1.2.6**), TAM and Treg immunosuppressive capabilities (**Section 1.3.3**) and resistance to ICB (**Section 1.4.4**), as well as relative ease of inhibition *in vivo* via direct antibody blockade. I show that low dose TGFβ is sufficient to protect these cell types from high dose LCL161, with protective effects plateauing likely because of TGFβR availability. I also show that GBM-secreted TGFβ is sufficient to confer protection, illustrating further multicellular communication driven mechanisms of resistance to SMC-based therapies. The protective effects on macrophages and microglia are in keeping with past work showing enhanced IAP expression following TGFβ treatment[530], further corroborated by the reestablishment of cytotoxicity following treatment with the dimeric SMC AZD5582. Future work will examine which IAPs are specifically upregulated and assess TGFβ, TGFβR, and IAP levels *in vivo*.

TGFβ has a wide range of context-dependent effects, and blockade has the potential to enhance immunotherapies for a wide array of cancers[649–651]. Introducing TGFβ blockade into current immunotherapeutic regimens is therefore an extremely promising strategy. However, this may be

associated with exacerbated immunotherapy-derived toxicities and disrupted tissue homeostasis, indicating that its application requires a nuanced approach and significant safety studies[652]. TGFβ or TGFβR blocking antibodies, small molecule inhibitors and TGFβ-producing enzyme inhibitors are nonetheless currently in clinical trials for multiple solid tumors, including in combination with αPD-1 or αCTLA4 ICB with promising early results[653–655]. TGFβ has been found to be a major contributor to $CD4^+$ CAR-T cell exhaustion, significantly reducing efficacy of adoptive cell therapies against solid tumors[656] and contributing significantly to ICB resistance for GBM. Direct IT delivery of antisense oligonucleotides against TGFβ2 showed promising preclinical and early clinical efficacy in extending patient survival administered following conventional therapy[657–659], although further clinical trials failed to show survival benefit[393]. TGFβ is highly expressed in GBM and plays key roles in disease aggression[660] and immunosuppression. Several clinical trials incorporating blockade of TGFβ2, TGFβR1, or broad TGFβ for GBM are underway or have been completed[661] and shown to be safe but with minimal clinical benefit[662–664]. In GL261 models, TGFβ blockade concurrent with GBM antigen vaccination resulted in significant anti-tumor immunity and significantly improved survival[366]. Similar survival improvements in GL261-bearing animals were seen when TGFβ blockade was combined with RT and αPD-L1[665,666]. I show that TGFβ represents a significant resistance factor for SMC-mediated TAM killing in an IAP-dependent manner, and *in vivo* blockade almost triples the number of long-term survivors in combination with HDSF LCL161 and αPD-1 ICB relative to the combination alone. LCL161 represents the major immunostimulant in peripheral lymphoid organs, with αTGFβ and αPD-1 treatments removing immunosuppressive and anti-apoptotic hurdles for maximal anti-GBM attack described previously. Elucidating the optimal timing and

dosing of TGFβ-blockade in SMC-based immunotherapies to maximize TAM clearance and GBM killing represent key future research goals.

5.0 Conclusions

I show that human and mouse GBM cells undergo cell death following IAP blockade, and that the sensitivities of murine GBM cells are maintained upon exposure to *in vivo* microenvironmental conditions. I demonstrate SMC-induced cell death occurs through apoptosis and necroptosis in CT2A and GL261 murine GBM lines, respectively. Both lines express immunomodulatory proteins, with GL261 uniquely showing inducible MHCII expression. Intracranial tumors formed from both cell lines are cured in response to SMC and αPD-1 ICB, and anti-GBM immunity is limited by CNS location. Together, these data indicate that GBM sensitivity to IAP blockade is maintained *in vivo* and improved SMC delivery and increased intratumoral inflammatory signaling represent key steps towards maximizing efficacy of SMC-based immunotherapies. I further show age negatively impacts cotherapy efficacy, and high tumor-infiltrating immune cell expression of IDO1 and KLRG1 reveal potential future combination targets.

I explored the impact of individual tumor infiltrating and CNS cell types on sensitivity of GBM cells to SMC-mediated cell death. Macrophages and microglia, key factors in GBM immunosuppression and aggressive biology, are killed by SMCs and consequently kill sensitized GBM cells. SMC treatment increases astrocyte reactivity surrounding GL261 tumors. Astrocytes enhance GBM growth and protect microglia from SMC cytotoxicity. Cotreatment with SMC and TNFα results in significantly greater GBM killing because of TNFα-induced astrocyte reactivity. Together, I show that TAMs represent a promising source of death signals for SMC-sensitized GBM cells contingent upon sufficient inflammation to overcome astrocyte protective effects.

I evaluated dose escalation of SMC *in vivo* and show significantly improved survival across both murine GBM cell lines in combination with ICB, plateauing at a point wherein tumors are cleared but on-target off-tumor toxicity prevails. I show SMCs potently increase T-cell activation markers in peripheral lymphoid organs, but at non-toxic doses these are not accompanied by changes in the tumor. I identify TGFβ as a significant limiting factor in SMC TAM killing capacity in an IAP-dependent manner and in efficacy of SMC and ICB cotherapy. I show TGFβ blockade nearly triples the number of cures in mice bearing GL261 tumors. Together, I show limiting factors in SMC-based GBM immunotherapies are extent of drug reaching tumor site, extent of intratumoral inflammatory signaling, CNS location and TGFβ. I propose TGFβ, IDO1 and KLRG1 inhibition as rational combinations with high dose SMC and ICB.

6.0 References

1. Birnbaum, M. J., Clem, R. J. & Miller, L. K. An apoptosis-inhibiting gene from a nuclear polyhedrosis virus encoding a polypeptide with Cys/His sequence motifs. *J. Virol.* **68**, 2521–2528 (1994).
2. Heng, T. S. P., Painter, M. W., & Immunological Genome Project Consortium. The Immunological Genome Project: networks of gene expression in immune cells. *Nat. Immunol.* **9**, 1091–1094 (2008).
3. Burm, S. M. *et al.* Inflammasome-induced IL-1β secretion in microglia is characterized by delayed kinetics and is only partially dependent on inflammatory caspases. *J. Neurosci. Off. J. Soc. Neurosci.* **35**, 678–687 (2015).
4. Fagerberg, L. *et al.* Analysis of the human tissue-specific expression by genome-wide integration of transcriptomics and antibody-based proteomics. *Mol. Cell. Proteomics MCP* **13**, 397–406 (2014).
5. Aguilar, C. & Latour, S. X-linked inhibitor of apoptosis protein deficiency: more than an X-linked lymphoproliferative syndrome. *J. Clin. Immunol.* **35**, 331–338 (2015).
6. Nielsen, O. H. & LaCasse, E. C. How genetic testing can lead to targeted management of XIAP deficiency-related inflammatory bowel disease. *Genet. Med. Off. J. Am. Coll. Med. Genet.* **19**, 133–143 (2017).
7. Cantarini, L. *et al.* Tumour necrosis factor receptor-associated periodic syndrome (TRAPS): State of the art and future perspectives. *Autoimmun. Rev.* **12**, 38–43 (2012).
8. Hrdinka, M. & Yabal, M. Inhibitor of apoptosis proteins in human health and disease. *Genes Immun.* **20**, 641–650 (2019).
9. LaCasse, E. C. *et al.* IAP-targeted therapies for cancer. *Oncogene* **27**, 6252–6275 (2008).
10. Rothe, M., Sarma, V., Dixit, V. M. & Goeddel, D. V. TRAF2-mediated activation of NF-kappa B by TNF receptor 2 and CD40. *Science* **269**, 1424–1427 (1995).
11. Hsu, H., Shu, H. B., Pan, M. G. & Goeddel, D. V. TRADD-TRAF2 and TRADD-FADD interactions define two distinct TNF receptor 1 signal transduction pathways. *Cell* **84**, 299–308 (1996).
12. Jensen, S., Seidelin, J. B., LaCasse, E. C. & Nielsen, O. H. SMAC mimetics and RIPK inhibitors as therapeutics for chronic inflammatory diseases. *Sci. Signal.* **13**, (2020).
13. Dumétier, B., Zadoroznyj, A. & Dubrez, L. IAP-Mediated Protein Ubiquitination in Regulating Cell Signaling. *Cells* **9**, 1118 (2020).
14. Yang, Y., Wu, J. & Wang, J. A database and functional annotation of NF-κB target genes. in (2016).
15. Beug, S. T., Conrad, D. P., Alain, T., Korneluk, R. G. & Lacasse, E. C. Combinatorial cancer immunotherapy strategies with proapoptotic small-molecule IAP antagonists. *Int. J. Dev. Biol.* **59**, 141–147 (2015).
16. Cheung, H. H. *et al.* Smac mimetic compounds potentiate interleukin-1beta-mediated cell death. *J. Biol. Chem.* **285**, 40612–40623 (2010).
17. Suzuki, Y., Nakabayashi, Y., Nakata, K., Reed, J. C. & Takahashi, R. X-linked Inhibitor of Apoptosis Protein (XIAP) Inhibits Caspase-3 and -7 in Distinct Modes. *J. Biol. Chem.* **276**, 27058–27063 (2001).
18. Scott, F. L. *et al.* XIAP inhibits caspase-3 and -7 using two binding sites: evolutionarily conserved mechanism of IAPs. *EMBO J.* **24**, 645–655 (2005).
19. Eckelman, B. P., Salvesen, G. S. & Scott, F. L. Human inhibitor of apoptosis proteins: why XIAP is the black sheep of the family. *EMBO Rep.* **7**, 988–994 (2006).

20. Silke, J., Verhagen, A. M., Ekert, P. G. & Vaux, D. L. Sequence as well as functional similarity for DIABLO/Smac and Grim, Reaper and Hid? *Cell Death Differ.* **7**, 1275–1275 (2000).
21. Du, C., Fang, M., Li, Y., Li, L. & Wang, X. Smac, a Mitochondrial Protein that Promotes Cytochrome c–Dependent Caspase Activation by Eliminating IAP Inhibition. *Cell* **102**, 33–42 (2000).
22. Gao, Z. *et al.* A dimeric Smac/diablo peptide directly relieves caspase-3 inhibition by XIAP. Dynamic and cooperative regulation of XIAP by Smac/Diablo. *J. Biol. Chem.* **282**, 30718–30727 (2007).
23. Srinivasula, S. M. *et al.* A conserved XIAP-interaction motif in caspase-9 and Smac/DIABLO regulates caspase activity and apoptosis. *Nature* **410**, 112–116 (2001).
24. Feltham, R. *et al.* Smac Mimetics Activate the E3 Ligase Activity of cIAP1 Protein by Promoting RING Domain Dimerization. *J. Biol. Chem.* **286**, 17015–17028 (2011).
25. Marusawa, H. *et al.* HBXIP functions as a cofactor of survivin in apoptosis suppression. *EMBO J.* **22**, 2729–2740 (2003).
26. Verhagen, A. M., Coulson, E. J. & Vaux, D. L. Inhibitor of apoptosis proteins and their relatives: IAPs and other BIRPs. *Genome Biol.* **2**, reviews3009.1 (2001).
27. Song, Z. *et al.* A Single Amino Acid Change (Asp 53→ Ala53) Converts Survivin from Anti-apoptotic to Pro-apoptotic. *Mol. Biol. Cell* **15**, 1287–1296 (2003).
28. Wheatley, S. P. & Altieri, D. C. Survivin at a glance. *J. Cell Sci.* **132**, (2019).
29. Westphal, D., Dewson, G., Czabotar, P. E. & Kluck, R. M. Molecular biology of Bax and Bak activation and action. *Biochim. Biophys. Acta BBA - Mol. Cell Res.* **1813**, 521–531 (2011).
30. Dewson, G. & Kluck, R. M. Mechanisms by which Bak and Bax permeabilise mitochondria during apoptosis. *J. Cell Sci.* **122**, 2801–2808 (2009).
31. Decaudin, D., Marzo, I., Brenner, C. & Kroemer, G. Mitochondria in chemotherapy-induced apoptosis: a prospective novel target of cancer therapy (review). *Int. J. Oncol.* **12**, 141–152 (1998).
32. Saelens, X. *et al.* Toxic proteins released from mitochondria in cell death. *Oncogene* **23**, 2861–2874 (2004).
33. Sevrioukova, I. F. Apoptosis-Inducing Factor: Structure, Function, and Redox Regulation. *Antioxid. Redox Signal.* **14**, 2545–2579 (2011).
34. Suzuki, Y. *et al.* A serine protease, HtrA2, is released from the mitochondria and interacts with XIAP, inducing cell death. *Mol. Cell* **8**, 613–621 (2001).
35. Liston, P. *et al.* Identification of XAF1 as an antagonist of XIAP anti-Caspase activity. *Nat. Cell Biol.* **3**, 128–133 (2001).
36. Galluzzi, L. *et al.* Molecular mechanisms of cell death: recommendations of the Nomenclature Committee on Cell Death 2018. *Cell Death Differ.* **25**, 486–541 (2018).
37. Chang, L. K., Putcha, G. V., Deshmukh, M. & Johnson, E. M. Mitochondrial involvement in the point of no return in neuronal apoptosis. *Biochimie* **84**, 223–231 (2002).
38. Kim, H.-E., Du, F., Fang, M. & Wang, X. Formation of apoptosome is initiated by cytochrome c-induced dATP hydrolysis and subsequent nucleotide exchange on Apaf-1. *Proc. Natl. Acad. Sci.* **102**, 17545–17550 (2005).
39. Srinivasula, S. M., Ahmad, M., Fernandes-Alnemri, T. & Alnemri, E. S. Autoactivation of procaspase-9 by Apaf-1-mediated oligomerization. *Mol. Cell* **1**, 949–957 (1998).

40. Acehan, D. *et al.* Three-dimensional structure of the apoptosome: implications for assembly, procaspase-9 binding, and activation. *Mol. Cell* **9**, 423–432 (2002).
41. Cain, K. *et al.* Apaf-1 oligomerizes into biologically active approximately 700-kDa and inactive approximately 1.4-MDa apoptosome complexes. *J. Biol. Chem.* **275**, 6067–6070 (2000).
42. Li, P. *et al.* Cytochrome c and dATP-dependent formation of Apaf-1/caspase-9 complex initiates an apoptotic protease cascade. *Cell* **91**, 479–489 (1997).
43. Rodriguez, J. & Lazebnik, Y. Caspase-9 and APAF-1 form an active holoenzyme. *Genes Dev.* **13**, 3179–3184 (1999).
44. Julien, O. & Wells, J. A. Caspases and their substrates. *Cell Death Differ.* **24**, 1380–1389 (2017).
45. Walsh, J. G. *et al.* Executioner caspase-3 and caspase-7 are functionally distinct proteases. *Proc. Natl. Acad. Sci.* **105**, 12815–12819 (2008).
46. Llambi, F. *et al.* A unified model of mammalian BCL-2 protein family interactions at the mitochondria. *Mol. Cell* **44**, 517–531 (2011).
47. Fletcher, J. I. *et al.* Apoptosis is triggered when prosurvival Bcl-2 proteins cannot restrain Bax. *Proc. Natl. Acad. Sci.* **105**, 18081–18087 (2008).
48. Czabotar, P. E. *et al.* Bax crystal structures reveal how BH3 domains activate Bax and nucleate its oligomerization to induce apoptosis. *Cell* **152**, 519–531 (2013).
49. Gavathiotis, E. *et al.* BAX Activation is Initiated at a Novel Interaction Site. *Nature* **455**, 1076–1081 (2008).
50. Letai, A. *et al.* Distinct BH3 domains either sensitize or activate mitochondrial apoptosis, serving as prototype cancer therapeutics. *Cancer Cell* **2**, 183–192 (2002).
51. Ren, D. *et al.* BID, BIM, and PUMA are essential for activation of the BAX- and BAK-dependent cell death program. *Science* **330**, 1390–1393 (2010).
52. O'Neill, K. L., Huang, K., Zhang, J., Chen, Y. & Luo, X. Inactivation of prosurvival Bcl-2 proteins activates Bax/Bak through the outer mitochondrial membrane. *Genes Dev.* **30**, 973–988 (2016).
53. Nagata, S. & Golstein, P. The Fas death factor. *Science* **267**, 1449–1456 (1995).
54. Nagata, S. Apoptosis by Death Factor. *Cell* **88**, 355–365 (1997).
55. Boldin, M. P. *et al.* A Novel Protein That Interacts with the Death Domain of Fas/APO1 Contains a Sequence Motif Related to the Death Domain. *J. Biol. Chem.* **270**, 7795–7798 (1995).
56. Kischkel, F. C. *et al.* Cytotoxicity-dependent APO-1 (Fas/CD95)-associated proteins form a death-inducing signaling complex (DISC) with the receptor. *EMBO J.* **14**, 5579–5588 (1995).
57. Kischkel, F. C. *et al.* Death Receptor Recruitment of Endogenous Caspase-10 and Apoptosis Initiation in the Absence of Caspase-8. *J. Biol. Chem.* **276**, 46639–46646 (2001).
58. Li, H., Zhu, H., Xu, C. J. & Yuan, J. Cleavage of BID by caspase 8 mediates the mitochondrial damage in the Fas pathway of apoptosis. *Cell* **94**, 491–501 (1998).
59. Wang, S. & El-Deiry, W. S. TRAIL and apoptosis induction by TNF-family death receptors. *Oncogene* **22**, 8628–8633 (2003).
60. Ashkenazi, A. & Dixit, V. M. Death receptors: signaling and modulation. *Science* **281**, 1305–1308 (1998).
61. Schwabe, R. F. & Luedde, T. Apoptosis and necroptosis in the liver: a matter of life and death. *Nat. Rev. Gastroenterol. Hepatol.* **15**, 738–752 (2018).

62. Lotocki, G., Alonso, O. F., Dietrich, W. D. & Keane, R. W. Tumor Necrosis Factor Receptor 1 and Its Signaling Intermediates Are Recruited to Lipid Rafts in the Traumatized Brain. *J. Neurosci.* **24**, 11010–11016 (2004).
63. Samuel, T. *et al.* Distinct BIR Domains of cIAP1 Mediate Binding to and Ubiquitination of Tumor Necrosis Factor Receptor-associated Factor 2 and Second Mitochondrial Activator of Caspases. *J. Biol. Chem.* **281**, 1080–1090 (2006).
64. Bertrand, M. J. M. *et al.* cIAP1 and cIAP2 Facilitate Cancer Cell Survival by Functioning as E3 Ligases that Promote RIP1 Ubiquitination. *Mol. Cell* **30**, 689–700 (2008).
65. Niu, J., Shi, Y., Iwai, K. & Wu, Z.-H. LUBAC regulates NF-κB activation upon genotoxic stress by promoting linear ubiquitination of NEMO. *EMBO J.* **30**, 3741–3753 (2011).
66. Kanayama, A. *et al.* TAB2 and TAB3 Activate the NF-κB Pathway through Binding to Polyubiquitin Chains. *Mol. Cell* **15**, 535–548 (2004).
67. Karin, M. How NF-κB is activated: the role of the IκB kinase (IKK) complex. *Oncogene* **18**, 6867–6874 (1999).
68. Van Herreweghe, F., Festjens, N., Declercq, W. & Vandenabeele, P. Tumor necrosis factor-mediated cell death: to break or to burst, that's the question. *Cell. Mol. Life Sci. CMLS* **67**, 1567–1579 (2010).
69. Feltham, R., Vince, J. E. & Lawlor, K. E. Caspase-8: not so silently deadly. *Clin. Transl. Immunol.* **6**, e124 (2017).
70. Tummers, B. & Green, D. R. Caspase-8; regulating life and death. *Immunol. Rev.* **277**, 76–89 (2017).
71. O'Donnell, M. A. *et al.* Caspase 8 inhibits programmed necrosis by processing CYLD. *Nat. Cell Biol.* **13**, 1437–1442 (2011).
72. Berghe, T. V., Linkermann, A., Jouan-Lanhouet, S., Walczak, H. & Vandenabeele, P. Regulated necrosis: the expanding network of non-apoptotic cell death pathways. *Nat. Rev. Mol. Cell Biol.* **15**, 135–147 (2014).
73. Dondelinger, Y. *et al.* RIPK3 contributes to TNFR1-mediated RIPK1 kinase-dependent apoptosis in conditions of cIAP1/2 depletion or TAK1 kinase inhibition. *Cell Death Differ.* **20**, 1381–1392 (2013).
74. Dhuriya, Y. K. & Sharma, D. Necroptosis: a regulated inflammatory mode of cell death. *J. Neuroinflammation* **15**, 199 (2018).
75. Choi, M. E., Price, D. R., Ryter, S. W. & Choi, A. M. K. Necroptosis: a crucial pathogenic mediator of human disease. *JCI Insight* **4**,.
76. Pasparakis, M. & Vandenabeele, P. Necroptosis and its role in inflammation. *Nature* **517**, 311–320 (2015).
77. Safa, A. R. c-FLIP, A MASTER ANTI-APOPTOTIC REGULATOR. *Exp. Oncol.* **34**, 176–184 (2012).
78. Tsuchiya, Y., Nakabayashi, O. & Nakano, H. FLIP the Switch: Regulation of Apoptosis and Necroptosis by cFLIP. *Int. J. Mol. Sci.* **16**, 30321–30341 (2015).
79. Safa, A. R. Roles of c-FLIP in Apoptosis, Necroptosis, and Autophagy. *J. Carcinog. Mutagen.* **Suppl 6**, (2013).
80. Walter, D. *et al.* Switch from type II to I Fas/CD95 death signaling on in vitro culturing of primary hepatocytes. *Hepatol. Baltim. Md* **48**, 1942–1953 (2008).
81. Jost, P. J. *et al.* XIAP discriminates between type I and type II FAS-induced apoptosis. *Nature* **460**, 1035–1039 (2009).

82. Dougan, M. *et al.* IAP inhibitors enhance co-stimulation to promote tumor immunity. *J. Exp. Med.* **207**, 2195–2206 (2010).
83. Fulda, S. & Vucic, D. Targeting IAP proteins for therapeutic intervention in cancer. *Nat. Rev. Drug Discov.* **11**, 109–124 (2012).
84. Melero, I. *et al.* Evolving synergistic combinations of targeted immunotherapies to combat cancer. *Nat. Rev. Cancer* **15**, 457–472 (2015).
85. Larkin, J. *et al.* Combined Nivolumab and Ipilimumab or Monotherapy in Untreated Melanoma. *N. Engl. J. Med.* **373**, 23–34 (2015).
86. Sayour, E. J. & Mitchell, D. A. Immunotherapy for Pediatric Brain Tumors. *Brain Sci.* **7**, (2017).
87. Sharma, P. & Allison, J. P. Immune Checkpoint Targeting in Cancer Therapy: Toward Combination Strategies with Curative Potential. *Cell* **161**, 205–214 (2015).
88. Topalian, S. L., Drake, C. G. & Pardoll, D. M. Immune checkpoint blockade: a common denominator approach to cancer therapy. *Cancer Cell* **27**, 450–461 (2015).
89. Preusser, M., Lim, M., Hafler, D. A., Reardon, D. A. & Sampson, J. H. Prospects of immune checkpoint modulators in the treatment of glioblastoma. *Nat. Rev. Neurol.* **11**, 504–514 (2015).
90. Postow, M. A. *et al.* Nivolumab and Ipilimumab versus Ipilimumab in Untreated Melanoma. *N. Engl. J. Med.* **372**, 2006–2017 (2015).
91. LCL161 | IAP Inhibitor | MedChemExpress. *MedchemExpress.com* https://www.medchemexpress.com/LCL161.html.
92. Liu, T., Zhang, L., Joo, D. & Sun, S.-C. NF-κB signaling in inflammation. *Signal Transduct. Target. Ther.* **2**, 17023 (2017).
93. Hayden, M. S., West, A. P. & Ghosh, S. NF-κB and the immune response. *Oncogene* **25**, 6758–6780 (2006).
94. Li, Q. & Verma, I. M. NF-kappaB regulation in the immune system. *Nat. Rev. Immunol.* **2**, 725–734 (2002).
95. Iacobazzi, D. *et al.* New Insights into NF-κB Signaling in Innate Immunity: Focus on Immunometabolic Crosstalks. *Biology* **12**, 776 (2023).
96. Michie, J., Kearney, C. J., Hawkins, E. D., Silke, J. & Oliaro, J. The Immuno-Modulatory Effects of Inhibitor of Apoptosis Protein Antagonists in Cancer Immunotherapy. *Cells* **9**, 207 (2020).
97. Beug, S. T. *et al.* Smac mimetics and innate immune stimuli synergize to promote tumor death. *Nat. Biotechnol.* **32**, 182–190 (2014).
98. Jensen, S., Seidelin, J. B., LaCasse, E. C. & Nielsen, O. H. SMAC mimetics and RIPK inhibitors as therapeutics for chronic inflammatory diseases. *Sci. Signal.* **13**, eaax8295 (2020).
99. Seyfrid, M., Marschall, V. & Fulda, S. Reactive oxygen species contribute toward Smac mimetic/temozolomide-induced cell death in glioblastoma cells. *Anticancer. Drugs* **27**, 953 (2016).
100. Berger, R. *et al.* NF-κB Is Required for Smac Mimetic-Mediated Sensitization of Glioblastoma Cells for γ-Irradiation–Induced Apoptosis. *Mol. Cancer Ther.* **10**, 1867–1875 (2011).
101. Cerna, D. *et al.* SMAC Mimetic/IAP Inhibitor Birinapant Enhances Radiosensitivity of Glioblastoma Multiforme. *Radiat. Res.* **195**, 549–560 (2021).

102. Wagner, L. *et al.* Smac mimetic sensitizes glioblastoma cells to Temozolomide-induced apoptosis in a RIP1- and NF-κB-dependent manner. *Oncogene* **32**, 988–997 (2013).
103. Marschall, V. & Fulda, S. Smac mimetic-induced upregulation of interferon-β sensitizes glioblastoma to temozolomide-induced cell death. *Cell Death Dis.* **6**, e1888 (2015).
104. Zhang, X. *et al.* YM155 decreases radiation-induced invasion and reverses epithelial–mesenchymal transition by targeting STAT3 in glioblastoma. *J. Transl. Med.* **16**, 79 (2018).
105. Rasmussen, B. K. *et al.* Epidemiology of glioma: clinical characteristics, symptoms, and predictors of glioma patients grade I-IV in the the Danish Neuro-Oncology Registry. *J. Neurooncol.* **135**, 571–579 (2017).
106. Davis, F. G. *et al.* Glioblastoma incidence rate trends in Canada and the United States compared with England, 1995–2015. *Neuro-Oncol.* **22**, 301–302 (2020).
107. Philips, A., Henshaw, D. L., Lamburn, G. & O'Carroll, M. J. Brain Tumours: Rise in Glioblastoma Multiforme Incidence in England 1995-2015 Suggests an Adverse Environmental or Lifestyle Factor. *J. Environ. Public Health* **2018**, 7910754 (2018).
108. Patel, A. P. *et al.* Global, regional, and national burden of brain and other CNS cancer, 1990–2016: a systematic analysis for the Global Burden of Disease Study 2016. *Lancet Neurol.* **18**, 376–393 (2019).
109. Ladomersky, E. *et al.* The Coincidence Between Increasing Age, Immunosuppression, and the Incidence of Patients With Glioblastoma. *Front. Pharmacol.* **10**, 200 (2019).
110. Schritz, A. *et al.* Systematic review and network meta-analysis of the efficacy of existing treatments for patients with recurrent glioblastoma. *Neuro-Oncol. Adv.* **3**, vdab052 (2021).
111. Stupp, R. *et al.* Radiotherapy plus concomitant and adjuvant temozolomide for glioblastoma. *N. Engl. J. Med.* **352**, 987–996 (2005).
112. Agarwala, S. S. & Kirkwood, J. M. Temozolomide, a novel alkylating agent with activity in the central nervous system, may improve the treatment of advanced metastatic melanoma. *The Oncologist* **5**, 144–151 (2000).
113. Wick, W., Platten, M. & Weller, M. New (alternative) temozolomide regimens for the treatment of glioma. *Neuro-Oncol.* **11**, 69–79 (2009).
114. Preuss, I. *et al.* O6-methylguanine-DNA methyltransferase activity in breast and brain tumors. *Int. J. Cancer* **61**, 321–326 (1995).
115. Rayfield, C. A. *et al.* Distinct Phenotypic Clusters of Glioblastoma Growth and Response Kinetics Predict Survival. *JCO Clin. Cancer Inform.* **2**, 1–14 (2018).
116. Hegi, M. E. *et al.* MGMT gene silencing and benefit from temozolomide in glioblastoma. *N. Engl. J. Med.* **352**, 997–1003 (2005).
117. Molinaro, A. M., Taylor, J. W., Wiencke, J. K. & Wrensch, M. R. Genetic and molecular epidemiology of adult diffuse glioma. *Nat. Rev. Neurol.* **15**, 405–417 (2019).
118. Verhaak, R. G. W. *et al.* An integrated genomic analysis identifies clinically relevant subtypes of glioblastoma characterized by abnormalities in PDGFRA, IDH1, EGFR and NF1. *Cancer Cell* **17**, 98 (2010).
119. Ravi, V. M. *et al.* Spatiotemporal heterogeneity of glioblastoma is dictated by microenvironmental interference. 2021.02.16.431475 Preprint at https://doi.org/10.1101/2021.02.16.431475 (2021).
120. Ravi, V. M. *et al.* Spatially resolved multi-omics deciphers bidirectional tumor-host interdependence in glioblastoma. *Cancer Cell* **40**, 639-655.e13 (2022).
121. McLendon, R. *et al.* Comprehensive genomic characterization defines human glioblastoma genes and core pathways. *Nature* **455**, 1061–1068 (2008).

122. Nozell, S. *et al.* The ING4 tumor suppressor attenuates NF-kappaB activity at the promoters of target genes. *Mol. Cell. Biol.* **28**, 6632–6645 (2008).
123. Alt, E. U. *et al.* TRAF3IP2, a novel therapeutic target in glioblastoma multiforme. *Oncotarget* **9**, 29772–29788 (2018).
124. Furnari, F. B. *et al.* Malignant astrocytic glioma: genetics, biology, and paths to treatment. *Genes Dev.* **21**, 2683–2710 (2007).
125. Ekstrand, A. J. *et al.* Genes for epidermal growth factor receptor, transforming growth factor alpha, and epidermal growth factor and their expression in human gliomas in vivo. *Cancer Res.* **51**, 2164–2172 (1991).
126. Libermann, T. A. *et al.* Amplification, enhanced expression and possible rearrangement of EGF receptor gene in primary human brain tumours of glial origin. *Nature* **313**, 144–147 (1985).
127. Gan, H. K., Cvrljevic, A. N. & Johns, T. G. The epidermal growth factor receptor variant III (EGFRvIII): where wild things are altered. *FEBS J.* **280**, 5350–5370 (2013).
128. Heimberger, A. B. *et al.* Prognostic Effect of Epidermal Growth Factor Receptor and EGFRvIII in Glioblastoma Multiforme Patients. *Clin. Cancer Res.* **11**, 1462–1466 (2005).
129. Voldborg, B. R., Damstrup, L., Spang-Thomsen, M. & Poulsen, H. S. Epidermal growth factor receptor (EGFR) and EGFR mutations, function and possible role in clinical trials. *Ann. Oncol. Off. J. Eur. Soc. Med. Oncol.* **8**, 1197–1206 (1997).
130. Narita, Y. *et al.* Mutant epidermal growth factor receptor signaling down-regulates p27 through activation of the phosphatidylinositol 3-kinase/Akt pathway in glioblastomas. *Cancer Res.* **62**, 6764–6769 (2002).
131. Nagane, M. *et al.* A common mutant epidermal growth factor receptor confers enhanced tumorigenicity on human glioblastoma cells by increasing proliferation and reducing apoptosis. *Cancer Res.* **56**, 5079–5086 (1996).
132. Nishikawa, R. *et al.* A mutant epidermal growth factor receptor common in human glioma confers enhanced tumorigenicity. *Proc. Natl. Acad. Sci. U. S. A.* **91**, 7727–7731 (1994).
133. Lammering, G., Valerie, K., Lin, P.-S., Hewit, T. H. & Schmidt-Ullrich, R. K. Radiation-induced activation of a common variant of EGFR confers enhanced radioresistance. *Radiother. Oncol. J. Eur. Soc. Ther. Radiol. Oncol.* **72**, 267–273 (2004).
134. Montgomery, R. B., Guzman, J., O'Rourke, D. M. & Stahl, W. L. Expression of oncogenic epidermal growth factor receptor family kinases induces paclitaxel resistance and alters beta-tubulin isotype expression. *J. Biol. Chem.* **275**, 17358–17363 (2000).
135. Simmons, M. L. *et al.* Analysis of complex relationships between age, p53, epidermal growth factor receptor, and survival in glioblastoma patients. *Cancer Res.* **61**, 1122–1128 (2001).
136. Li, J., Liang, R., Song, C., Xiang, Y. & Liu, Y. Prognostic significance of epidermal growth factor receptor expression in glioma patients. *OncoTargets Ther.* **11**, 731 (2018).
137. An, Z., Aksoy, O., Zheng, T., Fan, Q.-W. & Weiss, W. A. Epidermal growth factor receptor and EGFRvIII in glioblastoma: signaling pathways and targeted therapies. *Oncogene* **37**, 1561–1575 (2018).
138. Singh, S. K. *et al.* Identification of a cancer stem cell in human brain tumors. *Cancer Res.* **63**, 5821–5828 (2003).
139. Singh, S. K. *et al.* Identification of human brain tumour initiating cells. *Nature* **432**, 396–401 (2004).

140. Safa, A. R., Saadatzadeh, M. R., Cohen-Gadol, A. A., Pollok, K. E. & Bijangi-Vishehsaraei, K. Glioblastoma stem cells (GSCs) epigenetic plasticity and interconversion between differentiated non-GSCs and GSCs. *Genes Dis.* **2**, 152–163 (2015).
141. Mao, P. *et al.* Mesenchymal glioma stem cells are maintained by activated glycolytic metabolism involving aldehyde dehydrogenase 1A3. *Proc. Natl. Acad. Sci. U. S. A.* **110**, 8644–8649 (2013).
142. Brown, D. V. *et al.* Expression of CD133 and CD44 in glioblastoma stem cells correlates with cell proliferation, phenotype stability and intra-tumor heterogeneity. *PloS One* **12**, e0172791 (2017).
143. Richards, L. M. *et al.* Gradient of Developmental and Injury Response transcriptional states defines functional vulnerabilities underpinning glioblastoma heterogeneity. *Nat. Cancer* **2**, 157–173 (2021).
144. Thomas, T. M. & Yu, J. S. Metabolic regulation of glioma stem-like cells in the tumor micro-environment. *Cancer Lett.* **408**, 174–181 (2017).
145. Papale, M. *et al.* Hypoxia, Inflammation and Necrosis as Determinants of Glioblastoma Cancer Stem Cells Progression. *Int. J. Mol. Sci.* **21**, 2660 (2020).
146. Jijiwa, M. *et al.* CD44v6 regulates growth of brain tumor stem cells partially through the AKT-mediated pathway. *PloS One* **6**, e24217 (2011).
147. Li, G. *et al.* ALDH1A3 induces mesenchymal differentiation and serves as a predictor for survival in glioblastoma. *Cell Death Dis.* **9**, 1–11 (2018).
148. Xu, X. *et al.* Aldehyde dehydrogenases and cancer stem cells. *Cancer Lett.* **369**, 50–57 (2015).
149. Carén, H. *et al.* Glioblastoma Stem Cells Respond to Differentiation Cues but Fail to Undergo Commitment and Terminal Cell-Cycle Arrest. *Stem Cell Rep.* **5**, 829–842 (2015).
150. Ferrandez, E., Gutierrez, O., Segundo, D. S. & Fernandez-Luna, J. L. NFκB activation in differentiating glioblastoma stem-like cells is promoted by hyaluronic acid signaling through TLR4. *Sci. Rep.* **8**, 6341 (2018).
151. Pibuel, M. A., Poodts, D., Díaz, M., Hajos, S. E. & Lompardía, S. L. The scrambled story between hyaluronan and glioblastoma. *J. Biol. Chem.* **296**, 100549 (2021).
152. Hai, L. *et al.* Jagged1 is Clinically Prognostic and Promotes Invasion of Glioma-Initiating Cells by Activating NF-κB(p65) Signaling. *Cell. Physiol. Biochem. Int. J. Exp. Cell. Physiol. Biochem. Pharmacol.* **51**, 2925–2937 (2018).
153. Gimple, R. C., Bhargava, S., Dixit, D. & Rich, J. N. Glioblastoma stem cells: lessons from the tumor hierarchy in a lethal cancer. *Genes Dev.* **33**, 591–609 (2019).
154. Pistollato, F. *et al.* Intratumoral Hypoxic Gradient Drives Stem Cells Distribution and MGMT Expression in Glioblastoma. *Stem Cells* **28**, 851–862 (2010).
155. Schiffer, D. *et al.* Stem cell niches in glioblastoma: a neuropathological view. *BioMed Res. Int.* **2014**, 725921 (2014).
156. Murat, A. *et al.* Stem cell-related 'self-renewal' signature and high epidermal growth factor receptor expression associated with resistance to concomitant chemoradiotherapy in glioblastoma. *J. Clin. Oncol. Off. J. Am. Soc. Clin. Oncol.* **26**, 3015–3024 (2008).
157. Liu, G. *et al.* Analysis of gene expression and chemoresistance of CD133+ cancer stem cells in glioblastoma. *Mol. Cancer* **5**, 67 (2006).
158. Aderetti, D. A., Hira, V. V. V., Molenaar, R. J. & van Noorden, C. J. F. The hypoxic peri-arteriolar glioma stem cell niche, an integrated concept of five types of niches in human glioblastoma. *Biochim. Biophys. Acta Rev. Cancer* **1869**, 346–354 (2018).

159. Schiffer, D., Annovazzi, L., Casalone, C., Corona, C. & Mellai, M. Glioblastoma: Microenvironment and Niche Concept. *Cancers* **11**, 5 (2018).
160. Cheng, L. *et al.* Glioblastoma stem cells generate vascular pericytes to support vessel function and tumor growth. *Cell* **153**, 139–152 (2013).
161. Wang, X. *et al.* Reciprocal Signaling between Glioblastoma Stem Cells and Differentiated Tumor Cells Promotes Malignant Progression. *Cell Stem Cell* **22**, 514-528.e5 (2018).
162. Murphy, Á. C. *et al.* Activation of executioner caspases is a predictor of progression-free survival in glioblastoma patients: a systems medicine approach. *Cell Death Dis.* **4**, e629–e629 (2013).
163. Datta, S. R. *et al.* Akt phosphorylation of BAD couples survival signals to the cell-intrinsic death machinery. *Cell* **91**, 231–241 (1997).
164. Pommier, Y., Sordet, O., Antony, S., Hayward, R. L. & Kohn, K. W. Apoptosis defects and chemotherapy resistance: molecular interaction maps and networks. *Oncogene* **23**, 2934–2949 (2004).
165. Hill, V. K., Kim, J.-S., James, C. D. & Waldman, T. Correction of PTEN mutations in glioblastoma cell lines via AAV-mediated gene editing. *PLoS ONE* **12**, (2017).
166. Altomare, D. A. & Testa, J. R. Perturbations of the AKT signaling pathway in human cancer. *Oncogene* **24**, 7455–7464 (2005).
167. Wang, H. *et al.* Analysis of the activation status of Akt, NFkappaB, and Stat3 in human diffuse gliomas. *Lab. Investig. J. Tech. Methods Pathol.* **84**, 941–951 (2004).
168. Korkolopoulou, P. *et al.* Expression of nuclear factor-kappaB in human astrocytomas: relation to pI kappa Ba, vascular endothelial growth factor, Cox-2, microvascular characteristics, and survival. *Hum. Pathol.* **39**, 1143–1152 (2008).
169. Fan, X. *et al.* NOTCH Pathway Blockade Depletes CD133-Positive Glioblastoma Cells and Inhibits Growth of Tumor Neurospheres and Xenografts. *Stem Cells Dayt. Ohio* **28**, 5–16 (2010).
170. Lino, M. M., Merlo, A. & Boulay, J.-L. Notch signaling in glioblastoma: a developmental drug target? *BMC Med.* **8**, 72 (2010).
171. Furnari, F. B. *et al.* Malignant astrocytic glioma: genetics, biology, and paths to treatment. *Genes Dev.* **21**, 2683–2710 (2007).
172. Strik, H. *et al.* BCL-2 family protein expression in initial and recurrent glioblastomas: modulation by radiochemotherapy. *J. Neurol. Neurosurg. Psychiatry* **67**, 763–768 (1999).
173. Qiu, B., Wang, Y., Tao, J. & Wang, Y. Expression and correlation of Bcl-2 with pathological grades in human glioma stem cells. *Oncol. Rep.* **28**, 155–160 (2012).
174. Konnikova, L., Kotecki, M., Kruger, M. M. & Cochran, B. H. Knockdown of STAT3 expression by RNAi induces apoptosis in astrocytoma cells. *BMC Cancer* **3**, 23 (2003).
175. Hao, C. *et al.* Induction and intracellular regulation of tumor necrosis factor-related apoptosis-inducing ligand (TRAIL) mediated apotosis in human malignant glioma cells. *Cancer Res.* **61**, 1162–1170 (2001).
176. Cheung, H. H., Mahoney, D. J., LaCasse, E. C. & Korneluk, R. G. Down-regulation of c-FLIP Enhances Death of Cancer Cells by Smac Mimetic Compound. *Cancer Res.* **69**, 7729–7738 (2009).
177. Coupienne, I., Fettweis, G., Rubio, N., Agostinis, P. & Piette, J. 5-ALA-PDT induces RIP3-dependent necrosis in glioblastoma. *Photochem. Photobiol. Sci. Off. J. Eur. Photochem. Assoc. Eur. Soc. Photobiol.* **10**, 1868–1878 (2011).

178. Fianco, G. *et al.* Caspase-8 contributes to angiogenesis and chemotherapy resistance in glioblastoma. *eLife* **6**, e22593 (2017).
179. Aggarwal, B. B., Schwarz, L., Hogan, M. E. & Rando, R. F. Triple helix-forming oligodeoxyribonucleotides targeted to the human tumor necrosis factor (TNF) gene inhibit TNF production and block the TNF-dependent growth of human glioblastoma tumor cells. *Cancer Res.* **56**, 5156–5164 (1996).
180. Hayashi, S. *et al.* Expression of nuclear factor-kappa B, tumor necrosis factor receptor type 1, and c-Myc in human astrocytomas. *Neurol. Med. Chir. (Tokyo)* **41**, 187–195 (2001).
181. Valdés-Rives, S. A., Casique-Aguirre, D., Germán-Castelán, L., Velasco-Velázquez, M. A. & González-Arenas, A. Apoptotic Signaling Pathways in Glioblastoma and Therapeutic Implications. *BioMed Res. Int.* **2017**, (2017).
182. Beug, S. T. *et al.* Smac mimetics synergize with immune checkpoint inhibitors to promote tumour immunity against glioblastoma. *Nat. Commun.* **8**, 14278 (2017).
183. Guo, G. *et al.* Primary resistance to EGFR inhibition in glioblastoma is mediated by a TNF-JNK-Axl-ERK signaling axis. *Nat. Neurosci.* **20**, 1074–1084 (2017).
184. Luo, Z., Wang, B., Liu, H. & Shi, L. TNF Inhibitor Pomalidomide Sensitizes Glioblastoma Cells to EGFR Inhibition. *Ann. Clin. Lab. Sci.* **50**, 474–480 (2020).
185. Song, J. H., Bellail, A., Tse, M. C. L., Yong, V. W. & Hao, C. Human Astrocytes Are Resistant to Fas Ligand and Tumor Necrosis Factor-Related Apoptosis-Inducing Ligand-Induced Apoptosis. *J. Neurosci.* **26**, 3299–3308 (2006).
186. Greig, F. H. & Nixon, G. F. Phosphoprotein enriched in astrocytes (PEA)-15: A potential therapeutic target in multiple disease states. *Pharmacol. Ther.* **143**, 265–274 (2014).
187. Eisele, G. & Weller, M. Targeting apoptosis pathways in glioblastoma. *Cancer Lett.* **332**, 335–345 (2013).
188. Fulda, S., Wick, W., Weller, M. & Debatin, K.-M. Smac agonists sensitize for Apo2L/TRAIL- or anticancer drug-induced apoptosis and induce regression of malignant glioma in vivo. *Nat. Med.* **8**, 808–815 (2002).
189. Kim, E. H. *et al.* Arsenic trioxide sensitizes human glioma cells, but not normal astrocytes, to TRAIL-induced apoptosis via CCAAT/enhancer-binding protein homologous protein-dependent DR5 up-regulation. *Cancer Res.* **68**, 266–275 (2008).
190. Khan, M., Bi, Y., Qazi, J. I., Fan, L. & Gao, H. Evodiamine sensitizes U87 glioblastoma cells to TRAIL via the death receptor pathway. *Mol. Med. Rep.* **11**, 257–262 (2015).
191. Han, H. *et al.* Icaritin Sensitizes Human Glioblastoma Cells to TRAIL-Induced Apoptosis. *Cell Biochem. Biophys.* **72**, 533–542 (2015).
192. Ivanov, V. N. & Hei, T. K. Radiation-induced glioblastoma signaling cascade regulates viability, apoptosis and differentiation of neural stem cells (NSC). *Apoptosis Int. J. Program. Cell Death* **19**, 1736–1754 (2014).
193. Liu, J. *et al.* Synergistic effect of TRAIL and irradiation in elimination of glioblastoma stem-like cells. *Clin. Exp. Med.* **18**, 399–411 (2018).
194. Han, H. R., Park, S. A., Ahn, S., Jeun, S.-S. & Ryu, C. H. Evaluation of Combination Treatment Effect With TRAIL-secreting Mesenchymal Stem Cells and Compound C Against Glioblastoma. *Anticancer Res.* **39**, 6635–6643 (2019).
195. Xiao, C., Yang, B. F., Asadi, N., Beguinot, F. & Hao, C. Tumor Necrosis Factor-related Apoptosis-inducing Ligand-induced Death-inducing Signaling Complex and Its Modulation by c-FLIP and PED/PEA-15 in Glioma Cells*. *J. Biol. Chem.* **277**, 25020–25025 (2002).

196. Liang, J. *et al.* Comprehensive molecular characterization of inhibitors of apoptosis proteins (IAPs) for therapeutic targeting in cancer. *BMC Med. Genomics* **13**, 7 (2020).
197. Lopez, P. L. C. *et al.* Sensitization of Glioma Cells by X-Linked Inhibitor of Apoptosis Protein Knockdown. *Oncology* **83**, 75–82 (2012).
198. Zhen, H.-N. *et al.* Short hairpin RNA targeting survivin inhibits growth and angiogenesis of glioma U251 cells. *Int. J. Oncol.* **31**, 1111–1117 (2007).
199. Chakravarti, A. *et al.* Survivin enhances radiation resistance in primary human glioblastoma cells via caspase-independent mechanisms. *Oncogene* **23**, 7494–7506 (2004).
200. Chakravarti, A. *et al.* Quantitatively determined survivin expression levels are of prognostic value in human gliomas. *J. Clin. Oncol. Off. J. Am. Soc. Clin. Oncol.* **20**, 1063–1068 (2002).
201. Zhang, X. *et al.* YM155 decreases radiation-induced invasion and reverses epithelial-mesenchymal transition by targeting STAT3 in glioblastoma. *J. Transl. Med.* **16**, 79 (2018).
202. Lai, P. C. *et al.* Novel Survivin Inhibitor YM155 elicits Cytotoxicity in Glioblastoma Cell Lines with Normal or Deficiency DNA-Dependent Protein Kinase Activity. *Pediatr. Neonatol.* **53**, 199–204 (2012).
203. Guo, H. *et al.* Silencing of survivin using YM155 inhibits invasion and suppresses proliferation in glioma cells. *Cell Biochem. Biophys.* **71**, 587–593 (2015).
204. Jane, E. P. *et al.* YM-155 Potentiates the Effect of ABT-737 in Malignant Human Glioma Cells via Survivin and Mcl-1 Downregulation in an EGFR-Dependent Context. *Mol. Cancer Ther.* **12**, 326–338 (2013).
205. Fenstermaker, R. A. & Ciesielski, M. J. Challenges in the development of a survivin vaccine (SurVaxM) for malignant glioma. *Expert Rev. Vaccines* **13**, 377–385 (2014).
206. Fenstermaker, R. A. *et al.* Clinical study of a survivin long peptide vaccine (SurVaxM) in patients with recurrent malignant glioma. *Cancer Immunol. Immunother.* **65**, 1339–1352 (2016).
207. Tchoghandjian, A. *et al.* Inhibitor of apoptosis protein expression in glioblastomas and their in vitro and in vivo targeting by SMAC mimetic GDC-0152. *Cell Death Dis.* **7**, e2325–e2325 (2016).
208. Soubéran, A. *et al.* Inhibitor of Apoptosis Proteins Determines Glioblastoma Stem-Like Cell Fate in an Oxygen-Dependent Manner. *Stem Cells Dayt. Ohio* **37**, 731–742 (2019).
209. Zakaria, Z. *et al.* Patient-derived glioblastoma cells show significant heterogeneity in treatment responses to the inhibitor-of-apoptosis-protein antagonist birinapant. *Br. J. Cancer* **114**, 188–198 (2016).
210. Wang, D. *et al.* BIRC3 is a novel driver of therapeutic resistance in Glioblastoma. *Sci. Rep.* **6**, 21710 (2016).
211. Yang, W., Cooke, M., Duckett, C. S., Yang, X. & Dorsey, J. F. Distinctive effects of the cellular inhibitor of apoptosis protein c-IAP2 through stabilization by XIAP in glioblastoma multiforme cells. *Cell Cycle* **13**, 992–1005 (2014).
212. Wang, D. *et al.* BIRC3 is a biomarker of mesenchymal habitat of glioblastoma, and a mediator of survival adaptation in hypoxia-driven glioblastoma habitats. *Sci. Rep.* **7**, 9350 (2017).
213. Gressot, L. V. *et al.* Analysis of the inhibitors of apoptosis identifies BIRC3 as a facilitator of malignant progression in glioma. *Oncotarget* **8**, 12695–12704 (2017).
214. Lee, J. H. *et al.* Human glioblastoma arises from subventricular zone cells with low-level driver mutations. *Nature* **560**, 243–247 (2018).

215. Dufour, A. *et al.* Modeling the dynamics of oligodendrocyte precursor cells and the genesis of gliomas. *PLoS Comput. Biol.* **14**, e1005977 (2018).
216. Alcantara Llaguno, S. *et al.* Cell-of-origin susceptibility to glioblastoma formation declines with neural lineage restriction. *Nat. Neurosci.* **22**, 545–555 (2019).
217. Luk, K. C. & Sadikot, A. F. Glutamate and regulation of proliferation in the developing mammalian telencephalon. *Dev. Neurosci.* **26**, 218–228 (2004).
218. LoTurco, J. J., Owens, D. F., Heath, M. J., Davis, M. B. & Kriegstein, A. R. GABA and glutamate depolarize cortical progenitor cells and inhibit DNA synthesis. *Neuron* **15**, 1287–1298 (1995).
219. Kougioumtzidou, E. *et al.* Signalling through AMPA receptors on oligodendrocyte precursors promotes myelination by enhancing oligodendrocyte survival. *eLife* **6**, e28080 (2017).
220. Venkatesh, H. S. *et al.* Neuronal Activity Promotes Glioma Growth through Neuroligin-3 Secretion. *Cell* **161**, 803–816 (2015).
221. Venkatesh, H. S. *et al.* Targeting neuronal activity-regulated neuroligin-3 dependency in high-grade glioma. *Nature* **549**, 533–537 (2017).
222. Buckingham, S. C. *et al.* Glutamate release by primary brain tumors induces epileptic activity. *Nat. Med.* **17**, 1269–1274 (2011).
223. Campbell, S. L., Buckingham, S. C. & Sontheimer, H. Human glioma cells induce hyperexcitability in cortical networks. *Epilepsia* **53**, 1360–1370 (2012).
224. Campbell, S. L. *et al.* GABAergic disinhibition and impaired KCC2 cotransporter activity underlie tumor-associated epilepsy. *Glia* **63**, 23–36 (2015).
225. Venkatesh, H. S. *et al.* Electrical and synaptic integration of glioma into neural circuits. *Nature* **573**, 539–545 (2019).
226. Krishna, S. *et al.* Glioblastoma remodelling of human neural circuits decreases survival. *Nature* **617**, 599–607 (2023).
227. Drexler, R. *et al.* Epigenetic neural glioblastoma enhances synaptic integration and predicts therapeutic vulnerability. *bioRxiv* 2023.08.04.552017 (2023) doi:10.1101/2023.08.04.552017.
228. Varn, F. S. *et al.* Glioma progression is shaped by genetic evolution and microenvironment interactions. *Cell* **185**, 2184-2199.e16 (2022).
229. Venkataramani, V. *et al.* Glioblastoma hijacks neuronal mechanisms for brain invasion. *Cell* **185**, 2899-2917.e31 (2022).
230. Venteicher, A. S. *et al.* Decoupling genetics, lineages, and microenvironment in IDH-mutant gliomas by single-cell RNA-seq. *Science* **355**, eaai8478 (2017).
231. Filbin, M. G. *et al.* Developmental and oncogenic programs in H3K27M gliomas dissected by single-cell RNA-seq. *Science* **360**, 331–335 (2018).
232. Bandt, S. K. *et al.* The impact of high grade glial neoplasms on human cortical electrophysiology. *PLoS ONE* **12**, e0173448 (2017).
233. Esmaeili, M., Stensjøen, A. L., Berntsen, E. M., Solheim, O. & Reinertsen, I. The Direction of Tumour Growth in Glioblastoma Patients. *Sci. Rep.* **8**, 1199 (2018).
234. Parker, J. J. *et al.* Intratumoral heterogeneity of endogenous tumor cell invasive behavior in human glioblastoma. *Sci. Rep.* **8**, 18002 (2018).
235. Koh, I. *et al.* The mode and dynamics of glioblastoma cell invasion into a decellularized tissue-derived extracellular matrix-based three-dimensional tumor model. *Sci. Rep.* **8**, 4608 (2018).

236. Hyvärinen, T. *et al.* Co-stimulation with IL-1β and TNF-α induces an inflammatory reactive astrocyte phenotype with neurosupportive characteristics in a human pluripotent stem cell model system. *Sci. Rep.* **9**, 16944 (2019).
237. Lau, L. T. & Yu, A. C. Astrocytes produce and release interleukin-1, interleukin-6, tumor necrosis factor alpha and interferon-gamma following traumatic and metabolic injury. *J. Neurotrauma* **18**, 351–359 (2001).
238. Perriot, S. *et al.* Human Induced Pluripotent Stem Cell-Derived Astrocytes Are Differentially Activated by Multiple Sclerosis-Associated Cytokines. *Stem Cell Rep.* **11**, 1199–1210 (2018).
239. O'Brien, E. R., Howarth, C. & Sibson, N. R. The role of astrocytes in CNS tumors: pre-clinical models and novel imaging approaches. *Front. Cell. Neurosci.* **7**, 40 (2013).
240. Nagashima, G., Suzuki, R., Asai, J. & Fujimoto, T. Immunohistochemical analysis of reactive astrocytes around glioblastoma: an immunohistochemical study of postmortem glioblastoma cases. *Clin. Neurol. Neurosurg.* **104**, 125–131 (2002).
241. Diep, Y. N. *et al.* Astrocytic scar restricting glioblastoma via glutamate–MAO-B activity in glioblastoma-microglia assembloid. *Biomater. Res.* **27**, 71 (2023).
242. Brandao, M., Simon, T., Critchley, G. & Giamas, G. Astrocytes, the rising stars of the glioblastoma microenvironment. *Glia* **67**, 779–790 (2019).
243. Henrik Heiland, D. *et al.* Tumor-associated reactive astrocytes aid the evolution of immunosuppressive environment in glioblastoma. *Nat. Commun.* **10**, 2541 (2019).
244. Barcia, C. *et al.* Infiltrating CTLs in human glioblastoma establish immunological synapses with tumorigenic cells. *Am. J. Pathol.* **175**, 786–798 (2009).
245. Katz, A. M. *et al.* Astrocyte-specific expression patterns associated with the PDGF-induced glioma microenvironment. *PloS One* **7**, e32453 (2012).
246. Carrillo-de Sauvage, M. A. *et al.* CCL2-expressing astrocytes mediate the extravasation of T lymphocytes in the brain. Evidence from patients with glioma and experimental models in vivo. *PloS One* **7**, e30762 (2012).
247. Perelroizen, R. *et al.* Astrocyte immunometabolic regulation of the tumour microenvironment drives glioblastoma pathogenicity. *Brain* **145**, 3288–3307 (2022).
248. Okolie, O. *et al.* Reactive astrocytes potentiate tumor aggressiveness in a murine glioma resection and recurrence model. *Neuro-Oncol.* **18**, 1622–1633 (2016).
249. Chen, W. *et al.* Glioma cells escaped from cytotoxicity of temozolomide and vincristine by communicating with human astrocytes. *Med. Oncol.* **32**, 43 (2015).
250. Lin, Q., Liu, Z., Ling, F. & Xu, G. Astrocytes protect glioma cells from chemotherapy and upregulate survival genes via gap junctional communication. *Mol. Med. Rep.* **13**, 1329–1335 (2016).
251. Pustchi, S. E., Avci, N. G., Akay, Y. M. & Akay, M. Astrocytes Decreased the Sensitivity of Glioblastoma Cells to Temozolomide and Bay 11-7082. *Int. J. Mol. Sci.* **21**, 7154 (2020).
252. Civita, P., M. Leite, D. & Pilkington, G. J. Pre-Clinical Drug Testing in 2D and 3D Human In Vitro Models of Glioblastoma Incorporating Non-Neoplastic Astrocytes: Tunneling Nano Tubules and Mitochondrial Transfer Modulates Cell Behavior and Therapeutic Response. *Int. J. Mol. Sci.* **20**, 6017 (2019).
253. Gielen, P. R. *et al.* Connexin43 confers Temozolomide resistance in human glioma cells by modulating the mitochondrial apoptosis pathway. *Neuropharmacology* **75**, 539–548 (2013).

254. Rath, B. H., Wahba, A., Camphausen, K. & Tofilon, P. J. Coculture with astrocytes reduces the radiosensitivity of glioblastoma stem-like cells and identifies additional targets for radiosensitization. *Cancer Med.* **4**, 1705–1716 (2015).
255. Kober, C. *et al.* Microglia and astrocytes attenuate the replication of the oncolytic vaccinia virus LIVP 1.1.1 in murine GL261 gliomas by acting as vaccinia virus traps. *J. Transl. Med.* **13**, 216 (2015).
256. Carrano, A. *et al.* Human Cerebrospinal Fluid Modulates Pathways Promoting Glioblastoma Malignancy. *Front. Oncol.* **11**, 624145 (2021).
257. Mistry, A. M. *et al.* Influence of glioblastoma contact with the lateral ventricle on survival: a meta-analysis. *J. Neurooncol.* **131**, 125–133 (2017).
258. Jafri, N. F., Clarke, J. L., Weinberg, V., Barani, I. J. & Cha, S. Relationship of glioblastoma multiforme to the subventricular zone is associated with survival. *Neuro-Oncol.* **15**, 91–96 (2013).
259. Ihrie, R. A. & Álvarez-Buylla, A. Lake Front Property: A Unique Germinal Niche by the Lateral Ventricles of the Adult Brain. *Neuron* **70**, 674–686 (2011).
260. Steed, T. C. *et al.* Glioblastomas located in proximity to the subventricular zone (SVZ) exhibited enrichment of gene expression profiles associated with the cancer stem cell state. *J. Neurooncol.* **148**, 455–462 (2020).
261. Guyon, J., Chapouly, C., Andrique, L., Bikfalvi, A. & Daubon, T. The Normal and Brain Tumor Vasculature: Morphological and Functional Characteristics and Therapeutic Targeting. *Front. Physiol.* **12**, 622615 (2021).
262. Valdor, R. *et al.* Glioblastoma ablates pericytes antitumor immune function through aberrant up-regulation of chaperone-mediated autophagy. *Proc. Natl. Acad. Sci. U. S. A.* **116**, 20655–20665 (2019).
263. Oldendorf, W. H., Cornford, M. E. & Brown, W. J. The large apparent work capability of the blood-brain barrier: a study of the mitochondrial content of capillary endothelial cells in brain and other tissues of the rat. *Ann. Neurol.* **1**, 409–417 (1977).
264. Takakura, Y., Audus, K. L. & Borchardt, R. T. Blood-brain barrier: transport studies in isolated brain capillaries and in cultured brain endothelial cells. *Adv. Pharmacol. San Diego Calif* **22**, 137–165 (1991).
265. Sweeney, M. D., Zhao, Z., Montagne, A., Nelson, A. R. & Zlokovic, B. V. Blood-Brain Barrier: From Physiology to Disease and Back. *Physiol. Rev.* **99**, 21–78 (2019).
266. Butt, A. M., Jones, H. C. & Abbott, N. J. Electrical resistance across the blood-brain barrier in anaesthetized rats: a developmental study. *J. Physiol.* **429**, 47–62 (1990).
267. Kacem, K., Lacombe, P., Seylaz, J. & Bonvento, G. Structural organization of the perivascular astrocyte endfeet and their relationship with the endothelial glucose transporter: a confocal microscopy study. *Glia* **23**, 1–10 (1998).
268. Abbott, N. J., Rönnbäck, L. & Hansson, E. Astrocyte-endothelial interactions at the blood-brain barrier. *Nat. Rev. Neurosci.* **7**, 41–53 (2006).
269. Ronaldson, P. T. & Davis, T. P. Blood-brain barrier integrity and glial support: mechanisms that can be targeted for novel therapeutic approaches in stroke. *Curr. Pharm. Des.* **18**, 3624–3644 (2012).
270. Hawkins, B. T. & Davis, T. P. The blood-brain barrier/neurovascular unit in health and disease. *Pharmacol. Rev.* **57**, 173–185 (2005).
271. Bell, R. D. *et al.* Apolipoprotein E controls cerebrovascular integrity via cyclophilin A. *Nature* **485**, 512–516 (2012).

272. Mizee, M. R. *et al.* Retinoic Acid Induces Blood–Brain Barrier Development. *J. Neurosci.* **33**, 1660–1671 (2013).
273. Daneman, R. *et al.* Wnt/β-catenin signaling is required for CNS, but not non-CNS, angiogenesis. *Proc. Natl. Acad. Sci.* **106**, 641–646 (2009).
274. Liebner, S. *et al.* Wnt/β-catenin signaling controls development of the blood–brain barrier. *J. Cell Biol.* **183**, 409–417 (2008).
275. Alvarez, J. I. *et al.* The Hedgehog Pathway Promotes Blood-Brain Barrier Integrity and CNS Immune Quiescence. *Science* **334**, 1727–1731 (2011).
276. Erdő, F., Denes, L. & de Lange, E. Age-associated physiological and pathological changes at the blood-brain barrier: A review. *J. Cereb. Blood Flow Metab. Off. J. Int. Soc. Cereb. Blood Flow Metab.* **37**, 4–24 (2017).
277. van Tellingen, O. *et al.* Overcoming the blood-brain tumor barrier for effective glioblastoma treatment. *Drug Resist. Updat. Rev. Comment. Antimicrob. Anticancer Chemother.* **19**, 1–12 (2015).
278. Couto, M. *et al.* The interplay between glioblastoma and microglia cells leads to endothelial cell monolayer dysfunction via the interleukin-6-induced JAK2/STAT3 pathway. *J. Cell. Physiol.* **234**, 19750–19760 (2019).
279. Wijaya, J., Fukuda, Y. & Schuetz, J. D. Obstacles to Brain Tumor Therapy: Key ABC Transporters. *Int. J. Mol. Sci.* **18**, 2544 (2017).
280. Dunn, G. P., Bruce, A. T., Ikeda, H., Old, L. J. & Schreiber, R. D. Cancer immunoediting: from immunosurveillance to tumor escape. *Nat. Immunol.* **3**, 991–998 (2002).
281. Lasek, W. Cancer immunoediting hypothesis: history, clinical implications and controversies. *Cent.-Eur. J. Immunol.* **47**, 168–174 (2022).
282. Vesely, M. D. & Schreiber, R. D. Cancer Immunoediting: antigens, mechanisms and implications to cancer immunotherapy. *Ann. N. Y. Acad. Sci.* **1284**, 1–5 (2013).
283. Gubin, M. M. & Vesely, M. D. Cancer Immunoediting in the Era of Immuno-oncology. *Clin. Cancer Res.* **28**, 3917–3928 (2022).
284. O'Donnell, J. S., Teng, M. W. L. & Smyth, M. J. Cancer immunoediting and resistance to T cell-based immunotherapy. *Nat. Rev. Clin. Oncol.* **16**, 151–167 (2019).
285. Liu, S., Sun, Q. & Ren, X. Novel strategies for cancer immunotherapy: counter-immunoediting therapy. *J. Hematol. Oncol.J Hematol Oncol* **16**, 38 (2023).
286. Chen, D. S. & Mellman, I. Elements of cancer immunity and the cancer-immune set point. *Nature* **541**, 321–330 (2017).
287. Romagnani, S. Immunological tolerance and autoimmunity. *Intern. Emerg. Med.* **1**, 187–196 (2006).
288. Zhang, Y. & Zheng, J. Functions of Immune Checkpoint Molecules Beyond Immune Evasion. *Adv. Exp. Med. Biol.* **1248**, 201–226 (2020).
289. Mirzaei, R., Sarkar, S. & Yong, V. W. T Cell Exhaustion in Glioblastoma: Intricacies of Immune Checkpoints. *Trends Immunol.* **38**, 104–115 (2017).
290. Jiang, Y., Li, Y. & Zhu, B. T-cell exhaustion in the tumor microenvironment. *Cell Death Dis.* **6**, e1792–e1792 (2015).
291. Yi, J. S., Cox, M. A. & Zajac, A. J. T-cell exhaustion: characteristics, causes and conversion. *Immunology* **129**, 474–481 (2010).
292. Guo, Z., Zhang, R., Yang, A.-G. & Zheng, G. Diversity of immune checkpoints in cancer immunotherapy. *Front. Immunol.* **14**, (2023).

293. Brunet, J. F. *et al.* A new member of the immunoglobulin superfamily--CTLA-4. *Nature* **328**, 267–270 (1987).
294. Ishida, Y., Agata, Y., Shibahara, K. & Honjo, T. Induced expression of PD-1, a novel member of the immunoglobulin gene superfamily, upon programmed cell death. *EMBO J.* **11**, 3887–3895 (1992).
295. Kamali, A. N., Bautista, J. M., Eisenhut, M. & Hamedifar, H. Immune checkpoints and cancer immunotherapies: insights into newly potential receptors and ligands. *Ther. Adv. Vaccines Immunother.* **11**, (2023).
296. Arasanz, H. *et al.* PD1 signal transduction pathways in T cells. *Oncotarget* **8**, 51936–51945 (2017).
297. Lorenz, U. SHP-1 and SHP-2 in T cells: two phosphatases functioning at many levels. *Immunol. Rev.* **228**, 342–359 (2009).
298. Yang, W. *et al.* Protein Kinase 2 (CK2) Controls CD8+ T-cell Effector and Memory Function during Infection. *J. Immunol. Baltim. Md 1950* ji2101080 (2022) doi:10.4049/jimmunol.2101080.
299. Rao, N., Dodge, I. & Band, H. The Cbl family of ubiquitin ligases: critical negative regulators of tyrosine kinase signaling in the immune system. *J. Leukoc. Biol.* **71**, 753–763 (2002).
300. Duan, L., Reddi, A. L., Ghosh, A., Dimri, M. & Band, H. The Cbl family and other ubiquitin ligases: destructive forces in control of antigen receptor signaling. *Immunity* **21**, 7–17 (2004).
301. He, X. & Xu, C. Immune checkpoint signaling and cancer immunotherapy. *Cell Res.* **30**, 660–669 (2020).
302. Chen, D. S. & Mellman, I. Oncology Meets Immunology: The Cancer-Immunity Cycle. *Immunity* **39**, 1–10 (2013).
303. Mellman, I., Chen, D. S., Powles, T. & Turley, S. J. The cancer-immunity cycle: Indication, genotype, and immunotype. *Immunity* **56**, 2188–2205 (2023).
304. Medawar, P. B. Immunity to homologous grafted skin; the fate of skin homografts transplanted to the brain, to subcutaneous tissue, and to the anterior chamber of the eye. *Br. J. Exp. Pathol.* **29**, 58–69 (1948).
305. Murphy, J. B. & Sturm, E. CONDITIONS DETERMINING THE TRANSPLANTABILITY OF TISSUES IN THE BRAIN. *J. Exp. Med.* **38**, 183–197 (1923).
306. Hogan, B. M. & Bower, N. I. Lymphatics and the Brain. *Circ. Res.* **128**, 59–61 (2021).
307. Perry, V. H. A revised view of the central nervous system microenvironment and major histocompatibility complex class II antigen presentation. *J. Neuroimmunol.* **90**, 113–121 (1998).
308. Perry, V. H., Anthony, D. C., Bolton, S. J. & Brown, H. C. The blood-brain barrier and the inflammatory response. *Mol. Med. Today* **3**, 335–341 (1997).
309. Scott, B. *et al.* A role for non-MHC genetic polymorphism in susceptibility to spontaneous autoimmunity. *Immunity* **1**, 73–83 (1994).
310. Brabb, T. *et al.* Triggers of autoimmune disease in a murine TCR-transgenic model for multiple sclerosis. *J. Immunol. Baltim. Md 1950* **159**, 497–507 (1997).
311. Brabb, T. *et al.* In situ tolerance within the central nervous system as a mechanism for preventing autoimmunity. *J. Exp. Med.* **192**, 871–880 (2000).
312. Barker, C. F. & Billingham, R. E. Immunologically privileged sites. *Adv. Immunol.* **25**, 1–54 (1977).

313. Rustenhoven, J. & Kipnis, J. Brain borders at the central stage of neuroimmunology. *Nature* **612**, 417–429 (2022).
314. Mamuladze, T. & Kipnis, J. Type 2 immunity in the brain and brain borders. *Cell. Mol. Immunol.* **20**, 1290–1299 (2023).
315. Rustenhoven, J. *et al.* Functional characterization of the dural sinuses as a neuroimmune interface. *Cell* **184**, 1000-1016.e27 (2021).
316. Absinta, M. *et al.* Human and nonhuman primate meninges harbor lymphatic vessels that can be visualized noninvasively by MRI. *eLife* **6**, e29738 (2017).
317. Alves de Lima, K., Rustenhoven, J. & Kipnis, J. Meningeal Immunity and Its Function in Maintenance of the Central Nervous System in Health and Disease. *Annu. Rev. Immunol.* **38**, 597–620 (2020).
318. Louveau, A. *et al.* CNS lymphatic drainage and neuroinflammation are regulated by meningeal lymphatic vasculature. *Nat. Neurosci.* **21**, 1380–1391 (2018).
319. Antila, S. *et al.* Development and plasticity of meningeal lymphatic vessels. *J. Exp. Med.* **214**, 3645–3667 (2017).
320. Koh, L., Zakharov, A. & Johnston, M. Integration of the subarachnoid space and lymphatics: Is it time to embrace a new concept of cerebrospinal fluid absorption? *Cerebrospinal Fluid Res.* **2**, 6 (2005).
321. Iliff, J. J. *et al.* A Paravascular Pathway Facilitates CSF Flow Through the Brain Parenchyma and the Clearance of Interstitial Solutes, Including Amyloid β. *Sci. Transl. Med.* **4**, 147ra111 (2012).
322. Ding, Z. *et al.* The glymphatic system: a new perspective on brain diseases. *Front. Aging Neurosci.* **15**, (2023).
323. Iliff, J. J. *et al.* Impairment of Glymphatic Pathway Function Promotes Tau Pathology after Traumatic Brain Injury. *J. Neurosci.* **34**, 16180–16193 (2014).
324. Gao, Y., Liu, K. & Zhu, J. Glymphatic system: an emerging therapeutic approach for neurological disorders. *Front. Mol. Neurosci.* **16**, (2023).
325. Formolo, D. A. *et al.* Leveraging the glymphatic and meningeal lymphatic systems as therapeutic strategies in Alzheimer's disease: an updated overview of nonpharmacological therapies. *Mol. Neurodegener.* **18**, 26 (2023).
326. Merlini, A. *et al.* Distinct roles of the meningeal layers in CNS autoimmunity. *Nat. Neurosci.* **25**, 887–899 (2022).
327. Schläger, C. *et al.* Effector T-cell trafficking between the leptomeninges and the cerebrospinal fluid. *Nature* **530**, 349–353 (2016).
328. Lilius, T. O. *et al.* Dexmedetomidine enhances glymphatic brain delivery of intrathecally administered drugs. *J. Controlled Release* **304**, 29–38 (2019).
329. Herisson, F. *et al.* Direct vascular channels connect skull bone marrow and the brain surface enabling myeloid cell migration. *Nat. Neurosci.* **21**, 1209–1217 (2018).
330. Cugurra, A. *et al.* Skull and vertebral bone marrow are myeloid cell reservoirs for the meninges and CNS parenchyma. *Science* **373**, eabf7844 (2021).
331. Rustenhoven, J. *et al.* Age-related alterations in meningeal immunity drive impaired CNS lymphatic drainage. *J. Exp. Med.* **220**, e20221929 (2023).
332. Kierdorf, K. *et al.* Microglia emerge from erythromyeloid precursors via Pu.1- and Irf8-dependent pathways. *Nat. Neurosci.* **16**, 273–280 (2013).
333. Schulz, C. *et al.* A Lineage of Myeloid Cells Independent of Myb and Hematopoietic Stem Cells. *Science* **336**, 86–90 (2012).

334. Ginhoux, F. *et al.* Fate Mapping Analysis Reveals That Adult Microglia Derive from Primitive Macrophages. *Science* **330**, 841–845 (2010).
335. Carson, M. J., Reilly, C. R., Sutcliffe, J. G. & Lo, D. Disproportionate recruitment of CD8+ T cells into the central nervous system by professional antigen-presenting cells. *Am. J. Pathol.* **154**, 481–494 (1999).
336. Arcuri, C. *et al.* Microglia-glioma cross-talk: a two way approach to new strategies against glioma. *Front. Biosci. Landmark Ed.* **22**, 268–309 (2017).
337. Carson, M. J., Doose, J. M., Melchior, B., Schmid, C. D. & Ploix, C. C. CNS immune privilege: hiding in plain sight. *Immunol. Rev.* **213**, 48–65 (2006).
338. Greter, M. *et al.* Dendritic cells permit immune invasion of the CNS in an animal model of multiple sclerosis. *Nat. Med.* **11**, 328–334 (2005).
339. Kivisäkk, P. *et al.* Localizing central nervous system immune surveillance: Meningeal antigen-presenting cells activate T cells during experimental autoimmune encephalomyelitis. *Ann. Neurol.* **65**, 457–469 (2009).
340. Deleidi, M., Jäggle, M. & Rubino, G. Immune aging, dysmetabolism, and inflammation in neurological diseases. *Front. Neurosci.* **9**, 172 (2015).
341. Mrdjen, D. *et al.* High-Dimensional Single-Cell Mapping of Central Nervous System Immune Cells Reveals Distinct Myeloid Subsets in Health, Aging, and Disease. *Immunity* **48**, 380-395.e6 (2018).
342. Korin, B. *et al.* High-dimensional, single-cell characterization of the brain's immune compartment. *Nat. Neurosci.* **20**, 1300–1309 (2017).
343. Constantinescu, C. S. *et al.* Astrocytes as antigen-presenting cells: expression of IL-12/IL-23. *J. Neurochem.* **95**, 331–340 (2005).
344. Aloisi, F., Ria, F. & Adorini, L. Regulation of T-cell responses by CNS antigen-presenting cells: different roles for microglia and astrocytes. *Immunol. Today* **21**, 141–147 (2000).
345. Sofroniew, M. V. Astrocyte barriers to neurotoxic inflammation. *Nat. Rev. Neurosci.* **16**, 249–263 (2015).
346. Gimsa, U., Mitchison, N. A. & Brunner-Weinzierl, M. C. Immune privilege as an intrinsic CNS property: astrocytes protect the CNS against T-cell-mediated neuroinflammation. *Mediators Inflamm.* **2013**, 320519 (2013).
347. Steelman, A. J., Smith, R., Welsh, C. J. & Li, J. Galectin-9 protein is up-regulated in astrocytes by tumor necrosis factor and promotes encephalitogenic T-cell apoptosis. *J. Biol. Chem.* **288**, 23776–23787 (2013).
348. Schachtele, S. J., Hu, S., Sheng, W. S., Mutnal, M. B. & Lokensgard, J. R. Glial cells suppress postencephalitic CD8+ T lymphocytes through PD-L1. *Glia* **62**, 1582–1594 (2014).
349. Deczkowska, A., Amit, I. & Schwartz, M. Microglial immune checkpoint mechanisms. *Nat. Neurosci.* **21**, 779–786 (2018).
350. Liddelow, S. A. *et al.* Neurotoxic reactive astrocytes are induced by activated microglia. *Nature* **541**, 481–487 (2017).
351. Clarke, L. E. *et al.* Normal aging induces A1-like astrocyte reactivity. *Proc. Natl. Acad. Sci.* **115**, E1896–E1905 (2018).
352. Kearney, C. J. *et al.* PD-L1 and IAPs co-operate to protect tumors from cytotoxic lymphocyte-derived TNF. *Cell Death Differ.* **24**, 1705–1716 (2017).
353. Vredevoogd, D. W. *et al.* Augmenting Immunotherapy Impact by Lowering Tumor TNF Cytotoxicity Threshold. *Cell* **178**, 585-599.e15 (2019).

354. Müller-Sienerth, N. *et al.* SMAC mimetic BV6 induces cell death in monocytes and maturation of monocyte-derived dendritic cells. *PloS One* **6**, e21556 (2011).
355. Chesi, M. *et al.* IAP antagonists induce anti-tumor immunity in multiple myeloma. *Nat. Med.* **22**, 1411–1420 (2016).
356. Kearney, C. J. *et al.* Inhibitor of Apoptosis Proteins (IAPs) and Their Antagonists Regulate Spontaneous and Tumor Necrosis Factor (TNF)-induced Proinflammatory Cytokine and Chemokine Production *. *J. Biol. Chem.* **288**, 4878–4890 (2013).
357. Knights, A. J., Fucikova, J., Pasam, A., Koernig, S. & Cebon, J. Inhibitor of apoptosis protein (IAP) antagonists demonstrate divergent immunomodulatory properties in human immune subsets with implications for combination therapy. *Cancer Immunol. Immunother. CII* **62**, 321–335 (2013).
358. Pan, W. *et al.* A novel SMAC mimetic APG-1387 exhibits dual antitumor effect on HBV-positive hepatocellular carcinoma with high expression of cIAP2 by inducing apoptosis and enhancing innate anti-tumor immunity. *Biochem. Pharmacol.* **154**, 127–135 (2018).
359. Zahedi-Amiri, A., Malone, K., Beug, S. T., Alain, T. & Yeganeh, B. Autophagy in Tumor Immunity and Viral-Based Immunotherapeutic Approaches in Cancer. *Cells* **10**, 2672 (2021).
360. Singh, K. *et al.* Enhancing T Cell Chemotaxis and Infiltration in Glioblastoma. *Cancers* **13**, 5367 (2021).
361. Nicolas-Boluda, A. & Donnadieu, E. Obstacles to T cell migration in the tumor microenvironment. *Comp. Immunol. Microbiol. Infect. Dis.* **63**, 22–30 (2019).
362. Duerinck, J., Tuyaerts, S., Movahedi, K. & Neyns, B. Overcoming the immune suppressive nature of glioblastoma by leveraging the surgical intervention - current status and future perspectives. *Front. Immunol.* **14**, (2023).
363. Kiyokawa, J. *et al.* Modification of Extracellular Matrix Enhances Oncolytic Adenovirus Immunotherapy in Glioblastoma. *Clin. Cancer Res. Off. J. Am. Assoc. Cancer Res.* **27**, 889–902 (2021).
364. Didenko, V. V., Ngo, H. N., Minchew, C. & Baskin, D. S. Apoptosis of T lymphocytes invading glioblastomas multiforme: a possible tumor defense mechanism. *J. Neurosurg.* **96**, 580–584 (2002).
365. Jacobs, J. F. M. *et al.* Regulatory T cells and the PD-L1/PD-1 pathway mediate immune suppression in malignant human brain tumors. *Neuro-Oncol.* **11**, 394–402 (2009).
366. Ueda, R. *et al.* Systemic inhibition of transforming growth factor-beta in glioma-bearing mice improves the therapeutic efficacy of glioma-associated antigen peptide vaccines. *Clin. Cancer Res. Off. J. Am. Assoc. Cancer Res.* **15**, 6551–6559 (2009).
367. Mangani, D., Weller, M. & Roth, P. The network of immunosuppressive pathways in glioblastoma. *Biochem. Pharmacol.* **130**, 1–9 (2017).
368. Wang, J., Zhao, X. & Wan, Y. Y. Intricacies of TGF-β signaling in Treg and Th17 cell biology. *Cell. Mol. Immunol.* **20**, 1002–1022 (2023).
369. Heimberger, A. B. *et al.* Incidence and Prognostic Impact of FoxP3+ Regulatory T Cells in Human Gliomas. *Clin. Cancer Res.* **14**, 5166–5172 (2008).
370. El Andaloussi, A. & Lesniak, M. S. CD4+ CD25+ FoxP3+ T-cell infiltration and heme oxygenase-1 expression correlate with tumor grade in human gliomas. *J. Neurooncol.* **83**, 145–152 (2007).

371. Thornton, A. M. & Shevach, E. M. CD4+CD25+ immunoregulatory T cells suppress polyclonal T cell activation in vitro by inhibiting interleukin 2 production. *J. Exp. Med.* **188**, 287–296 (1998).
372. Fontenot, J. D., Rasmussen, J. P., Gavin, M. A. & Rudensky, A. Y. A function for interleukin 2 in Foxp3-expressing regulatory T cells. *Nat. Immunol.* **6**, 1142–1151 (2005).
373. Annacker, O., Asseman, C., Read, S. & Powrie, F. Interleukin-10 in the regulation of T cell-induced colitis. *J. Autoimmun.* **20**, 277–279 (2003).
374. Thomas, D. A. & Massagué, J. TGF-beta directly targets cytotoxic T cell functions during tumor evasion of immune surveillance. *Cancer Cell* **8**, 369–380 (2005).
375. Miska, J. *et al.* HIF-1α Is a Metabolic Switch between Glycolytic-Driven Migration and Oxidative Phosphorylation-Driven Immunosuppression of Tregs in Glioblastoma. *Cell Rep.* **27**, 226-237.e4 (2019).
376. Friebel, E. *et al.* Single-Cell Mapping of Human Brain Cancer Reveals Tumor-Specific Instruction of Tissue-Invading Leukocytes. *Cell* **181**, 1626-1642.e20 (2020).
377. Tran Thang, N. N. *et al.* Immune Infiltration of Spontaneous Mouse Astrocytomas Is Dominated by Immunosuppressive Cells from Early Stages of Tumor Development. *Cancer Res.* **70**, 4829–4839 (2010).
378. Gabrusiewicz, K. *et al.* Characteristics of the Alternative Phenotype of Microglia/Macrophages and its Modulation in Experimental Gliomas. *PLOS ONE* **6**, e23902 (2011).
379. Sattiraju, A. *et al.* Spatial patterning and immunosuppression of glioblastoma immune contexture in hypoxic niches. 2022.03.01.482530 Preprint at https://doi.org/10.1101/2022.03.01.482530 (2022).
380. Ye, X. *et al.* Tumor-Associated Microglia/Macrophages Enhance the Invasion of Glioma Stem-like Cells via TGF-β1 Signaling Pathway. *J. Immunol.* **189**, 444–453 (2012).
381. Yi, L. *et al.* Glioma-initiating cells: A predominant role in microglia/macrophages tropism to glioma. *J. Neuroimmunol.* **232**, 75–82 (2011).
382. Coniglio, S. J. *et al.* Microglial Stimulation of Glioblastoma Invasion Involves Epidermal Growth Factor Receptor (EGFR) and Colony Stimulating Factor 1 Receptor (CSF-1R) Signaling. *Mol. Med.* **18**, 519–527 (2012).
383. Gutmann, D. H. & Kettenmann, H. Microglia/Brain Macrophages as Central Drivers of Brain Tumor Pathobiology. *Neuron* **104**, 442–449 (2019).
384. Chen, Z. *et al.* Cellular and Molecular Identity of Tumor-Associated Macrophages in Glioblastoma. *Cancer Res.* **77**, 2266–2278 (2017).
385. Poon, C. C. *et al.* Differential microglia and macrophage profiles in human IDH-mutant and -wild type glioblastoma. *Oncotarget* **10**, 3129–3143 (2019).
386. Hambardzumyan, D., Gutmann, D. H. & Kettenmann, H. The role of microglia and macrophages in glioma maintenance and progression. *Nat. Neurosci.* **19**, 20–27 (2016).
387. Umemura, N. *et al.* Tumor-infiltrating myeloid-derived suppressor cells are pleiotropic-inflamed monocytes/macrophages that bear M1- and M2-type characteristics. *J. Leukoc. Biol.* **83**, 1136–1144 (2008).
388. Coniglio, S. J. & Segall, J. E. Review: molecular mechanism of microglia stimulated glioblastoma invasion. *Matrix Biol. J. Int. Soc. Matrix Biol.* **32**, 372–380 (2013).
389. Sottoriva, A. *et al.* Cancer Stem Cell Tumor Model Reveals Invasive Morphology and Increased Phenotypical Heterogeneity. *Cancer Res.* **70**, 46–56 (2010).

390. Yu, S. & Bian, X. Enrichment of Cancer Stem Cells Based on Heterogeneity of Invasiveness. *Stem Cell Rev. Rep.* **5**, 66–71 (2009).
391. Suzumura, A., Sawada, M., Yamamoto, H. & Marunouchi, T. Transforming growth factor-beta suppresses activation and proliferation of microglia in vitro. *J. Immunol. Baltim. Md 1950* **151**, 2150–2158 (1993).
392. Wu, A. *et al.* Glioma cancer stem cells induce immunosuppressive macrophages/microglia. *Neuro-Oncol.* **12**, 1113–1125 (2010).
393. Bogdahn, U. *et al.* Targeted therapy for high-grade glioma with the TGF-β2 inhibitor trabedersen: results of a randomized and controlled phase IIb study. *Neuro-Oncol.* **13**, 132–142 (2011).
394. Poon, C. C., Sarkar, S., Yong, V. W. & Kelly, J. J. P. Glioblastoma-associated microglia and macrophages: targets for therapies to improve prognosis. *Brain J. Neurol.* **140**, 1548–1560 (2017).
395. da Fonseca, A. C. C. *et al.* Microglial stress inducible protein 1 promotes proliferation and migration in human glioblastoma cells. *Neuroscience* **200**, 130–141 (2012).
396. Forsyth, P. A. *et al.* Gelatinase-A (MMP-2), gelatinase-B (MMP-9) and membrane type matrix metalloproteinase-1 (MT1-MMP) are involved in different aspects of the pathophysiology of malignant gliomas. *Br. J. Cancer* **79**, 1828–1835 (1999).
397. Markovic, D. S., Glass, R., Synowitz, M., Rooijen, N. van & Kettenmann, H. Microglia Stimulate the Invasiveness of Glioma Cells by Increasing the Activity of Metalloprotease-2. *J. Neuropathol. Exp. Neurol.* **64**, 754–762 (2005).
398. Klemm, F. *et al.* Interrogation of the Microenvironmental Landscape in Brain Tumors Reveals Disease-Specific Alterations of Immune Cells. *Cell* **181**, 1643-1660.e17 (2020).
399. Rodrigues, J. C. *et al.* Normal human monocytes exposed to glioma cells acquire myeloid-derived suppressor cell-like properties. *Neuro-Oncol.* **12**, 351–365 (2010).
400. Alban, T. J. *et al.* Global immune fingerprinting in glioblastoma patient peripheral blood reveals immune-suppression signatures associated with prognosis. *JCI Insight* **3**, e122264, 122264 (2018).
401. Yeini, E. *et al.* P-selectin axis plays a key role in microglia immunophenotype and glioblastoma progression. *Nat. Commun.* **12**, 1912 (2021).
402. Hu, X. *et al.* Meningeal lymphatic vessels regulate brain tumor drainage and immunity. *Cell Res.* **30**, 229–243 (2020).
403. Song, E. *et al.* VEGF-C-driven lymphatic drainage enables immunosurveillance of brain tumours. *Nature* **577**, 689–694 (2020).
404. Strong, M. J. *et al.* Bone metastasis from glioblastoma: a systematic review. *J. Neurooncol.* **158**, 379–392 (2022).
405. Fecci, P. E. *et al.* Increased regulatory T-cell fraction amidst a diminished CD4 compartment explains cellular immune defects in patients with malignant glioma. *Cancer Res.* **66**, 3294–3302 (2006).
406. Fecci, P. E. *et al.* Systemic anti-CD25 monoclonal antibody administration safely enhances immunity in murine glioma without eliminating regulatory T cells. *Clin. Cancer Res. Off. J. Am. Assoc. Cancer Res.* **12**, 4294–4305 (2006).
407. Gustafson, M. P. *et al.* Systemic immune suppression in glioblastoma: the interplay between CD14+HLA-DRlo/neg monocytes, tumor factors, and dexamethasone. *Neuro-Oncol.* **12**, 631–644 (2010).

408. Ayasoufi, K. *et al.* Brain cancer induces systemic immunosuppression through release of non-steroid soluble mediators. *Brain J. Neurol.* **143**, 3629–3652 (2020).
409. Chongsathidkiet, P. *et al.* Sequestration of T cells in bone marrow in the setting of glioblastoma and other intracranial tumors. *Nat. Med.* **24**, 1459–1468 (2018).
410. Lamano, J. B. *et al.* Glioblastoma-Derived IL6 Induces Immunosuppressive Peripheral Myeloid Cell PD-L1 and Promotes Tumor Growth. *Clin. Cancer Res.* **25**, 3643–3657 (2019).
411. Ahluwalia, M. S. *et al.* Correlation of higher levels of soluble TNF-R1 with a shorter survival, independent of age, in recurrent glioblastoma. *J. Neurooncol.* **131**, 449–458 (2017).
412. Waldman, A. D., Fritz, J. M. & Lenardo, M. J. A guide to cancer immunotherapy: from T cell basic science to clinical practice. *Nat. Rev. Immunol.* **20**, 651–668 (2020).
413. Rosenberg, S. A. *et al.* Durable complete responses in heavily pretreated patients with metastatic melanoma using T-cell transfer immunotherapy. *Clin. Cancer Res. Off. J. Am. Assoc. Cancer Res.* **17**, 4550–4557 (2011).
414. Hong, J. J. *et al.* Successful treatment of melanoma brain metastases with adoptive cell therapy. *Clin. Cancer Res. Off. J. Am. Assoc. Cancer Res.* **16**, 4892–4898 (2010).
415. Weathers, S.-P. *et al.* Glioblastoma-mediated Immune Dysfunction Limits CMV-specific T Cells and Therapeutic Responses: Results from a Phase I/II Trial. *Clin. Cancer Res. Off. J. Am. Assoc. Cancer Res.* **26**, 3565–3577 (2020).
416. Beatty, G. L. & O'Hara, M. Chimeric antigen receptor-modified T cells for the treatment of solid tumors: Defining the challenges and next steps. *Pharmacol. Ther.* **166**, 30–39 (2016).
417. Harris, D. T. & Kranz, D. M. Adoptive T Cell Therapies: A Comparison of T Cell Receptors and Chimeric Antigen Receptors. *Trends Pharmacol. Sci.* **37**, 220–230 (2016).
418. Wu, L., Wei, Q., Brzostek, J. & Gascoigne, N. R. J. Signaling from T cell receptors (TCRs) and chimeric antigen receptors (CARs) on T cells. *Cell. Mol. Immunol.* **17**, 600–612 (2020).
419. Srivastava, S. & Riddell, S. R. Engineering CAR-T cells: Design concepts. *Trends Immunol.* **36**, 494–502 (2015).
420. Abate-Daga, D. & Davila, M. L. CAR models: next-generation CAR modifications for enhanced T-cell function. *Mol. Ther. Oncolytics* **3**, 16014 (2016).
421. Bonifant, C. L., Jackson, H. J., Brentjens, R. J. & Curran, K. J. Toxicity and management in CAR T-cell therapy. *Mol. Ther. Oncolytics* **3**, 16011 (2016).
422. Pang, Y., Hou, X., Yang, C., Liu, Y. & Jiang, G. Advances on chimeric antigen receptor-modified T-cell therapy for oncotherapy. *Mol. Cancer* **17**, 91 (2018).
423. June, C. H. & Sadelain, M. Chimeric Antigen Receptor Therapy. *N. Engl. J. Med.* **379**, 64–73 (2018).
424. Goutnik, M. *et al.* Advancements in chimeric antigen receptor-expressing T-cell therapy for glioblastoma multiforme: Literature review and future directions. *Neuro-Oncol. Adv.* **6**, vdae025 (2024).
425. Singh, N. *et al.* Impaired Death Receptor Signaling in Leukemia Causes Antigen-Independent Resistance by Inducing CAR T-cell Dysfunction. *Cancer Discov.* **10**, 552–567 (2020).
426. Maude, S. L. *et al.* Chimeric antigen receptor T cells for sustained remissions in leukemia. *N. Engl. J. Med.* **371**, 1507–1517 (2014).
427. Choi, B. D. *et al.* CAR-T cells secreting BiTEs circumvent antigen escape without detectable toxicity. *Nat. Biotechnol.* **37**, 1049–1058 (2019).

428. Brown, C. E. *et al.* Optimization of IL13Rα2-Targeted Chimeric Antigen Receptor T Cells for Improved Anti-tumor Efficacy against Glioblastoma. *Mol. Ther. J. Am. Soc. Gene Ther.* **26**, 31–44 (2018).
429. Ahmed, N. *et al.* HER2-Specific Chimeric Antigen Receptor-Modified Virus-Specific T Cells for Progressive Glioblastoma: A Phase 1 Dose-Escalation Trial. *JAMA Oncol.* **3**, 1094–1101 (2017).
430. Shen, L. *et al.* The efficacy of third generation anti-HER2 chimeric antigen receptor T cells in combination with PD1 blockade against malignant glioblastoma cells. *Oncol. Rep.* **42**, 1549–1557 (2019).
431. Brown, C. E. *et al.* Glioma IL13Rα2 is associated with mesenchymal signature gene expression and poor patient prognosis. *PloS One* **8**, e77769 (2013).
432. Debinski, W., Gibo, D. M., Hulet, S. W., Connor, J. R. & Gillespie, G. Y. Receptor for interleukin 13 is a marker and therapeutic target for human high-grade gliomas. *Clin. Cancer Res. Off. J. Am. Assoc. Cancer Res.* **5**, 985–990 (1999).
433. Brown, C. E. *et al.* Stem-like tumor-initiating cells isolated from IL13Rα2 expressing gliomas are targeted and killed by IL13-zetakine-redirected T Cells. *Clin. Cancer Res. Off. J. Am. Assoc. Cancer Res.* **18**, 2199–2209 (2012).
434. Kahlon, K. S. *et al.* Specific recognition and killing of glioblastoma multiforme by interleukin 13-zetakine redirected cytolytic T cells. *Cancer Res.* **64**, 9160–9166 (2004).
435. Brown, C. E. *et al.* Bioactivity and Safety of IL13Rα2-Redirected Chimeric Antigen Receptor CD8+ T Cells in Patients with Recurrent Glioblastoma. *Clin. Cancer Res. Off. J. Am. Assoc. Cancer Res.* **21**, 4062–4072 (2015).
436. Johnson, L. A. *et al.* Rational development and characterization of humanized anti-EGFR variant III chimeric antigen receptor T cells for glioblastoma. *Sci. Transl. Med.* **7**, 275ra22 (2015).
437. Shen, C.-J. *et al.* Chimeric antigen receptor containing ICOS signaling domain mediates specific and efficient antitumor effect of T cells against EGFRvIII expressing glioma. *J. Hematol. Oncol.J Hematol Oncol* **6**, 33 (2013).
438. Jiang, H. *et al.* Selective Targeting of Glioblastoma with EGFRvIII/EGFR Bitargeted Chimeric Antigen Receptor T Cell. *Cancer Immunol. Res.* **6**, 1314–1326 (2018).
439. Bullain, S. S. *et al.* Genetically engineered T cells to target EGFRvIII expressing glioblastoma. *J. Neurooncol.* **94**, 373–382 (2009).
440. Morgan, R. A. *et al.* Recognition of glioma stem cells by genetically modified T cells targeting EGFRvIII and development of adoptive cell therapy for glioma. *Hum. Gene Ther.* **23**, 1043–1053 (2012).
441. Goff, S. L. *et al.* Pilot Trial of Adoptive Transfer of Chimeric Antigen Receptor-transduced T Cells Targeting EGFRvIII in Patients With Glioblastoma. *J. Immunother. Hagerstown Md 1997* **42**, 126–135 (2019).
442. Bagley, S. J. *et al.* Intrathecal bivalent CAR T cells targeting EGFR and IL13Rα2 in recurrent glioblastoma: phase 1 trial interim results. *Nat. Med.* (2024) doi:10.1038/s41591-024-02893-z.
443. Rodriguez, A., Brown, C. & Badie, B. Chimeric antigen receptor T-cell therapy for glioblastoma. *Transl. Res.* **187**, 93–102 (2017).
444. Alsajjan, R. & Mason, W. P. Bispecific T-Cell Engagers and Chimeric Antigen Receptor T-Cell Therapies in Glioblastoma: An Update. *Curr. Oncol. Tor. Ont* **30**, 8501–8549 (2023).

445. Vora, P. *et al.* The Rational Development of CD133-Targeting Immunotherapies for Glioblastoma. *Cell Stem Cell* **26**, 832-844.e6 (2020).
446. Sampson, J. H. *et al.* An epidermal growth factor receptor variant III-targeted vaccine is safe and immunogenic in patients with glioblastoma multiforme. *Mol. Cancer Ther.* **8**, 2773–2779 (2009).
447. Sampson, J. H. *et al.* Greater chemotherapy-induced lymphopenia enhances tumor-specific immune responses that eliminate EGFRvIII-expressing tumor cells in patients with glioblastoma. *Neuro-Oncol.* **13**, 324–333 (2011).
448. Sampson, J. H. *et al.* Immunologic Escape After Prolonged Progression-Free Survival With Epidermal Growth Factor Receptor Variant III Peptide Vaccination in Patients With Newly Diagnosed Glioblastoma. *J. Clin. Oncol.* **28**, 4722–4729 (2010).
449. Schuster, J. *et al.* A phase II, multicenter trial of rindopepimut (CDX-110) in newly diagnosed glioblastoma: the ACT III study. *Neuro-Oncol.* **17**, 854–861 (2015).
450. Weller, M. *et al.* Rindopepimut with temozolomide for patients with newly diagnosed, EGFRvIII-expressing glioblastoma (ACT IV): a randomised, double-blind, international phase 3 trial. *Lancet Oncol.* **18**, 1373–1385 (2017).
451. Platten, M. *et al.* A vaccine targeting mutant IDH1 in newly diagnosed glioma. *Nature* **592**, 463–468 (2021).
452. Iwami, K. *et al.* Peptide-pulsed dendritic cell vaccination targeting interleukin-13 receptor α2 chain in recurrent malignant glioma patients with HLA-A*24/A*02 allele. *Cytotherapy* **14**, 733–742 (2012).
453. Liau, L. M. *et al.* First results on survival from a large Phase 3 clinical trial of an autologous dendritic cell vaccine in newly diagnosed glioblastoma. *J. Transl. Med.* **16**, 142 (2018).
454. Erblich, B., Zhu, L., Etgen, A. M., Dobrenis, K. & Pollard, J. W. Absence of colony stimulation factor-1 receptor results in loss of microglia, disrupted brain development and olfactory deficits. *PloS One* **6**, e26317 (2011).
455. Nandi, S. *et al.* The CSF-1 receptor ligands IL-34 and CSF-1 exhibit distinct developmental brain expression patterns and regulate neural progenitor cell maintenance and maturation. *Dev. Biol.* **367**, 100–113 (2012).
456. Elmore, M. R. P. *et al.* Colony-stimulating factor 1 receptor signaling is necessary for microglia viability, unmasking a microglia progenitor cell in the adult brain. *Neuron* **82**, 380–397 (2014).
457. Yan, D. *et al.* Inhibition of colony stimulating factor-1 receptor abrogates microenvironment-mediated therapeutic resistance in gliomas. *Oncogene* **36**, 6049–6058 (2017).
458. Quail, D. F. *et al.* The tumor microenvironment underlies acquired resistance to CSF-1R inhibition in gliomas. *Science* **352**, aad3018 (2016).
459. Butowski, N. *et al.* Orally administered colony stimulating factor 1 receptor inhibitor PLX3397 in recurrent glioblastoma: an Ivy Foundation Early Phase Clinical Trials Consortium phase II study. *Neuro-Oncol.* **18**, 557–564 (2016).
460. Hu, F. *et al.* Glioma-derived versican promotes tumor expansion via glioma-associated microglial/macrophages Toll-like receptor 2 signaling. *Neuro-Oncol.* **17**, 200–210 (2015).
461. Reilly, M. *et al.* Randomized, double-blind, placebo-controlled, dose-escalating phase I, healthy subjects study of intravenous OPN-305, a humanized anti-TLR2 antibody. *Clin. Pharmacol. Ther.* **94**, 593–600 (2013).

462. von Roemeling, C. A. *et al.* Therapeutic modulation of phagocytosis in glioblastoma can activate both innate and adaptive antitumour immunity. *Nat. Commun.* **11**, 1508 (2020).
463. Hutter, G. *et al.* Microglia are effector cells of CD47-SIRPα antiphagocytic axis disruption against glioblastoma. *Proc. Natl. Acad. Sci. U. S. A.* **116**, 997–1006 (2019).
464. Zhang, P. *et al.* Therapeutic targeting of tumor-associated myeloid cells synergizes with radiation therapy for glioblastoma. *Proc. Natl. Acad. Sci. U. S. A.* **116**, 23714–23723 (2019).
465. Reardon, D. A. *et al.* Effect of Nivolumab vs Bevacizumab in Patients With Recurrent Glioblastoma: The CheckMate 143 Phase 3 Randomized Clinical Trial. *JAMA Oncol.* **6**, 1003–1010 (2020).
466. Lim, M. *et al.* Phase III trial of chemoradiotherapy with temozolomide plus nivolumab or placebo for newly diagnosed glioblastoma with methylated MGMT promoter. *Neuro-Oncol.* **24**, 1935–1949 (2022).
467. Araujo Moura, A. W. *et al.* Nivolumab for newly and recurrent glioblastoma multiforme treatment: A systematic review and meta-analysis. *J. Oncol. Pharm. Pract.* **29**, 1736–1747 (2023).
468. Schalper, K. A. *et al.* Neoadjuvant nivolumab modifies the tumor immune microenvironment in resectable glioblastoma. *Nat. Med.* **25**, 470–476 (2019).
469. Cloughesy, T. F. *et al.* Neoadjuvant anti-PD-1 immunotherapy promotes a survival benefit with intratumoral and systemic immune responses in recurrent glioblastoma. *Nat. Med.* **25**, 477–486 (2019).
470. Omuro, A. *et al.* Nivolumab with or without ipilimumab in patients with recurrent glioblastoma: results from exploratory phase I cohorts of CheckMate 143. *Neuro-Oncol.* **20**, 674–686 (2018).
471. Antonios, J. P. *et al.* PD-1 blockade enhances the vaccination-induced immune response in glioma. *JCI Insight* **1**, e87059 (2016).
472. Touat, M. *et al.* Mechanisms and therapeutic implications of hypermutation in gliomas. *Nature* **580**, 517–523 (2020).
473. Aslan, K. *et al.* Heterogeneity of response to immune checkpoint blockade in hypermutated experimental gliomas. *Nat. Commun.* **11**, 931 (2020).
474. Fu, W. *et al.* Single-Cell Atlas Reveals Complexity of the Immunosuppressive Microenvironment of Initial and Recurrent Glioblastoma. *Front. Immunol.* **11**, 835 (2020).
475. Lynch, H. E. *et al.* Thymic involution and immune reconstitution. *Trends Immunol.* **30**, 366–373 (2009).
476. Aw, D. & Palmer, D. B. The origin and implication of thymic involution. *Aging Dis.* **2**, 437–443 (2011).
477. Messaoudi, I., Lemaoult, J., Guevara-Patino, J. A., Metzner, B. M. & Nikolich-Zugich, J. Age-related CD8 T cell clonal expansions constrict CD8 T cell repertoire and have the potential to impair immune defense. *J. Exp. Med.* **200**, 1347–1358 (2004).
478. Bourgeois, C., Kassiotis, G. & Stockinger, B. A major role for memory CD4 T cells in the control of lymphopenia-induced proliferation of naive CD4 T cells. *J. Immunol. Baltim. Md 1950* **174**, 5316–5323 (2005).
479. Cicin-Sain, L. *et al.* Loss of naive T cells and repertoire constriction predict poor response to vaccination in old primates. *J. Immunol. Baltim. Md 1950* **184**, 6739–6745 (2010).
480. Sierra, A., Gottfried-Blackmore, A. C., McEwen, B. S. & Bulloch, K. Microglia derived from aging mice exhibit an altered inflammatory profile. *Glia* **55**, 412–424 (2007).

481. Henry, C. J., Huang, Y., Wynne, A. M. & Godbout, J. P. Peripheral lipopolysaccharide (LPS) challenge promotes microglial hyperactivity in aged mice that is associated with exaggerated induction of both pro-inflammatory IL-1beta and anti-inflammatory IL-10 cytokines. *Brain. Behav. Immun.* **23**, 309–317 (2009).
482. Zhai, L. *et al.* Molecular Pathways: Targeting IDO1 and Other Tryptophan Dioxygenases for Cancer Immunotherapy. *Clin. Cancer Res. Off. J. Am. Assoc. Cancer Res.* **21**, 5427–5433 (2015).
483. Ladomersky, E. *et al.* Advanced Age Increases Immunosuppression in the Brain and Decreases Immunotherapeutic Efficacy in Subjects with Glioblastoma. *Clin. Cancer Res. Off. J. Am. Assoc. Cancer Res.* **26**, 5232–5245 (2020).
484. Amoozgar, Z. *et al.* Targeting Treg cells with GITR activation alleviates resistance to immunotherapy in murine glioblastomas. *Nat. Commun.* **12**, 2582 (2021).
485. Mathios, D. *et al.* Anti-PD-1 antitumor immunity is enhanced by local and abrogated by systemic chemotherapy in GBM. *Sci. Transl. Med.* **8**, 370ra180 (2016).
486. Park, J. *et al.* Effect of combined anti-PD-1 and temozolomide therapy in glioblastoma. *Oncoimmunology* **8**, e1525243 (2019).
487. Karachi, A. *et al.* Modulation of temozolomide dose differentially affects T-cell response to immune checkpoint inhibition. *Neuro-Oncol.* **21**, 730–741 (2019).
488. Chen, Z. *et al.* The SMAC Mimetic APG-1387 Sensitizes Immune-Mediated Cell Apoptosis in Hepatocellular Carcinoma. *Front. Pharmacol.* **9**, (2018).
489. Burton, A. M., Ligman, B. R., Kearney, C. A. & Murray, S. E. SMAC mimetics inhibit human T cell proliferation and fail to augment type 1 cytokine responses. *Cell. Immunol.* **384**, 104674 (2023).
490. Rizk, J. *et al.* SMAC mimetics promote NIK-dependent inhibition of CD4+ TH17 cell differentiation. *Sci. Signal.* **12**, eaaw3469 (2019).
491. Kawalkowska, J. Z., Ogbechi, J., Venables, P. J. & Williams, R. O. cIAP1/2 inhibition synergizes with TNF inhibition in autoimmunity by down-regulating IL-17A and inducing Tregs. *Sci. Adv.* **5**, eaaw5422 (2019).
492. Roesler, S., Eckhardt, I., Wolf, S. & Fulda, S. Cooperative TRAIL production mediates IFNα/Smac mimetic-induced cell death in TNFα-resistant solid cancer cells. *Oncotarget* **7**, 3709–3725 (2016).
493. Morrish, E., Brumatti, G. & Silke, J. Future Therapeutic Directions for Smac-Mimetics. *Cells* **9**, 406 (2020).
494. Chang, Y.-C. & Cheung, C. H. A. An Updated Review of Smac Mimetics, LCL161, Birinapant, and GDC-0152 in Cancer Treatment. *Appl. Sci.* **11**, 335 (2021).
495. Juergens, R. A. *et al.* A dose-finding study of the SMAC mimetic Debio 1143 when given in combination with avelumab to patients with advanced solid malignancies. *J. Clin. Oncol.* **37**, 2599–2599 (2019).
496. Afsahi, A. *et al.* LCL161 enhances expansion and survival of engineered anti-tumor T cells but is restricted by death signaling. *Front. Immunol.* **14**, 1179827 (2023).
497. Chang, Y.-C. *et al.* The SMAC mimetic LCL161 is a direct ABCB1/MDR1-ATPase activity modulator and BIRC5/Survivin expression down-regulator in cancer cells. *Toxicol. Appl. Pharmacol.* **401**, 115080 (2020).
498. da Hora, C. C. *et al.* Sustained NF-κB-STAT3 signaling promotes resistance to Smac mimetics in Glioma stem-like cells but creates a vulnerability to EZH2 inhibition. *Cell Death Discov.* **5**, 72 (2019).

499. Marques-Torrejon, M. A., Gangoso, E. & Pollard, S. M. Modelling glioblastoma tumour-host cell interactions using adult brain organotypic slice co-culture. *Dis. Model. Mech.* **11**, dmm031435 (2018).
500. van Vloten, J. P. *et al.* Quantifying Antigen-Specific T Cell Responses When Using Antigen-Agnostic Immunotherapies. *Mol. Ther. Methods Clin. Dev.* **13**, 154–166 (2019).
501. Beug, S. T. *et al.* Combination of IAP Antagonists and TNF-α-Armed Oncolytic Viruses Induce Tumor Vascular Shutdown and Tumor Regression. *Mol. Ther. Oncolytics* **10**, 28–39 (2018).
502. Seyfried, T. N., el-Abbadi, M. & Roy, M. L. Ganglioside distribution in murine neural tumors. *Mol. Chem. Neuropathol.* **17**, 147–167 (1992).
503. Zimmerman, H. M. & Arnold, H. Experimental Brain Tumors. I. Tumors Produced with Methylcholanthrene*. *Cancer Res.* **1**, 919–938 (1941).
504. Fraser, H. Astrocytomas in an inbred mouse strain. *J. Pathol.* **103**, 266–270 (1971).
505. Maes, W. & Van Gool, S. W. Experimental immunotherapy for malignant glioma: lessons from two decades of research in the GL261 model. *Cancer Immunol. Immunother. CII* **60**, 153–160 (2011).
506. Serano, R. D., Pegram, C. N. & Bigner, D. D. Tumorigenic cell culture lines from a spontaneous VM/Dk murine astrocytoma (SMA). *Acta Neuropathol. (Berl.)* **51**, 53–64 (1980).
507. Martínez-Murillo, R. & Martínez, A. Standardization of an orthotopic mouse brain tumor model following transplantation of CT-2A astrocytoma cells. *Histol. Histopathol.* **22**, 1309–1326 (2007).
508. McKelvey, K. J. *et al.* Temporal and spatial modulation of the tumor and systemic immune response in the murine Gl261 glioma model. *PLOS ONE* **15**, e0226444 (2020).
509. Sampson, J. H. *et al.* Characterization of a spontaneous murine astrocytoma and abrogation of its tumorigenicity by cytokine secretion. *Neurosurgery* **41**, 1365–1372; discussion 1372-1373 (1997).
510. Ashley, D. M., Kong, F. M., Bigner, D. D. & Hale, L. P. Endogenous Expression of Transforming Growth Factor β1 Inhibits Growth and Tumorigenicity and Enhances Fas-mediated Apoptosis in a Murine High-Grade Glioma Model1. *Cancer Res.* **58**, 302–309 (1998).
511. Seystahl, K. *et al.* Biological Role and Therapeutic Targeting of TGF-β3 in Glioblastoma. *Mol. Cancer Ther.* **16**, 1177–1186 (2017).
512. Marsh, J., Mukherjee, P. & Seyfried, T. N. Akt-dependent proapoptotic effects of dietary restriction on late-stage management of a phosphatase and tensin homologue/tuberous sclerosis complex 2-deficient mouse astrocytoma. *Clin. Cancer Res. Off. J. Am. Assoc. Cancer Res.* **14**, 7751–7762 (2008).
513. Binello, E., Qadeer, Z. A., Kothari, H. P., Emdad, L. & Germano, I. M. Stemness of the CT-2A Immunocompetent Mouse Brain Tumor Model: Characterization *In Vitro*. *J. Cancer* **3**, 166–174 (2012).
514. Szatmári, T. *et al.* Detailed characterization of the mouse glioma 261 tumor model for experimental glioblastoma therapy. *Cancer Sci.* **97**, 546–553 (2006).
515. Allam, A. H. & Russell, S. M. Establishing a multiplex imaging panel to study T cell development in the thymus in mouse. *STAR Protoc.* **3**, 101472 (2022).
516. Fulda, S. Cell death-based treatment of glioblastoma. *Cell Death Dis.* **9**, 1–8 (2018).

517. Miles, M. A., Caruso, S., Baxter, A. A., Poon, I. K. H. & Hawkins, C. J. Smac mimetics can provoke lytic cell death that is neither apoptotic nor necroptotic. *Apoptosis* **25**, 500–518 (2020).
518. Heckmann, B. L., Tummers, B. & Green, D. R. Crashing the computer: apoptosis vs. necroptosis in neuroinflammation. *Cell Death Differ.* **26**, 41–52 (2019).
519. Kasamatsu, T. Implications of Senescent T Cells for Cancer Immunotherapy. *Cancers* **15**, 5835 (2023).
520. Li, L., Wan, S., Tao, K., Wang, G. & Zhao, E. KLRG1 restricts memory T cell antitumor immunity. *Oncotarget* **7**, 61670–61678 (2016).
521. Zhang, J., He, T., Xue, L. & Guo, H. Senescent T cells: a potential biomarker and target for cancer therapy. *EBioMedicine* **68**, 103409 (2021).
522. Jaggi, U. *et al.* Increased phagocytosis in the presence of enhanced M2-like macrophage responses correlates with increased primary and latent HSV-1 infection. *PLoS Pathog.* **16**, e1008971 (2020).
523. Ali, H. *et al.* Selective killing of human M1 macrophages by Smac mimetics alone and M2 macrophages by Smac mimetics and caspase inhibition. *J. Leukoc. Biol.* **110**, 693–710 (2021).
524. Wu, M. *et al.* Serum-free media and the immunoregulatory properties of mesenchymal stem cells in vivo and in vitro. *Cell. Physiol. Biochem. Int. J. Exp. Cell. Physiol. Biochem. Pharmacol.* **33**, 569–580 (2014).
525. Sriram, K., Benkovic, S. A., Hebert, M. A., Miller, D. B. & O'Callaghan, J. P. Induction of gp130-related cytokines and activation of JAK2/STAT3 pathway in astrocytes precedes up-regulation of glial fibrillary acidic protein in the 1-methyl-4-phenyl-1,2,3,6-tetrahydropyridine model of neurodegeneration: key signaling pathway for astrogliosis in vivo? *J. Biol. Chem.* **279**, 19936–19947 (2004).
526. Khalsa, J. K. *et al.* Immune phenotyping of diverse syngeneic murine brain tumors identifies immunologically distinct types. *Nat. Commun.* **11**, 3912 (2020).
527. Graham, K. & Unger, E. Overcoming tumor hypoxia as a barrier to radiotherapy, chemotherapy and immunotherapy in cancer treatment. *Int. J. Nanomedicine* **13**, 6049–6058 (2018).
528. Magnussen, A. L. & Mills, I. G. Vascular normalisation as the stepping stone into tumour microenvironment transformation. *Br. J. Cancer* **125**, 324–336 (2021).
529. Sorensen, A. G. *et al.* A 'vascular normalization index' as potential mechanistic biomarker to predict survival after a single dose of cediranib in recurrent glioblastoma patients. *Cancer Res.* **69**, 5296–5300 (2009).
530. Van Themsche, C., Chaudhry, P., Leblanc, V., Parent, S. & Asselin, E. XIAP gene expression and function is regulated by autocrine and paracrine TGF-β signaling. *Mol. Cancer* **9**, 216 (2010).
531. Hennessy, E. J. *et al.* Discovery of a Novel Class of Dimeric Smac Mimetics as Potent IAP Antagonists Resulting in a Clinical Candidate for the Treatment of Cancer (AZD5582). *J. Med. Chem.* **56**, 9897–9919 (2013).
532. Moon, J.-H. *et al.* A novel small-molecule IAP antagonist, AZD5582, draws Mcl-1 down-regulation for induction of apoptosis through targeting of cIAP1 and XIAP in human pancreatic cancer. *Oncotarget* **6**, 26895–26908 (2015).

533. Sharp, D. A., Lawrence, D. A. & Ashkenazi, A. Selective knockdown of the long variant of cellular FLICE inhibitory protein augments death receptor-mediated caspase-8 activation and apoptosis. *J. Biol. Chem.* **280**, 19401–19409 (2005).
534. Henrich, C. J. *et al.* Withanolide E sensitizes renal carcinoma cells to TRAIL-induced apoptosis by increasing cFLIP degradation. *Cell Death Dis.* **6**, e1666–e1666 (2015).
535. Lee, S.-R. *et al.* Accelerated degradation of cFLIPL and sensitization of the TRAIL DISC-mediated apoptotic cascade by pinoresinol, a lignan isolated from Rubia philippinensis. *Sci. Rep.* **9**, 13505 (2019).
536. Riley, J. S., Malik, A., Holohan, C. & Longley, D. B. DED or alive: assembly and regulation of the death effector domain complexes. *Cell Death Dis.* **6**, e1866–e1866 (2015).
537. Yaacoub, K. *et al.* The Identification of New c-FLIP Inhibitors for Restoring Apoptosis in TRAIL-Resistant Cancer Cells. *Curr. Issues Mol. Biol.* **46**, 710–728 (2024).
538. Karlsson, M. *et al.* A single–cell type transcriptomics map of human tissues. *Sci. Adv.* **7**, eabh2169 (2021).
539. Sjöstedt, E. *et al.* An atlas of the protein-coding genes in the human, pig, and mouse brain. *Science* **367**, eaay5947 (2020).
540. Tissue expression of PEA15 - Summary - The Human Protein Atlas. https://www.proteinatlas.org/ENSG00000162734-PEA15/tissue.
541. Ricci-Vitiani, L. *et al.* Absence of Caspase 8 and High Expression of PED Protect Primitive Neural Cells from Cell Death. *J. Exp. Med.* **200**, 1257–1266 (2004).
542. Ceccatelli, S., Tamm, C., Sleeper, E. & Orrenius, S. Neural stem cells and cell death. *Toxicol. Lett.* **149**, 59–66 (2004).
543. Wei, Y. On the Quest of Cellular Functions of PEA-15 and the Therapeutic Opportunities. *Pharmaceuticals* **8**, 455–473 (2015).
544. Ramos, J. W. *et al.* Death Effector Domain Protein PEA-15 Potentiates Ras Activation of Extracellular Signal Receptor-activated Kinase by an Adhesion-independent Mechanism. *Mol. Biol. Cell* **11**, 2863–2872 (2000).
545. Sung, J.-H. *et al.* Identification of proteins regulated by estradiol in focal cerebral ischemic injury—A proteomics approach. *Neurosci. Lett.* **477**, 66–71 (2010).
546. Zabel, C. *et al.* Comparative proteomics in neurodegenerative and non-neurodegenerative diseases suggest nodal point proteins in regulatory networking. *J. Proteome Res.* **5**, 1948–1958 (2006).
547. Koh, P.-O. Ferulic acid prevents the cerebral ischemic injury-induced decreases of astrocytic phosphoprotein PEA-15 and its two phosphorylated forms. *Neurosci. Lett.* **511**, 101–105 (2012).
548. Araujo, H. A., Danziger, N., Cordier, J., Glowinski, J. & Chneiweiss, H. Characterization of PEA-15, a major substrate for protein kinase C in astrocytes. *J. Biol. Chem.* (1993).
549. Kubes, M., Cordier, J., Glowinski, J., Girault, J. A. & Chneiweiss, H. Endothelin induces a calcium-dependent phosphorylation of PEA-15 in intact astrocytes: identification of Ser104 and Ser116 phosphorylated, respectively, by protein kinase C and calcium/calmodulin kinase II in vitro. *J. Neurochem.* **71**, 1307–1314 (1998).
550. Trencia, A. *et al.* Protein Kinase B/Akt Binds and Phosphorylates PED/PEA-15, Stabilizing Its Antiapoptotic Action. *Mol. Cell. Biol.* **23**, 4511–4521 (2003).
551. Renganathan, H., Vaidyanathan, H., Knapinska, A. & Ramos, J. W. Phosphorylation of PEA-15 switches its binding specificity from ERK/MAPK to FADD. *Biochem. J.* **390**, 729–735 (2005).

552. Sulzmaier, F. J., Opoku-Ansah, J. & Ramos, J. W. Phosphorylation is the switch that turns PEA-15 from tumor suppressor to tumor promoter. *Small GTPases* **3**, 173–177 (2012).
553. Glading, A., Koziol, J. A., Krueger, J. & Ginsberg, M. H. PEA-15 Inhibits Tumor Cell Invasion by Binding to Extracellular Signal-Regulated Kinase 1/2. *Cancer Res.* **67**, 1536–1544 (2007).
554. Siegelin, M. D., Habel, A. & Gaiser, T. Epigalocatechin-3-gallate (EGCG) downregulates PEA15 and thereby augments TRAIL-mediated apoptosis in malignant glioma. *Neurosci. Lett.* **448**, 161–165 (2008).
555. Eckert, A. *et al.* The PEA-15/PED protein protects glioblastoma cells from glucose deprivation-induced apoptosis via the ERK/MAP kinase pathway. *Oncogene* **27**, 1155–1166 (2008).
556. Tong, X. *et al.* Survivin is a prognostic indicator in glioblastoma and may be a target of microRNA-218. *Oncol. Lett.* **18**, 359–367 (2019).
557. Dahan, P. *et al.* Ionizing radiations sustain glioblastoma cell dedifferentiation to a stem-like phenotype through survivin: possible involvement in radioresistance. *Cell Death Dis.* **5**, e1543–e1543 (2014).
558. Reiszadeh-Jahromi, S. *et al.* Sepantronium Bromide (YM155), A Small Molecule Survivin Inhibitor, Promotes Apoptosis by Induction of Oxidative Stress, Worsens the Behavioral Deficits and Develops an Early Model of Toxic Demyelination: In Vivo and In-Silico Study. *Neurochem. Res.* **44**, 2482–2498 (2019).
559. West, T. J. *et al.* A Cell Type Selective YM155 Prodrug Targets Receptor-Interacting Protein Kinase 2 to Induce Brain Cancer Cell Death. *J. Am. Chem. Soc.* **145**, 8355–8363 (2023).
560. Householder, K. T. *et al.* Abstract B21: Use of polymeric nanoparticles for the delivery of YM155 to glioma cells in vitro and in vivo. *Cancer Res.* **75**, B21 (2015).
561. Rosa, R., Monteleone, F., Zambrano, N. & Bianco, R. In Vitro and In Vivo Models for Analysis of Resistance to Anticancer Molecular Therapies. *Curr. Med. Chem.* **21**, 1595–1606 (2014).
562. Huang, D. *et al.* Interleukin-8 mediates resistance to antiangiogenic agent sunitinib in renal cell carcinoma. *Cancer Res.* **70**, 1063–1071 (2010).
563. Rini, B. I. & Atkins, M. B. Resistance to targeted therapy in renal-cell carcinoma. *Lancet Oncol.* **10**, 992–1000 (2009).
564. Ugurel, S. *et al.* In vitro Drug Sensitivity Predicts Response and Survival after Individualized Sensitivity-Directed Chemotherapy in Metastatic Melanoma: A Multicenter Phase II Trial of the Dermatologic Cooperative Oncology Group. *Clin. Cancer Res.* **12**, 5454–5463 (2006).
565. Saberian, C., Sperduto, P. & Davies, M. A. Targeted therapy strategies for melanoma brain metastasis. *Neuro-Oncol. Adv.* **3**, v75–v85 (2021).
566. Di Giacomo, A. M. *et al.* Immunotherapy for brain metastases and primary brain tumors. *Eur. J. Cancer* **179**, 113–120 (2023).
567. Musca, B. *et al.* The immune cell landscape of glioblastoma patients highlights a myeloid-enriched and immune suppressed microenvironment compared to metastatic brain tumors. *Front. Immunol.* **14**, 1236824 (2023).
568. Kute, T. E. *et al.* Breast tumor cells isolated from in vitro resistance to trastuzumab remain sensitive to trastuzumab anti-tumor effects in vivo and to ADCC killing. *Cancer Immunol. Immunother.* **58**, 1887–1896 (2009).

569. Sallusto, F. & Lanzavecchia, A. Heterogeneity of CD4+ memory T cells: functional modules for tailored immunity. *Eur. J. Immunol.* **39**, 2076–2082 (2009).
570. Shin, S. *et al.* Novel antitumor therapeutic strategy using CD4+ T cell-derived extracellular vesicles. *Biomaterials* **289**, 121765 (2022).
571. Hunder, N. N. *et al.* Treatment of metastatic melanoma with autologous CD4+ T cells against NY-ESO-1. *N. Engl. J. Med.* **358**, 2698–2703 (2008).
572. Kreiter, S. *et al.* Mutant MHC class II epitopes drive therapeutic immune responses to cancer. *Nature* **520**, 692–696 (2015).
573. Linnemann, C. *et al.* High-throughput epitope discovery reveals frequent recognition of neo-antigens by CD4+ T cells in human melanoma. *Nat. Med.* **21**, 81–85 (2015).
574. Ott, P. A. *et al.* An immunogenic personal neoantigen vaccine for patients with melanoma. *Nature* **547**, 217–221 (2017).
575. Tran, E. *et al.* Cancer immunotherapy based on mutation-specific CD4+ T cells in a patient with epithelial cancer. *Science* **344**, 641–645 (2014).
576. Bawden, E. G. *et al.* CD4+ T cell immunity against cutaneous melanoma encompasses multifaceted MHC II–dependent responses. *Sci. Immunol.* **9**, eadi9517 (2024).
577. Cachot, A. *et al.* Tumor-specific cytolytic CD4 T cells mediate immunity against human cancer. *Sci. Adv.* **7**, eabe3348 (2021).
578. Malyshkina, A., Brüggemann, A., Paschen, A. & Dittmer, U. Cytotoxic CD4+ T cells in chronic viral infections and cancer. *Front. Immunol.* **14**, (2023).
579. Park, S., Anderson, N. L., Canaria, D. A. & Olson, M. R. Granzyme-Producing CD4 T Cells in Cancer and Autoimmune Disease. *ImmunoHorizons* **5**, 909–917 (2021).
580. Poncette, L., Bluhm, J. & Blankenstein, T. The role of CD4 T cells in rejection of solid tumors. *Curr. Opin. Immunol.* **74**, 18–24 (2022).
581. Tay, R. E., Richardson, E. K. & Toh, H. C. Revisiting the role of CD4+ T cells in cancer immunotherapy—new insights into old paradigms. *Cancer Gene Ther.* **28**, 5–17 (2021).
582. Venkatesh, H., Tracy, S. I. & Farrar, M. A. Cytotoxic CD4 T cells in the mucosa and in cancer. *Front. Immunol.* **14**, (2023).
583. Han, S. *et al.* Tumour-infiltrating CD4+ and CD8+ lymphocytes as predictors of clinical outcome in glioma. *Br. J. Cancer* **110**, 2560–2568 (2014).
584. Guo, W. *et al.* Upregulation of HLA-II related to LAG-3+ CD4+ T cell infiltration is associated with patient outcome in human glioblastoma. *Cancer Sci.* (2024) doi:10.1111/cas.16128.
585. Wang, J. *et al.* Vaccination with Designed Neopeptides Induces Intratumoral, Cross-reactive CD4+ T-cell Responses in Glioblastoma. *Clin. Cancer Res. Off. J. Am. Assoc. Cancer Res.* **28**, 5368–5382 (2022).
586. Khan, S. M. *et al.* Impact of CD4 T cells on intratumoral CD8 T-cell exhaustion and responsiveness to PD-1 blockade therapy in mouse brain tumors. *J. Immunother. Cancer* **10**, e005293 (2022).
587. Kesidou, E. *et al.* CNS Ageing in Health and Neurodegenerative Disorders. *J. Clin. Med.* **12**, 2255 (2023).
588. Lee, J. & Kim, H.-J. Normal Aging Induces Changes in the Brain and Neurodegeneration Progress: Review of the Structural, Biochemical, Metabolic, Cellular, and Molecular Changes. *Front. Aging Neurosci.* **14**, 931536 (2022).
589. Swenson, B. L., Meyer, C. F., Bussian, T. J. & Baker, D. J. Senescence in aging and disorders of the central nervous system. *Transl. Med. Aging* **3**, 17–25 (2019).

590. Aiello, A. *et al.* Immunosenescence and Its Hallmarks: How to Oppose Aging Strategically? A Review of Potential Options for Therapeutic Intervention. *Front. Immunol.* **10**, (2019).
591. Fulop, T. *et al.* Immunosenescence and Inflamm-Aging As Two Sides of the Same Coin: Friends or Foes? *Front. Immunol.* **8**, 1960 (2018).
592. Terekhova, M. *et al.* Single-cell atlas of healthy human blood unveils age-related loss of NKG2C+GZMB−CD8+ memory T cells and accumulation of type 2 memory T cells. *Immunity* **56**, 2836-2854.e9 (2023).
593. Weyand, C. M. & Goronzy, J. J. Aging of the Immune System. Mechanisms and Therapeutic Targets. *Ann. Am. Thorac. Soc.* **13**, S422–S428 (2016).
594. Zhai, L. *et al.* Infiltrating T Cells Increase IDO1 Expression in Glioblastoma and Contribute to Decreased Patient Survival. *Clin. Cancer Res. Off. J. Am. Assoc. Cancer Res.* **23**, 6650–6660 (2017).
595. Hamilton, J. A. G. & Henry, C. J. Aging and immunotherapies: New horizons for the golden ages. *Aging Cancer* **1**, 30–44 (2020).
596. Ladomersky, E. *et al.* Advanced age negatively impacts survival in an experimental brain tumor model. *Neurosci. Lett.* **630**, 203–208 (2016).
597. Fulop, T. *et al.* Potential role of immunosenescence in cancer development. *Ann. N. Y. Acad. Sci.* **1197**, 158–165 (2010).
598. Johnson, M. *et al.* Advanced Age in Humans and Mouse Models of Glioblastoma Show Decreased Survival from Extratumoral Influence. *Clin. Cancer Res.* **29**, 4973–4989 (2023).
599. Gorgoulis, V. *et al.* Cellular Senescence: Defining a Path Forward. *Cell* **179**, 813–827 (2019).
600. Riviere-Cazaux, C. *et al.* An untapped window of opportunity for glioma: targeting therapy-induced senescence prior to recurrence. *Npj Precis. Oncol.* **7**, 1–12 (2023).
601. Fletcher-Sananikone, E. *et al.* Elimination of Radiation-Induced Senescence in the Brain Tumor Microenvironment Attenuates Glioblastoma Recurrence. *Cancer Res.* **81**, 5935–5947 (2021).
602. Aasland, D. *et al.* Temozolomide Induces Senescence and Repression of DNA Repair Pathways in Glioblastoma Cells via Activation of ATR-CHK1, p21, and NF-κB. *Cancer Res.* **79**, 99–113 (2019).
603. Beltzig, L. *et al.* Senescence Is the Main Trait Induced by Temozolomide in Glioblastoma Cells. *Cancers* **14**, 2233 (2022).
604. Newlands, E. S., Stevens, M. F., Wedge, S. R., Wheelhouse, R. T. & Brock, C. Temozolomide: a review of its discovery, chemical properties, pre-clinical development and clinical trials. *Cancer Treat. Rev.* **23**, 35–61 (1997).
605. Milanovic, M. *et al.* Senescence-associated reprogramming promotes cancer stemness. *Nature* **553**, 96–100 (2018).
606. Salam, R. *et al.* Cellular senescence in malignant cells promotes tumor progression in mouse and patient Glioblastoma. *Nat. Commun.* **14**, 441 (2023).
607. Beltzig, L., Christmann, M. & Kaina, B. Abrogation of Cellular Senescence Induced by Temozolomide in Glioblastoma Cells: Search for Senolytics. *Cells* **11**, 2588 (2022).
608. Schwarzenbach, C. *et al.* Targeting c-IAP1, c-IAP2, and Bcl-2 Eliminates Senescent Glioblastoma Cells Following Temozolomide Treatment. *Cancers* **13**, 3585 (2021).
609. Colville, A. *et al.* Death-seq identifies regulators of cell death and senolytic therapies. *Cell Metab.* **35**, 1814-1829.e6 (2023).

610. Bollu, L. R. *et al.* Identification and Characterization of a Novel Indoleamine 2,3-Dioxygenase 1 Protein Degrader for Glioblastoma. *J. Med. Chem.* **65**, 15642–15662 (2022).
611. Kesarwani, P. *et al.* Tryptophan Metabolism Contributes to Radiation-Induced Immune Checkpoint Reactivation in Glioblastoma. *Clin. Cancer Res.* **24**, 3632–3643 (2018).
612. Ladomersky, E. *et al.* IDO1 Inhibition Synergizes with Radiation and PD-1 Blockade to Durably Increase Survival Against Advanced Glioblastoma. *Clin. Cancer Res. Off. J. Am. Assoc. Cancer Res.* **24**, 2559–2573 (2018).
613. Campian, J. L. *et al.* Preliminary results of a phase II study of retifanlimab (PD-1 inhibitor) plus or minus epacadostat (IDO1 inhibitor) in combination with bevacizumab and hypofractionated radiotherapy for recurrent glioblastoma: NCT03532295. *J. Clin. Oncol.* **40**, 2058–2058 (2022).
614. Tang, K., Wu, Y.-H., Song, Y. & Yu, B. Indoleamine 2,3-dioxygenase 1 (IDO1) inhibitors in clinical trials for cancer immunotherapy. *J. Hematol. Oncol.J Hematol Oncol* **14**, 68 (2021).
615. Burris, H. A. *et al.* A phase Ib dose escalation study of combined inhibition of IDO1 (GDC-0919) and PD-L1 (atezolizumab) in patients (pts) with locally advanced or metastatic solid tumors. *J. Clin. Oncol.* **35**, 105–105 (2017).
616. Li, M. *et al.* The indoleamine 2,3-dioxygenase pathway controls complement-dependent enhancement of chemo-radiation therapy against murine glioblastoma. *J. Immunother. Cancer* **2**, 21 (2014).
617. Conte, D. *et al.* Inhibitor of apoptosis protein cIAP2 is essential for lipopolysaccharide-induced macrophage survival. *Mol. Cell. Biol.* **26**, 699–708 (2006).
618. McComb, S. *et al.* cIAP1 and cIAP2 limit macrophage necroptosis by inhibiting Rip1 and Rip3 activation. *Cell Death Differ.* **19**, 1791–1801 (2012).
619. Kavanagh, E., Rodhe, J., Burguillos, M. A., Venero, J. L. & Joseph, B. Regulation of caspase-3 processing by cIAP2 controls the switch between pro-inflammatory activation and cell death in microglia. *Cell Death Dis.* **5**, e1565–e1565 (2014).
620. Rajalingam, K. *et al.* IAP-IAP Complexes Required for Apoptosis Resistance of C. trachomatis–Infected Cells. *PLOS Pathog.* **2**, e114 (2006).
621. Barca, O., Carneiro, C., Costoya, J. A., Señarís, R. M. & Arce, V. M. Resistance of neonatal primary astrocytes against Fas-induced apoptosis depends on silencing of caspase 8. *Neurosci. Lett.* **479**, 206–210 (2010).
622. Wosik, K., Becher, B., Ezman, A., Nalbantoglu, J. & Antel, J. P. Caspase 8 expression and signaling in Fas injury–resistant human fetal astrocytes. *Glia* **33**, 217–224 (2001).
623. Yew, D. T., Ping Li, W. & Liu, W. K. Fas and activated caspase 8 in normal, Alzheimer and multiple infarct brains. *Neurosci. Lett.* **367**, 113–117 (2004).
624. Germano, I. M., Uzzaman, M., Benveniste, R. J., Zaurova, M. & Keller, G. Apoptosis in human glioblastoma cells produced using embryonic stem cell-derived astrocytes expressing tumor necrosis factor-related apoptosis-inducing ligand. *J. Neurosurg.* **105**, 88–95 (2006).
625. Riddick, E., Evans, S., Rousch, J., Gwebu, E. & Banerjee, H. N. Identification of death receptors DR4 and DR5 in HTB-12 astrocytoma cell lines and determination of TRAIL sensitivity. *J. Solid Tumors* **3**, 20–26 (2013).
626. Aravalli, R. N., Hu, S., Rowen, T. N., Gekker, G. & Lokensgard, J. R. Differential apoptotic signaling in primary glial cells infected with herpes simplex virus 1. *J. Neurovirol.* **12**, 501–510 (2006).

627. Sharif, A. *et al.* The expression of PEA-15 (phosphoprotein enriched in astrocytes of 15 kDa) defines subpopulations of astrocytes and neurons throughout the adult mouse brain. *Neuroscience* **126**, 263–275 (2004).
628. Ishigaki, S. *et al.* X-Linked inhibitor of apoptosis protein is involved in mutant SOD1-mediated neuronal degeneration. *J. Neurochem.* **82**, 576–584 (2002).
629. Solaroglu, I., Tsubokawa, T., Cahill, J. & Zhang, J. H. Anti-apoptotic effect of Granulocyte-Colony Stimulating Factor after focal cerebral ischemia in the rat. *Neuroscience* **143**, 965–974 (2006).
630. Choi, C. *et al.* Fas ligand and Fas are expressed constitutively in human astrocytes and the expression increases with IL-1, IL-6, TNF-alpha, or IFN-gamma. *J. Immunol. Baltim. Md 1950* **162**, 1889–1895 (1999).
631. de la Monte, S. M., Sohn, Y. K. & Wands, J. R. Correlates of p53- and Fas (CD95)-mediated apoptosis in Alzheimer's disease. *J. Neurol. Sci.* **152**, 73–83 (1997).
632. Falsig, J., Latta, M. & Leist, M. Defined inflammatory states in astrocyte cultures: correlation with susceptibility towards CD95-driven apoptosis. *J. Neurochem.* **88**, 181–193 (2004).
633. Vernet-der Garabedian, B., Derer, P., Bailly, Y. & Mariani, J. Innate immunity in the Grid2Lc/+mouse model of cerebellar neurodegeneration: glial CD95/CD95L plays a non-apoptotic role in persistent neuron loss-associated inflammatory reactions in the cerebellum. *J. Neuroinflammation* **10**, 829 (2013).
634. Saxena, T. *et al.* Engineering Controlled Peritumoral Inflammation to Constrain Brain Tumor Growth. *Adv. Healthc. Mater.* **8**, e1801076 (2019).
635. Aktas, O., Schulze-Topphoff, U. & Zipp, F. The role of TRAIL/TRAIL receptors in central nervous system pathology. *Front. Biosci. J. Virtual Libr.* **12**, 2912–2921 (2007).
636. Bechmann, I. *et al.* Astrocyte-induced T cell elimination is CD95 ligand dependent. *J. Neuroimmunol.* **132**, 60–65 (2002).
637. Bellgrau, D. *et al.* A role for CD95 ligand in preventing graft rejection. *Nature* **377**, 630–632 (1995).
638. Giuliani, F., Goodyer, C. G., Antel, J. P. & Yong, V. W. Vulnerability of human neurons to T cell-mediated cytotoxicity. *J. Immunol. Baltim. Md 1950* **171**, 368–379 (2003).
639. Griffith, T. S., Brunner, T., Fletcher, S. M., Green, D. R. & Ferguson, T. A. Fas Ligand-Induced Apoptosis as a Mechanism of Immune Privilege. *Science* **270**, 1189–1192 (1995).
640. Hunt, J. S., Vassmer, D., Ferguson, T. A. & Miller, L. Fas ligand is positioned in mouse uterus and placenta to prevent trafficking of activated leukocytes between the mother and the conceptus. *J. Immunol.* **158**, 4122–4128 (1997).
641. Kwidzinski, E. *et al.* Self-tolerance in the immune privileged CNS: lessons from the entorhinal cortex lesion model. *J. Neural Transm. Suppl.* 29–49 (2003) doi:10.1007/978-3-7091-0643-3_2.
642. Castaneyra-Ruiz, L. *et al.* Intraventricular dimethyl sulfoxide (DMSO) induces hydrocephalus in a dose-dependent pattern. *Heliyon* **10**, e27295 (2024).
643. Zhang, C. *et al.* Effects of dimethyl sulfoxide on the morphology and viability of primary cultured neurons and astrocytes. *Brain Res. Bull.* **128**, 34–39 (2017).
644. Barzegar Behrooz, A., Talaie, Z. & Syahir, A. Nanotechnology-Based Combinatorial Anti-Glioblastoma Therapies: Moving from Terminal to Treatable. *Pharmaceutics* **14**, 1697 (2022).

645. Di Filippo, L. D., Duarte, J. L., Luiz, M. T., de Araújo, J. T. C. & Chorilli, M. Drug Delivery Nanosystems in Glioblastoma Multiforme Treatment: Current State of the Art. *Curr. Neuropharmacol.* **19**, 787–812 (2021).
646. Gregory, J. V. *et al.* Systemic brain tumor delivery of synthetic protein nanoparticles for glioblastoma therapy. *Nat. Commun.* **11**, 5687 (2020).
647. Roque, D. *et al.* Nanoparticle-Based Treatment in Glioblastoma. *J. Pers. Med.* **13**, 1328 (2023).
648. Miller, M. A. *et al.* Tumour-associated macrophages act as a slow-release reservoir of nano-therapeutic Pt(IV) pro-drug. *Nat. Commun.* **6**, 8692 (2015).
649. de Streel, G. & Lucas, S. Targeting immunosuppression by TGF-β1 for cancer immunotherapy. *Biochem. Pharmacol.* **192**, 114697 (2021).
650. Derynck, R., Turley, S. J. & Akhurst, R. J. TGFβ biology in cancer progression and immunotherapy. *Nat. Rev. Clin. Oncol.* **18**, 9–34 (2021).
651. Groeneveldt, C., Hall, T. van, Burg, S. H. van der, Dijke, P. ten & Montfoort, N. van. Immunotherapeutic Potential of TGF-β Inhibition and Oncolytic Viruses. *Trends Immunol.* **41**, 406–420 (2020).
652. Dahmani, A. & Delisle, J.-S. TGF-β in T Cell Biology: Implications for Cancer Immunotherapy. *Cancers* **10**, 194 (2018).
653. Batlle, E. & Massagué, J. Transforming Growth Factor-β Signaling in Immunity and Cancer. *Immunity* **50**, 924–940 (2019).
654. Chen, S.-Y., Mamai, O. & Akhurst, R. J. TGFβ: Signaling Blockade for Cancer Immunotherapy. *Annu. Rev. Cancer Biol.* **6**, 123–146 (2022).
655. Metropulos, A. E., Munshi, H. G. & Principe, D. R. The difficulty in translating the preclinical success of combined TGFβ and immune checkpoint inhibition to clinical trial. *eBioMedicine* **86**, (2022).
656. Ledergor, G. *et al.* CD4+ CAR-T cell exhaustion associated with early relapse of multiple myeloma after BCMA CAR-T cell therapy. *Blood Adv.* bloodadvances.2023012416 (2024) doi:10.1182/bloodadvances.2023012416.
657. Hau, P., Jachimczak, P. & Bogdahn, U. Treatment of malignant gliomas with TGF-beta2 antisense oligonucleotides. *Expert Rev. Anticancer Ther.* **9**, 1663–1674 (2009).
658. Schlingensiepen, K.-H. *et al.* Targeted tumor therapy with the TGF-beta 2 antisense compound AP 12009. *Cytokine Growth Factor Rev.* **17**, 129–139 (2006).
659. Vallières, L. Trabedersen, a TGFbeta2-specific antisense oligonucleotide for the treatment of malignant gliomas and other tumors overexpressing TGFbeta2. *IDrugs Investig. Drugs J.* **12**, 445–453 (2009).
660. Joseph, J. V. *et al.* TGF-β promotes microtube formation in glioblastoma through thrombospondin 1. *Neuro-Oncol.* **24**, 541–553 (2022).
661. Han, J., Alvarez-Breckenridge, C. A., Wang, Q.-E. & Yu, J. TGF-β signaling and its targeting for glioma treatment. *Am. J. Cancer Res.* **5**, 945–955 (2015).
662. den Hollander, M. W. *et al.* 89zr-GC1008 PET imaging and GC1008 treatment of recurrent glioma patients. *J. Clin. Oncol.* **31**, 2050–2050 (2013).
663. Rodon, J. *et al.* First-in-Human Dose Study of the Novel Transforming Growth Factor-β Receptor I Kinase Inhibitor LY2157299 Monohydrate in Patients with Advanced Cancer and Glioma. *Clin. Cancer Res.* **21**, 553–560 (2015).

664. Rodón, J. *et al.* Pharmacokinetic, pharmacodynamic and biomarker evaluation of transforming growth factor-β receptor I kinase inhibitor, galunisertib, in phase 1 study in patients with advanced cancer. *Invest. New Drugs* **33**, 357–370 (2015).
665. Lan, Y. *et al.* Simultaneous targeting of TGF-β/PD-L1 synergizes with radiotherapy by reprogramming the tumor microenvironment to overcome immune evasion. *Cancer Cell* **39**, 1388-1403.e10 (2021).
666. Reiners, O. *et al.* Abstract PO-049: TGFβ and PD-L1 inhibition in combination with radiotherapy can overcome glioblastoma resistance to immunotherapies. *Clin. Cancer Res.* **27**, PO-049 (2021).